

Development of Silane based Coating for Corrosion Protection of Magnesium alloy for Biomedical Implant Application

Submitted in partial fulfillment of the requirements

for the degree of

Doctor of Philosophy

of the

Indian Institute of Technology, Bombay, India

and

Monash University, Australia

by

Swati

Supervisors:

Prof. A.S. Khanna (IIT Bombay)

and

Prof. R.K. Singh Raman (Monash University)



The course of study for this award was developed jointly by the Indian Institute of Technology, Bombay and Monash University, Australia and given academic recognition by each of them. The programme was administered by The IITB-Monash Research Academy

(Year 2015)

DECLARATION

I declare that this written submission represents my ideas in my own words and where others' ideas or words have been included, I have adequately cited and referenced the original sources. I also declare that I have adhered to all principles of academic honesty and integrity and have not misrepresented or fabricated or falsified any idea/data/fact/source in my submission. I understand that any violation of the above will be cause for disciplinary action by the Institute and can also evoke penal action from the sources which have thus not been properly cited or from whom proper permission has not been taken when needed.

Notice 1

Under the Copyright Act 1968, this thesis must be used only under the normal conditions of scholarly fair dealing. In particular no results or conclusions should be extracted from it, nor should it be copied or closely paraphrased in whole or in part without the written consent of the author. Proper written acknowledgement should be made for any assistance obtained from this thesis.

Notice 2

I certify that I have made all reasonable efforts to secure copyright permissions for third-party content included in this thesis and have not knowingly added copyright content to my work without the owner's permission.

Student Name: **Swati**

IITB ID: 10411411

████████████████████

Date: 23/07/2015

Place: IIT Bombay, Mumbai

ACKNOWLEDGEMENTS

Completion of this doctoral dissertation is possible with the support of several people. I would like to express my sincere gratitude to all of them. Firstly and most importantly I would like to express my deepest gratitude to my advisor, Prof. A.S. Khanna, for his valuable guidance, scholarly expertise, patience and consistent encouragement I received throughout the research work. I appreciate his vast knowledge and skill in many areas and his assistance in writing reports (proposals, publications and this thesis).

I wish to thank my advisor, Prof. R.K. Singh Raman, for giving me the opportunity to get trained in his lab in Monash University and offering invaluable assistance and guidance. He has been very encouraging and supportive. He always made himself available to clarify my doubts despite his busy schedule. His support, knowledge and encouragement made this research possible. I thank both of my guides for giving me abundant help and guidance in preparing paper work for publication during the course of my research work.

I must also acknowledge my research committee member Prof. A.S. Panwar for helping me with any technical questions and editorial comments in reviewing my annual progress reports and providing valuable suggestions. I would also thank IITB-Monash Research Academy for all the cooperative support throughout the tenure of my work.

My colleagues, Ravindra Puri, Narayanan, Karan and Rajkumar, have all extended their support in a very special way, and I gained a lot from them, through their personal and scholarly interactions, their suggestions at various points of my research programme. I also acknowledge my old pals, Narayani, Ruchi, Garima and Gunjan for their well wishes. Thank you all so much for the laughs and encouragement and for making my Ph.D journey a little easier to handle. I would also appreciate, Ms Saumya Nigam, for working with me to develop biological tests and for teaching me how to work with cells.

But most of all I would like to thank my family, for their blessings, unconditional love and support throughout my journey. I thank my parents who raised me with a love of science and supported me in all my pursuit. I would like to thank my brothers, sister and also my brother in-

law for his support all the time during this journey. And most of all, my loving, supportive, encouraging, and patient husband Mr. Prateet Jain whose faithful support during this Ph.D. is so appreciated. I would like to thank my little daughter Sanvi for being so sweet and for sacrificing her own precious time with me for my research.

Above all, I owe it all to Almighty God for granting me the wisdom, health and strength to undertake this research task and enabling me to its completion.

ABSTRACT

Biomaterials are used in several medical applications today, such as fixation devices, replacements and surgical equipment. Implants are typical examples of a biomaterial application and there are several different implant materials used today. Conventional implant materials include stainless steels, cobalt-chromium alloys, alumina, polymers (methyl methacrylate), polyethylene etc. There are several impediments associated with long term presence of implants inside body, including allergy and sensitization. After the healing and curing, the implant is removed by a second surgery which is not only costly but also very painful. To make this process simpler, less painful and cost effective, there is a need for alternative methodology, called the use of temporary biodegradable implants. The purpose of biodegradable implant is to support tissue regeneration and healing by material degradation and simultaneous implant replacement through the surrounding tissues. In recent years there has been increased amount of focus on magnesium and its alloys for their potential use as biodegradable implant materials. Magnesium is biocompatible; has excellent mechanical properties; is natural for human body, and seems to stimulate new bone formation. However, a serious problem with magnesium is its high corrosion rate with consistent hydrogen gas formation which delays the healing process. Hence, there is need for controlling their degradation rate, by some surface modification.

In this research work magnesium based alloy system containing calcium and zinc was investigated (Mg-6Zn-Ca alloy) which are supposed to be non-toxic in the body. The work focused on to mitigate/delay the corrosion rate of the alloy by development of silane based coating systems for effective corrosion resistance and selecting the coating chemistry to provide biocompatibility. Two different types of silane based coating systems were studied and developed. Phosphonate silane approach (DEPETES with MTEOS and BTESPT as precursor) and non-Phosphonate silanes approach (GPTMS with MTEOS) were used to develop coating. As developed coatings were subjected to various detailed characterization techniques like, scanning electron microscopy (SEM) and energy dispersive X-ray analysis (EDAX) and the cross-linking in the coating was studied using Fourier transform infrared spectroscopy (FTIR) and performance evaluation, using Electrochemical Impedance Spectroscopy (EIS),

Potentiodynamic polarization, hydrogen evolution and pH change. Further, biological response of human osteoblast cell line on the developed coating system was studied. The in vitro cytotoxicity studies were performed on human osteoblast cells MG-63 to observe cell morphology, attachment, proliferation and differentiation. It was found that the silane coated alloy shows an improved corrosion resistance and biocompatibility as compared to bare Mg-6Zn-Ca alloy.

TABLE OF CONTENTS

Section	Title	Page No.
I	Abstract	v
II	Contents	vii
III	List of Figures	xiii
IV	List of Tables	xxi
V	List of abbreviations	xxii
Chapter 1 - Introduction		1
Chapter 2 – Literature review		
2.1	Background	7
2.2	Corrosion of magnesium alloy	8
2.2.1	Types of corrosion in magnesium	10
2.2.1.1	Galvanic corrosion	10
2.2.1.2.	Localized corrosion	10
2.2.1.3	Stress corrosion cracking (SCC)	11
2.3	Biomaterials	11
2.3.1	History of biomaterials	11
2.3.2	Classification of biomaterials	12
2.3.2.1	Polymers	13
2.3.2.2	Ceramics	14
2.3.2.4	Metals	14
2.4	Magnesium as a biodegradable implant material	16
2.4.1	A short history of application of magnesium as body implant	16

2.4.2	Advantages of Magnesium Alloy as body implant	17
2.4.3	Problems with magnesium Alloy as body implant	19
2.4.4	Corrosion Resistance Improvement	20
2.4.4.1	Alloying	20
2.4.4.2	Effect of alloying elements on physical and toxicological properties of magnesium	26
2.4.4.3	Surface modification of magnesium and its alloys	30
2.5	Organosilane Coating	45
2.5.1	Surface treatment	47
2.5.2	Silane hydrolysis	47
2.5.3	Application methods	49
2.5.4	Silanes for coating implants and in pharmaceutical application	49
2.5.5	Effect of functionalities on corrosion performance of silanes coatings	53
2.5.6	Diethylphosphonatoethyltriethoxy-silane (DEPETES)	53
2.5.7	Glycidoxypropyltrimethoxysilane (GPTMS)	57
2.5.8	Bis-silanes like bis-[triethoxysilylpropyl] tetrasulfide (BTESPT)	60
2.6	Biological testing of biomaterials	66
2.6.1	Categories of Evaluation	67
2.6.2	The most common assays for determining cytotoxicity	67
2.6.2.1	Neutral red (NR)	67
2.6.2.2	MTT ((3-(4,5-dimethylthiazol-2-yl)-2,5-diphenyltetrazoliumbromide)) assay	67
2.6.2.3	XTT(2,3-bis-(2-methoxy-4-nitro-5-sulfophenyl)-2H-tetrazolium-5-carboxanilide)	68
2.6.2.4	BrDU (5-bromo-2'-deoxyuridine)	68

2.6.2.5	Alkaline phosphatase activity	68
2.6.3	Advantages and Disadvantages	69
2.6.4	Experimental Procedure	69
2.6.5	Kinds of cytotoxicity tests:	70
2.6.5.1	Extract test	70
2.6.5.2	Direct contact test	70
2.6.5.3	Indirect contact test	70
2.7	Gaps in the literature:	71
2.8	Aims and Objectives	72
Chapter 3 – Experimental Work		
3.1	Materials, reagents and test environment	74
3.1.1	Material	74
3.1.2	Reagents	75
3.1.3	In-vitro Corrosion test environment	75
3.1.4	In-vitro Biocompatibility test environment	75
3.2	Experimental Methodology and Procedure	76
3.2.1.	Preparation of alloy sample	76
3.2.2	Alkaline Surface Pretreatment	77
3.2.3	Coating procedure	77
3.2.3.1	Investigation with 2-Diethylphosphatoethyl triethoxysilane (DEPETES) and Methyl triethoxysilane (MTEOS)	77
3.2.3.2	Investigation with 2-Diethylphosphatoethyl triethoxysilane (DEPETES) and Bis-[3-(triethoxysilyl) propyl]tetrasulfide (BTESPT)	78
3.2.3.3	Investigation with Glycidoxypropyltrimethoxysilane (GPTMS) and MTEOS	79

3.3	Characterization of as developed sol-gel coatings	79
3.3.1	Structural analysis of various modified sol-gel coatings	79
3.3.2	Surface Morphology of various sol -gel coatings	80
3.3.3	Corrosion resistance of various modified sol -gel coatings	80
3.3.4	Mechanical Properties of various modified sol -gel coatings	82
3.3.5	In-vitro biocompatibility tests	82
3.3.5.1	Cell Culture	82
3.3.5.2	Cell morphology and attachment	83
3.3.5.3	Cell viability and proliferation	83
3.3.5.4	Alkaline phosphatase activity assay	84
3.3.5.5	Statistical Analysis	84
Chapter 4 – Results and Discussion		
4.1	Surface pretreatment of Mg-6Zn-Ca alloy	85
4.2	Development, Characterization and Evaluation of Coating systems	91
4.2.1	DEPETES: MTEOS based coating system	91
A)	Study of hydrolysis of 2-Diethylphosphatoethyl triethoxysilane (DEPETES)	92
B)	Methyl triethoxy silane (MTEOS) hydrolysis at two different pH	94
C)	Curing at two different temperatures	95
4.2.1.1	Surface characterization of the silane coated alloy	96
A)	Structural Analysis (by Fourier transform infrared spectroscopy (FTIR))	96
B)	Surface morphology and chemical analysis of silane coated alloy	98
4.2.1.2	Performance Evaluation of DEPETES: MTEOS silane coated Mg-6Zn-Ca alloy	100

A)	Electrochemical investigation of DEPETES: MTEOS silane coated Mg 6Zn-Ca alloy	100
B)	Time dependent degradation of 1:4 DEPETES: MTEOS coated alloy	105
C)	Hydrogen Evolution	107
D)	pH study	109
4.2.1.3	Mechanical analysis of the silane coating on the Mg-6Zn-Ca alloy	110
4.2.1.4	Post Corrosion Analysis of 1:4 DEPETES: MTEOS coated alloy	110
4.2.2	DEPETES:BTESPT based coating system	113
A)	BTESPT hydrolysis study at two different pH	114
B)	Curing at two different temperatures	115
4.2.2.1	Surface characterization of the silane coated alloy	115
A)	Structural Analysis – by Fourier transform infrared spectroscopy (FTIR)	116
B)	Surface morphology and chemical analysis of silane coated alloy	117
4.2.2.2	Performance Evaluation of DEPETES: BTESPT silane coated Mg-6Zn-Ca alloy	119
A)	Electrochemical investigation of silane coated Mg-6Zn-Ca alloy	119
B)	Time dependent degradation of 1:4 DEPETES: BTESPT coated alloy	124
C)	Hydrogen Evolution	126
D)	pH study	127
4.2.2.3	Mechanical analysis of the DEPETES:BTESPT silane coating on the Mg-6Zn-Ca alloy	127
4.2.2.4	Post Corrosion Analysis of 1:4 DEPETES: BTESPT coated alloy	128
4.2.3	GPTMS:MTEOS based coating system	130
4.2.3.1	Surface characterization of silane coated alloy	130

A)	Structural Analysis –by Fourier transform infrared spectroscopy (FTIR)	131
B)	Morphology, chemical and mechanical properties of silane coated alloy	132
4.2.3.2	Performance Evaluation of GPTMS:MTEOS silane coated Mg-6Zn-Ca alloy	133
A)	Electrochemical investigation of GPTMS:MTEOS silane coated alloy	133
B)	Time dependent degradation of GPTMS: MTEOS coated alloys	137
C)	Hydrogen Evolution	142
D)	pH study	143
4.2.3.3	Post corrosion analysis	143
4.3	In vitro biocompatibility tests	145
4.3.1	Biocompatibility investigation of GPTMS: MTEOS coating system	145
4.3.1.1	Cell morphology and attachment observations	145
4.3.1.2	Cell viability and proliferation	147
4.3.1.3	Alkaline phosphatase activity (ALP) assay	149
4.3.2	Biocompatibility investigation of DEPETES:BTESPT coating system	150
4.3.2.1	Cell morphology and attachment observations	150
4.3.2.2	Cell viability and proliferation	151
4.3.2.3	Alkaline phosphatase activity (ALP) assay	152
4.3.2.4	XRD Analysis of formed corrosion products on the coated surface in DMEM	153
Chapter 5 – General Discussion		155
Chapter 6 - Conclusion		165
Future Scope		166
References		

List of Figures

Figure No.	Captions	Page No.
1.1	Different types of metallic implant materials	2
1.2	Real/possible applications of biodegradable magnesium implants: (a) cardiovascular stents (BIOTRONIK, Berlin, Germany, under clinical trial), (b) MAGNEZIX screw (received CE mark in Europe), (c) microclip for laryngeal microsurgery (pure magnesium), (d) biodegradable orthopaedic implants, (e) wound-closing devices (WZ21)	3
2.1	Pourbaix diagram for magnesium-water system at 25 ⁰ C	9
2.2	a) Microgalvanic corrosion. b) Microgalvanic corrosion	10
2.3	Pitting corrosion site at the surface of a magnesium component	11
2.4	Global market of orthopedic implants	12
2.5	Averaged hydrogen evolution for different magnesium alloys	21
2.6	Polarization curves and b) impedance spectra of AZ91 and Mg–2Zn–0.2X (X = Ca, Mn, Si) alloys recorded after 1 h exposure to Ringer’s physiological solution at 37°C	22
2.7	a) EIS curves and b) Potentiodynamic polarization curves of the alloys AZ91 alloys (with and without Ca) in <i>m</i> -SBF at 36.5°C	23
2.8	Polarization curves of the extruded Mg–Zn–Mn alloys with different Zn content	24
2.9	Polarization and EIS plots for Mg and Mg-Zn alloys in physiological environment	26
2.10	Behavior of HeLa cells on differently pre-treated Mg surfaces as well as on glass: (a) cell density after 24 h in cell culture and (b) SEM image of a cell attached to the surface of Mg soaked in <i>m</i> -SBF	31
2.11	a) Nyquist plot and (b) Potentiodynamic polarization curves of untreated and alkali-treated AZ91 magnesium alloy pre-exposed SBF for 1 h at the nominal body temperature (36.58°C)	32

2.12	Cell morphology after 1, 3, and 5 days incubation on bare and Ca-P coated Mg alloy and pure Ti	33
2.13	Growth of L929 cells vs culturing time on the naked Mg, the Ca-P coated Mg and the pure Ti	34
2.14	Scanning electron microscopy (SEM) images of the MC3T3-E1 cells that were cultured on the (a) and (b) bare, (c) and (d) MgF ₂ coated, and (e) and (f) HA/MgF ₂ coated Mg samples for 5 and 24 h, respectively	35
2.15	(a) DNA levels that were measured from the cells that adhered to the samples after culturing for 24 h and (b) DNA and ALP activity levels of the MC3T3-E1 cells that were cultured on the bare, MgF ₂ coated, and HA/MgF ₂ coated Mg for 4 and 10 days	36
2.16	(a) Potentiodynamic polarization curves (b) Variation of pH and (c) hydrogen gas evolution in the SBF for bare and HA-coated Mg	37
2.17	SEM images of the MC3T3-E1 cells on (A) the bare Mg, (B) HA-coated Mg samples after 1 day of culturing, (C) bare Mg and (D) HA-coated after 5 days of culturing	38
2.18	(a) DNA levels of the MC3T3-E1 cells that were cultured for 5 days and (b) ALP activity levels of the MC3T3-E1 cells that were cultured for 14 days	39
2.19	(a) The hydrogen evolution volume (b) the change of pH of Hank's solution incubating bare and MgF ₂ -coated Mg-1Ca alloy as a function of the immersion time (c) Nyquist plots and (d) potentiodynamic polarization curves of bare and MgF ₂ -coated Mg-1Ca alloy in Hank's solution	40
2.20	Morphologies of MG63 cells on (a) bare Mg-1Ca alloy, (b) MgF ₂ -coated Mg-1Ca alloy and MC3T3 cells on (c) bare Mg-1Ca alloy, (d) MgF ₂ -coated Mg-1Ca alloy	40
2.21	Polarization curves of uncoated and coated Mg-6Zn alloy in 0.9% NaCl solution	41
2.22	FE-SEM micrographs of cell morphology after different culture times, (a) 1 day culture, 2% PLGA coating, (b) 2 days culture, 2% PLGA coating, (c) 3 days culture, 2% PLGA coating, (d) 1 day culture, uncoated, (e) 2 days culture, uncoated and (f) 3 days culture, uncoated	42

2.23	Potentiodynamic polarization curves of bare and coated Mg alloy in SBF solution at $36.5 \pm 0.5^\circ\text{C}$	43
2.24	(a) SEM image of MAO coating with cells and (b) The typical SEM image of composite coating	43
2.25	Impedance spectra of Mg, Mg-OH, Mg-B, Mg-B-A and Mg-B-A-heparin samples	45
2.26	Representative SEM micrographs of platelets on (A) Mg-B-A and (B) Mg-B-A-heparin. The scale bars represent $2 \mu\text{m}$	45
2.27	Structure of organofunctional silane	46
2.28	Schematic representation of silane hydrolysis, condensation and bond formation with the substrate	48
2.29	Hydrolysis and condensation rate of a typical silane	49
2.30	Schematic of sol–gel processing of hybrid coatings with phosphonate functionalities	54
2.31	(a) Potentiodynamic scans and (b) electrochemical impedance spectra of the sol–gel coatings with phosphonate groups after 30 min immersion in dilute Harrison's solution. The hybrid sol–gel coatings was formulated with different PHS to TEOS molar ratio	55
2.32	Potentiodynamic scans of the phosphonate-functionalized coatings obtained by sol– gel processing of PHS and different silane co-reagents at constant (1:4) molar ratio (substrate—AZ31B; in dilute Harrison's solution)	56
2.33	Structure of GPTMS	57
2.34	Potentiodynamic scans of AA 2024-T3 coated with SNAP coatings prepared with different crosslinking agents (1A (O), 2A (Δ), 3A (\blacktriangledown), DETA($_$)), and bare AA2024-T3 (\times).The inset is corrosion current densities and corrosion potentials estimated by Tafel analysis	59
2.35	Structure of BTESPT	60
2.36	Bonding mechanism in (a) bis-silane and (b) mono-silane with Al substrate	61
2.37	EIS Bode plots of AA2024-T3 alloy and the alloy with three different	62

	pretreatments immersed in 0.1N NaCl for 24 h	
2.38	Bode plots of bis-sulfur silane-treated AA 2024-T3 during immersion in a neutral 0.6 M NaCl solution for different durations (upto 20 days)	63
2.39	EIS Bode plots obtained for the bare AZ31 Mg alloy and for the same alloy pre-treated with BTESPT, BTESPT+Ce(NO ₃) ₃ and BTESPT+La(NO ₃) ₃ after 24 h of immersion in 0.005M NaCl	64
2.40	Bode plots of silane-treated AA 2024-T3 panels in a 0.6M NaCl solution (pH 6.5) after 32 days of exposure	65
3.1	Work flow chart	74
3.2	Schematic representation of different stages of the pre-treating procedure	77
3.3	(a) Schematic representation and (b) Lab setup of in vitro electrochemical set-up	81
3.4	(a) Schematic illustration and (b) Lab set up of the evolved hydrogen volume measurement	81
3.5	Mounted magnesium alloy samples immersed in DMEM in petridish	83
4.1	SEM micrograph of a) bare Mg-6Zn-Ca alloy b) EDAX of point 2 in the SEM micrograph, (c) intermetallics and (d) EDAX of point 1 of the intermetallics	87
4.2	SEM micrographs of the surface morphology of the Mg-6Zn-Ca alloy with alkali pretreatment for different durations: (a) 24 h, (b) 48 h, (c) 72 h and (d) 240 h.	88
4.3	SEM micrographs of crosssections of Mg-6Zn-Ca alloy with alkali pretreatment for different durations: (a) 24 h, (b) 48 h, (c) 72 h and (d) 240 h.	89
4.4	Potentiodynamic polarization of different pretreated samples as compared to bare in <i>m</i> -SBF at (36.5 ± 0.5) °C	90
4.5	Time dependent FTIR spectra of hydrolysis and condensation of DEPETS batch 1	92
4.6	Comparative spectra of batch 1 and batch 2 DEPETES after 24 h hydrolysis	93

4.7	Time dependent FTIR Spectra to study hydrolysis and condensation of MTEOS at a) pH 5, b) pH 4	94
4.8	FTIR spectra of cured sample of DEPETES:MTEOS at 100 and 120°C	96
4.9	FTIR spectra of cured alkali-pretreated alloy dipped in mixtures of silanes in different DEPETES: MTEOS volume ratios: (a) 1:1, (b) 1:2, (c) 1:3 and (d) 1:4	97
4.10	SEM micrograph of crosssectional thickness of the 1:4 DEPETES:MTEOS coated sample	98
4.11	SEM micrographs of the surface morphology of alkali-pretreated alloy dipped in mixtures of silanes in different DEPETES: MTEOS volume ratios of: (a) 1:1, (b) 1:2, (c) 1:3 and (d) 1:4.	98
4.12	a) SEM micrograph, (b) EDAX graph and (c) Elemental analysis of 1:4 DEPETES:MTEOS coated sample	100
4.13	Potentiodynamic polarization in <i>m</i> -SBF at (36.5 ± 0.5) °C of the alloy coated with different DEPETES:MTEOS ratios of coating formulations	101
4.14	Bode plots in <i>m</i> -SBF at (36.5 ± 0.5) °C of the alloy coated with different DEPETES: MTEOS ratios of coating formulations.	102
4.15	(a) The electrical equivalent circuit fitted to the experimentally obtained impedance data of the bare Mg-6Zn-Ca alloy, (b) DEPETES:MTEOS (1:4) coated sample	103
4.16	Bode plots of the alloy silane coated with DEPETES: MTEOS ratio of 1:4, after different durations of immersion in <i>m</i> -SBF at (36.5 ± 0.5) °C	106
4.17	Hydrogen evolution of bare and coated alloys, as a function of immersion time <i>m</i> -SBF at (36.5 ± 0.5) °C.	109
4.18	Variation of pH as a function of immersion time <i>m</i> -SBF at (36.5 ± 0.5) °C.	110
4.19	SEM micrographs of: (a) bare Mg-6Zn-Ca alloy and (b) 1:4 DEPETES: MTEOS-coated samples, (c) EDAX of 1:4 MTEOS-coated samples, after immersion for 110 hrs in <i>m</i> -SBF at (36.5 ± 0.5) °C	112
4.20	XRD spectra of the 1:4 DEPETES: MTEOS coated alloy after immersion for 110 h in <i>m</i> -SBF at (36.5 ± 0.5) °C	113
4.21	Time dependent FTIR Spectra study of hydrolysis and condensation of	114

	Tetrasulfide silane at a) pH 6.5, b) pH 5	
4.22	FTIR spectra of cured sample of DEPETES: BTESPT at 100°C and 120°C	115
4.23	FTIR spectra of cured alkali-pretreated alloy dipped in mixtures of silanes in different DEPETES: BTESPT volume ratios: (a) 1:1, (b) 1:2, (c) 1:3 and (d) 1:4	116
4.24	SEM micrographs of crosssectional thickness of the 1:4 DEPETES:BTESPT coated sample	117
4.25	SEM micrographs of the surface morphology of alkali-pretreated alloy dipped in mixtures of silanes in different DEPETES: BTESPT volume ratios of: (a) 1:1, (b) 1:2, (c) 1:3 and (d) 1:4.	118
4.26	(a) SEM micrograph, (b) EDAX graph and (c) Elemental analysis of 1:4 DEPETES:BTESPT coated sample	119
4.27	Potentiodynamic polarization in <i>m</i> -SBF at (36.5 ± 0.5) °C of the alloy coated with different DEPETES: BTESPT ratios of coating formulations	120
4.28	Bode plots in <i>m</i> -SBF at (36.5 ± 0.5) °C of the alloy coated with different DEPETES: BTESPT ratios of coating formulations.	121
4.29	The electrical equivalent circuit that fits the experimentally-obtained impedance data of sample coated with a mixture of DEPETES and BTESPT	122
4.30	Bode plots of the alloy silane coated with DEPETES: BTESPT ratio of 1:4, after different durations of immersion in <i>m</i> -SBF at (36.5 ± 0.5) °C.	125
4.31	Hydrogen evolution of bare and coated alloys, as a function of immersion time <i>m</i> -SBF at (36.5 ± 0.5) °C	127
4.32	Variation of pH as a function of immersion time <i>m</i> -SBF at (36.5 ± 0.5) °C	128
4.33	a) SEM micrograph, b) EDAX of 1:4 DEPETES:BTESPT-coated samples, after immersion for 216 hrs in <i>m</i> -SBF at (36.5 ± 0.5) °C	129
4.34	XRD spectra of the 1:4 DEPETES: BTESPT coated alloy after immersion for 216 hrs in <i>m</i> -SBF at (36.5 ± 0.5) °C	130
4.35	FTIR spectra of cured alkali-pretreated alloy dipped in mixtures of silanes in different GPTMS: MTEOS volume ratios: (a) 1:1, (b) 2:1 and (c) 3:1	131

4.36	SEM micrographs of crosssectional thickness of the 3:1 GPTMS: MTEOS coated sample	132
4.37	SEM micrographs of the surface morphology of alkali-pretreated alloy dipped in mixtures of silanes in different GPTMS: MTEOS volume ratios of: (a) 1:1, (b) 2:1, (c) 3:1 and (d) EDAX elemental analysis of 3:1 GPTMS: MTEOS coated specimen	133
4.38	Potentiodynamic polarization in <i>m</i> -SBF at (36.5 ± 0.5) °C of the alloy coated with different GPTMS:MTEOS ratios of coating formulations	134
4.39	Bode plots in <i>m</i> -SBF at (36.5 ± 0.5) °C of the alloy coated with different GPTMS:MTEOS ratios of coating formulations.	136
4.40	The electrical equivalent circuit that fits the experimentally-obtained impedance data of sample coated with a mixture of GPTMS:MTEOS	137
4.41 (a)	Bode plots of the alloy silane coated with, 1:1 GPTMS:MTEOS, after different durations of immersion in <i>m</i> -SBF at (36.5 ± 0.5) °C .	139
4.41 (b)	Bode plots of the alloy silane coated with, 2:1 GPTMS:MTEOS, after different durations of immersion in <i>m</i> -SBF at (36.5 ± 0.5) °C .	139
4.41 (c)	Bode plots of the alloy silane coated with, 3:1 GPTMS:MTEOS, after different durations of immersion in <i>m</i> -SBF at (36.5 ± 0.5) °C .	140
4.42	Hydrogen evolution of bare and coated alloys, as a function of immersion time <i>m</i> -SBF at (36.5 ± 0.5) °C.	142
4.43	Variation of pH as a function of immersion time <i>m</i> -SBF at (36.5 ± 0.5) °C.	143
4.44	a) SEM micrographs, (b) EDAX of 3:1 GPTMS:MTEOS-coated samples, after immersion for 280 h in <i>m</i> -SBF at (36.5 ± 0.5) °C	144
4.45	XRD spectra of the 3:1 GPTMS: MTEOS coated alloy after immersion for 280 h in <i>m</i> -SBF at (36.5 ± 0.5) °C	144
4.46	Electron micrographs depicting attachment of the MG-63 cells after culturing for 1, 3, 7 and 14 day on bare Mg-6Zn-Ca and GPTMS:MTEOS silane coated Mg-6Zn-Ca	146
4.47	Electron micrographs depicting attachment of the MG-63 cells after culturing for 1, 3, 7 and 14 day on bare Mg-6Zn-Ca and GPTMS:MTEOS silane coated Mg-6Zn-Ca.	147

4.48	(a) Percentage cell proliferation observed on bare Mg-6Zn-Ca and GPTMS:MTEOS coated Mg-6Zn-Ca calculated against positive control; at $p < 0.05$ level the difference of means were found to be significantly different (b) DNA content of MG-63 cells on the bare Mg-6Zn-Ca and GPTMS:MTEOS coated Mg-6Zn-Ca	148
4.49	Percentage ALP activity of MG-63 cells cultured on bare Mg-6Zn-Ca and GPTMS:MTEOS coated Mg-6Zn-Ca calculated against ALP activity observed in positive control MG-63 cells; at $p < 0.05$, 0.01 and 0.001 level the difference of means were found to be significantly different between bare Mg-6Zn-Ca and GPTMS:MTEOS coated Mg-6Zn-Ca	149
4.50	Electron micrographs depicting attachment of the MG-63 cells after culturing for 1, 3, 7 and 14 day on bare Mg-6Zn-Ca and DEPOTES:BTESPT silane coated Mg-6Zn-Ca.	150
4.51	(a) Percentage cell proliferation observed on bare Mg-6Zn-Ca and DEPOTES:BTESPT coated Mg-6Zn-Ca calculated against positive control; at $p < 0.05$ level the difference of means were found to be significantly different (b) DNA content of MG-63 cells on the bare Mg-6Zn-Ca and DEPOTES:BTESPT coated Mg-6Zn-Ca	151
4.52	Percentage ALP activity of MG-63 cells cultured on bare Mg6ZnCa and DEPOTES:BTESPT coated Mg-6Zn-Ca calculated against ALP activity observed in positive control MG-63 cells	152
4.53	XRD images of the MG-63 cells on (a) bare Mg6ZnCa alloy, (b) DEPOTES:BTESPT coated Mg-6Zn-Ca alloy and (d) GPTMS:MTEOS coated Mg6ZnCa samples after culturing in DMEM	150
5.1	Proposed biological response of phosphonato silane based coating system	157
5.2	Proposed reaction mechanism for the developed Phosphonato silane based sol-gel coating	160
5.3	Schematic representation of hydrolysis and condensation of GPTMS and MTEOS	161
5.4	Schematic degradation diagram, (a) initial surface condition of the coated magnesium alloy and (b) degraded polymeric coating upon degradation	162
5.5	Mechanism for formation of Ca/Mg phosphates and carbonates	163

List of Tables

2.1	Historical overview of reports on magnesium and its biomedical application in historical order	17
2.2	Summary of physical and mechanical properties of various implant materials compared with bone	18
2.3	Toxicology, pathophysiology and effect of alloying elements on Mg	27
2.4	Silanes used as coating implants and in pharmaceutical applications	50
3.1	Compositions of the alloy (wt %)	75
3.2	Composition of modified-simulated body fluid (<i>m</i> -SBF)/liter	76
4.1	Elemental Analysis of the base alloy and intermetallics point 1 and 2	87
4.2	Corrosion potential and corrosion current densities derived from plots in Figure 4.4	91
4.3	Corrosion potential and corrosion current densities derived from plots in Figure 4.13	102
4.4	Calculated parameters of the proposed EEC for the uncoated sample	104
4.5	Calculated parameters of the proposed EEC for the DEPOTES: MTEOS coated Samples after the simulation of experimental data	104
4.6	Values of the different components in the EEC after the simulation of experimental data for the time dependent degradation of 1:4 (DEPTES: MTEOS) coated sample	107
4.7	Corrosion potential and corrosion current densities derived from plots in Figure 4.27.	120
4.8	Impedance at the lowest frequency for the bare and coated alloys, derived from plots in Figure 4.28	122
4.9	Parameters calculated using EEC in Figure 4.29 for the alloy coated with different ratios of DEPOTES: BTESPT, and dipped in <i>m</i> -SBF	123
4.10	Parameters calculated using EEC in Figure 4.29 for the alloy coated with the DEPOTES: BTESPT volume ratio of 1:4, dipped in <i>m</i> -SBF for different durations	125
4.11	Corrosion potential and corrosion current densities derived from plots in Figure 4.38	135
4.12	Impedance at the lowest frequency for the bare and coated alloys, derived from plots in Figure 4.39	136
4.13.	Parameters calculated using EEC in Figure 4.40 for the alloy coated with the GPTMS: MTEOS 1:1, dipped in <i>m</i> -SBF at (36.5 ± 0.5) °C for different durations	140
4.14	Parameters calculated using EEC in Figure 4.40 for the alloy coated with the GPTMS: MTEOS 2:1, dipped in <i>m</i> -SBF for different durations	141
4.15	Parameters calculated using EEC in Figure 4.40 for the alloy coated	141

List of abbreviations

1. DEPOTES Diethylphosphatoethyltriethoxysilane
2. BTESPT bis-[3-(triethoxysilyl) propyl] tetrasulfide
3. GPTMS Glycidoxypropyltrimethoxysilane
4. MTEOS Methyltriethoxysilane
5. HEPES 2-(4-(2-hydroxyethyl)-1-piperazinyl) ethanesulfonic acid
6. *m*-SBF *modified*-Simulated body fluid
7. DMEM Dulbecco's Minimum Essential Medium
8. PBS Phosphate Buffered Saline
9. ALP Alkaline phosphatase
10. EIS Electrochemical impedance spectroscopy
11. EEC Electrical Equivalent Circuit
12. CPE Constant phase element
13. SEM Scanning Electron Microscopy
14. ESEM Environmental Scanning Electron Microscopy
15. FTIR Fourier transform infrared spectroscopy
16. XRD X-ray diffraction
17. EDAX Energy Dispersive X-ray analysis

Chapter1

Introduction

Biomaterials play a dominant role in medical field, whether it is an organ replacement or drug delivery system. It is defined as a material, synthetic or natural, when placed in human body triggers no significant adverse biological reaction and aims to bring back original function of natural living tissues and organ in the body to provide an opportunity for the patient to resume normal life style [1, 2].

The use of metals is not new in the medical area and its use as an implant is dated since prehistoric times. As early as 4000 years back, the Egyptians and Romans had used linen for sutures, iron and gold for dental applications and wood for toe replacement but there was very little knowledge about the problem of corrosion. Teflon, nylon, stainless steel and titanium were some of the other materials which were put into use after World war II [3]. About one million patients worldwide are treated annually for total replacement of arthritic hips and knee joints. Requirement for joint replacement continues to grow as people damage themselves more through hard sports or get injured in road accidents. Internal and external bone-fracture fixation provides a major application for implant material as clips, pins, bone-plates, screws, intramedullary nails, and external fixators as shown in Fig. 1.1

Metals are known for their high strength and toughness compared to ceramics and polymers. Varieties of metals have been used as permanent implants but the most prominent ones include stainless steel, type 316 L, titanium and its alloys and Co-Cr alloys. SS 316L has appropriate corrosion resistance, excellent mechanical properties and superior biocompatibility. It is the most economic biocompatible material with easy availability. On the other hand, Ti and its alloys possess excellent corrosion resistance and superior mechanical properties and biocompatibility, but it is costly. These metals can be used in hard tissue replacements as well as an external fixation device like screw, nails and plates [3].



Figure 1.1: Different types of metallic implant materials [4]

But there are a few serious concerns associated with these permanent implants, such as possible release of toxic metallic ions and/or particles through corrosion or wear processes that may eventually result in the loss of an implant's biocompatibility, and can result in physical irritation, and inability to adapt to growth and changes in the human body. The elastic moduli of current metallic implants are not well matched with that of natural bone tissue, resulting in stress shielding effects that can lead to reduced stimulation of new bone growth. In use of such materials as temporary implants, there is a need for a second surgical procedure to remove the

implant after the tissue has sufficiently healed. This second surgery leads to additional cost that can create chances of infection [3, 5, 6].

Therefore, there has been a need of alternative materials to eliminate above problems. One of the options is the use of biodegradable implant material like HA/PLLA polymers, ceramics, bioactive glasses that can dissolve in the body after the healing of the tissues. But they have limited applications because of unsatisfactory mechanical strength of such material. In addition, polymeric materials are more expensive as compared to conventional metallic implants. An alternative to biodegradable polymer implant is the biodegradable metallic implants that have received great attention due to their high load bearing ability. In this regard biodegradable magnesium metallic implants are very attractive. A few examples of magnesium alloy implants that were surgically introduced in the body, as fasteners for bones, such as screws, plates or nails, intestinal clips, vascular clips and stents etc. are shown in Fig. 2[6-13].



Figure 1.2 : Real/possible applications of biodegradable magnesium implants: (a) cardiovascular stents (BIOTRONIK, Germany, under clinical trial), (b) MAGNEZIX screw (received CE mark in Europe), (c) microclip (pure magnesium), (d) biodegradable implants, (e) wound-closing devices (WZ21)[14] .

Magnesium is one of the lightest structural metals with outstanding mechanical and physical properties such as high strength-to-weight ratio. This makes magnesium alloys attractive for light weight applications like transportation (aerospace and automobiles) to improve fuel efficiency and performance [15]. Magnesium alloys are becoming increasingly attractive temporary orthopedic implants, particularly because of a few of their properties which are similar to those of human bones. Magnesium and magnesium alloys are exceptionally lightweight with density ranging from 1.74 to 2.0 g/cm³, which is close to that of the bone (1.8 – 2.1 g/cm³). The fracture toughness of magnesium is greater than ceramic biomaterials (eg. Hydroxyapatite), while the elastic modulus (41–45 GPa) is close to that of the bone (3-20GPa) that avoids the stress shielding effect as compared to traditional metallic implants (namely, titanium alloys, Co-Cr alloy and stainless steels). Magnesium is not only biocompatible but also essential to the human metabolism as a cofactor for many enzymes, and thus, unlike the traditional implants materials, the degradation products of magnesium are not toxic to human physiology. Further, magnesium ions that are produced as a result of the degradation are reported to aid the growth and healing of tissues and stimulate bone formation. Magnesium alloys are also considerably cheaper than the traditional implant alloys [5, 6, 9, 10, 16-20].

Since the beginning of the 2000s, magnesium alloys have been extensively studied as biodegradable implants as bone fixation devices, cardiovascular stents and tissue engineering scaffolds. The major limitation arises because of the high corrosion rate of magnesium alloys in the physiological environment (pH of 7.4–7.6). Sensitivity to impurities in the alloy and lack of passive film below pH 11 accounts for different types of magnesium corrosion problems, such as , general, galvanic corrosion, pitting corrosion and stress corrosion cracking [21]. As a result, magnesium alloys may lose their mechanical integrity in the aggressive physiological environment before tissues have sufficient time to heal. Also, new tissue formation and cell proliferation are unfavorably affected by hydrogen evolution and increase in pH around implantation region during degradation process.

In this biomedical application, it is proposed to advantageously exploit the high susceptibility of corrosion of magnesium, i.e. the very shortcoming of magnesium alloys that prevents them from their wider use in the automobile and aerospace industries. However, biodegradable implants should have controlled rate of corrosion which can be achieved by modification of the alloy composition and/or the surface modification of the alloy to achieve the required corrosion resistance during the initial period where mechanical strength is required[22].Retarding the rate of corrosion of Mg is considered to be the more suitable strategy because a corrosion rate of Mg implant implies a decrease in the extent of alkalization and hydrogen evolution, which would facilitate the human body to gradually absorb or consume the corrosion products formed during magnesium degradation. The approach towards this suggests three main possibilities: (i) use of high purity Mg; (ii) appropriate alloying; and (iii) surface treatment or coating. High purity Mg, though, useful in controlling the rate of corrosion better than alloys or that by surface treatment, is not highly promising because of low strength of pure Mg.

Addition of an alloying element to magnesium can be restricted to much lower levels due to toxicity and bio-compatibility issues. Release of magnesium ions from corroding magnesium alloys should not cause toxicity and may even have beneficial effects on cells and tissues [23].A corrosion resistant coating can significantly delay the initiation of biodegradation of magnesium alloy. The coating should be non-toxic and also the breakdown products of the coating should be biodegradable [9, 10]. A few preliminary trials for improving the corrosion resistance of Mg implants have been reported in the literature, including carbonate treatment [24],fluoride treatment [25], phosphating treatment [26], electrodeposition of hydroxyapatite coating acting as a physical barrier [27], as the micro-arc oxidation (MAO) to deposit ceramic coatings on surface of metals.

Research on magnesium and its alloy for light weight applications has picked up considerably for automobile applications. But recently they are also considered as a potential candidate for temporary implant material with suitable non toxic alloying elements and its controlled dissolution. Aim of the present research work is to look for a suitable alloy and to control the

dissolution of magnesium alloy by development of hybrid sol-gel coatings using various organo-silanes.

Thesis outline

The goal of the thesis is to develop a biodegradable coated magnesium alloy for orthopaedic biodegradable metallic implant application. Silane based coating on magnesium is done for its potential application as a biodegradable orthopaedic metallic implant material by delaying its corrosion rate. This thesis is structured into five chapters. Chapter 2 focuses on the literature review of the previous work on corrosion in magnesium, biomaterials, various biodegradable magnesium alloy and coatings, silanes and cytotoxicity test. In chapter 3, the experimental protocols and techniques are discussed, pre-treatment process, coating deposition process, various experiments such as, SEM, FTIR, Electrochemical investigation, hydrogen evolution and biocompatibility studies using in-vitro cell culture technique. In chapter 4, the results of the experiments are discussed using SEM-Edax, FTIR, corrosion analysis and cytotoxicity. Chapter 5 focuses on the summary and general discussion about the overall work. Chapter 6 concludes the thesis.

Chapter 2

Literature Review

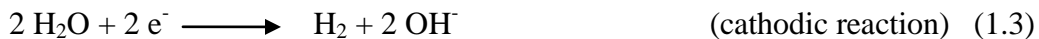
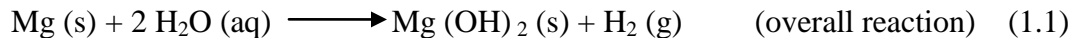
2.1 Background

Magnesium is the lightest of all the engineering and structural metals, having a density of 1.74 g/cm^3 . It is 35% lighter than aluminum (2.7 g/cm^3) and over four times lighter than steel (7.86 g/cm^3). Use of Mg alloys results in 22% to 70% weight reduction as compared to other metals. Alloying magnesium with aluminium, manganese, rare earths, thorium, zinc or zirconium increases the strength to weight ratio making them important materials for applications where weight reduction is important [15]. In recent years, use of magnesium in the auto sector has been increasing. Automobile manufacturers, Volkswagen recently made a considerable use of magnesium in their Beetle model. But Porsche was the first work with a magnesium engine in 1928. Automotive industry is embracing manufacture of lighter, more environmentally friendly, safer and cheaper cars. The leading automakers are concentrating on the reduction of car weight and limiting the amount of exhaust emissions due to legislative and consumers' requirements for safer, cleaner vehicles. Weight reduction, not only saves energy but it also reduces greenhouse gas emissions. High-strength steels, Al and composites are already being used to reduce weight, but additional reduction could be achieved by greater use of low-density magnesium and its alloys. Magnesium also has high thermal conductivity, high dimensional stability, good electromagnetic shielding characteristics, high damping characteristics, good machinability and can be easily recycled. Therefore, it finds number of applications including automobile and

computer parts, aerospace components, mobile phones, sporting goods, handheld tools and household equipment [28, 29]. Considerable research has been undertaken on magnesium processing, alloy development, joining, surface treatment, corrosion resistance, and mechanical properties improvement. Magnesium has even been suggested for use as metallic implants due to its low weight and inherent biocompatibility[6]. Unfortunately, magnesium has a few undesirable properties including poor corrosion and wear resistance, poor creep resistance and high chemical reactivity that has hindered its widespread use in many application [30, 31].

2.2 Corrosion of Magnesium alloy

The corrosion resistance of magnesium and its alloy is poor because of a very high electrochemical activity of magnesium (standard reduction potential of pure magnesium is -2.37 V vs. standard hydrogen electrode)[32], micro-galvanic corrosion caused by second phase particles and impurities which act as local cathodes accelerating dissolution in the adjacent alloy matrix that has a less passive surface film composed of a mixture of MgO and Mg(OH)₂ film provides reasonable corrosion protection in air, but becomes unstable in aqueous or in high humidity environments [33]. Magnesium dissolution in aqueous environments generally proceeds by electrochemical reaction with water to produce magnesium hydroxide and hydrogen gas as shown in the equations below. These equations also suggest that this mechanism is insensitive to the oxygen concentration [21, 34].



Moreover, the presence of several anions such as, chloride, sulphate and nitrate in the aqueous solution either hinder the formation of the surface film or disrupts the existing film, which in turn accelerates the corrosion rate [21, 34].

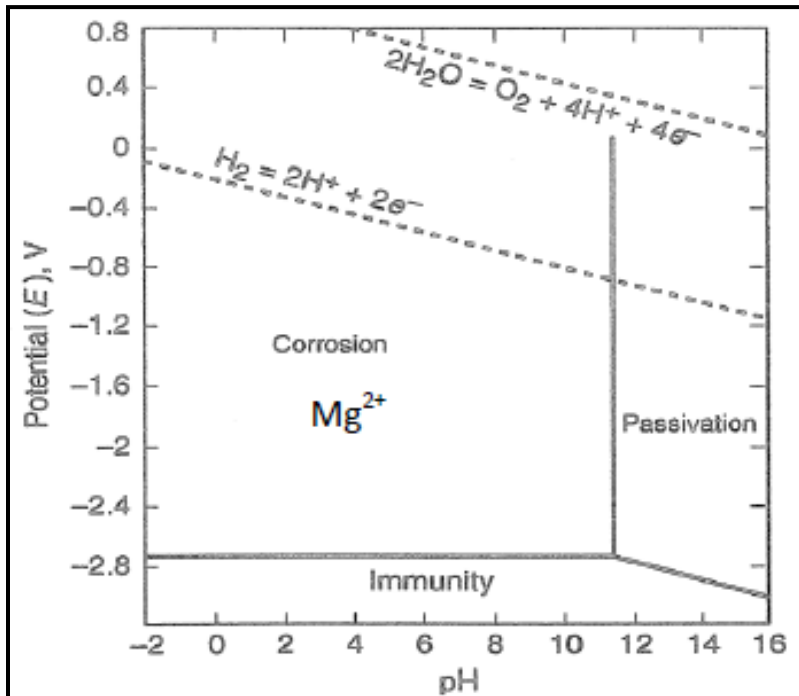


Figure 2.1: Pourbaix diagram for magnesium-water system at 25⁰C [35]

The poor corrosion resistance of magnesium alloys can be summarized by Pourbaix diagram in figure 2.1. This diagram clearly suggests (Figure 2.1), Mg^{2+} to be stable species in solution over most of the potential – pH range. The only potential – pH domain in which magnesium is stable is well below the domain in which water is stable; therefore magnesium reduces water and, hydrogen evolution is the cathodic reaction. At pH greater than about 11.5, a passive film of $Mg(OH)_2$ protects the magnesium from corrosion.

Sensitivity to impurities (as discussed later) and lack of passive film below pH 11 account for different types of magnesium corrosion problems, such as general, galvanic corrosion, pitting corrosion and stress corrosion cracking [21].

2.2.1 Types of corrosion in magnesium

Magnesium and its alloys are extremely susceptible to different forms of corrosion but in the context of implant application in osteosynthesis, following corrosion mechanisms need to be considered.

2.2.1.1 Galvanic Corrosion

Two types of galvanic corrosion occur in magnesium (Figure 2.2)

Macro-galvanic corrosion, occurs when magnesium is coupled with a metal such as steel, because Mg is the most active engineering metal and its corrosion potential is more negative than all other engineering metals.

Micro-galvanic corrosion is caused by secondary phases or impurities which act as cathodes and form micro cells with magnesium matrix as anodes having lower corrosion potential[31, 34].

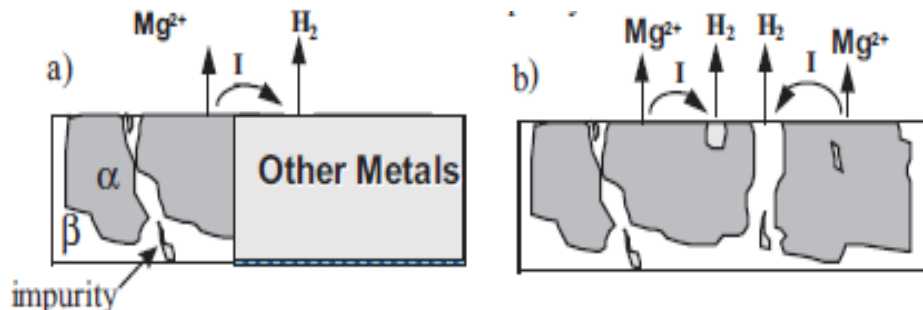


Fig 2.2 a) Microgalvaniccorrosion. b) Microgalvaniccorrosion[34]

2.2.1.2. Localized Corrosion

Magnesium is a naturally passive metal that undergoes pitting corrosion at its equilibrium corrosion potential, E_{corr} , when exposed to chloride ions in a non-oxidizing medium. Pitting corrosion of Mg results from the rapid corrosion of small-localized areas where protective surface oxide layer gets damaged /disrupted. The pits are small, highly corrosive and continue to grow downwards, perforating the metal matrix. In the case of Al-containing alloys that develop

$Mg_{17}Al_{12}$, pits are often formed due to selective attack along the $Mg_{17}Al_{12}$ network which is followed by the undercutting and falling out of grains.

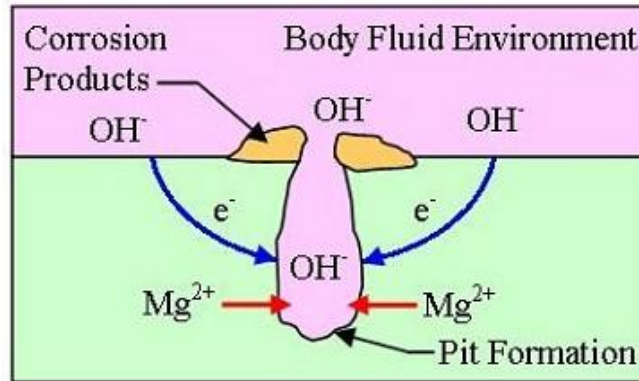


Figure 2.3: Pitting corrosion site at the surface of a magnesium component[36]

2.2.1.3 Stress Corrosion Cracking (SCC)

Magnesium alloys are susceptible to SCC. In general, the localized disruptions in MgO and $Mg(OH)_2$ surface layer (such as due to pitting) provides sites for entry of hydrogen into the alloy matrix, causing hydrogen embrittlement. It is noted that magnesium can produce hydrogen even under anodically polarized conditions. However, the recent studies have demonstrated that Mg alloys suffer SCC due to a mixed mechanism of hydrogen embrittlement and crack tip dissolution [34, 37, 38].

2.3 Biomaterials

2.3.1 History of biomaterials

Biomaterials Science is applied in multiple fields including medical implants, biosensors and biochips for diagnostics, tissue engineering, bioelectronics, artificial photosynthesis and biomimetic materials. Biomaterials have been used for diseased tissues dating back more than

2000 years, as a wooden teeth and glass eyes. By the end of the 20th century, many materials had been attempted for use as surgical implants. In 1902, gold was used as the interphase between the articular heads of the implant. This experiment proved to be successful, which led to further studies on chemically inert and stable materials [1]. Current biomaterials generally consist of non-living materials which can be basically divided into several groups: synthetic and natural polymers, ceramics, metals and composites. Common examples of medical devices include: sutures, supportive meshes, needles, orthopedic, osteosynthetic, vascular grafts, stents, etc. The biomaterials employed must possess good mechanical integrity, non-toxicity and pronounced chemical stability. In recent years, the demand for biomaterials has been increasing with relative proportion of senior citizens in society as a result of the demand for replacement of failed tissue and organs with biomaterials and artificial devices.

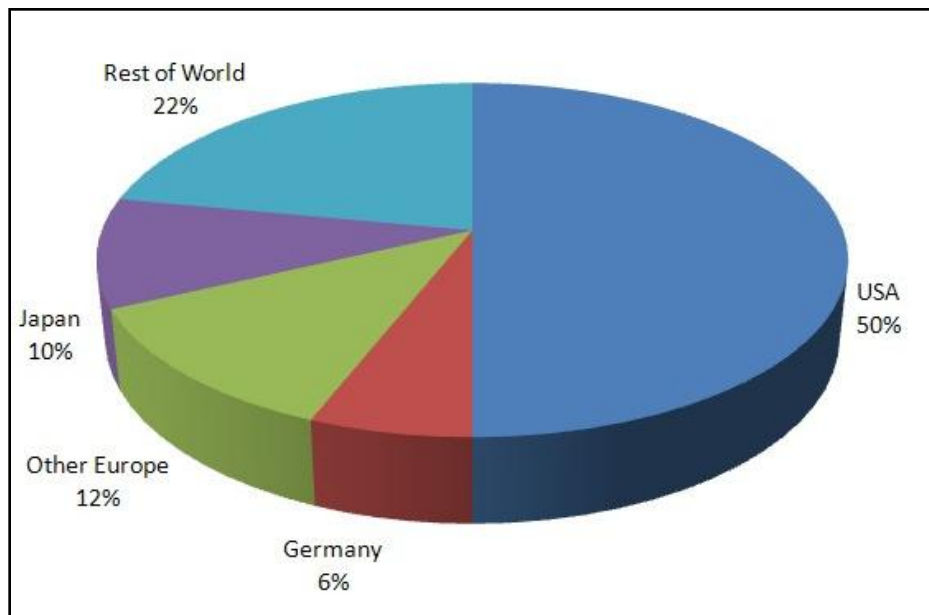


Figure2.4: Global market of orthopedic implants[39]

2.3.2 Classification of Biomaterials

Biomaterials are classified into three classes: class I materials [8, 10], which have no direct contact with bodily tissues, class II materials that are intermittently in contact with tissues and

class III materials that are constantly in contact with tissue and are prone to unwanted ion leaching [8]. The latter can be categorized into three types: bio-inert, bioactive and biodegradable. Currently approved and commonly used Class III metallic biomaterials include stainless steels, titanium and cobalt-chromium based alloys used as permanent implants.

Permanent implants such as a hip replacement remain in the body for much longer duration, whereas implants such as plates, wires and screws are required for the function of assisting the healing process. After the healing and curing, the temporary implants are removed by a second surgery which is not only an additional cost but also duress to the patient [6, 9, 40]. Also with these current metallic biomaterials, there is a possibility of release of toxic metallic ions through corrosion or wear processes that leads to inflammatory responses and thereby reduced biocompatibility. It is an attractive concept that such implants harmlessly degrade away within the human. This is where the alternative methodology of using biodegradable implants becomes extremely attractive. The purpose of temporary biodegradable implant is to support healing of the tissues with material degradation and simultaneous implant replacement through the surrounding tissues. So, biodegradable temporary implants (bioabsorbable) are materials that can be gradually dissolved, absorbed, consumed, or excreted from the body, so that there is no need for a second surgery to remove the implant [9]. A biodegradable material needs to fulfill its purpose as a biomaterial as well as be able to degrade within the body and degradation products have to be chemically and physically stable and biocompatible and must pass through and out of the body in a safe way, i.e. it cannot cause permanent or temporary irritation or inflammation. The implant must maintain adequate mechanical properties when degrading and not fall into pieces or break causing physical injury.

2.3.2.1 Polymers

Polymers are long chain, organic molecules and are versatile in their properties and composition. They are considered to be the most extensively used biomaterials. Some common natural polymers include heparin, DNA, and collagen. Advantages of using polymers in biomedical applications are versatility, reasonably low cost and ease of manufacturing. Over the past 35

years, biodegradable polymers have evolved. These materials when implanted are gradually replaced by tissues generated in-vivo and break down into a non toxic product that is later removed by the body. Common examples of degradable synthetic polymers are Poly (lactide-coglycolide) (PLGA), polyanhydrides and polycaprolactone, while chitin, starch, collagen and glycosaminoglycans are polymers that degrade naturally. Polymers offer the benefit of being intrinsically resistant to environmental attack. However, even with these attractive properties, biopolymers have low mechanical strength when compared to ceramics and metals, which has resulted in them being used in soft tissue reconstruction and low-load bearing applications only, thus, avoiding risk for yield, fatigue, wear, creep, and fracture [41, 42].

2.3.2.2 Ceramics

Ceramic materials for oral implants were investigated and used some 30–40 years ago. Ceramics are nonmetallic, inorganic materials that have biological inertness and high hardness. They possess exceptional biocompatibility properties with bone cells and tissues. Metallic oxides, carbides and sulfides are examples of ceramics [42-44]. Also ceramics have low electrical conductivity, high melting point, and low thermal conductivity. They are categorized as: bioreactive, completely reabsorbable and bio inert. Bioceramics that are resorbable degrade over a period of time with simultaneous tissue replacement in orthopedic applications. Materials such as hydroxyapatite, calcium phosphate and calcium sulfate dehydrate are few examples of reabsorbable bioceramics. During the resorption process the mechanical properties of these materials greatly diminishes, which results in a considerable decrease in load-bearing capacity. The key feature of bioreactive bioceramics is the capability of the material to bond chemically and interact with normal tissues at its interface. But there application is limited by their poor mechanical properties and brittleness. Unlike Mg and its alloys, bioceramics such as HAP, tend to be brittle, have low fracture toughness and are not as resilient.

2.3.2.4 Metals

Metals and alloys have a wide range of applications as devices for fracture fixation, partial and total joint replacement, braces, prostheses for hard tissue replacement, and active devices such as

electrodes, stents and as well as dental amalgams. The high modulus and yield stress along with the ductility of metals make them appropriate for load-bearing applications. Although metals exhibit high strength and toughness, they can be susceptible to chemical and electrochemical degradation. A unique consideration for the biocompatibility of metals is that corrosion may occur in physiological situations. Corrosion leads to the progressive weakening of the deteriorating material and releases products into the surroundings which could possibly lead to adverse effects. Noble metals, such as platinum, silver and gold are inert and are not subject to corrosion reactions. Some metals form an inert, adherent surface layer of protective oxide that prevents further reactivity between the biological system and the metal. A majority of metals are not useful biomaterials because of corrosion and biocompatibility concerns. The most common alloys that are currently in use are titanium (Ti)-containing, cobalt-chromium, stainless steel and shape memory alloys.

Surgical grade 316L implants corrode in the human body environment and release Fe, Cr and Ni ions and these ions are found to be powerful allergens and even carcinogens. Studies on retrieved implants show that more than 90% of the failure of implants of 316L stainless steel are due to pitting and crevice corrosion attack [45].

Cobalt-chromium alloys perform similar to stainless steel with enhanced corrosion resistance and slightly higher or comparable mechanical properties; however, metal ions have been observed to be leaching into the tissues.

Titanium and its alloys are used extensively due to their low density and good mechanical properties, which give these alloys a high strength-to-weight ratio as well as a favorable biocompatibility profile. The good biocompatibility profile is due to an adherent surface oxide layer. Ti alloys are ideal due to their distinctive properties in applications which require high load-bearing [46, 47]. A unique nickel-titanium alloy known as nitinol possesses all the

properties of Ti but also has shape memory, fatigue resistance, super elasticity, force hysteresis and kink resistance [48].

2.4 Magnesium as a biodegradable implant material

Stainless steel, cobalt-chromium, and titanium alloys have been the primary biomaterials used for load-bearing applications. However, the need has grown for structural materials in temporary implant that provide short-term structural support and can be reabsorbed into the body after healing. Most of the currently used implants are only biocompatible and not bioabsorbable. Magnesium provides the combination of bioabsorbability and high specific strength [13].

Mg has been found to be a very useful biomaterial in the areas of cardiovascular and orthopedic devices. Though Mg has low corrosion resistance, its mechanical properties are advantageous. Neither the platinum group of metals nor tantalum has the required mechanical properties, though they do exhibit high corrosion resistance.

2.4.1 A short history of application of magnesium as body implant

Magnesium-based materials were first introduced for orthopedic applications as early as the beginning of the 20th century. Payr in 1900 proposed Mg as a potential implant for musculoskeletal applications, such as fixator pins, nails, wires, cramps, sheets and plate. Lambotte in 1906 reported the use of a pure Mg plate along with gold plated steel nails to fix a lower leg bone fracture. However, the in-vivo corrosion of the implant was too rapid as it degraded in just 8 days and a large amount of gas was observed beneath the skin. However, on the positive side it was concluded that Mg is absorbable in the body. An overview of the research on magnesium for biomedical applications is given in Table 2.1.

Recent research in this area has been undertaken in animals and humans using different magnesium alloys [6, 10, 17, 19]. Till now magnesium alloys have been researched for osteosynthetic applications, such as, as screws, plates and bio-batteries for pacemakers, etc.

2.4.2 Advantages of magnesium alloys as body implant

Magnesium alloys have an advantage over current biodegradable implants made up of polymers (such as HA/PLLA), ceramics, bioactive glasses which have limited applications because of their unsatisfactory mechanical strength. Magnesium alloy implants can act as fasteners for bones, such as screws, plates or nails, intestinal clips, vascular clips and stents etc [6-13].

Table 2.1 Historical overview of reports on magnesium and its biomedical application in historical order [11]

Author	Year	Magnesium (alloy)	Supplier	Application	Human/ animal model
Huse	1878	Pure magnesium	Not reported	Wires as ligature	Humans
Payr	1892– 1905	High-purity Mg	I. and C.W. Rohrbeck, Vienna, Austria, Al und Mg Fabrik Hemelingen, Germany	Tubes (intestine, vessel, nerve connector), plates, arrows, wire, sheets, rods	Humans, guinea pigs, rabbits, pigs, dogs
Höpfner	1903	Pure magnesium	Not reported	Magnesium cylinders as vessel connectors	Dogs
Chlumský	1900– 1905	High-purity Mg	Friedrich Wosch Company, Germany	Tubes, sheets and cylinder intestine connector, arthoplastik	Humans, rabbits, dogs
Lambotte	1906– 1932	Pure Mg (99.7%)	Not reported	Rods, plates, screws	Humans, rabbits, dogs
Lespinasse	1910	Metallic magnesium	Not reported	Ring-plates for anastomosis	Dogs
Groves	1913		Not reported	Intramedullar pegs in bone	Rabbits
Andrews	1917	Pure Mg, mix. of eq. part: Mg/Al, Mg/Cd, Mg/Zn	Not reported	Wires, clips as ligature, anastomosis	Dogs
Seelig	1924	Pure Mg (99.99%), distilled in vacuum	American Mg Cooperation, Niagra Falls, New York	Wires, strips, bands	Rabbits
Glass	1925	Pure Mg (99.8–99.9%)	Al und Mg Fabrik, Hemelingen, Germany	Magnesium arrows	Humans, rats, cats
Heinzhoff	1928	Pure magnesium	Not reported	Magnesium arrows	Rabbits
Verbrugge	1933– 1937	Dow Metal: Mg–Al6–Zn3–Mn0.2%–wt, Elektron Mg– Al8%–wt.	Dow Chemical Corp., USA Griesheim-Elektron, Germany	Plate, band, screws, pegs	Humans, dogs, rats, rabbits
McBride	1938	Mg–Mn3%–wt., Mg–Al4–Mn0.3%–wt.	Not reported	Sheet, plate, band, screw, peg, wire	Humans, dogs
Nogara	1939	Elektron (alloy not specified)	Griesheim-Elektron, Germany	Rods	Rabbits
Троцкий	1948	Mg–Cd	Not reported	Plate, screws, rod-plate	Humans
Maier	1940	Magnesium	I.G. Farben Industry AG, Bitterfeld, Germany	Band, suture from woven Mg wires, fusiform pins	Humans, rabbits
Stone	1951	Mg–Al2%–wt. pure magnesium	Aluminium Company of America, OH, USA	Wires for clotting aneurysms	Dogs
Fontenier	1975	Ind.-grade purity: Domal Mg (99.9%), T.L.H. Mg not reported Lab-grade purity: "zone fondue" Mg, R69 Mg MgMn1.5%–wt., MgAlGAZ8%, GAZ6%, GAZ3%	Not reported	Anodes for implantable batteries to feed pacemaker	Dogs
Wexler	1980	Mg–Al2%–wt.	McMaster Univ. Med., Canada	Wires intravascular	Rats
Hussl	1981	Pure Mg (99.8%)	Goodfellow Metals Ltd., GB	Wires for hemangioma treatment	Rats, rabbits
Wiiflingseder	1981	Pure Mg (99.8%)	Goodfellow Metals Ltd., GB	Wires for hemangioma treatment	Humans

The major advantages of magnesium alloys are:

- 1) Magnesium is biocompatible, essential in human metabolism and is the fourth most abundant cation in the human body, with estimated 25 g magnesium stored in human body and approximately half of the total content stored in bone tissue. Excess magnesium is harmlessly secreted along with the urine. Magnesium is a cofactor for many enzymes and stabilizes the structures of DNA and RNA[20].
- 2) Magnesium and magnesium alloys are exceptionally lightweight with density ranging from 1.74 to 2.0 g/cm³, which is close to that of the bone (1.8 – 2.1 g/cm³).The fracture toughness of magnesium is greater than ceramic biomaterials (eg HA), while the elastic modulus (41–45 GPa) is close to that of the bone (3-20GPa) that avoids the stress shielding effect which emerges from the difference in stiffness/Young’s modulus between implant and bone and which diminishes the healing process, bone growth and implant stability. It is a condition that emerges when a metal implant takes all the loads that would have otherwise been taken by the bone and allowed the development of its load bearing capability[49].
- 3) Magnesium has standard electrode potential of – 2.37 V, and bare magnesium metal can slowly corrode away in the Cl⁻ containing physiologic environment. Therefore, magnesium alloys could be developed as a new biodegradable metal, taking advantage of their fast corrosion rate in the physiological environment [6, 50].

Table 2.2 Summary of physical and mechanical properties of various implant materials compared with bone[18]

Property	Natural bone	Magnesium	Ti Alloy	Co-Cr Alloy	Stainless steel
Density(g/cm ³)	1.8-2.1	1.74-2.0	4.4-4.5	8.3-9.2	7.9-8.1
Elastic Modulus(GPa)	3-20	41-45	110-117	230	189-205
Yield Strength(MPa)	130-180	65-100	758-1117	450-1000	170-310
Toughness(MPa m ^{1/2})	3-6	15-40	55-115	-	50-200

2.4.3 Problems with magnesium alloy as body implant

The unfortunate complication with the current magnesium alloys being used as body implants is that, magnesium alloys tend to corrode too quickly in the physiological environment (in pH = 7.4–7.6), thereby losing their mechanical integrity before the tissues have sufficient time to heal. The implant should be maintained in the body for more than 12 weeks to allow sufficient time for healing [9, 51, 52]. However, current magnesium based implant material can only retain mechanical integrity for about 6-8 weeks. Also, the degradation of magnesium alloys always leads to hydrogen evolution and alkalization of the aqueous environment. The evolved hydrogen bubbles from a corroding magnesium implant will accumulate as gas pockets adjacent to the implant which will delay and lead to necrosis of tissues as the gas pockets can cause separation of tissues and tissue layers. Also, local alkalization can unfavorably affect the pH dependent physiological reaction balances in the vicinity of the magnesium implant and may even lead to an alkaline poisoning effect if the local in-vivo pH value exceeds 7.8 in that region [6, 9, 10, 50].

Hence there is a need to slow down the biodegradation rate of magnesium that Mg^{2+} ions, H_2 bubbles and OH^- ions are generated more slowly which may allow the human body to gradually adjust with the degradation products. All of these can be controlled with the retardation of corrosion (i.e., improvement of corrosion resistance).

In recent years various studies dealt with the biodegradation behaviour of different Mg alloys mostly in vitro, but also in vivo. So far no standard procedure for evaluation of the biodegradation is available. Bio-corrosion behaviour is analysed by different techniques such as immersion testing and evaluation of the corrosion rate either by measuring the mass loss or the evolved hydrogen gas, by potentiodynamic or by electrochemical impedance spectroscopy. The tests were performed in various body-similar fluids, such as simulated body fluid (SBF), artificial plasma or Hank's solution that reflect the ion composition and pH of human blood, Minimum Essential Medium, MEM (Invitrogen), which is a proprietary form of the well known Eagle's essential medium. MEM, often used as a tissue culture media and is said to be closer to physiological conditions due to the addition of a variety of amino acids and vitamins (in addition

to salts) that are present in human plasma [9, 40, 53-58]. But most of the in - vitro corrosion studies are carried out in modified-simulated body fluid (m-SBF) maintained at a temperature of 36.5 ± 0.5 °C. *m*-SBF was chosen because it does not suffer changes in ion concentrations and pH over a period of up to 8 weeks [55]. Large amounts of buffering agents such as HCO_3^- , HPO_4^{2-} . Tris- HCl and HEPES, consumes the generated OH^- and mediates the abrupt changes in the pH [40].

2.4.4 Corrosion resistance improvement

In order to control the corrosion rate and life of magnesium implants in the human body, i.e. to provide sufficient time to the body to deal with the degradation products and for initial healing process around the magnesium implant, two approaches are most appropriate: Alloying and Surface coating [59].

2.4.4.1 Alloying

Alloying has been employed effectively to improve the mechanical properties and corrosion resistance of magnesium [6, 60, 61]. Elements like Fe, Ni, Cu, and Co have extremely deleterious effects on the corrosion properties of Mg, rapidly increasing the degradation rate. Studies have revealed that the decrease in the levels of these impurities profoundly decreases the corrosion rate. However, pure magnesium cannot be used due to the low yield strength for orthopedics and other load bearing applications [9].

Alloying elements can be added to increase the strength of pure Mg, but alloying elements should be selected carefully to maintain the biocompatibility for implant application. Among the magnesium alloys developed and used, there are two primary groups of magnesium-based alloys, magnesium-aluminum alloys and magnesium-rare earth alloys:

A. Alloys with aluminium

- AZ 91(9 wt% Al, 1 wt% Zn, 0.005wt%Fe,< 0.002wt% Cu, and <0.002wt% Ni)
- AZ 31(3wt% Al, 1 wt% Zn, 0.005wt%Fe,< 0.002wt% Cu, and <0.002wt% Ni)
- AZ91Ca(9 wt% Al, 1 wt% Zn, 0.005wt%Fe,< 0.002wt% Cu, <0.002wt% Ni and Ca)
- And alloys like AE 42 having both aluminium and rare earths

B. Alloys without aluminium

- Mg-1.0Zn(1 wt% Zn, 0.02 wt% Fe, 0.002 wt% Cu, 0.001 wt% Ni)
- Mg-2Zn-0.2 Mn, Mg- 1.0Zn-1.2 Mn
- Mg- Zn- Ca alloys
- Mg-Rare earth alloys like ZE 41(4 wt% Zn, 1 wt% RE, .4-1 wt% Zr, 0.005wt% Fe, 0.1 wt% Cu, 0.01wt% Ni), WE 43, LAE442
- Mg-Ca-Zn metallic glasses

Song [9] studied the biodegradation of different magnesium alloys, commercial purity (CP) magnesium, high purity (HP) magnesium and magnesium alloy (viz. AZ91, ZE41, Mg1.0Zn and Mg2Zn0.2Mn) in *m*-SBF and compared their average rate of hydrogen evolution as shown in Figure 2.5.

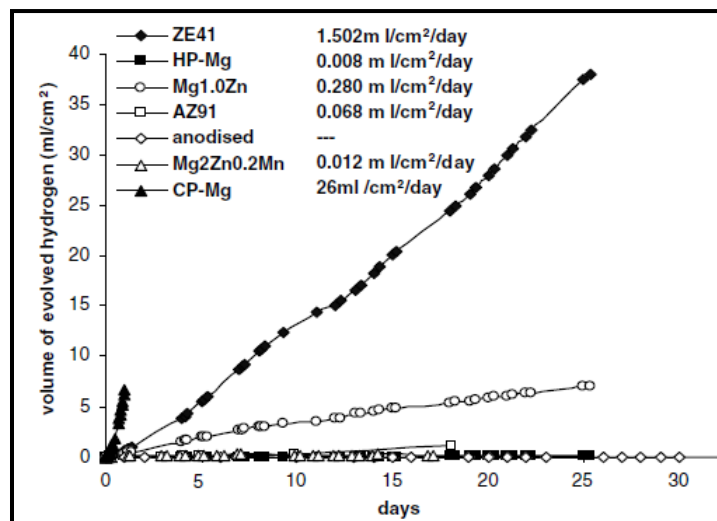


Fig 2.5 Averaged hydrogen evolution for different magnesium alloys [9]

The effect of removal of impurities from the alloy on biodegradability was shown and it was found that the hydrogen evolution of HP-Mg in comparison with commercial purity Mg (CP-Mg) was remarkably decreased. But high purity Mg (HP-Mg) has yield strength (cast Mg typically <55 MPa) lower than natural bone (e.g. femur ~110 MPa). Also, the lowest corrosion rate was observed in case of AZ91 and Mg-Zn-Mn alloy but they both have elements that are found to be toxic (see Table 2.3) [9]. So a corrosion resistant coating on the alloy may be a viable option for delaying the biodegradation.

The bio-corrosion behavior of Mg-2Zn-0.2X (X = Ca, Mn, Si) alloys was investigated (Figure 2.6) in Ringer's physiological solution and compared with that of the AZ91 magnesium alloy. Superior corrosion resistance of the AZ91 alloys with respect to Mg-2Zn-0.2Ca and Mg-2Zn-0.2Si alloys were observed. The corrosion resistance of Mg-2Zn-0.2Mn alloy was superior to that of AZ91 which was ascribed to enhanced protective properties of the Mg(OH)₂ surface layer due to the incorporation of manganese in the hydroxide layer[62].

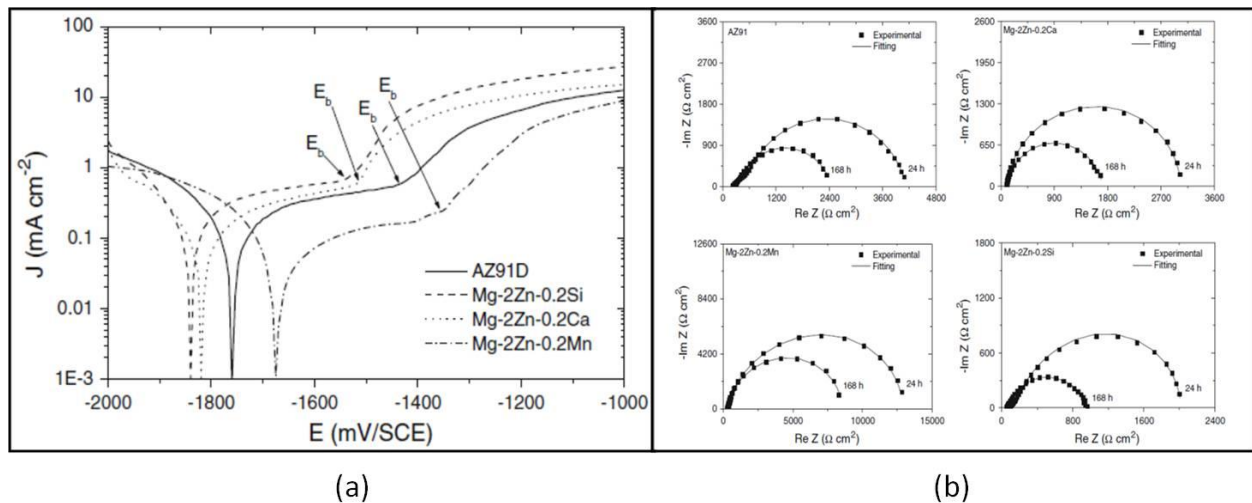


Fig 2.6: a) Polarization curves and b) impedance spectra of AZ91 and Mg-2Zn-0.2X (X = Ca, Mn, Si) alloys recorded after 1 h exposure to Ringer's physiological solution at 37°C [62]

The in-vivo corrosion of LAE442 and WE43 were investigated by Witte et al [63] and compared with AZ31 and AZ91. A much slow corrosion rate was recorded for LAE442, while AZ31, AZ91 and WE43 were found to degrade at similar rates.

Kannan et al [17] reported that the Ca addition to AZ91 alloy helps in refining the microstructure of Mg alloy, thereby improving the corrosion resistance of AZ91 (Figure 2.7). The impedance results showed AZ91Ca alloy had two-fold greater in polarization resistance (R_p) as compared to AZ91 alloy. Film resistance R_f of AZ91Ca alloy was found to be five-times greater than that of AZ91 alloy. This showed the higher stability of the surface film formed on AZ91Ca alloy than on AZ91 alloy. The E_{corr} of AZ91Ca alloy is ~ 140 mV nobler in comparison with AZ91 alloy. But AZ61Ca alloy showed no significant change in the E_{corr} in comparison with AZ91 alloy. This was attributed to the net effect of Ca addition and lower Al level. Al addition is known to shift the corrosion potential of magnesium alloys towards noble direction [17].

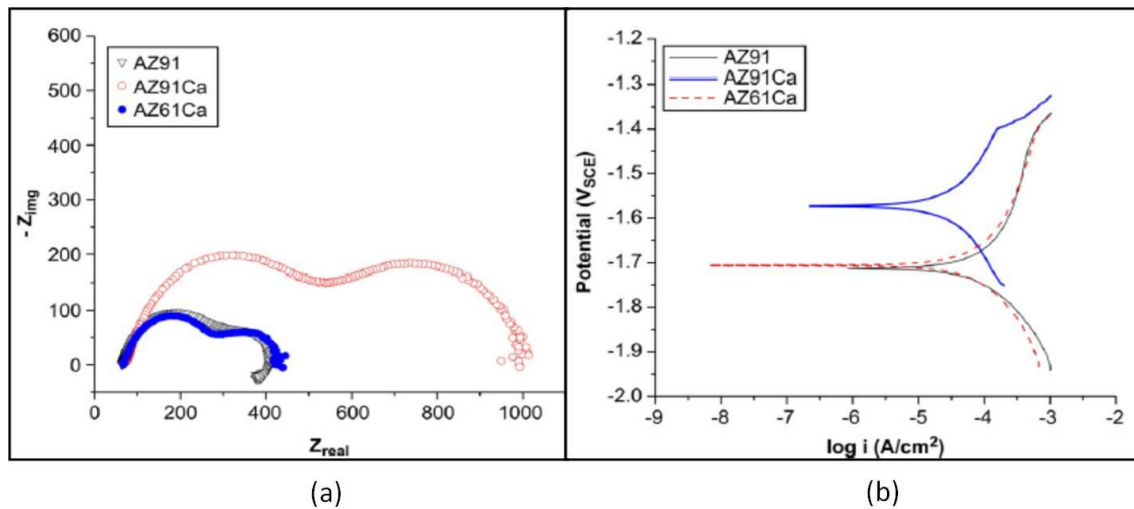


Fig 2.7: a) EIS curves and b) Potentiodynamic polarization curves of the alloys AZ91 alloys (with and without Ca) in *m*-SBF at 36.5°C [17]

Different compositions of Mg-Mn-Zn alloys were studied [64, 65] (Figure 2.8) and was found that the fine Mg_7Zn_3 and Al-Mn phases acts as the micro cathode sites and magnesium matrix as

the micro anode sites. With the increase in Zn content, more Mg_7Zn_3 phase forms, providing more micro anode–cathode sites, that impairs corrosion resistance. The increase in Zn content moved the corrosion potential, E_{corr} , to a more negative direction and reduced the corrosion resistance.

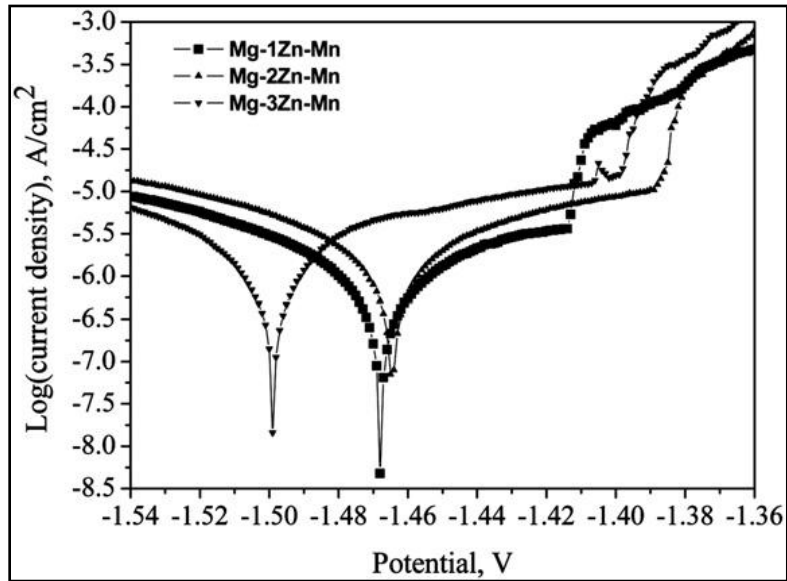


Fig 2.8: Polarization curves of the extruded Mg–Zn–Mn alloys with different Zn contents [65]

In each case, a long plateau was found in the anodic region, showing that a passivation film was formed on the surface in the immersion to protect the magnesium samples from corrosion attack (Figure 2.8). Broadest passivation stage was observed for Mg–3Zn–1Mn alloy. The passivation stage becomes broader with the increasing Zn content and the coexistence of HPO_4^{2-} , $H_2PO_4^-$ and Ca^{2+} , as well as Mg^{2+} and Zn^{2+} which induce precipitation of phosphates on the surface of magnesium alloy and thereby provide protection to the alloy. No cytotoxicity was detected but blood hemolysis was determined, indicating that high Zn containing magnesium alloys cause damage to blood system due to the corrosion which increased the pH of the blood system causing serious hemolysis at $pH > 10.2$.

Mg-Ca, Mg-Zn and Mg-Zn-Ca-Mn alloys have been investigated for their use as bio-implants. Recently, Li et al. [66] developed binary Mg-Ca alloys for use as biodegradable materials within bone. The bio-corrosion rate of as-cast Mg-1Ca alloy was found to be greater than conventional alloys, viz. AZ31, AZ91D, WE43 and LAE442. However, the biocompatibility tests of Mg-1Ca alloy also demonstrated its qualification as orthopedic biodegradable alloy [66]. Li et al. also reported that a mixture of $Mg(OH)_2$ and HA precipitated on the surface of Mg-1Ca alloy with the extended in-vivo implantation time of about one month. However, if the Ca content exceeds 1 wt% it may lead to the deterioration in corrosion properties as well as their mechanical properties, as a result of enhanced micro-galvanic corrosion caused by a very brittle inter-metallic Mg_2Ca phase.

Zhang et al. [67] studied the binary Mg-Zn alloy as a degradable biomedical material and reported that Mg-Zn has more noble corrosion potential as compared to pure Mg (Figure 2.9). The corrosion products formed on Mg-Zn alloy in the physiological environment are hydroxyapatite (HA), $Mg(OH)_2$ and other Mg/Ca phosphate that helps in reducing the corrosion rate in later stage of degradation.

MgZnCa glasses have been reported to have superior mechanical and corrosion resistance as compared to their crystalline counterparts [68, 69]. A significant decrease in corrosion rate and hydrogen evolution was observed and was attributed to the homogenous single-phase structure of MgZnCa glass and the development of passivating surface layers of ZnO and $ZnCO_3$. These are attractive because of extended solubility of alloying elements to give single homogeneous phase structure and absence of any second phases, which improves mechanical properties as well as corrosion resistance (as minimizes the micro galvanic corrosion due to absence of secondary precipitates). The alloy has uniform corrosion morphology.

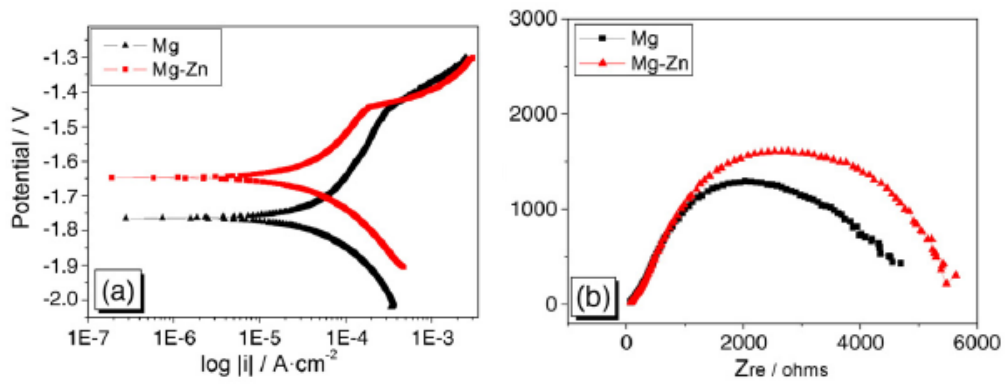


Fig 2.9: Polarization and EIS plots for Mg and Mg-Zn alloys in physiological environment [67]

2.4.4.2 Effect of alloying elements on physical and toxicological properties of magnesium

Li et al. [66] reported calcium addition to improve corrosion resistance of Mg alloys by Ca addition also enhanced the formation of hydroxyapatite (HA) layer during prolonged immersion in *m*-SBF. The Ca^{2+} available from corrosion of Mg alloy and *m*-SBF are incorporated into the layer of $\text{Mg}(\text{OH})_2$. Ca^{2+} ions act as nucleation sites for HA formation by attaching to negatively charged ions $(\text{PO}_4)^{3-}$ and $(\text{CO}_3)^{2-}$ available from the surrounding fluid to form Ca-P enriched surface layer which crystallizes into the bone-like apatite.

Zinc is also reported to be one of the essential elements in human body. Human requirement for Zn is estimated to be 15 mg per day [70, 71]. Zn addition is known to improve the mechanical properties of magnesium alloys through a solid solution hardening mechanism [32].

It is essential that the alloying elements released due to in-vivo dissolution of Mg alloy are non-toxic. Therefore, it is necessary to establish the influence of released alloying elements on the human cells or cell lines through the standard in-vitro test [72, 73]. Most studies on the corrosion resistance of magnesium alloys with coatings have been carried out on Al- and/or rare earth (RE) containing alloys. Both Al and RE are generally believed to be toxic to human health [9, 60, 72,

74-76]. Therefore, Mg-6Zn-Ca alloys, i.e., free from both Al and RE (as selected for the present study may be an ideal choice for bioimplant application). Mg, Ca and Zn are essential elements having no toxic effect in the body [50]

Table 2.3 Toxicology, pathophysiology and effect of alloying elements on Mg
[9, 12, 13, 32, 50]

Alloying element	Pathophysiology/Toxicology	Effect on physical properties of magnesium
Aluminium	<p>Risk factor in causing Alzheimer's disease(neurotoxicity)[60, 76]</p> <p>Can cause muscle fiber damage</p> <p>Decrease osteoblast viability</p> <p>Combines with phosphates of body causing lack of phosphates inducing dementia[9]</p>	<p>Increases strength and hardness, widens the freezing range and makes the alloy easy to cast</p>
Magnesium	<p>Essential trace element in the body</p> <p>Activator of many enzymes, co-regulator of protein synthesis, energy metabolism, cell proliferation and stabilizer of DNA and RNA</p>	
Calcium	<p>Essential trace element in the body</p> <p>Activator or stabilizer of enzymes, stored in bone and teeth.</p> <p>Calcium content could enhance the</p>	<p>Serves dual role in casting alloys when added prior to pouring it decreases the oxidation of metal as well as during subsequent heat treatments, improves</p>

	formation of precipitates of calcium and phosphates in the implant periphery.	rollability of magnesium sheets, mechanical properties are also improved due to solution strengthening [17].
Manganese	<p>Important in metabolic cycle of lipids, amino acids and carbohydrates</p> <p>Influences the function of the immune system, bone formation, blood clotting, neurotransmitter synthesis.</p> <p>But poisonous effects on cell viability even by Mg-1Mn alloy [40].</p>	Increases yield strength, removes iron and other heavy impurities to increase corrosion resistance [26, 65]
Zinc	<p>Essential trace element, appears in all enzyme classes.</p> <p>Essential for immune system, Cofactor for specific enzymes in bone and cartilage.</p> <p>Believed to stimulate bone formation. [26, 65].</p>	Increases the strength of the alloy by precipitation hardening [32, 64].
Silicon	<p>Essential element in mammals [9]</p> <p>Cross linking agent of connective tissue base membrane structures.</p> <p>Necessary for growth and bone calcification.</p>	Increases fluidity of metal in the molten state.
Lithium	Used in treatment of depressive psychosis but reduces kidney life and	Its addition decreases the strength but increases the

	<p>central nervous system disorders.</p> <p>Shifts the body pH greater than 11.5 and this in-vivo alkalization is hazardous to human body[9].</p>	ductility.
Zirconium	Causes liver/lung/breast/nasopharyngeal cancer [9].	Helps in grain refinement but cannot be added to the alloys containing Al and Mn because it forms stable compounds with them and is removed from solid solution.
Nickel	<p>known to give rise to allergic skin diseases [77].</p> <p>Reproductive disorders and effects on foetues after nickel exposure have convincingly been demonstrated in animal experiments[77].</p>	Harmful impurity in magnesium alloys. When present even in small amount it decreases the corrosion resistance of the magnesium alloys[32].
Y and Rare earths(Pr, Ce, Lu,Gd, Dy, La, Nd)	<p>Accumulates in bone and liver</p> <p>Y have inflammatory reaction and effects the viability of macrophages[78]</p> <p>La, Pr, Ce – hepatotoxic by inducing fatty liver</p> <p>La, Nd, Eu, Ce, Pr – inflammatory response on cells [72].</p> <p>Gd - interferes with hepatic function by altering RNA polymerase II activity even at low concentration[78] can cause</p>	<p>Addition of rare earths increases the strength.</p> <p>Increases alloys castability and enhances mechanical performance [79].</p>

	<p>renal failure [75].</p> <p>Yb - have influence on inflammatory genes of human cells.</p> <p>Induces toxicity to human body[9]</p> <p>Nd and Y resides in the degrading site (alloy WE43) even after 18 weeks post implantation.</p>	
--	--	--

2.4.4.3 Surface modification of magnesium and its alloys

Alloying may be an option for controlling the corrosion rate of magnesium but it is still a challenge to develop new alloys with optimum performance due to the low solubility of many elements in magnesium [59]. Therefore, a suitable coating is an attractive option for improving the corrosion resistance of magnesium alloys. Protective coatings for temporary implants should act as temporary barrier to slow down degradation while enhancing biocompatibility [6, 59]. These coatings generally fall into two categories: conversion coatings and deposited coatings. The simplest example of a conversion coating on magnesium and its alloys is the magnesium hydroxide layer that forms upon exposure to the aqueous environment. However, the protection of this passivation layer is limited in an environment containing aggressive ions such as chloride ions in physiological environment is one such example. Therefore, advanced coating methods are being investigated such as chemical treatment, anodization and ion implantation [31]. However, chemical conversion coatings still play an important role as a pre-treatment for many coatings as they have been shown to significantly enhance the adhesion of the deposited coatings [34]. For biomedical applications, besides corrosion protection, coatings must possess some additional functions, such as an enhancement of biocompatibility or osteointegration in the case of orthopedic applications, bioactivity, antibiotic ability, or local drug delivery ability. Furthermore, the coatings should allow biodegradation of the temporary implant at a desired rate, and hence they should offer only a limited barrier function.

There are quite a large number of surface treatment methods used for improving the corrosion resistance of Mg and its alloys [80], but they have been developed primarily for Mg alloys for industrial applications. On the other hand, a few preliminary studies are reported for improving the corrosion resistance of Mg implants, including passivation by alkaline pretreatment, carbonate treatment [24], fluoride treatment [25], phosphating treatment [26], electro deposition of HA coating, acting as a physical barrier [27], microarc oxidation (MAO). Some of these coatings are of ceramic nature that have been shown to provide both corrosion and wear resistance to AZ91D alloy in the Hank's solution.

Simple passivation treatments of Mg and its alloys in NaOH solution can provide protection during the initial phases of corrosion. Immersion in a solution with a stable pH of >11 forms a passive layer of MgO/Mg(OH)₂. Cell culture tests, however, showed that even though the oxide/hydroxide passive layer can decrease the initial surface reactivity when in contact with cell culture medium, the effect was not durable. Lorenz et al [81] studied the effect of pure Mg surface passivation on human HeLa cells and mouse fibroblasts in cell culture experiments. As shown in Figure 2.10 pure Mg being highly reactive in the cell culture medium, led to a pH shift in the alkaline direction, therefore, cell death on pure magnesium samples without treatment occurred within 1 day, whereas surface passivation enabled survival of a large number of cells on Mg. The best initial cell adhesion was observed for Mg samples incubated in simulated body fluid (*m*-SBF), which leads to the formation of a biomimetic, amorphous Ca/Mg-phosphate layer with high surface roughness.

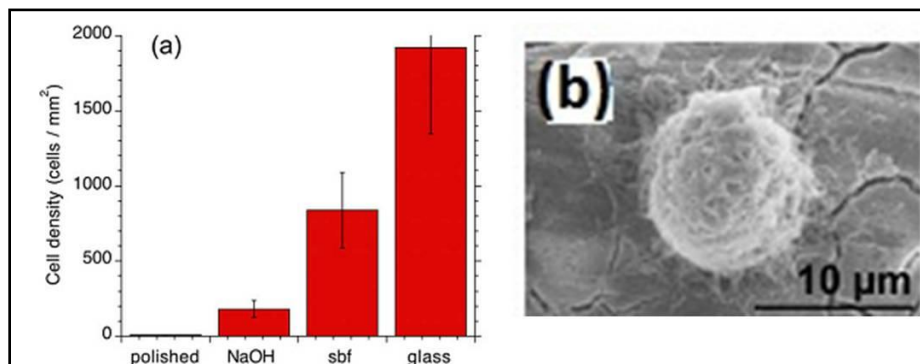


Figure 2.10: Behavior of HeLa cells on differently pre-treated Mg surfaces as well as on glass: (a) cell density after 24 h in cell culture and (b) SEM image of a cell attached to the surface of Mg soaked in *m*-SBF[81]

The effect of alkaline pre-treatment [53, 54] was also studied by Kannan et al on AZ91 alloy in IM NaOH for 24 h and 48 h. The Nyquist plots of the untreated and alkaline-treated alloy are shown in Figure 2.11 (a). The alkaline treatment is seen to have improved the polarization resistance of the untreated alloy by an order of magnitude. The alloy treated with alkali for 24 h and 48 h exhibited R_p values of $1 \pm 0.04 \times 10^4 \Omega \text{ cm}^2$ and $1.2 \pm 0.1 \times 10^4 \Omega \text{ cm}^2$, respectively. A longer period of alkali-treatment, however, did not provide any additional beneficial effect. The potentiodynamic polarization curves of untreated and alkali-treated alloys are shown in Figure 2.11 (b). The E_{corr} of alkali treated alloys shifted towards active direction by 70–80 mV when compared with that of untreated alloy. Further, a passivation-kind of behavior was observed in the anodic polarization curve of alkali-treated alloys. A passive-like region was found to be slightly extended in case of 48 hrs alkali-treated alloy and the break-down potentials of the alkali treated alloys were quite close to the E_{corr} of the untreated alloy, suggesting that the film was mainly composed of $\text{Mg}(\text{OH})_2$.

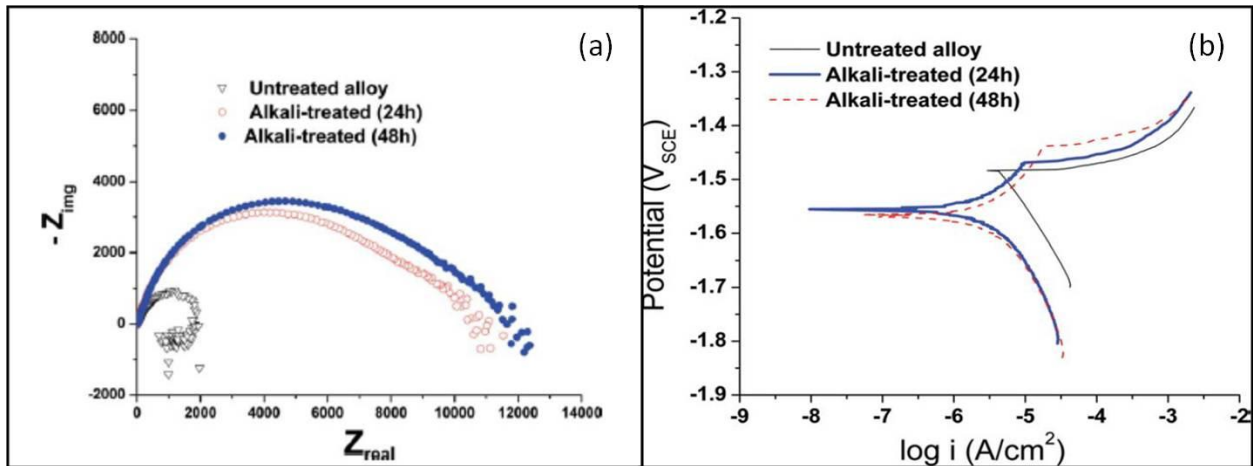


Figure 2.11: (a) Nyquist plot and (b) Potentiodynamic polarization curves of untreated and alkali-treated AZ91 magnesium alloy pre-exposed SBF for 1 h at the nominal body temperature (36.58°C)[53]

Xu et al [23] coated Mg–Mn–Zn alloy with calcium phosphate by a phosphating treatment to improve the surface bioactivity of the magnesium alloy. Cytocompatibility tests showed that the cells on the surface of the bare Mg alloys were round in morphology during the whole incubation

period, whereas for the Ca–P coated Mg alloy, the cells were elongated after 1-day of incubation (Figure 2.12). Some cells spread across the surface and contacted with each other. After 3-day culture, the cells and the excreted matrices were found to be connected together, and after 5-day culture, no difference in the morphology of the cells was found in comparison with that incubated for 3 days. Coated Mg sample and the pure Ti samples show significantly better cell response than the naked Mg sample during the whole incubation period. In addition, the cells on the surface of the Ca–P coated Mg alloy excreted more matrix than the cells on the surface of the pure Ti did.

In cell proliferation study (Figure 2.13), the cell activity represented by the cell number was found to increase with culture time, indicating that a cell could attach and proliferate on the surface of the samples. In comparison with the naked Mg alloy, the cell number on the surfaces of the Ca–P coated Mg alloy and the pure Ti showed a significant increase at all time intervals, indicating that both the Ca–P coated Mg alloy and Ti have better surface bioactivity than the naked Mg alloy.

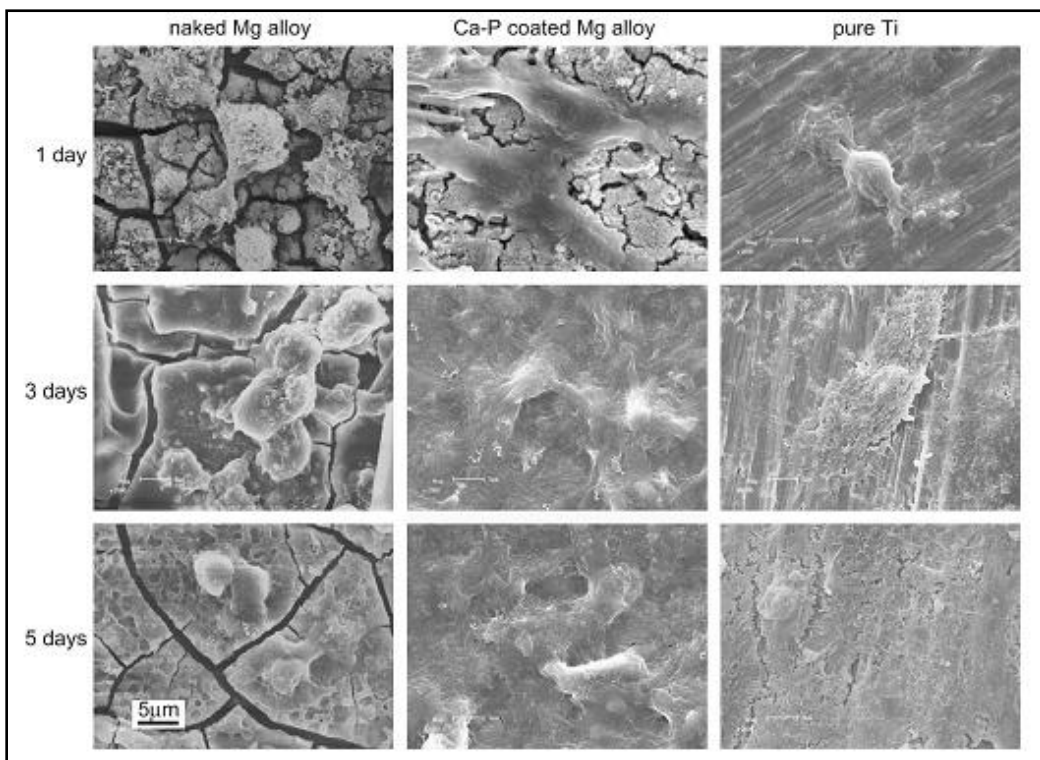


Figure 2.12: Cell morphology after 1, 3, and 5 days incubation on bare and Ca-P coated Mg alloy and pure Ti[23]

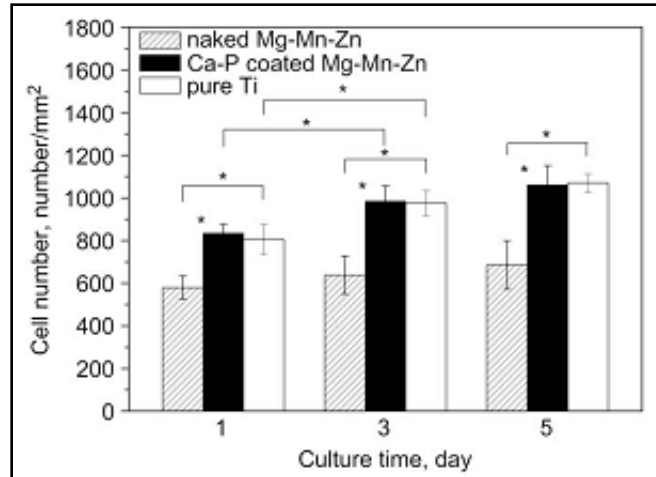


Figure 2.13: Growth of L929 cells vs culturing time on the naked Mg, the Ca-P coated Mg and the pure Ti [23]

Jo et al [82] studied hydroxyapatite coating on magnesium with MgF_2 interlayer for enhanced corrosion resistance and biocompatibility. The HA/ MgF_2 double coating exhibited a slightly better corrosion resistance than the single MgF_2 coating in the immersion tests as the coating layer protected Mg against corrosion and reduced the alkalization of the medium in the vicinity of Mg. The in-vitro cell culture results demonstrated that the double coating layer had enhanced cell proliferation and differentiation levels. Figure 2.14 shows the morphology of the preosteoblast cells that were cultured for 5 and 24 h on the bare Mg, the Mg that was coated with MgF_2 and the Mg that was coated with MgF_2 and HA. After 5 h, a few cells were found attached to the surface of the bare Mg in Figure 2.14a. Even after culturing for 24 h, the cells were still adhered with no significant morphology changes. In case of MgF_2 surface more cells were found to be attached. For the HA coated samples with the MgF_2 interlayer, most of the cells were well attached to the coating surface and spread out after 5 h (Figure. 2.14e). After culturing for 24 h, the cells were considerably flattened on the rough coating surface, in Figure. 2.14f. The cells that were cultured on the bare Mg exhibited a poor cell proliferation, whereas the proliferation levels were significantly higher on the coated Mg samples (Figure 2.15). The cells that were cultured on the HA coating layer exhibited a significantly higher alkaline phosphatase activity level than the bare and MgF_2 -coated Mg. The results indicated that the HA coating improved the in vitro cellular responses of Mg and the MgF_2 coating layer.

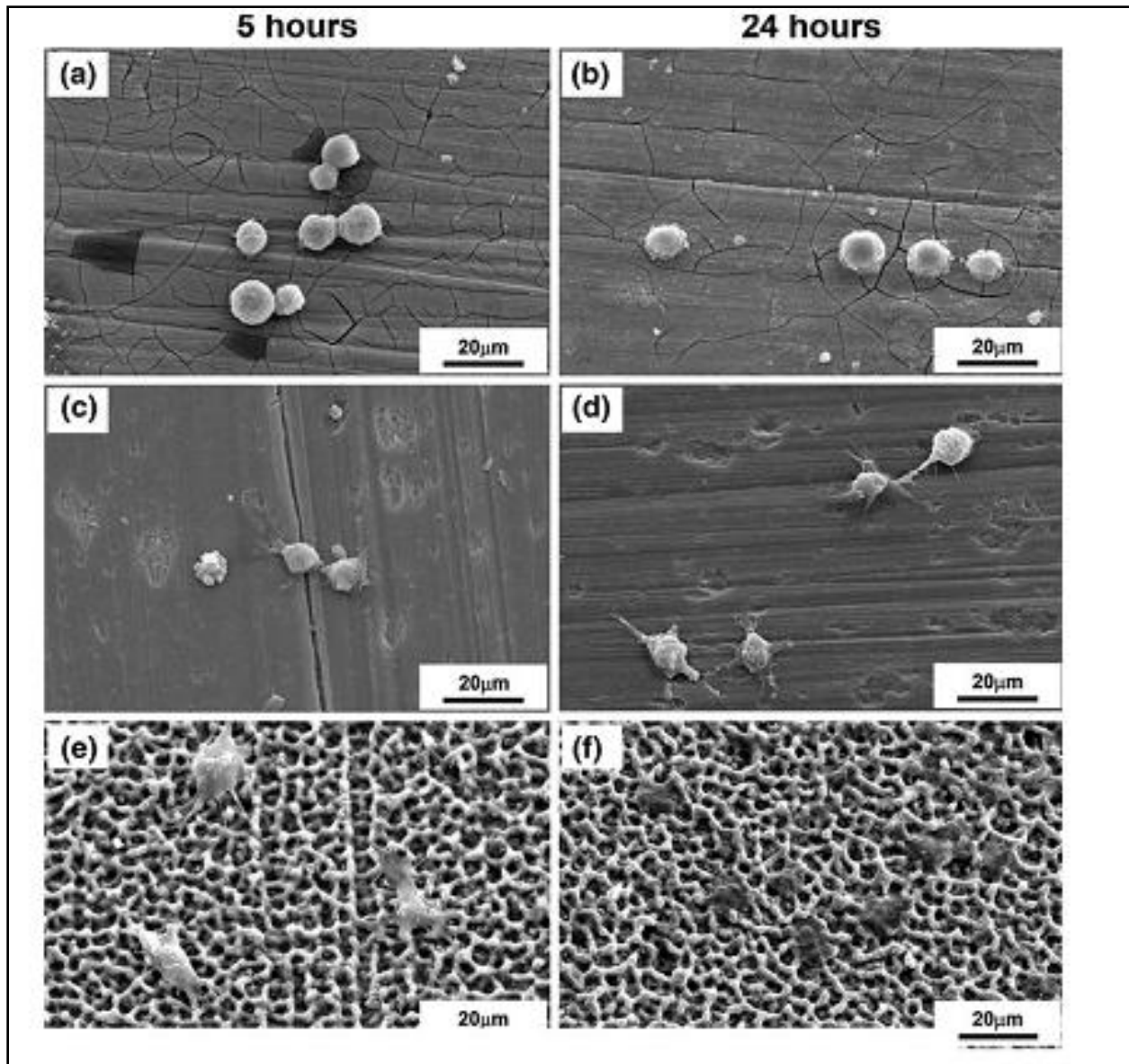
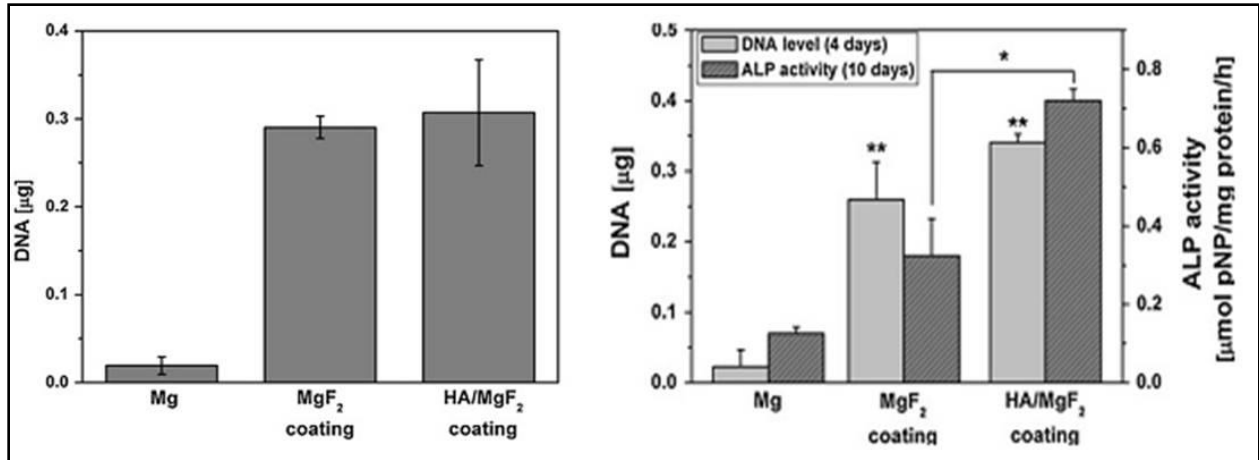


Figure 2.14: Scanning electron microscopy (SEM) images of the MC3T3-E1 cells that were cultured on the (a) and (b) bare, (c) and (d) MgF₂ coated, and (e) and (f) HA/MgF₂ coated Mg samples for 5 and 24 h, respectively [82].

Kim et al [83] studied the corrosion resistance and biological response by in-vitro cell tests using MC3T3-E1 preosteoblast cells to observe cell attachment, viability and differentiation on hydroxyapatite coated magnesium alloy in comparison to bare Mg alloy.



(a)

(b)

Figure 2.15: (a) DNA levels that were measured from the cells that adhered to the samples after culturing for 24 h and (b) DNA and ALP activity levels of the MC3T3-E1 cells that were cultured on the bare, MgF₂ coated, and HA/MgF₂ coated Mg for 4 and 10 days[82]

The corrosion resistances of the Mg and HA-coated Mg were determined by electrochemical polarization tests in the SBF, as shown in Figure 2.16 (a). The HA-coated Mg showed much lower I_{corr} and higher R_p than the bare Mg, while E_{corr} of the coated alloy was shifted in the positive direction. The change in the pH (Figure 2.16 (b)) of the solution with HA-coated samples was observed to be considerably lower than that of the untreated samples for immersion times up to 120 h. Furthermore, the evolved hydrogen (Figure 2.16 (c)) from the samples with a HA coating exhibited a trend similar to the pH change; that is, a much smaller amount of hydrogen was evolved from the alloy with an HA coating than from the bare Mg. The corrosion resistance of Mg was significantly improved due to HA coating as HA coating acted as a protective layer enhancing the corrosion resistance of Mg quite substantially.

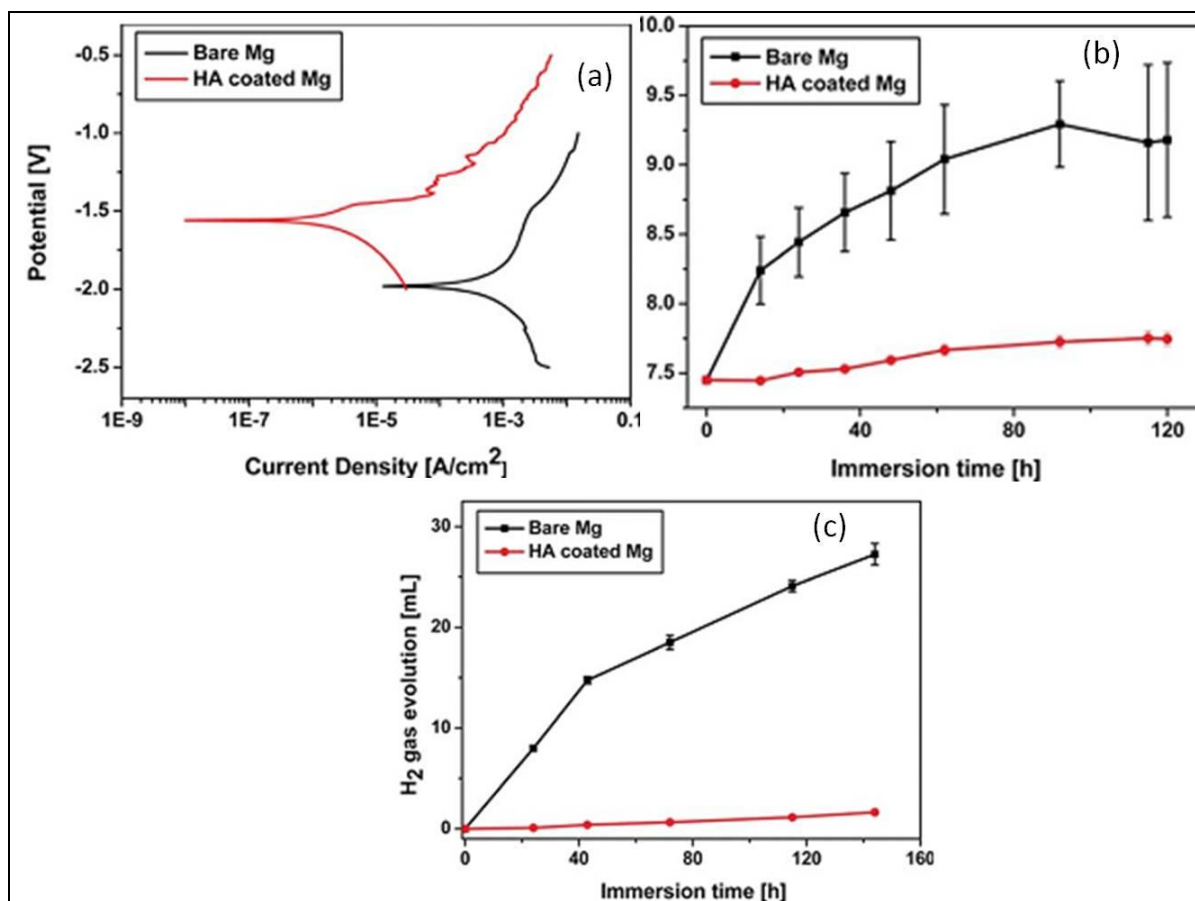


Figure 2.16 : (a) Potentiodynamic polarization curves (b) Variation of pH and (c) hydrogen gas evolution in the SBF for bare and HA-coated Mg [83]

Further, in cytotoxicity test, SEM images (Figure 2.17) showed the presence of only few cells with a spherical shape attached to the surface of the bare Mg sample whereas in the case of the coated sample, considerably more cells were attached to the HA surface and spread well with an active cytoskeletal extension after 1 day of culturing. The morphologies of the pre-osteoblast cells after 5 days of culturing on the bare Mg and HA-coated Mg samples are shown in Figure 2.17(A,B). The bare Mg sample showed no noticeable cells attached on its cracked surface probably due to the fast corrosion of Mg. On the other hand, the HA-coated Mg showed that cells were attached and spread well with an active cytoskeletal extension [Figure. 2.17(B)], suggesting its good biocompatibility *in vitro*. Also cell proliferation was evaluated by DNA quantification after 5 days of culturing. The DNA content from the bare samples was found to be

close to zero, whereas that from the HA-coated samples showed a considerably higher level. To evaluate the cell differentiation, ALP activities were also measured, as shown in Figure 2.18. After 14 days of culturing, the cells cultured on Mg with an HA layer exhibited ALP activity similar to that of Thermanox VR and slightly lower than that of HA. However, it should be noted that the ALP activity of bare Mg could not be measured because of the fast in-vitro corrosion of Mg, which would not allow the active proliferation and differentiation of cells.

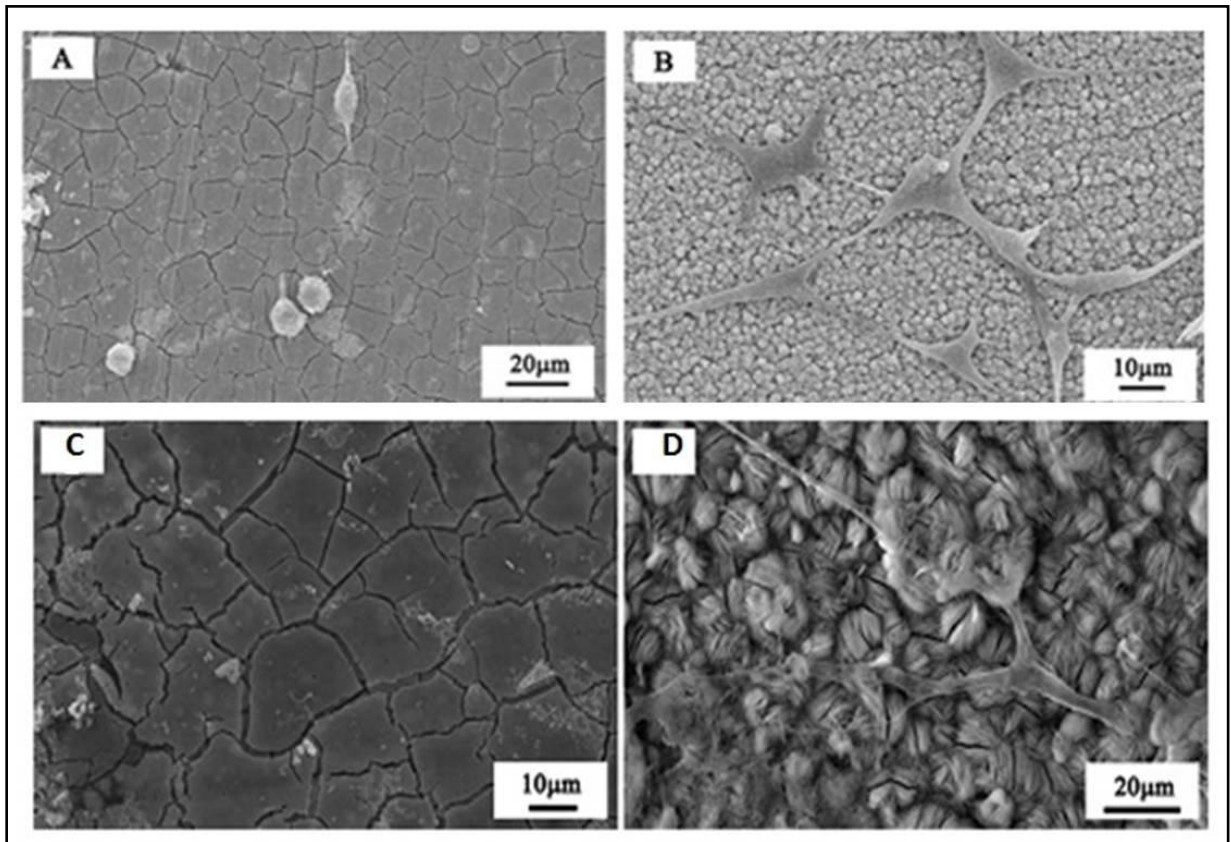


Figure 2.17: SEM images of the MC3T3-E1 cells on (A) the bare Mg, (B) HA-coated Mg samples after 1 day of culturing, (C) bare Mg and (D) HA-coated after 5 days of culturing[83]

Li et al [84] studied the corrosion resistance and cytotoxicity of MgF_2 coatings on Mg-Ca alloy deposited via vacuum evaporation deposition method. In the immersion studies (Figure 2.19 (a)) hydrogen evolution volume of both samples showed approximately linear relationship with the

immersion time, but the bare Mg–1Ca alloy released much more hydrogen than the MgF₂-coated alloy. Smaller increase in pH (Figure 2.19(b)) of the immersion solution also indicated the MgF₂ coating protected the Mg–1Ca alloy from fast degradation. The MgF₂-coated Mg–1Ca alloy exhibited a much higher polarization resistance than the bare Mg 1Ca alloy and the corrosion current density of the MgF₂-coated Mg–1Ca alloy was half of that of the bare Mg–Ca alloy.

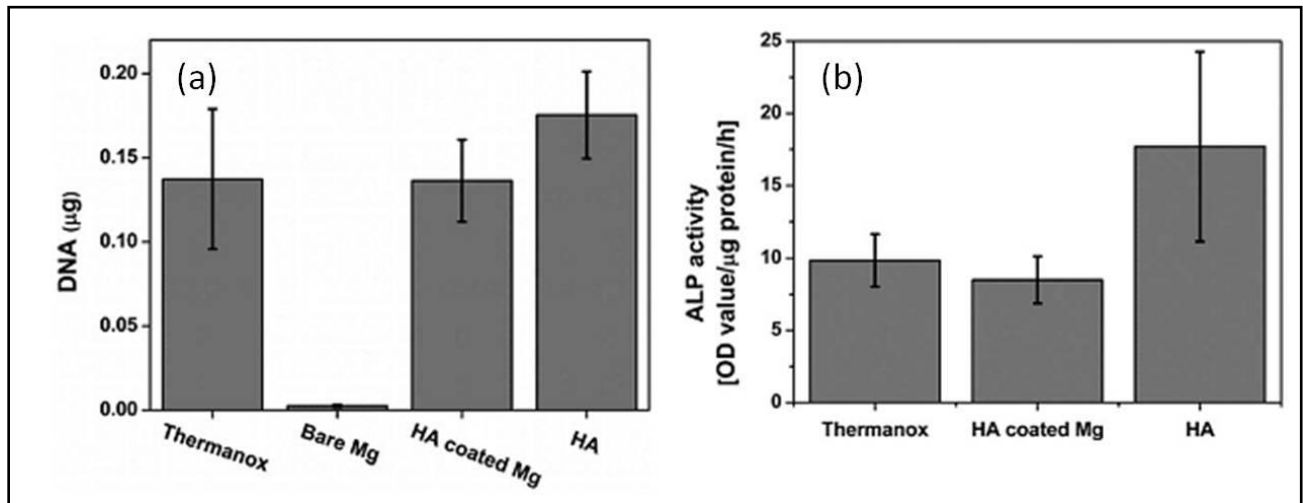


Figure 2.18:(a)DNA levels of the MC3T3-E1 cells that were cultured for 5 days and (b) ALP activity levels of the MC3T3-E1 cells that were cultured for 14 days [83]

In cytotoxicity test, only a few round shape MG63 cells shape and hardly any MC3T3-E1 cells were observed on the bare Mg–1Ca surface (Figure 2.20). The MgF₂ film effectively retarded corrosion of the Mg–1Ca, so both MG63 and MC3T3-E1 cells exhibited healthy configuration with an extended morphology on the substrate.

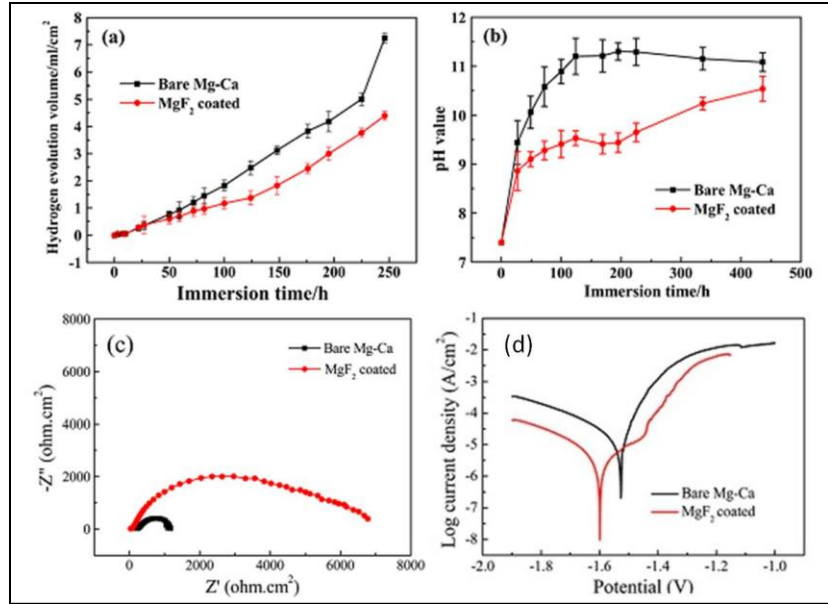


Figure 2.19: (a) The hydrogen evolution volume (b) the change of pH of Hank's solution incubating bare and MgF₂-coated Mg-1Ca alloy as a function of the immersion time (c) Nyquist plots and (d) potentiodynamic polarization curves of bare and MgF₂-coated Mg-1Ca alloy in Hank's solution [84]

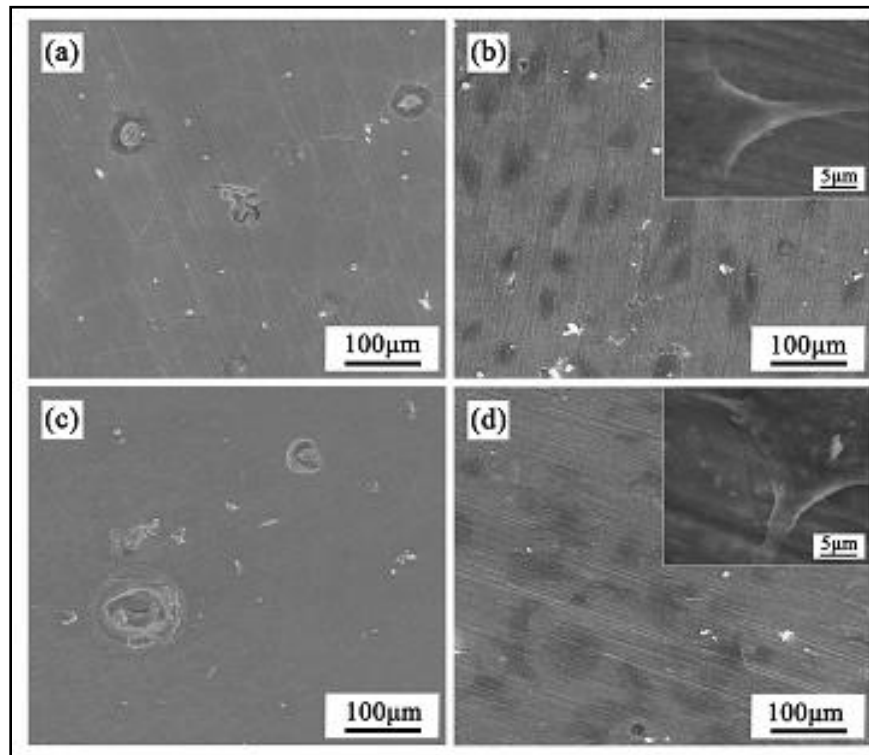


Figure 2.20: Morphologies of MG63 cells on (a) bare Mg-1Ca alloy, (b) MgF₂-coated Mg-1Ca alloy and MC3T3 cells on (c) bare Mg-1Ca alloy, (d) MgF₂-coated Mg-1Ca alloy [84]

Zhang et al [85] developed MAO, a ceramic coating directly on the surface of AZ91D Mg alloy, that greatly improved the corrosion and wear resistances of the alloy. The mass loss of untreated AZ91D alloy was 15 times that of the MAO coated alloy. With the coating the corrosion potential of the bare Mg alloy shifted from -1.5786 V to -0.43019 V and the corrosion current was reduced from 0.028703 A/cm² to 2.0456 x10⁻⁷ A/cm². But the disadvantage with this coating is the localized heating at the surface during MAO coating process. Also the coatings produced are brittle ceramic material that may not have the desired mechanical properties [27].

Coating materials can be metallic, inorganic or organic. Of these, organic-based coatings are the most widely used for biomedical applications because of their good biocompatibility, biodegradability and the availability of functional groups that can be used for further surface modification [59]. However, an appropriate coating on magnesium needs to have excellent adhesion properties as well as the ability to enhance the biocompatibility and slow the corrosion rate [35]. Li et al [86] produced a polylactic-co-glycolic acid (PLGA) coating on Mg6Zn substrates. Polarization test in NaCl solution (Figure 2.21) reported a decrease in degradation rate due to the presence of the biopolymer coating. The thicker (72 μm) coating showed lower corrosion resistance than the thin (33 μm) coating, probably due to voids and flaws in the coating system. Direct cell culture tests with mouse osteoblast-like MC3T3-E1 cells on the thin coatings revealed enhanced cell attachment (Figure 2.22).

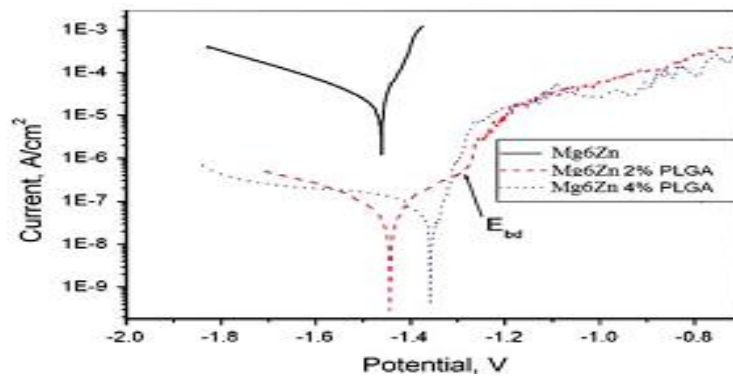


Figure 2.21: Polarization curves of uncoated and coated Mg–6Zn alloy in 0.9% NaCl solution [86]

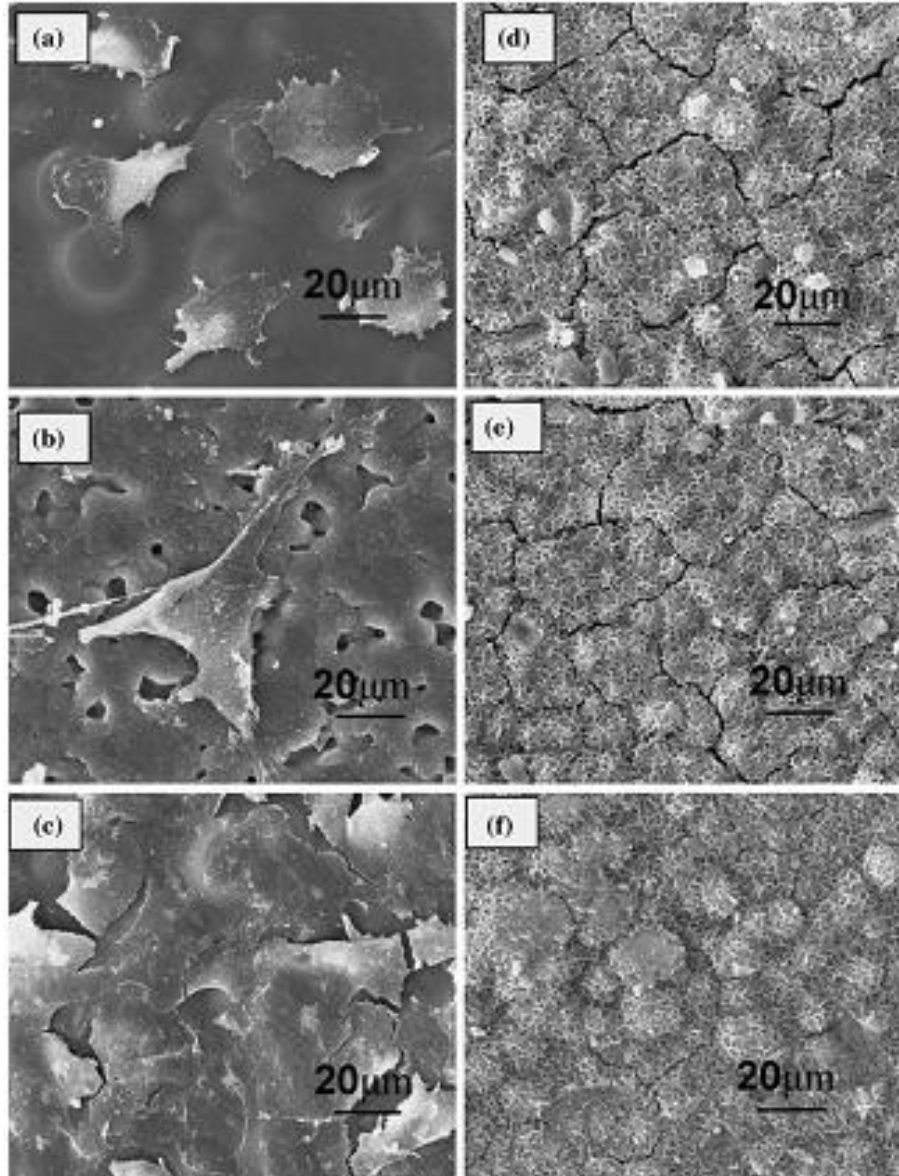


Figure 2.22: FE-SEM micrographs of cell morphology after different culture times, (a) 1 day culture, 2% PLGA coating, (b) 2 days culture, 2% PLGA coating, (c) 3 days culture, 2% PLGA coating, (d) 1 day culture, uncoated, (e) 2 days culture, uncoated and (f) 3 days culture, uncoated[86]

Gao et al. [87] developed a 2 step coating process that comprised preliminary PEO treatment of substrate followed by immersion in an organic phase solution of propolis, ethanol and Polylactic acid. The samples were immersed several times in above solution and then dried. The corrosion resistance (Figure 2.23) in SBF was found to be improved due to the composite coating.

Furthermore, the coating showed improved cell adhesion and proliferation using whartons jelly derived mesenchymal stem cells (Figure 2.24).

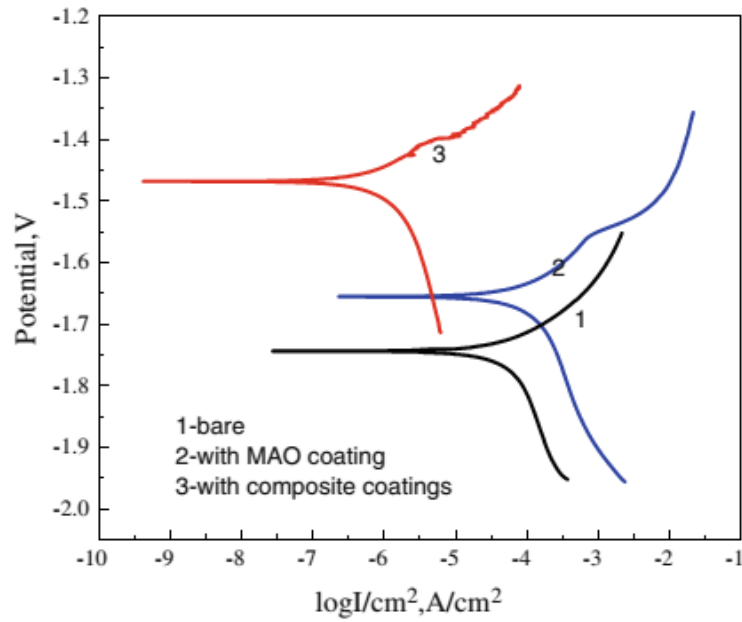


Figure 2.23: Potentiodynamic polarization curves of bare and coated Mg alloy in SBF solution at $36.5 \pm 0.5^\circ\text{C}$ [87]

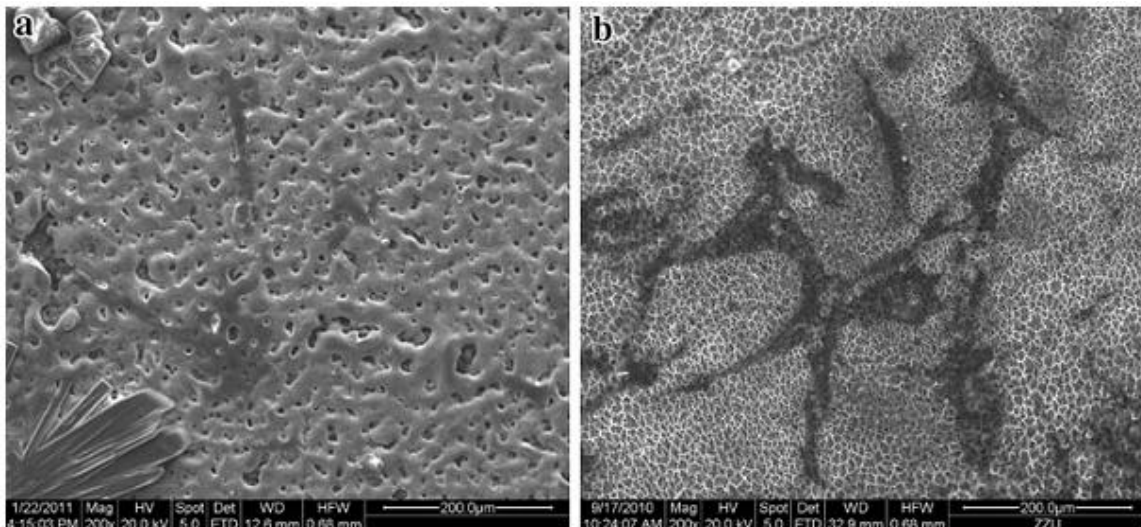


Figure 2.24: (a) SEM image of MAO coating with cells and (b) The typical SEM image of composite coating [87]

Among all the coating technologies, silane-based anti-corrosive coatings on Mg alloys have proven to be effective, economical and environment friendly. When in contact with water silanes are hydrolyzed to yield silanol groups (Si-OH) that gets attached to hydrated metal surfaces (metal-OH) via the formation of Si-O-metal bonds. The silanol groups undergo crosslinking to form siloxane bonds (Si-O-Si), resulting in an organic protective layer chemically bound to the metallic substrate. Silanes can provide functional moieties that enable further attachment of bioactive molecules to enhance the interfacial interaction of metal implants with surrounding cells and tissue.

Huang et al. [88, 89] applied degradable poly (lactic acid) coatings (by dipping) on pure Mg implant on which a silane-coupling agent was first coated in order to improve adhesion strength between Mg samples and poly lactic acid. The preliminary result showed that the coating could offer an effective protection against corrosion, dependent on reduction in mass loss of coating on pure Mg in Hank's solutions.

Liu et al [90] developed a bi-functionalized anti-corrosive silane coating on AZ31 magnesium alloy with bis-triethoxysilyl ethane to immobilize a layer of crosslinked silane coating with good corrosion resistance and then using 3-amino-propyltrimethoxysilane to impart amine functionality to the magnesium surface. They further modified the surface with a view of increasing the thrombo-resistance of biomedical implants. The coated sample was called Mg-B-A-Heparin compared with bare alloy; Mg-B-A heparin exhibited both an improved corrosion resistance (Figure 2.25) and reduced platelet adhesion (Figure 2.26). This surface modification strategy, controlled corrosion resistance and inhibited platelet adhesion on the magnesium alloy surface, thereby, improving blood compatibility with biodegradable magnesium implants.

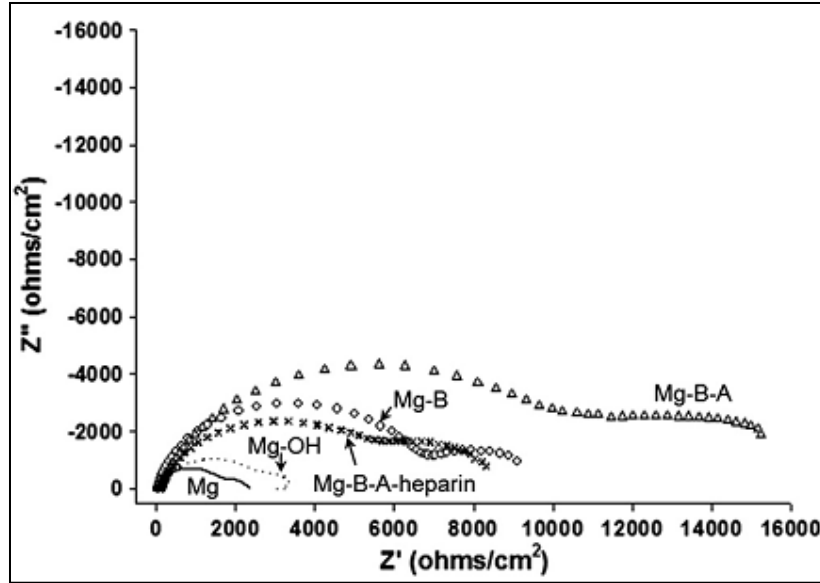


Figure 2.25: Impedance spectra of Mg, Mg-OH, Mg-B, Mg-B-A and Mg-B-A-heparin samples

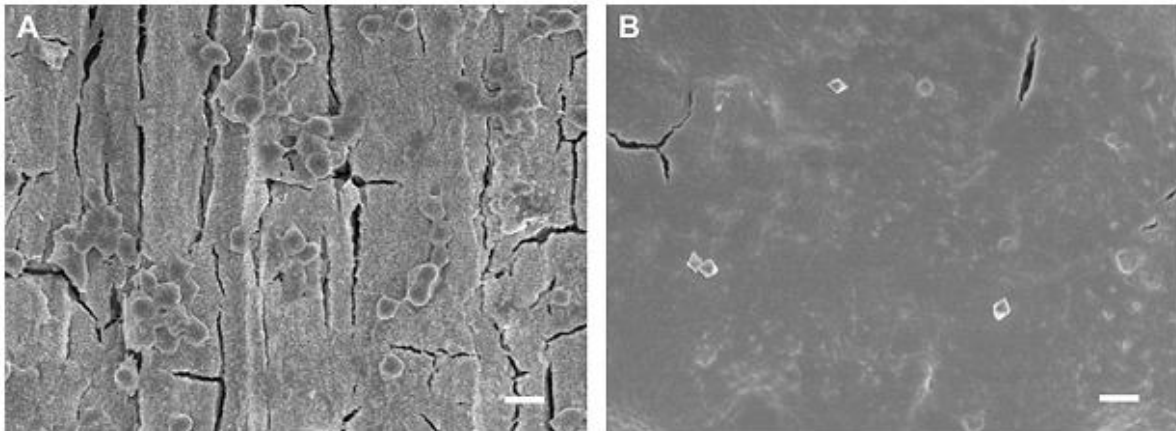


Figure 2.26: Representative SEM micrographs of platelets on (A) Mg-B-A and (B) Mg-B-A-heparin. The scale bars represent 2 μm

2.5 Organosilane Coating

Organofunctional silane class of materials is of great interest for a wide range of applications due to their excellent performance as coupling agents between organic and inorganic materials. Silane based anti-corrosive coatings on aluminum, steel and Mg alloys have been proven to be

effective, economical and environmentally benign. [80, 91-93]. Moreover, it has been reported that organosilane coatings can also improve scratch resistance, and enhance wear resistance of a number of different metals. They are important alternative to chromate containing coating which is toxic to both human health and the environment because of their toxicity and environmental hazards. Their successful applications on metals, combined with the outstanding biocompatibility, have inspired researchers to utilize organosilane coating onto Mg alloy substrates to achieve the ideal controlled biodegradable implant material.

The two criteria need to be fulfilled by the coating system for implant applications are: (a) to provide corrosion resistance and (b) the coating should be non-toxic and biocompatible. Silanes, that are emerging as an attractive alternative for improving corrosion resistance of the metallic substrates [33, 91, 94], are also attractive for implant application since they can fulfill (Figure 2.21) both the criteria.

The coupling ability of silanes is attributed to their unique chemical structure, which is given by, $R-(CH_2)_n-Si-X_3$, where R is any organofunctional group, CH_2 is the linker and X is the hydrolysable group. When a silane is used for modification of a polymeric-inorganic interface, the organofunctional group as well as the hydrolysable groups of silane independently bond with the polymer and inorganic surfaces. Silanes form oxane bonds with the hydroxyl groups of inorganic substrates as well as can form covalent bonds with suitable functional groups of different polymers [91].

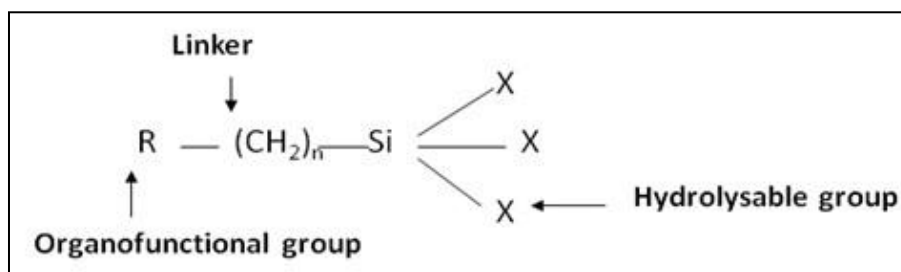


Figure 2.27: Structure of organofunctional silane

On the basis of the number of the hydrolysable groups, silanes are of two types, viz., monosilane, having three hydrolysable groups and bis-silane, having six hydrolysable groups. Though monosilanes have been widely used on different metal substrates, bis-silanes are reported to provide superior corrosion protection[91].

2.5.1 Surface treatment

The interaction of silanes with metallic surfaces profoundly depends on nature and preparation of the inorganic surfaces. The cleaning of the metal substrates prior to the film deposition is an important step in bonding process. Alkaline cleaning has been reported to be the best pretreatment before the application of silanes [95, 96]. Moreover, from the “chemical bonding theory” of Plueddeman [97] it can be expected that oxide surfaces with a high number density of hydroxyl groups will be preferred. It has also been reported that acid or neutral cleaners are less desirable compared to alkaline cleaners. The effect of surface pretreatment on aluminum has also showed that the amount of hydroxyl groups at the aluminum surface provided by the different pretreatments strongly influence the initiation and the formation of non-functional silane films [91]. The effect of different types of alkali pretreatments on the corrosion resistance of silane coated ZE41 was also investigated [98] and the nature of alkaline pre-treatments were found to profoundly influence the corrosion resistance of the coated alloy. This improvement in corrosion resistance was superior in the case of a pre-treatment that results in the formation of a uniform hydroxide film on the surface, which facilitates formation of a protective silane film on the substrate [98]. In summary, the interaction of the silane coupling agents with the metals seems to be dependent on the condition of the metallic surface and pretreatments [91].

2.5.2 Silane hydrolysis

Before application on any substrate, silanes needs to be hydrolyzed so that they have sufficient silanol Si—OH groups to interact with the metal substrate hydroxyl. Usually, silanes are applied from dilute water solutions onto the metal surface. In the solution, the silanes are hydrolyzed and silanol groups are formed.

After hydrolysis, the hydrolyzed silanols undergo condensation reactions, resulting in slow polymerization. Both hydrolysis and condensation reactions are acid or base catalyzed and solution pH is the major factor governing the stability of silanes in aqueous solutions. The factors influencing the kinetics and equilibrium of hydrolysis and condensation of silanes in solutions are the nature of the organofunctional groups, the concentration of silanes and water, the value of the solution pH, temperature, and the aging of the solution [95].

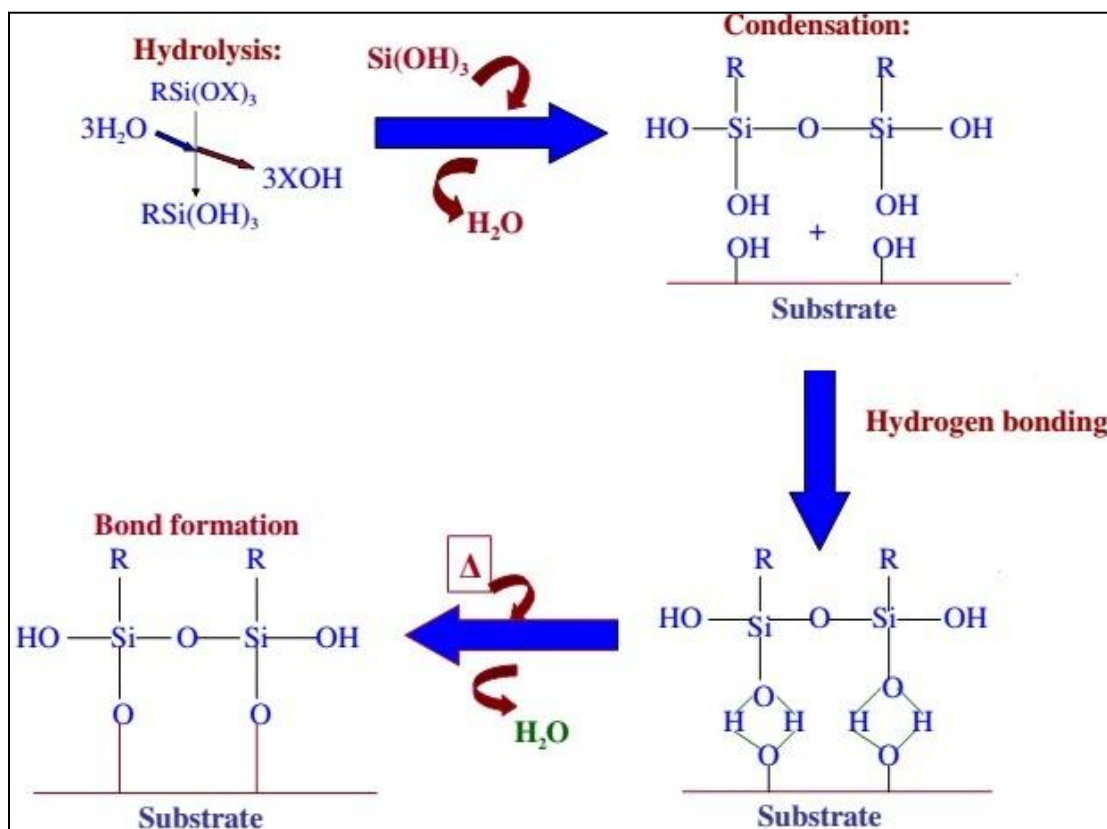


Figure 2.28: Schematic representation of silane hydrolysis, condensation and bond formation with the substrate

Figure 2.29 shows the pH dependency of the hydrolysis and condensation reactions of a typical silane. Under acidic or basic conditions, the rates of both hydrolysis and condensation reactions are high, while at or near neutral pH they are slow. When the reactions are OH^- catalyzed, a high rate of condensation is favored with rapid gelation and when reactions are H^+ catalyzed, a high

rate of hydrolysis is favored with slow gelation. Hydrolysis and condensation will proceed simultaneously unless one of them is limited under specific conditions.

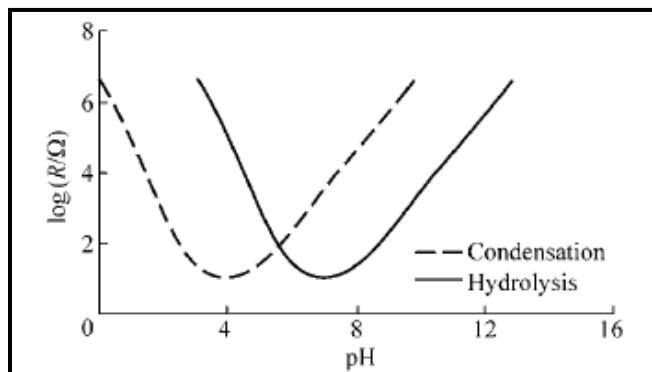


Fig 2.29: Hydrolysis and condensation rate of a typical silane [95]

2.5.3 Application methods

The methods of deposition of silane compounds involve dipping, solution casting techniques, microwave and vapor deposition techniques [95].

2.5.4 Silanes for coating implants and in pharmaceutical application

Silanes have been employed for implants, subcutaneous and intramuscular administration mainly for cancer, neurological and orthopedic applications [99]. Silane modified surfaces have been widely used as model surfaces for drug delivery and biological interactions, including protein absorption and cellular and bacterial adhesion [99, 100] because silica is a biocompatible natural component of the body, that does not affect the pH of the surrounding tissues, reducing the risk of inflammation. They are being used as coatings which provide easy, flexible and effective strategy for drug delivery.

There are various silanes which have been used for coating implants, in pharmaceutical application like drug delivery and for corrosion resistance like phosphonate silanes,

diethylphosphonatoethyltriethoxy-silane $[(C_2H_5O)_2-PO-(CH_2)_2-Si-(OC_2H_5)_3]$ (DEPETES) [101, 102], tetraethoxysilane (TEOS) [103], bis sulphur silanes like bis-[3-(triethoxysilyl)propyl]tetrasulfide(BTESPT), glycidoxypropyltrimethoxysilane (GPTMS), Methyltriethoxysilane (MTEOS) [103], bis(triethoxysilyl)hexane [104]. Applications of such silanes are summarized in the Table 2.5. The second factor which has to be taken in consideration before selecting the silane for the coating system is the corrosion resistance provided by the given silane.

Table 2.4: Silanes used as coating implants and in pharmaceutical applications

S.No.	Silane	Application
1.	3-aminopropyl triethoxysilane	<p>Used for surface modification of silicon microdevices used as bioadhesives agents in oral drug delivery. (Bioadhesive agents are used to enhance contact of the peptide to the intestinal wall. Such local delivery to sites in the gastrointestinal tract allows greater adsorption and stability) [105].</p> <p>As a coating to improve the corrosion resistance on magnesium alloy stents [106]</p> <p>For surface modification of magnetic nanoparticles to be used in drug delivery [107]</p> <p>For functionalization of metallic magnesium with protein layer by acting as linker molecules [108]</p> <p>Used for chemical modification of titanium implant surfaces for covalent attachments of</p>

		<p>biological molecules [109].</p> <p>Aminoalkylsilanes were selected as the spacer molecules because they possess two functional groups, one at each extremity. The silane group was used for attachment to the titanium oxide surface while the amino group was used to couple biological molecules at the opposite end and alkyl spacer can increase the stimulatory effect of biological molecules, such as growth factors immobilized on activated polymers [110]</p> <p>Used in synthesis of cell adhesive hydrogels which are used as scaffolds or for drug delivery [111]</p> <p>Used in surface modification of hydroxyapatite which is a bio-active material that has good biocompatibility, non-toxicity and an ability of promoting bone growth and conjoining with human bone and has been widely used in various medical applications such as orthopedic and maxillofacial applications [112]</p> <p>Can be used in drug delivery [100, 113]</p>
2.	Tetraethoxysilane (TEOS)	<p>Can be used in drug delivery like for coating the surface for controlled release of vitamin B1 from mesoporous silica tablets [114]</p> <p>Can be used with BTSE for controlled</p>

		<p>release of drug from silica xerogels [115]</p> <p>Can be used as precursor for the silica matrix along with tetramethylorthosilicate</p> <p>It has been reported that silanes causes no adverse tissue reactions and degrade in the body to Si(OH)_4 which is eliminated through kidney in the urine [116].</p> <p>Used as coating with MTES for stainless steel implants [117]</p> <p>But the problem with using TEOS solely will be during the curing of film, it can develop cracks and pores during curing</p>
3.	bis-1,2-(triethoxysilyl)ethane (BTSE)	<p>Used as barrier coating on stents along with amino alkylsilane[118]</p> <p>Used along with TEOS for surface modification of silica xerogels used in drug delivery [115, 116]</p>
4.	bis(trimethoxysilyl)hexane	Used for silica matrix for controlled release of drugs [114]
5.	bis(triethoxysilyl)hexane	Used for coating of drug loaded mesoporous silica [119]
6.	bissulphursilanes	Used as coating on magnesium alloys stents
7.	bis(trimethoxysilyl propyl)amine	<p>Used in drug delivery [114]</p> <p>But are highly hydrophilic [120]</p>

8.	Phosphonatosilanes	Found to be non toxic and are used in drug delivery like coating nanoparticles for neural interfaces [101, 102, 121]
9.	Glycidoxypropyltrimethoxysilane	Used in drug delivery [122, 123], as adhesion promoter, in drug delivery systems [124]

2.5.5 Effect of functionalities on corrosion performance of silanes coatings

From the above literature strongly negative charged surfaces such as PO_4H_2 , COOH and OH^- terminated surfaces, have a greater induction capability for the heterogeneous nucleation and growth of HA as calcium and phosphorus tend to bind to this hydrated oxide layer [125]. Calcium phosphate coated implants enhanced bonding of bone with the implant surfaces, in addition to accelerating bone growth. The hydroxyl group functionality ($-\text{OH}$) represents a neutral, hydrophilic surface. Early research into surface functionality suggested that an increase in oxygen containing functionalities was proportional to cell growth [125, 126] but being hydrophilic do not provide good stable coating [127].

Amine group ($-\text{NH}_2$) functionality displays a positive charge to the biomaterial surface. Studies show favorable protein conformations after adsorption to the positively charge $-\text{NH}_2$ surface [126] but amino silanes protonates during hydrolysis and attracts Cl^- and might not provide desirable corrosion resistance [127].

2.5.6 Diethylphosphonatoethyltriethoxy-silane (DEPETES)

Phosphonato silanes like Diethylphosphonatoethyltriethoxy-silane $[(\text{C}_2\text{H}_5\text{O})_2\text{-PO-(CH}_2)_2\text{-Si-(OC}_2\text{H}_5)_3]$ based coatings demonstrate superior corrosion protection performance for the magnesium AZ31B alloy [128, 129]. Potentially, both functionalities of this compound (trialkoxo silane and trialkoxyphosphonate) are hydrolysable. However, since the ethoxy-

phosphonate groups are more stable in dilute acetic acid environment, initially, DEPETES undergoes acid-catalyzed reactions of hydrolysis and condensation through its triethoxy-silane structural fragment as shown in the Figure 2.30, crosslinking with TEOS. The self-condensation of DEPETES silane leads to water soluble products and unstable coatings. To increase the stability of the coating, silica content of the coating was increased by adding TEOS with DEPETES silane at different molar ratios and it was found that P-O-Mg bond is more hydrolytically stable on coating/substrate interface than the Si-O-Mg bond.

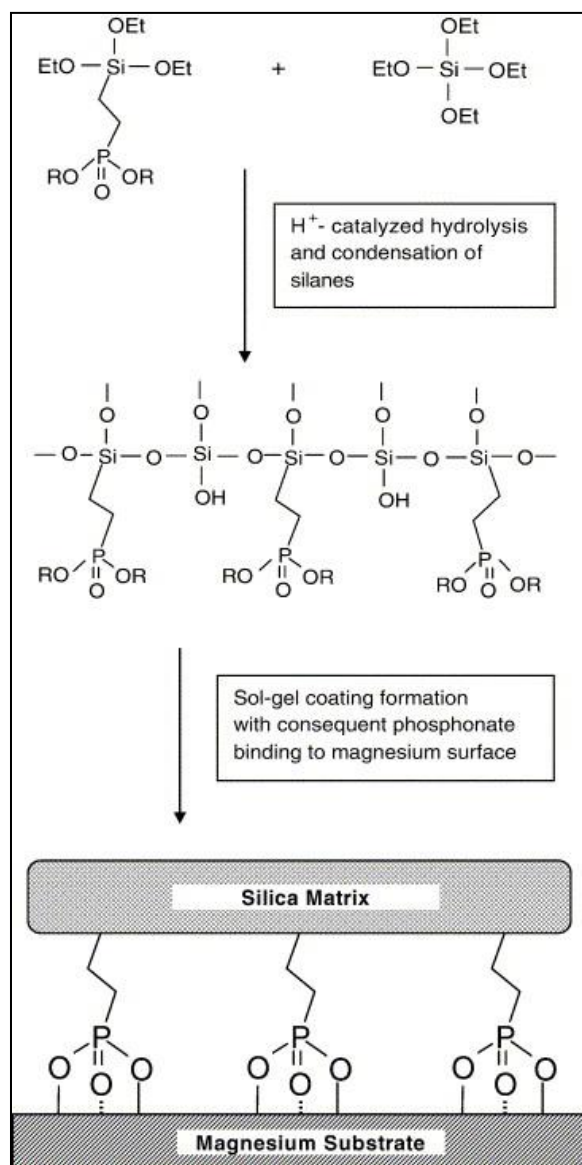


Figure 2.30: Schematic of sol-gel processing of hybrid coatings with phosphonate functionalities [128]

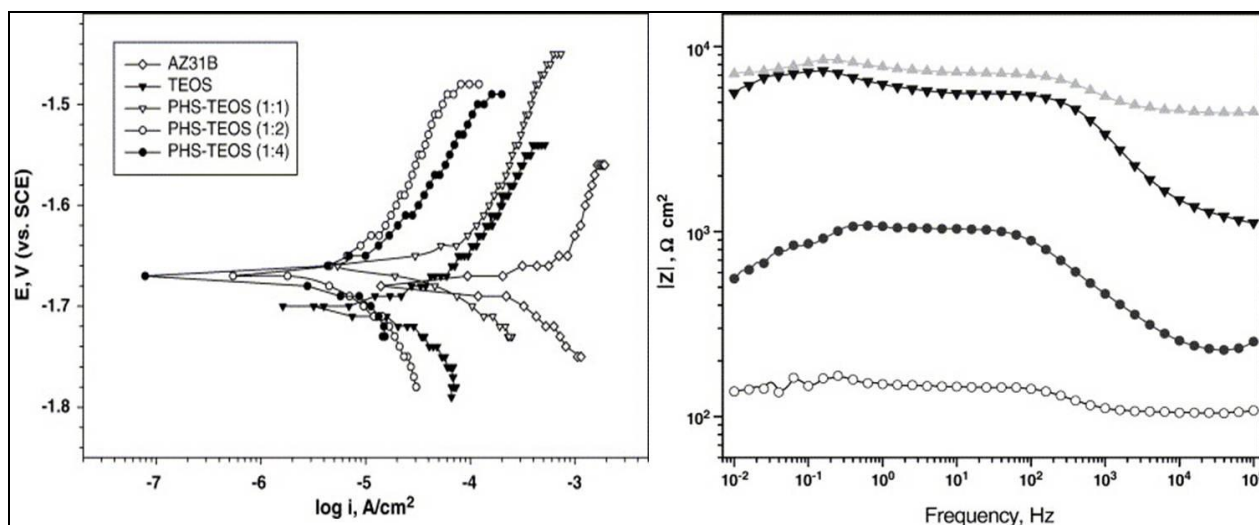


Figure 2.31: (a) Potentiodynamic scans and (b) electrochemical impedance spectra of the sol-gel coatings with phosphonate groups after 30 min immersion in dilute Harrison's solution. The hybrid sol-gel coatings were formulated with different PHS to TEOS molar ratio [128]

The corrosion protection of the resulting coatings was examined using the potentiodynamic polarization technique. The anodic polarization scans shown in Figure 2.31 demonstrated a significant improvement in corrosion performance of the coating as suggested by the substantial suppression of the corrosion current. The decrease in corrosion current was observed for the sample coated with silica (TEOS) film compared to uncoated magnesium sample and a further decrease in corrosion current for the coatings processed with the increasing amount of DEPOTES. However, as the content of DEPOTES is increased to a 1:1 molar ratio, the reversal in corrosion resistance was observed because of instability of coating material in water when it was processed with an excess of the phosphonato-silane in the coating system [128]. The EIS Bode plots for the coated and uncoated (control) AZ31B (Figure 2.31(b)) suggested a large increase in impedance modulus in the following order of samples: uncoated «silica coated» coated with 1:4 or 1:2 PHS: TEOS film. The observed enhancement in coatings performance was because of the presence of phosphonate functionalities within the organo-silicate matrix as their chemical bonding to the alloy surface directly affects stability and barrier properties of the coating/substrate interface [128].

Khramov et al [129] studied the effect of various silane co-reagents like Tetraethoxysilane (TEOS), methyltriethoxysilane (MTEOS), dimethyldiethoxysilane (DMDES) with DEPETES on corrosion resistance. It was found that the corrosion protection decreases in the order of the increased hydrophobicity of the materials: DEPETES–TEOS > DEPETES–MTEOS > DEPETES–DMDES (Figure 2.32). The DEPETES–TEOS coating showed highest corrosion protection, whereas DEPETES–DMDES coating showed limited corrosion protection. This was explained by the possibly lower crosslinking density of the PHS–DMDES films (due to lower amount of the silanol groups) and the possible nanoscale phase separation due to increasing differences between the hydrophilic silica and hydrophobic methyl-siloxane clusters, leading to increased porosity (i.e., lower film barrier properties).

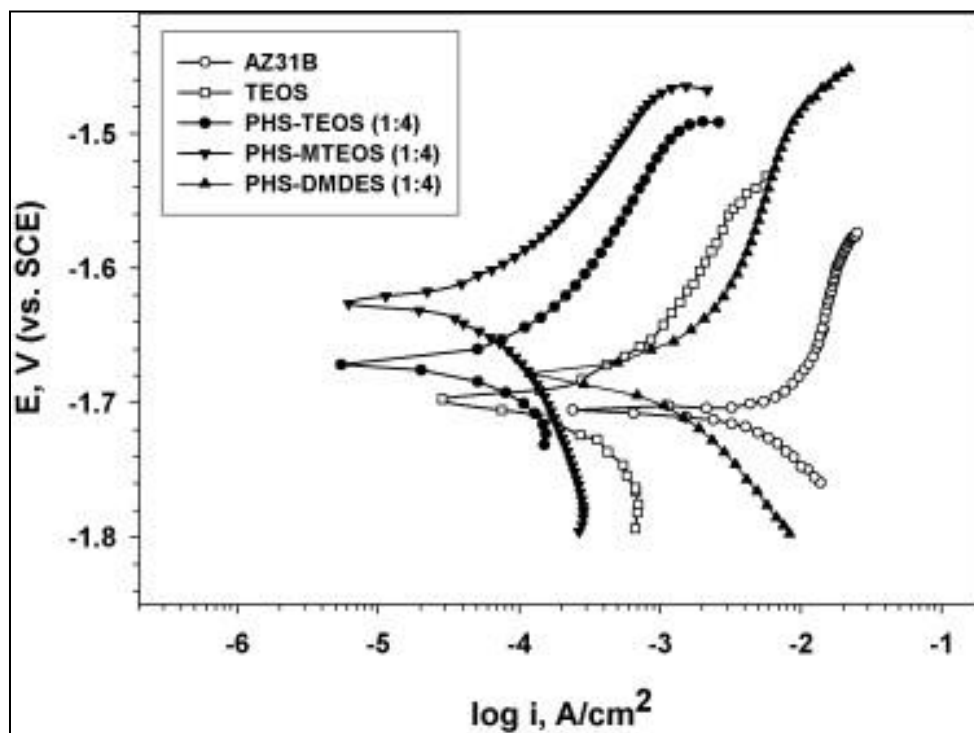


Figure 2.32: Potentiodynamic scans of the phosphonate-functionalized coatings obtained by sol–gel processing of PHS and different silane co-reagents at constant (1:4) molar ratio (substrate—AZ31B; in dilute Harrison’s solution) [129]

2.5.7 Glycidoxypropyltrimethoxysilane (GPTMS)

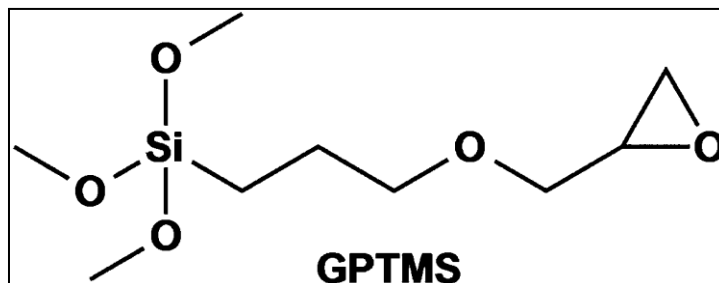


Figure 2.33: Structure of GPTMS

3-glycidoxypropyltrimethoxysilane (GPTMS) is most commonly used epoxy silane. It is a reactive chemical containing a glycidoxy organic group and a trimethoxy group (Figure 2.33). Possessing both organic and inorganic reactivity, GPTMS can react with organic resins as well as the surface of inorganic material such as ferrous alloy, aluminum alloys, and silica. GPTMS has been used in transparent abrasion-resistant hybrid coatings for polymers and metals. Hydrolysis of the methoxy groups gives silanol groups which can subsequently condense to form the silica network. The Si atom in GPTMS is tri-functional in terms of reactive methoxy groups with an epoxy rings which can be opened and polymerized to form a linear poly(ethylene oxide) organic network. Cross-links between the two networks arise either from the pre-existing link in the GPTMS molecule, by direct reaction of silanols with epoxy rings, or by condensation of silanols with hydroxyl of the opened epoxy rings. The uncatalyzed ring opening reaction occurs at a useful rate only at elevated temperature and so thermal curing is required. However, all the condensation reactions are catalyzed by other metals (Al, Ti, Zr) introduced into the sol-gel system. However GPTMS is hydrophilic and can result in a very poor coating in terms of corrosion resistance but hydrophobic silane films can somehow be obtained from hydrophilic silanes, such as addition of silane crosslinkers such as TEOS in small amounts to increase the film hydrophobicity by increasing the crosslink density of the films [95].

Pathak et al [130] studied the coating prepared by hydrolysis and condensation of methyltrimethoxysilane (MTMS) and GPTMS in the presence of acid catalyst and amino functional organosilanes namely 3-aminopropyltrimethoxysilane (1N), *N*-(2-aminoethyl)-3-aminopropyltrimethoxysilane (2N) as hardeners. The optimum concentration of GPTMS to hardeners (1N and 2N) and the effect of MTMS:GPTMS molar ratios on corrosion resistance of coatings were studied. Corrosion resistance and porosity in coatings were measured by potentiodynamic polarization studies and electrochemical impedance analysis.

They also synthesized organically modified silane (ormosil) coating for corrosion protection of aluminum alloy[131]. GPTMS/MTMS sol-gel solution was prepared by hydrolysis and condensation of 3-glycidoxypropyltrimethoxysilane (GPTMS) and methyltrimethoxysilane (MTMS) in aqueous solution of 0.05M acetic acid in molar ratios 3:1. To prepare the ormosil coating solutions, a crosslinking agent hexamethoxymethylmelamine (HMMM) and a blocked acid catalyst *p*-toluenesulphonic (*p*-TSA) were combined with the sol-gel solution for aluminium substrate.

Davis et al [132] studied the effect of heat treatment and the amine/epoxy ratio on the formation silica/epoxy hybrid network polymer. Epoxy-based inorganic-organic hybrid polymers were prepared using GPTMS and Diethylenetriamine as a crosslinking agent by a sol-gel process. The precursor, GPTMS, possesses both epoxy and silicon alkoxide functionality and so interlinked inorganic-organic networks can be formed.

Zandi-zand et al [133] developed a hybrid coating on 1050 aluminum by hydrolysis and condensation of GPTMS and tetramethoxysilane in the presence of an acidic catalyst and bisphenol A as cross-linking agent. The hybrid coatings thus developed were found to be relatively dense, uniform and defect free. Khramov et al. [134] prepared a amino-silane conversion coating for aluminum alloys by self-assembled nanophase particle (SNAP) coating process. SNAP solution was prepared by a drop-wise addition of a mixture of

Tetramethoxysilane (TMOS) and 3-glycidoxypropyltrimethoxysilane(GPTMS) (1:3 ratio) to 0.05M acetic acid at constant stirring for 1h and applied on aluminum by dip coating method. Four crosslinking agents were used are as follow:

- Diethylenetriamine (DETA)
- Aminopropyltrimethoxysilane(1A)
- 3-(2-aminoethyl)aminopropyltrimethoxysilane (2A)
- 3-(Trimethoxysilyl)propyl diethylenetriamine (3A)

Corrosion current density (I_{corr}) and corrosion potential (E_{corr}) of coated aluminum substrate with different crosslinking agent were investigated by Tafel method. The corrosion resistance of the coating, as shown in Figure 2.34, increased with the number of amino functionalities.

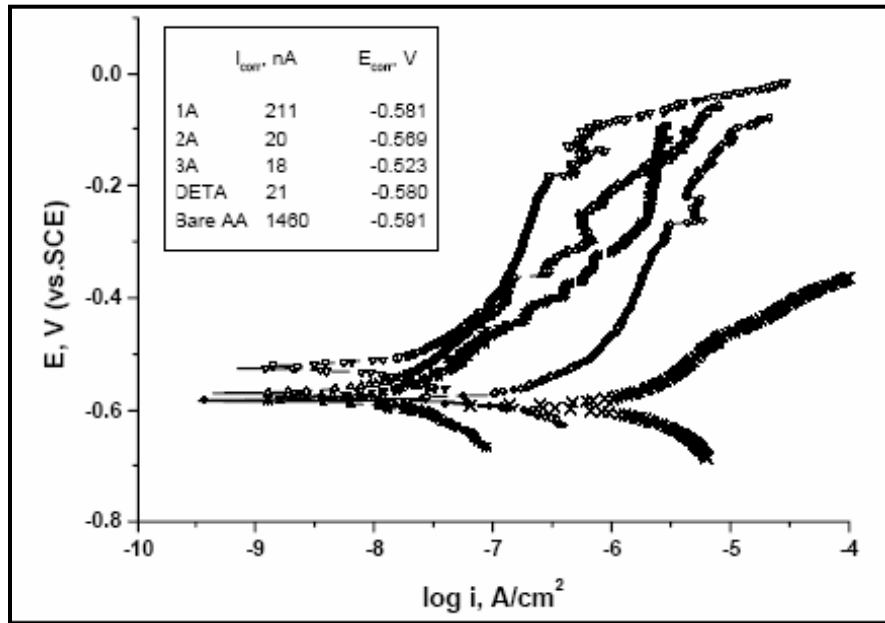


Figure 2.34: Potentiodynamic scans of AA 2024-T3 coated with SNAP coatings prepared with different crosslinking agents (1A (O), 2A (Δ), 3A (▼), DETA(□)), and bare AA 2024-T3 (×). The inset is corrosion current densities and corrosion potentials estimated by

Tafel analysis

2.5.8 Bis-silanes like bis-[triethoxysilylpropyl]tetrasulfide (BTESPT)

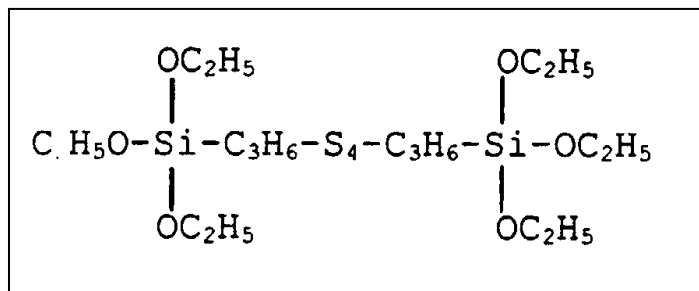


Figure 2.35: Structure of BTESPT

Studies have shown that bis-silanes show superior protection on metal surfaces, especially when used in conjunction with organofunctional mono-silane treatments for adhesion to other organic layers. These compounds have structures $X_3\text{Si}(\text{CH}_2)_n\text{Y}(\text{CH}_2)_n\text{SiX}_3$ or can exist with no functional group with the following structure $X_3\text{Si}(\text{CH}_2)_m\text{SiX}_3$ (Figure 2.35). They enhance performance by depositing a more pronounced hydrophobic polysiloxane layer (Si-O-Si linkages) during condensation, but still allow chemical coupling using the functional group present either in the dipodal silane itself or with a mono-silane solution additive [95].

The stronger interfacial adhesion of bis-silanes is one of the key factors that contribute to their impressive corrosion performance on metals, as compared to mono-silanes. It is imperative to understand the bonding mechanisms for bis-silanes and mono-silanes to the Al substrate. Each bis-silane molecule contains 6 hydrolysable-OR groups; this is twice as many as those in the mono-silane molecule. When silanes are hydrolyzed completely, each bis-silane molecule would generate 6 SiOH groups available for the subsequent reactions while each mono-silane molecule only has 3 SiOH groups. The metal substrate treated with the hydrolyzed and condensed silane forms M-O-Si covalent bonds formed at the metal silane interface and, Si-O-Si bonds within the silane films. Since the number of SiOH groups of the bis-silane molecules is twice that of the mono-silane molecules, bis-silane molecules are capable of reacting more effectively with the

metal substrate forming an interface with a high density of M-O-Si bonds and simultaneously building up a crosslinked silane film (i.e., Si-O-Si network) of an appreciable thickness on the top. Mono-silane molecules, however, cannot achieve this since each monosilane can only generate 3 Si-OH groups. A comparison of the possible interfacial regions formed in these two systems is presented in Figure. 2.36. On this basis, it is reasonable to expect that the bis-silanes have a stronger adhesion to the metal substrate than the mono-silanes[135].

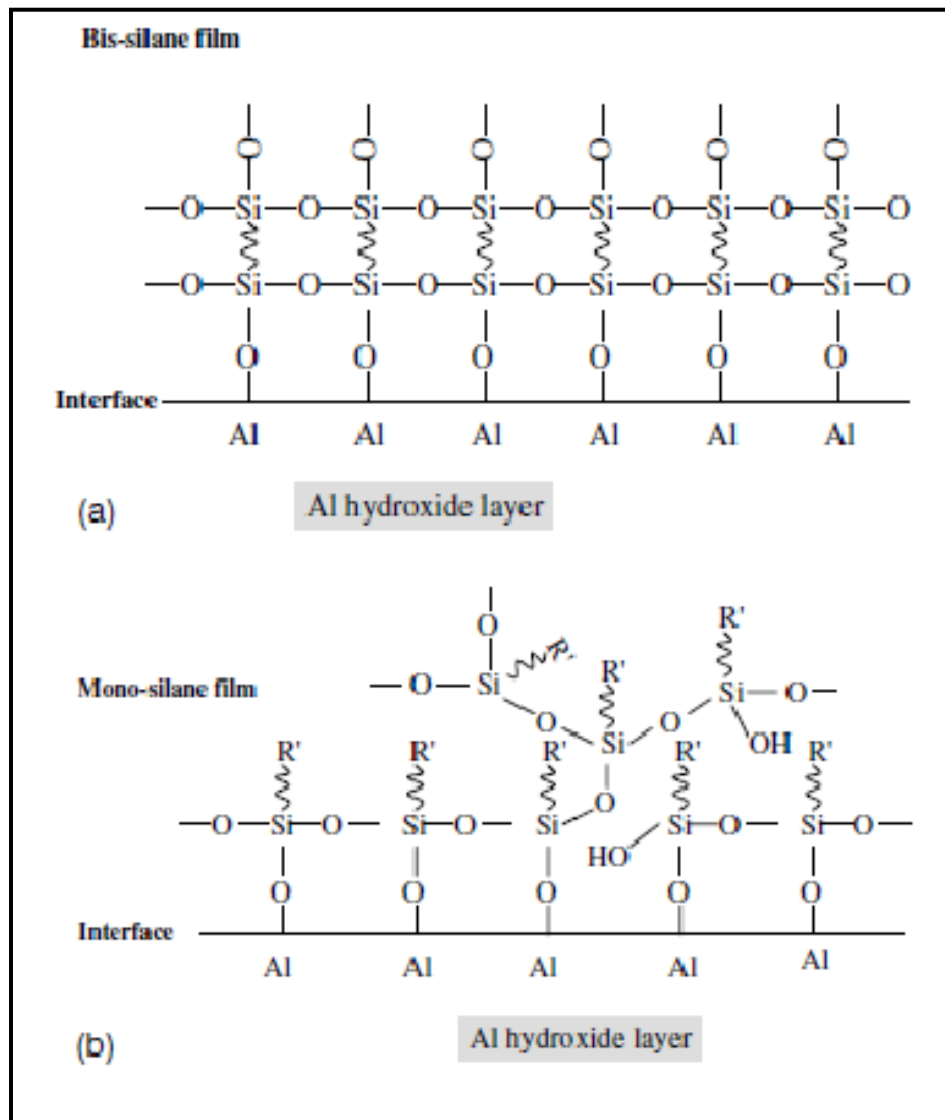


Figure 2.36: Bonding mechanism in (a) bis-silane and (b) mono-silane with Al substrate [135]

Sulphur based silanes might show superior protection because S chain of the bis-sulfur silane in the corrosion protection of AA 2024-T3 could provide a hydrophobic nature. [135]

Cabral et al [136] carried out a did comparative study on the corrosion resistance of AA2024-T3 pre-treated with three different silane solutions, viz; 1,2-bis(triethoxysilyl)ethane (BTSE), BTESPT and γ mercaptopropyltrimethoxysilane (γ -MPS) (Figure 2.37).

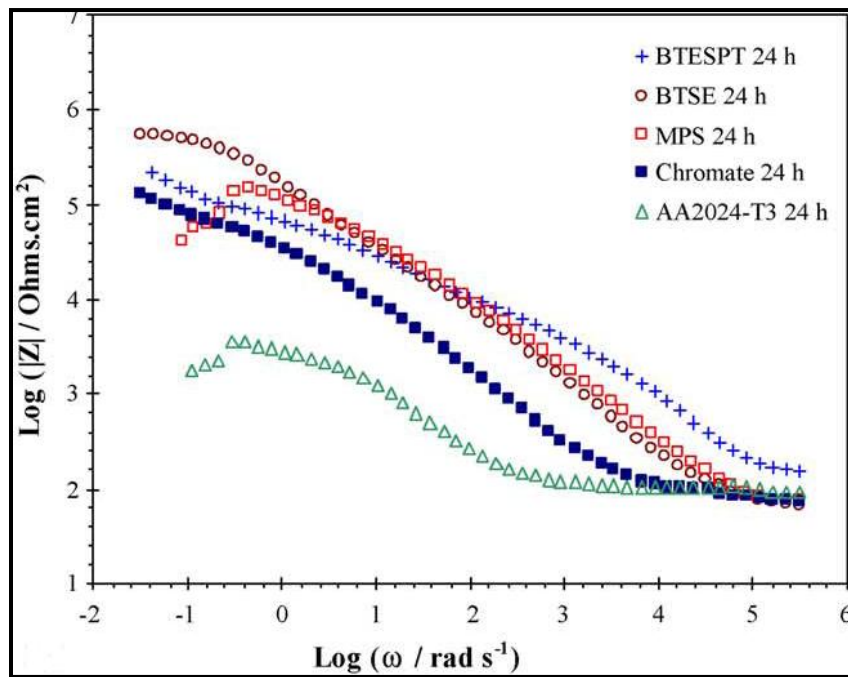


Figure 2.37: EIS Bode plots of AA2024-T3 alloy and the alloy with three different pretreatments immersed in 0.1N NaCl for 24 h [136]

It was concluded that Bis-silanes lead to thicker and more homogeneous films, whereas the mono-silane leads to thinner and relatively non-uniform films. The former also has higher capability to form Al-O-Si bonds at the interface. Though all silanes provided some protection, for the BTESPT pretreated system the charge transfer resistance is more than an order of magnitude greater than those pretreated with BTSE and MPS. These results account for higher corrosion resistance of the substrate pre-treated with BTESPT.

Danqing Zhu and van Ooij also studied the corrosion protection of AA 2024-T3 by films of BTESPT in a neutral 0.6 M NaCl solution (Figure 2.38) [135].

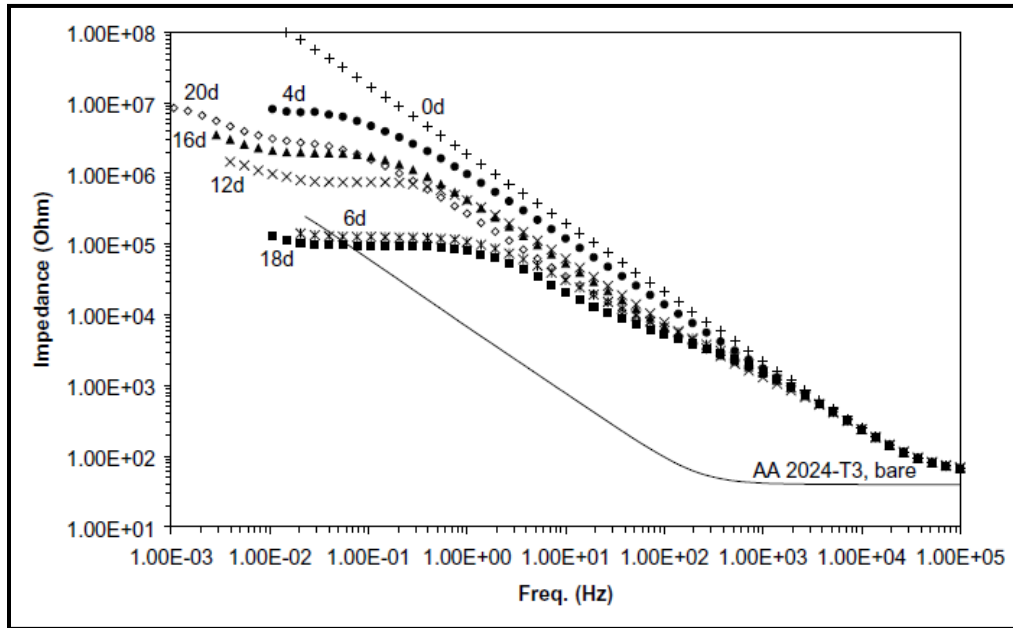


Figure 2.38: Bode plots of bis-sulfur silane-treated AA 2024-T3 during immersion in a neutral 0.6 M NaCl solution for different durations (upto 20 days) [135]

Zhu and Van Ooij[135]gave two major failure modes for silane-treated metal systems, since both result in shortcuts between the substrate and the electrolyte and thus accelerate the pitting of the substrate afterwards. Therefore, a high resistance of silane-treated systems to film cracking and delamination is required for corrosion protection. The former can be achieved by curing the silane film at an elevated temperature for a longer time to decrease film porosity. The latter, however, is mainly determined by the nature of interfacial adhesion. In general, the stronger the adhesion of the silane films to the substrate, the greater the resistance of the film.

Montemor and Ferreira [33] studied the effect BTESPT pre-treatments modified with cerium nitrate or with lanthanum nitrate on the AZ31Mg alloys. The samples were tested during immersion in 0.005M NaCl (Figure. 2.39).

They concluded that pre-treatments for the AZ31 Mg alloy using BTEPST silane solutions provided corrosion protection. The addition of cerium nitrate or lanthanum nitrate to the silane solutions further improved the barrier properties of the silane films and decreased the corrosion rate of the metallic substrate.

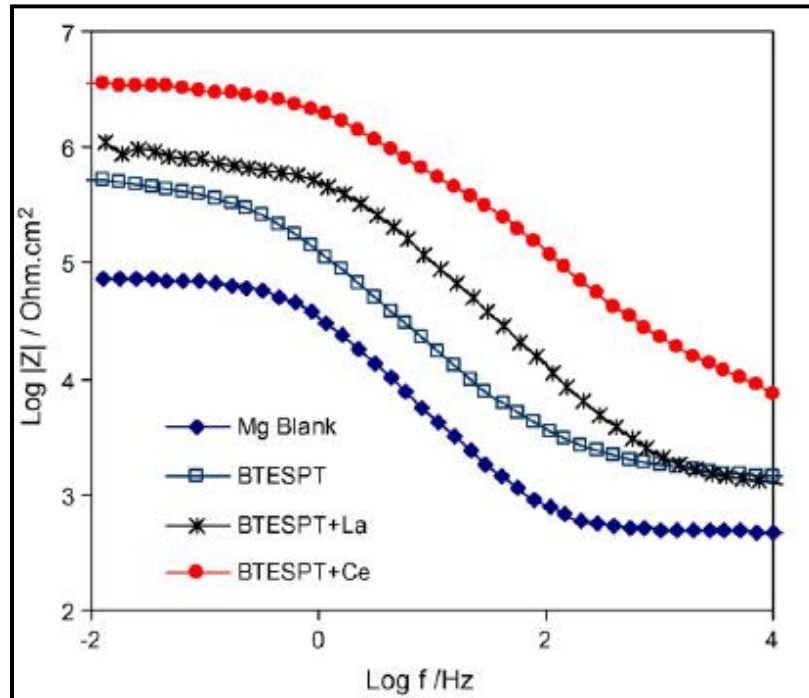


Figure 2.39: EIS Bode plots obtained for the bare AZ31 Mg alloy and for the same alloy pre-treated with BTESPT, BTESPT+Ce(NO₃)₃ and BTESPT+La(NO₃)₃ after 24 h of immersion in 0.005M NaCl[33]

When the silane film is immersed in the aggressive electrolyte there is deterioration of the outer layers of the film. This may cause leaching of cerium ions and La incorporated in the outer layers of the siloxane matrix to the vicinity of the anodic areas where they precipitate in the form of

Ce(III) or Ce(IV) hydroxides and La(III) hydroxides. These species are more insoluble than can be more effective in hindering the cathodic activity hindering the corrosion reactions.

Danqing and van Ooij [137] also studied corrosion resistance of AA 2024-T3 and hot-dip galvanized steel (HDG) after treatment with BTESPT, bis-[trimethoxysilylpropyl]amine (bis-amino silane), and their mixture in 0.6M NaCl (Figure 2.40).

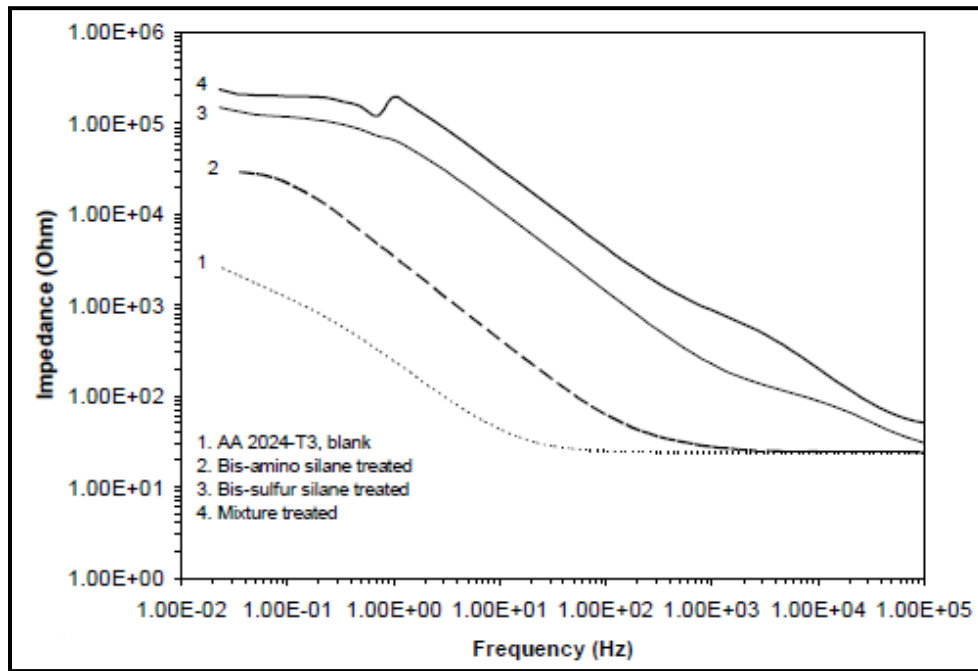


Figure 2.40: Bode plots of silane-treated AA 2024-T3 panels in a 0.6M NaCl solution (pH 6.5) after 32 days of exposure [137]

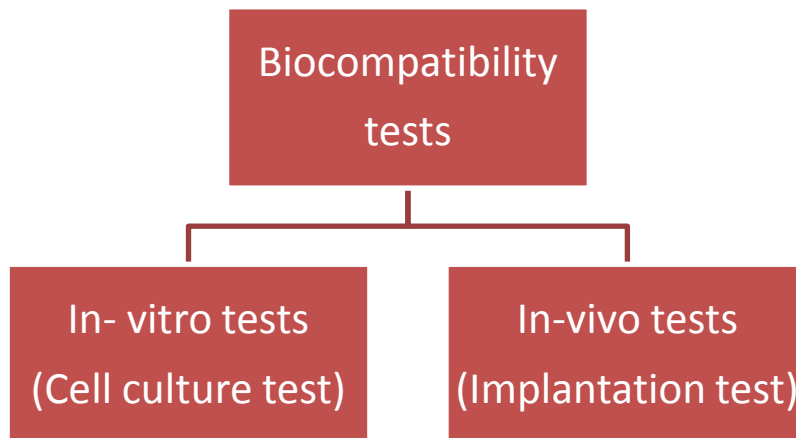
The results showed that hydrophilic bis-amino silane did not offer good corrosion protection on either of the metals because bis-amino silane film tends to be positively charged. This promotes ingress of anions like Cl^- ions as well as water into the film by electrostatic attraction. As a result, corrosion readily proceeds at the interface hydrophobic bis-sulfur silane performed very well on AA 2024-T3, but failed on HDG. The failure occurred from non-uniform film coverage on HDG owing to an insufficient wetting of bis-sulfur silane solution on the Zn oxide on HDG. Local corrosion initiates at defective sites which were poorly covered by the silane film.

Therefore, Sol–gel protective coatings on metal and alloy surfaces can improve their corrosion resistance in various corrosive mediums and practical applications.

2.6 Biological testing of biomaterials

Without any surface modification the initially high reactivity of Mg surface and the consistent hydrogen evolution does not enable adhesion and survival of cells on the surface and hence delay the bone healing process. Application of surface coating on the alloy can significantly increase the cell survival rate by initially enhancing the cell adhesion on the surface.

Biomaterials are evaluated using in vitro and in vivo conditions.



In vitro cytotoxicity test

Tests are done in test tube, cell culture dish, i.e. outside a living organism. The in vitro tests for cytotoxicity assess the response of cells in culture to direct contact with devices or to their extracts. The biological response of the samples has been evaluated by in vitro cell tests using MC3T3-E1 preosteoblast, L-929 mouse cell line, MG-63 osteosarcoma human cell line etc to observe cell attachment, viability and differentiation.

Cytotoxicity tests are performed to evaluate the bio-compatibility of a bio-medical material and/or device. The requirement of *in vitro* cytotoxicity tests has been driven by the need to rapidly evaluate the potential toxicity of large numbers of compounds, to limit animal experimentation whenever possible, and to carry out tests with small quantities of compound.

2.6.1 Categories of Evaluation

The endpoints measured in cytotoxicity determination can be grouped into the following categories of evaluation:

- a. Assessments of cell damage by morphological means
- b. Measurements of cell damage
- c. Measurements of cell growth and proliferation
- d. Measurements of specific aspects of cellular metabolism

There are several means of producing results in each of these four categories.

2.6.2 The most common assays for determining cytotoxicity

Measurement of cell viability and proliferation forms the basis for numerous *in vitro* assays of a cell population's response to external factors. There are several assays to determine the cell response:

2.6.2.1 Neutral red (NR)

The NR assay investigates the viability parameter, based on the physical uptake of neutral red.

2.6.2.2 MTT ((3-(4,5-dimethylthiazol-2-yl)-2,5-diphenyltetrazoliumbromide)) assay

1. MTT assay determines the metabolic activity.

2. The MTT Cell Proliferation Assay measures the cell proliferation rate and conversely, when metabolic events lead to apoptosis or necrosis, the reduction in cell viability.
3. The reduction of tetrazolium salts is now widely accepted as a reliable way to examine cell proliferation. The yellow tetrazolium MTT (3-(4, 5-dimethylthiazolyl-2)-2, 5-diphenyltetrazolium bromide) is reduced by metabolically active cells, in part by the action of dehydrogenase enzymes, to generate reducing equivalents such as NADH and NADPH.
4. The resulting intracellular purple formazan can be solubilized and quantified by spectrophotometric means.

2.6.2.3 XTT(2,3-bis-(2-methoxy-4-nitro-5-sulfophenyl)-2H-tetrazolium-5-carboxanilide)

1. Has been proposed to replace MTT, yielding higher sensitivity and a higher dynamic range.
2. The formed formazan dye is water soluble, avoiding a final solubilization step

2.6.2.4 BrDU (5-bromo-2'-deoxyuridine)

1. BrdU incorporated into cellular DNA during cell proliferation using an anti-BrdU antibody. When cells are cultured with labeling medium that contains BrdU, the pyrimidine analog is incorporated in place of thymidine into the newly synthesized DNA of proliferating cells.
2. The magnitude of the absorbance for the developed color is proportional to the quantity of BrdU incorporated into cells, which is a direct indication of cell proliferation.

2.6.2.5 Alkaline phosphatase activity

1. Any condition that affects bone growth or causes increased activity of bone cells can affect ALP levels.
2. Is used to study cell differentiation over a period of time.

3. During this reaction, pNPP (p-nitrophenyl phosphate) was converted into pNP (p-nitrophenol) in the presence of ALP, and therefore, the pNP production rate was proportional to the ALP activity [82, 83].

2.6.3 Advantages and Disadvantages

1. MTT, XTT and NR assays are widely accepted in bio-compatibility and cytotoxicity studies for the assessment of viability and growth of cells because they are easy, fast and cheap [138-140], non-radioactive and work specifically with living and metabolically active cells, not with dead cells or erythrocyte.
2. However, Fischer et al. [141] have shown that tetrazolium-salt-based assays, i.e. MTT, which are widely used in practice, are influenced by the corrosion products of Mg-based alloys. This can lead to false results of cell viability for Mg-based alloys. They also suggested the alternative to these tetrazolium-salt-based assays, which can be BrdU assay, LDH assay and Alkaline phosphatase activity test [140].

2.6.4 Experimental Procedure

In general, the experimental technique for determining cytotoxicity involves mainly four steps, which are:

- a. Grow cells in a specified medium
- b. Add compound and incubate for definite time period
- c. Perform testing to find out the cell viability
- d. Perform data analysis

ISO standard 10993-5 (Biological evaluation of medical devices - Part 5: Tests for in vitro cytotoxicity) describes test methods to assess the in vitro cytotoxicity of medical devices [142].

2.6.5 Kinds of cytotoxicity tests

2.6.5.1 Extract test

Few days prior to the cell seeding, the samples are incubated in cell culture medium for a definite time period under cell culture conditions in multiwell well plates. The obtained extracts then are applied to the cells in different concentrations (100%, 75%, 50% and 25%) and the dilution of the extracts is made with cell culture medium.

2.6.5.2 Direct contact test

In this method, a piece of test material is placed directly onto cells growing on culture medium. The cells are then incubated. During incubation, leachable chemicals in the test material can diffuse into the culture medium and contact the cell layer.

2.6.5.3 Indirect contact test

In this method, a thin layer of nutrient-supplemented agar is placed over the cultured cells. The test material (or an extract of the test material dried on filter paper) is placed on top of the agar layer, and the cells are incubated. A zone of malformed, degenerative or lysed cells under and around the test material indicates cytotoxicity.

Generally direct contact methods have various advantages, because they mimic physiological conditions but the choice of one or more of these categories depends upon the nature of the sample to be evaluated, the potential site of use and the nature of the use.

2.7 Gaps in the literature

Surface modification plays an important role in practical applications of magnesium-based alloys as evaluated by the reported in-vitro and in-vivo tests. By surface modification, better corrosion resistance and surface biocompatibility of magnesium and its alloys have been achieved. Although these surface modification methods proved to be a big achievement in improving the biomedical performance of magnesium alloy, several gaps has been observed in the existing coating systems for their application as bioimplants:

- 1) Most of the in-vitro corrosion studies reported so far is on magnesium alloys either with aluminum or rare earths as alloying elements, i.e. the elements that are considered to be unfavorable for implant application.
- 2) Surface pre-treatments like alkaline pretreatment or phosphate pretreatment provides corrosion resistance for a short interval of time (1-2 days). After this duration, the high reactivity of magnesium surface leaves the alloy incompatible.
- 3) Among developed coatings, micro arc oxidation (MAO) coating provides enhanced corrosion resistance and high adhesion strength to substrate. However, the long-term corrosion resistance of this coating is not satisfactory because of its surface porous structure. Also MAO coating is brittle in nature. PEO coating also lack surface biocompatibility for cell attachment and proliferation on its surface. So more efforts should be directed to improving its surface biocompatibility. Reducing the porosity of the coating by optimizing the preparation parameters needed to be further investigated for practical application.
- 4) Inorganic coatings, like HA and calcium phosphate based coatings, the concern is about the lack of adhesive strength. So for this kind of coatings, an improvement in adhesion strength to magnesium substrate needs to be investigated.
- 5) For ion implantation, the modified layer is very thin. So the enhancement of corrosion resistance for magnesium-based materials is not satisfactory for long term application.
- 6) Silane based coating developed on magnesium alloy thus, showed a maximum coating life of about 42 h which is insufficient to be used as an implant material.

- 7) Incomplete literature is available about time dependent degradation of any developed coating to provide an idea about the life of coating, biocompatibility/toxicity of the post corrosion products formed after the degradation.

2.8 Aims and Objectives

Metallic implants such as titanium, stainless steel, and cobalt-chromium alloys are commonly used as permanent body implants to provide stability to the damaged bone tissue. However, in some cases these implants become unnecessary after healing has occurred. Therefore biodegradable metallic materials such as magnesium and its alloys are very attractive due to their outstanding mechanical strength and relatively non-toxic degradation products. Unfortunately, the poor corrosion resistance of magnesium in physiological environment has limited its clinical application as an orthopedic implant material. Therefore, the overall objective of this thesis is to develop a biocompatible protective coating that can slow down the dissolution of a biodegradable magnesium alloy (Mg-6Zn-Ca) in the early stages of healing while enhancing the biocompatibility of the alloy.

Therefore, the main objectives of the present research are:

- a) Optimization of the surface treatment of Mg-6Zn-Ca alloy in NaOH before application of silane based coating.
- b) Development of a phosphonato – silane and a non-phosphonato silane based coating systems for effective corrosion resistance and biocompatibility with the human body as an implant material.
- c) To characterize the corrosion resistance of the coated alloy in simulated body fluid and the associated mechanism via hydrogen evolution, pH study, electrochemical impedance spectroscopy and potentiodynamic polarization tests for corrosion evaluation.
- f) In-vitro cytotoxicity tests for the final compositions of the coating system.

MG-63 human osteoblast cell morphology, cell attachment, proliferation and differentiation over a period of time on the coated sample as compared to bare Mg-6Zn-Ca alloy.

Chapter 3

Experimental Work

The experimental work consists of the development of silane based sol gel coatings to control the corrosion of chosen magnesium alloy Mg-6Zn-Ca as body implant in the physiological environment. Three coating systems using different silanes and on Mg-6Zn-Ca alloy samples were tested. Silane coating formulations used were:

- 1) Phosphonate silane based coating formulation
- 2) Non-phosphonate silane based coating formulation

Coatings were applied using dipping method and cured at optimum temperatures for adequate period. The coating morphology was characterized using Scanning Electron Microscopy (SEM), Energy Dispersive X-ray analysis (EDAX), X-ray diffraction (XRD) and the crosslinking in the coating was studied using Fourier Transform Infrared Spectroscopy (FTIR). Corrosion resistance of the coatings was evaluated using potentiodynamic polarization and electrochemical impedance spectroscopy (EIS). During immersion test, hydrogen evolution and pH variation, were also monitored for both bare and coated alloys. Mechanical properties of coatings were also evaluated using crosshatch adhesion and pencil hardness.

The biological response of the samples was evaluated by in-vitro cell tests using human osteosarcoma cells MG-63 to observe cell attachment, viability and differentiation. Fig 3.1 presents the work flow chart of the test program.

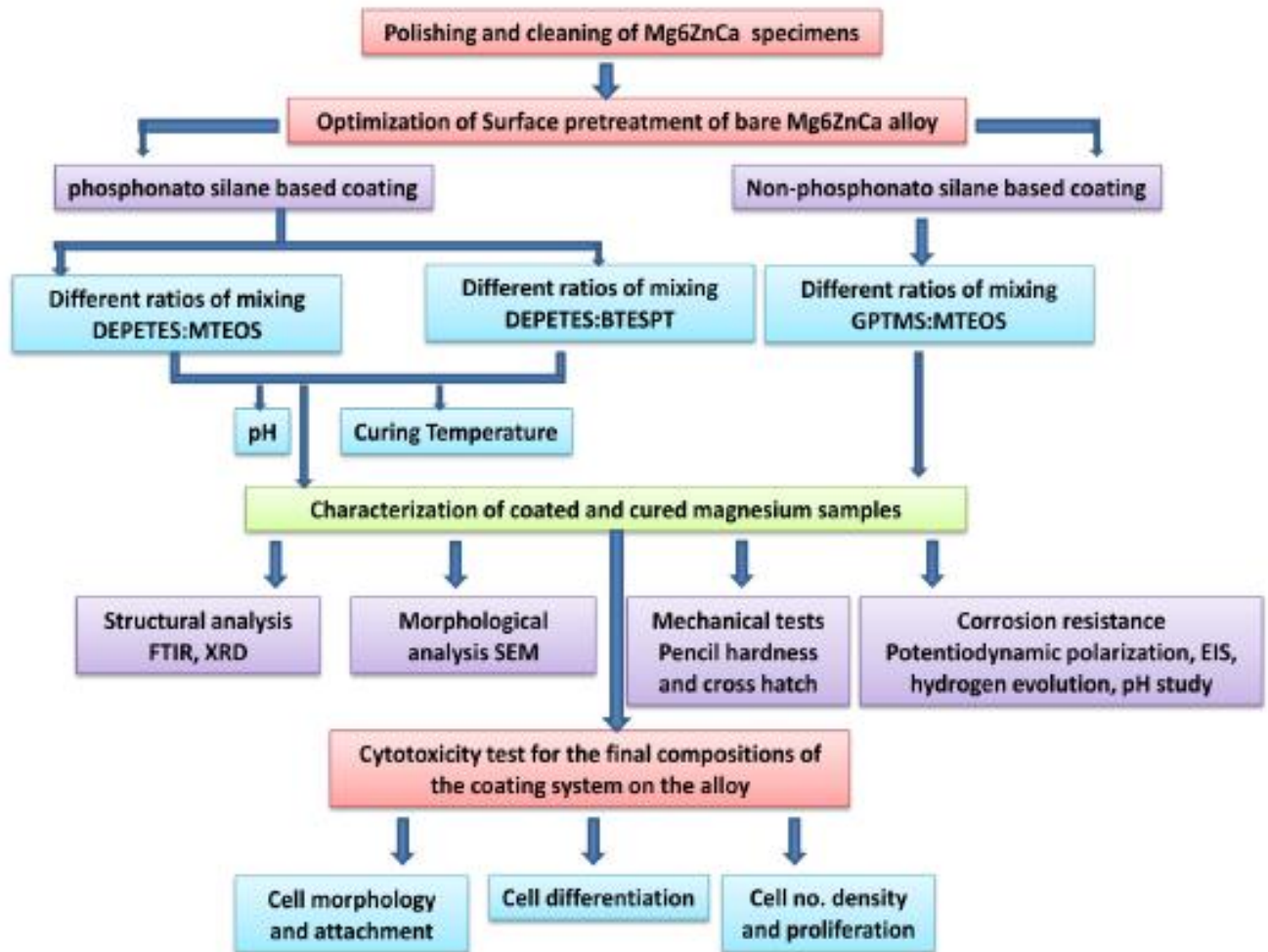


Figure 3.1: Work flow chart

3.1 Materials, reagents and test environment

3.1.1 Material

Magnesium alloy used in the present study was received from Monash University and the composition was determined by Inductively Coupled Plasma Optical Emission Spectroscopy (ICP-OES) as shown in Table 3.1.

3.1.2 Reagents

Diethylphosphatoethyltriethoxysilane (DEPETES), Methyl triethoxysilane (MTEOS), Glycidoxypropyltrimethoxysilane (GPTMS) and bis-[3-(triethoxysilyl) propyl] tetrasulfide (BTESPT) silane were procured from Gelest and Sigma Aldrich, respectively. Ethanol, glacial acetic acid and NaOH were procured from Merck.

3.1.3 In-vitro Corrosion test environment

In-vitro corrosion tests were carried out in modified-simulated body fluid (*m*-SBF) that was maintained at 36.5 ± 0.5 °C throughout the testing. The composition of *m*-SBF is given in Table 3.2. The solution was buffered with 2-(4-(2-hydroxyethyl)-1-piperazinyl) ethanesulfonic acid (HEPES) to simulate the physiological pH of 7.4. This pH was verified for each test.

3.1.4 In-vitro Biocompatibility test environment

A human osteosarcoma cell line MG-63 was used to assess the cell response to the sample surfaces. Prior to the cell seeding, the samples (bare Mg-6Zn-Ca and coated Mg-6Zn-Ca alloy samples) were sterilized with 70% ethanol and dried on a clean bench under UV irradiation. Cells were passaged at about 80% confluency. The pre-incubated cells were seeded on samples at densities of 10^5 cells/cm² to evaluate the cell attachment, proliferation and differentiation behavior, respectively. Dulbecco's modified eagle medium (Himedia) with the addition of 5% fetal bovine serum and 1% penicillin–streptomycin was used as the cell culture medium and the cells were cultured in a humidified incubator in air atmosphere containing 5% CO₂ at 37°C for different time period.

Table 3.1: Compositions of the alloy (wt %)

Alloy	Zn	Ca	Mg	Fe	Cu	Ni	Si
Mg-6Zn-Ca	6	1	Bal	0.001	0.003	0.0005	0.005

Table 3.2: Composition of modified-simulated body fluid (*m*-SBF)/liter [143]

Reagents	Amount
NaCl (g)	5.403
NaHCO ₃ (g)	0.504
Na ₂ CO ₃ (g)	0.426
KCl (g)	0.225
K ₂ HPO ₄ .3H ₂ O (g)	0.23
MgCl ₂ .6H ₂ O (g)	0.311
0.2M NaOH (ml)	100
HEPES (g)	17.892
CaCl ₂ (g)	0.293
Na ₂ SO ₄ (g)	0.072
1M NaOH (ml)	15

3.2 Experimental Methodology and Procedure

3.2.1. Preparation of alloy sample

Coupons of Mg-6Zn-Ca alloy were abraded using SiC papers up to 1500 grit, rinsed with deionized water and acetone and alkali-pretreated with a view of producing a uniform hydroxide layer on the alloy samples before silane coating. The pretreated coupons were rinsed with deionized water, and finally dried with compressed air.

3.2.2 Alkaline Surface Pretreatment

Influence of the following three surface pre-treatments before silane coating on the protective performance was investigated.

- 1) Treatment 1: Sample was ground to 2500 grit finish, rinsed with deionized water, degreased with acetone and dried with compressed air and stored in a desiccator for 24 h.
- 2) Treatment 2: Sample was ground to 2500 grit finish, rinsed with deionized water, degreased with acetone and dried with compressed air. It was then immersed in 3M NaOH (pH 12) solution for 24 h (25°C) to produce a uniform hydroxide layer on the sample.
- 3) Treatment 3: Immersed in 3M NaOH (pH 12) for 48 h (25°C)
- 4) Treatment 4: Immersed in 3M NaOH (pH 12) for 72 h (25°C)
- 5) Treatment 5: Immersed in hot 3M NaOH (pH 12) (Temp. 30° C) for 10 days

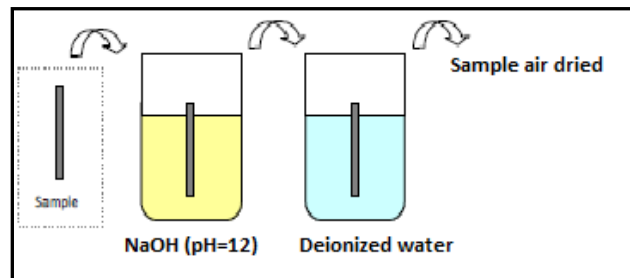


Figure 3.2: Schematic representation of different stages of the pre-treating procedure

3.2.3 Coating procedure

3.2.3.1 Investigation with 2-Diethylphosphatoethyl triethoxysilane (DEPETES) and Methyl triethoxysilane (MTEOS)

Silane mixtures with different ratios of a phosphonosilane (DEPETES) and a Methyl triethoxysilane (MTEOS) were deposited on the optimized alkali-pretreated alloy samples by the sol-gel process and dipping technique.

In the present study, the established conditions were employed for the hydrolysis of Methyltriethoxysilane (MTEOS), i.e., the 3/22/75 (v/v/v) ratio of silane, water and methanol were used as the base solution for hydrolysis and subsequent condensation. Acetic acid was added for accelerating the kinetics and pH of the hydrolysed solution and was maintained at pH 4.5. The silane solution was then stirred for 48 h at room temperature to ensure complete hydrolysis of the silane.

Hydrolysis of 2-Diethylphosphatoethyltriethoxysilane (DEPETES) was carried out in a solution of water and ethanol. The 5/50/44 volume ratio of silane, water and ethanol and acetic acid was added to maintain pH 5 and hydrolyzed for 24 hrs.

The samples with optimized alkali pretreatment of 10 days were immersed for 5 to 7 min in the silane solutions of different DEPETES:MTEOS mixing ratios, *viz.*, 1:1, 1:2, 1:3 and 1:4 (by vol), and then allowed to dry in air for 15 min. This coating was subjected to curing at 120 °C for 1 h.

3.2.3.2 Investigation with 2-Diethylphosphatoethyl triethoxysilane (DEPETES) and Bis-[3-(triethoxysilyl) propyl]tetrasulfide (BTESPT)

A 5 vol % BTESPT solution was prepared by adding the silane to a mixture of deionized (DI) water and ethanol. The ratio of bis-sulfur silane/DI water/ethanol was 5/5/90 (v/v/v). The natural pH of the solution was 6.5. The silane solution was stirred for an hour and then held for three days before use, to allow the maximum hydrolysis of all the Si-OEt to Si-OH, i.e., to ensure that a sufficient number of active SiOH groups were generated in the solution for the condensation reactions [33].

Hydrolysis of DEPETES was carried out in a solution of DI water and ethanol (5/50/44 volume ratio of silane, water and ethanol). 1 vol% acetic acid was added to maintain pH 5, before leaving the solution for hydrolysis for 24 h.

The samples with optimized alkali pretreatment of 10 days were immersed for 5 to 7 min in the silane solutions of different DEPETES:BTESPT mixing ratios, *viz.*, 1:1, 1:2, 1:3 and 1:4 (by vol), and then allowed to dry in air for 15 min. This coating was subjected to curing at 120 °C for 1 h.

3.2.3.3 Investigation with Glycidoxypropyltrimethoxysilane (GPTMS) and MTEOS

GPTMS and MTEOS were mixed together in different molar ratios, *viz.*, 1:1, 2:1 and 3:1. To the mixture, 0.05M acetic acid was added which results in silane-to-water weight % ratio of 15:85. The solution was aged in a closed container for 3 days under continued stirring at ambient temperature [134]. The pretreated specimens were immersed for 5-7 minutes in the silane solutions of different GPTMS:MTEOS mixing ratios, and then allowed to dry in air for 15 min. This coating was subjected to curing at 120 °C for 1 h.

3.3 Characterization of as developed sol-gel coatings

3.3.1 Structural analysis of various modified sol-gel coatings

Fourier transform infrared (FTIR) spectroscopy was used to characterize the structure of sol-gel coatings, using a Perkin Elmer ATR spectrum 100 FTIR spectrometer, at a resolution of 4 cm⁻¹ for 32 scans. This technique was used for determining the extent of crosslinking, which was established by comparing the IR spectra corresponding to Si-O-Si bonds.

3.3.2 Surface Morphology of various sol -gel coatings

The morphology of the various films was closely observed by using scanning electron microscopy (SEM) (Model no.S3400, Hitachi) and the samples exposed to cells were analyzed using environmental scanning electron microscopy (ESEM, Quanta 200FEG). For SEM examination of the cross sections, the samples were cold mounted edge-on and polished. Samples were required to be gold-coated prior to SEM to avoid charging due to the less conductive silane and hydroxide layers. Electron Dispersive X-ray spectroscopy (EDAX) analysis was carried out where elemental distribution is assessed by using X-mapping for determination of the elemental distribution of groups like, Zn, Ca, P and Si on the coated surface.

3.3.3 Corrosion resistance of various modified sol -gel coatings

Potentiodynamic polarization and electrochemical impedance spectroscopy (EIS) were performed in an *m*-SBF medium using a three electrode system(samples with an exposed area of 0.636 cm² acted as the working electrode, a platinum mesh as a counter electrode and a saturated calomel electrode(SCE)as the reference electrode) using a Bio-logic SP-300 Potentiostat. During the electrochemical testing, a submersible pump and water bath were used to simulate the *in vitro* flow rate of the body fluid and the normal body temperature (36.5 ± 0.5 °C), respectively. A flow rate of 2.5 ml/min was maintained, which is similar to the flow rate reported in the literature [144-146]. Open circuit potential was monitored for 3000 s to confirm its stability. Potentiodynamic polarization tests were carried out starting at 250 mV negative to the E_{corr} at a scan rate of 0.5 mV/s.

For the EIS tests, a sinusoidal potential wave of amplitude 10 mV was applied at E_{corr} . The impedance response was measured over frequencies between 1 MHz and 10 mHz, recording 10 points per decade of frequency; the data was analyzed using ZsimpWin software. Each electrochemical test was duplicated to examine the reproducibility of the results.

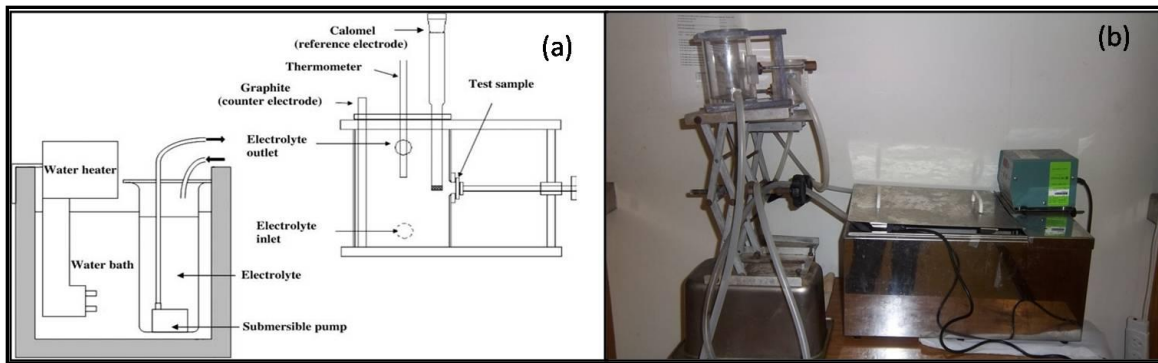


Fig 3.3:(a) Schematic representation [147] and (b) Lab setup of in vitro electrochemical set-up

A hydrogen evolution test was carried out by collecting evolved H_2 in a measuring cylinder above the corroding samples placed in *m*-SBF at $37\text{ }^\circ\text{C}$, as shown in Figure 3.3. Each sample, of dimensions $28 \times 22\text{ mm}^2$ of the bare Mg-6Zn-Ca alloy and the silane-coated sample was placed at the bottom of a 1000 ml beaker in a 500 ml solution of *m*- SBF at approximately $37\text{ }^\circ\text{C}$ for 216 hrs. The hydrogen evolution rates were monitored as a function of immersion time. Using the set-up shown in Figure 3.4, triplicate runs were carried out to examine reproducibility of the hydrogen evolution data [148].The pH of the immersion solution was monitored every 24 h, using a pH meter (Model: sp-701; Suntex).

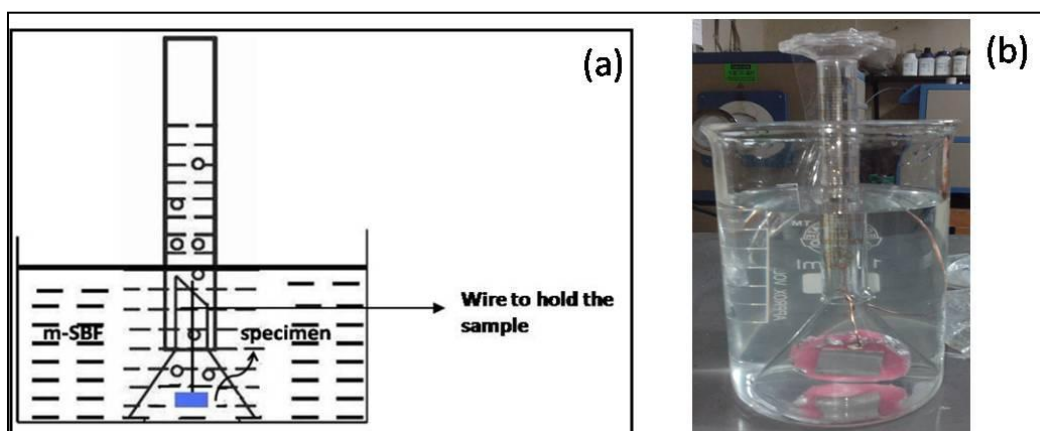


Figure 3.4: (a) Schematic illustration and (b) Lab set up of the evolved hydrogen volume measurement

3.3.4 Mechanical Properties of various modified sol -gel coatings

Adhesion of the coating layer with the sample was assessed according to the ASTM D3359 standard test method using Cross Hatch Cutter. In this test, eleven cuts were made in two directions using the cutter at right angles to each other to form a grid of small squares. A pressure-sensitive adhesive tape was applied over the lattice and removed by pulling in a single smooth action. Adhesion was then assessed by comparing the fraction of coating removed from grid of squares against the ASTM standard ratings. Hardness and scratch resistance of the coating were measured using Pencil Hardness Tester according to ASTM D 1522. The pencil hardness test is a constant-load scratch test. It uses pencil leads of different hardness grades as the scratch stylus. The hardest pencil grade that does not cause damage to the coated sample is considered as the pencil hardness of the coating.

3.3.5 In-vitro biocompatibility tests

3.3.5.1 Cell Culture

MG-63, a human-derived osteosarcoma cell line, was cultured in Dulbecco's Minimum Essential Medium (DMEM) supplemented with 10% foetal bovine serum and antibiotic/antimycotics at 37°C in a humidified 5% CO₂ environment. When approximately 85-90% confluent, the cells were treated with trypsin-EDTA solution for detachment and counted under an optical microscope using a haemocytometer. For a typical experiment, 1×10^6 cells were counted and seeded over the alloy specimen, of dimensions $1 \times 1 \text{ cm}^2$ mounted over acrylic resin, in a 35 mm sterile petri dish in the supplemented tissue culture medium for 1, 3, 7 and 14 days at 37 °C in a 5% CO₂ environment. The tissue culture medium was replaced when exhausted. The cells after the given time intervals, were harvested from alloy specimen and analyzed as described below. MG-63 cells grown in petridish directly and grown on bare Mg-6Zn-Ca alloy specimen were considered as positive and negative controls respectively.



Figure 3.5: Mounted magnesium alloy samples immersed in DMEM in petridish

3.3.5.2 Cell morphology and attachment observations

After culturing for 1, 3, 7 and 14 days, the attached cells were observed by ESEM (Quanta 200FEG). Prior to the SEM observations, the media was removed from the petridish and specimen was fixed with 3% glutaraldehyde for 5-6 h, and incubated in freshly made 1% carbonyldiimidazole for 30 min. The specimen was then rinsed with PBS 3-4 times and sequentially dehydrated in graded ethanol (30, 50, 70, 90 and 100%) for 10 min each. The dehydrated specimens were dried in vacuum and coated with platinum for observation under ESEM.

3.3.5.3 Cell viability and proliferation

Cell proliferation activity was evaluated using a Cyquant cell proliferation assay kit (Invitrogen) as mentioned in the manufacturer's protocol. Towards this end, the adhered cells were detached using trypsin-EDTA solution and centrifuged to obtain a cell pellet. This cell pellet was suspended in the fluorescent dye solution having cell lysis buffer. The fluorescence of this lysed cell pellet was recorded using a multi-well plate reader (Thermo Varioskan Flash Multimode Reader) at excitation wavelength of 480 and emission wavelength of 520 nm. The measured fluorescence values were used to calculate the DNA content (expressed in $\mu\text{g}/\text{cell}$) against a DNA standard curve; $R^2 = 0.997$ (prepared as directed by manufacturer's manual). This fluorescence was also used to determine the percentage proliferation activity of the cells represented against the control cells according to the following equation

$$\% \text{ Cell Proliferation} = \frac{\text{Flrsof cells from specimen harnessed at time 't'}}{\text{Flrsof control cell harnessed at time 't'}} \times 100$$

The cell proliferation is directly proportional to the number of viable cells and thus a standard curve, depicting a linear relation between cell number density and the fluorescence was developed according to the manufacturer's manual ($R^2 = 0.987$).

3.3.5.4 Alkaline phosphatase activity assay

ALP activity assay measurement offers an effective way to detect the bioactivity of biomaterials pertaining to osteoblast cells' responses of differentiation and mineralization. To evaluate cell differentiation, the activity of alkaline phosphatase (ALP) was determined using colorimetric assay kit (Millipore, India) with minor modifications [149]. For ALP determination, the cells were washed with PBS and detached from the specimen and centrifuged to obtain a cell pellet. These cells were lysed by 30% triton-X 100 and the lysate was put in 96-well plate and mixed with 50 μ l of working assay solution. The plate was then incubated for 1 hr at 37 °C in an incubator. After an hour, the 96-well plate was shaken for 2 min and the absorbance was measured at 570 nm (Thermo Varioskan Flash Multimode Reader). For the different time intervals, the ALP activity was calculated against the standard plot. The standard plot depicted a linear behavior between the absorbance and the ALP activity from a known quantity of MG-63 cells ($R^2 = 0.989$).

3.3.5.5 Statistical Analysis

The experimental results were represented as the mean \pm standard deviation of three independent experiments performed at different times (n=3). The statistical analyses were performed using the statistics functionality of Origin 9.1 software. Two sample *t* test was performed and the difference with $p < 0.05$ (*), $p < 0.01$ (**) and $p < 0.001$ (***) was considered significantly different with an assumption of equal variance.

Chapter 4

Results and Discussion

This chapter presents results of the coatings developed, detailed characterization of these coatings and their performance evaluation. The important sections are: pre-treatment of the alloy, development of coating systems, characterization of coatings, performance evaluation of coatings both in-vitro corrosion and in-vitro biocompatibility tests.

4.1 Surface pretreatment of Mg-6Zn-Ca alloy

It is well-established that the availability of a uniform hydroxide layer improves bonding/adhesion of the silane to the surface hydroxide of the alloy [98]. Proper alkali pretreatment is known to have profound influence on corrosion resistance of magnesium alloys [98]. Magnesium is very reactive and it is also well known that magnesium passivates at $\text{pH} > 11.5$ (alkaline medium) (refer section 2.5.1) [95, 98]. Alkaline cleaning has been reported to be the best pretreatment before the application of silanes. Therefore, alkali pretreatment was carried out for different durations to establish an optimum condition for developing a hydroxide layer that provided suitable surface condition for silane coating.

Exposure time and alkalinity level are two important parameters which are responsible for the formation of uniform and adherent hydroxide on the magnesium alloy surface. In the following

pretreatment process, we are trying to establish the best condition and time to give suitable pre-treatment of the alloy. Specimens with 1500 grit surface finish — rinsed with deionized water, degreased with acetone and dried with compressed air, were subjected to different pretreatments:

- In the first set of pretreatment, specimens were simply stored in desiccators for 24 h.
- In the second set, specimens were immersed in a 3M NaOH (pH 12) solution for 24, 48, and 72 h (25°C).
- In the third set, specimens were held for 10 days in hot 3M NaOH (pH 12) at 30 °C, subjecting them to a more rigorous alkaline treatment, with a view to achieving a comparatively crack-free surface hydroxide layer.

To understand the surface morphology of the alkaline pretreated specimen, it was also necessary to study the microstructure of bare Mg-6Zn-Ca alloy. Figure 4.1 shows SEM micrographs and EDAX results of the bare Mg-6Zn-Ca alloy and the intermetallics phase, present in the microstructure of the alloy. The EDAX graph of the point 2 in the matrix shows the presence of high Mg concentration and less of Zn and Ca, whereas EDAX graph at point 1 in the intermetallics phase shows the presence of Zn and Ca, both along with Mg. The presence of Zn and Ca can be attributed to the presence of intermetallics/secondary phases like $\text{Ca}_x\text{Mg}_y\text{Zn}_z$.

The secondary phases (intermetallics) have a different standard potential as compared to Mg matrix which accelerates the corrosion rate due to different electrochemical behaviors of α -Mg and precipitates. Therefore, the selective attack along the boundary of the Mg specimen and second phase occurs [150-152].

The surface morphology micrographs of the alkali-pretreated alloy (Figure 4.2) revealed that the pre-treatment had etched the alloy grain boundaries. However, the intensity of the etching decreased as the pre-treatment time increased from 24 h to 240 h because of the formation of thick and uniform hydroxide film.

When we pre-treat the samples with NaOH, it chemically reacts with the Mg matrix to form Mg (OH)₂ leaving the secondary phases unreacted. This may also give rise to depression on the surface due to undercutting feature on the hydroxide surface above the secondary phases in all the pretreated samples whereas 240 h exposure during pretreatment showed less of this effect due to the formation of a robust hydroxide on the surface.

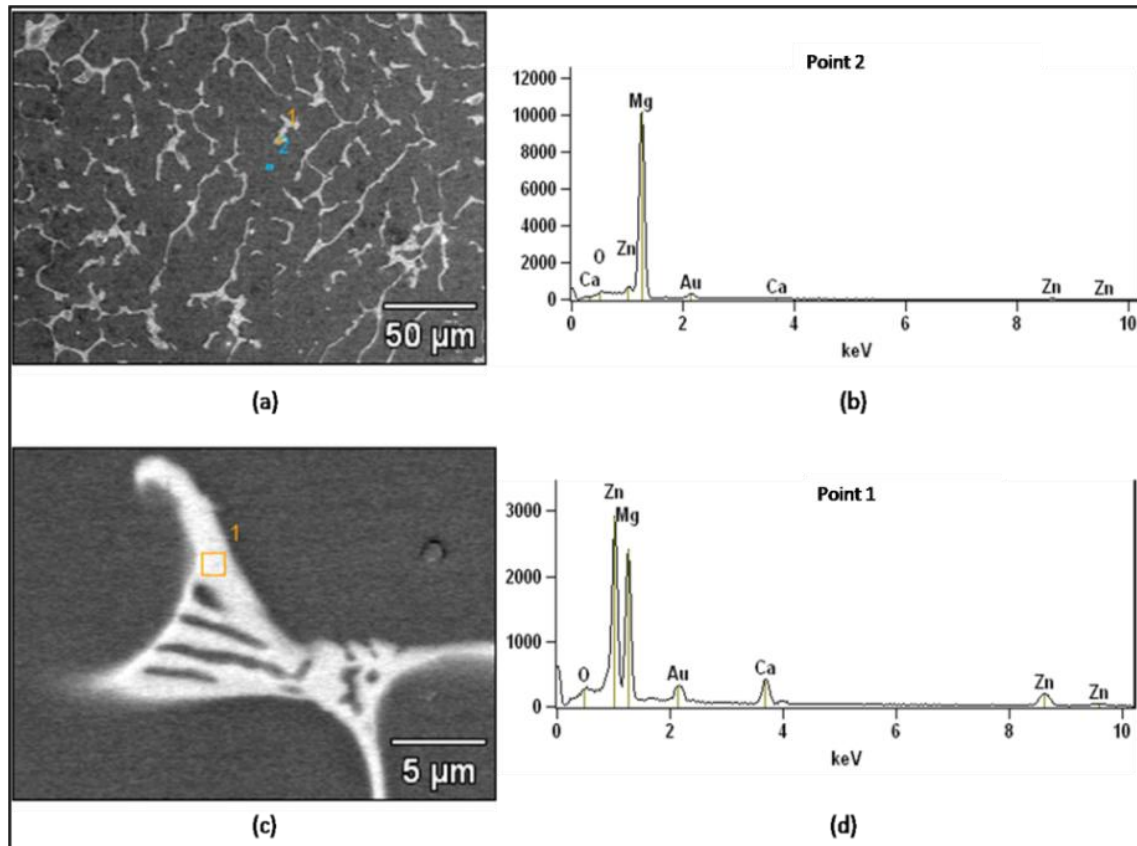


Figure 4.1: SEM micrograph of a) bare Mg-6Zn-Ca alloy b) EDAX of point 2 in the SEM micrograph, (c) intermetallics and (d) EDAX of point 1 of the intermetallics

Table: 4.1 Elemental Analysis of the base alloy and intermetallics point 1 and 2

Elements	O (wt%)	Mg (wt%)	Ca (wt%)	Zn (wt%)
Point 1 (intermetallics)	2.08	36.54	7.92	53.46
Point 2 (base alloy)	2.22	90.10	0.00	7.68

Also, Figure 4.3 reveals the thickness of the hydroxide generated during the pretreatment process for different durations. Figure 4.3 shows formation of thin hydroxide of an average thickness of 3-4 μm for 24 and 48 h pretreated samples, whereas the hydroxide layer was relatively thicker for sample pre-dipped for 72 h (8 μm) and 240 h (9.5 μm).

Therefore, the considerably thicker and less defective feature of the alloy surface/hydroxide film that developed in 240 h of alkali pretreatment (Figure 4.2d and 4.3d) was taken as the best condition for the silane coating.

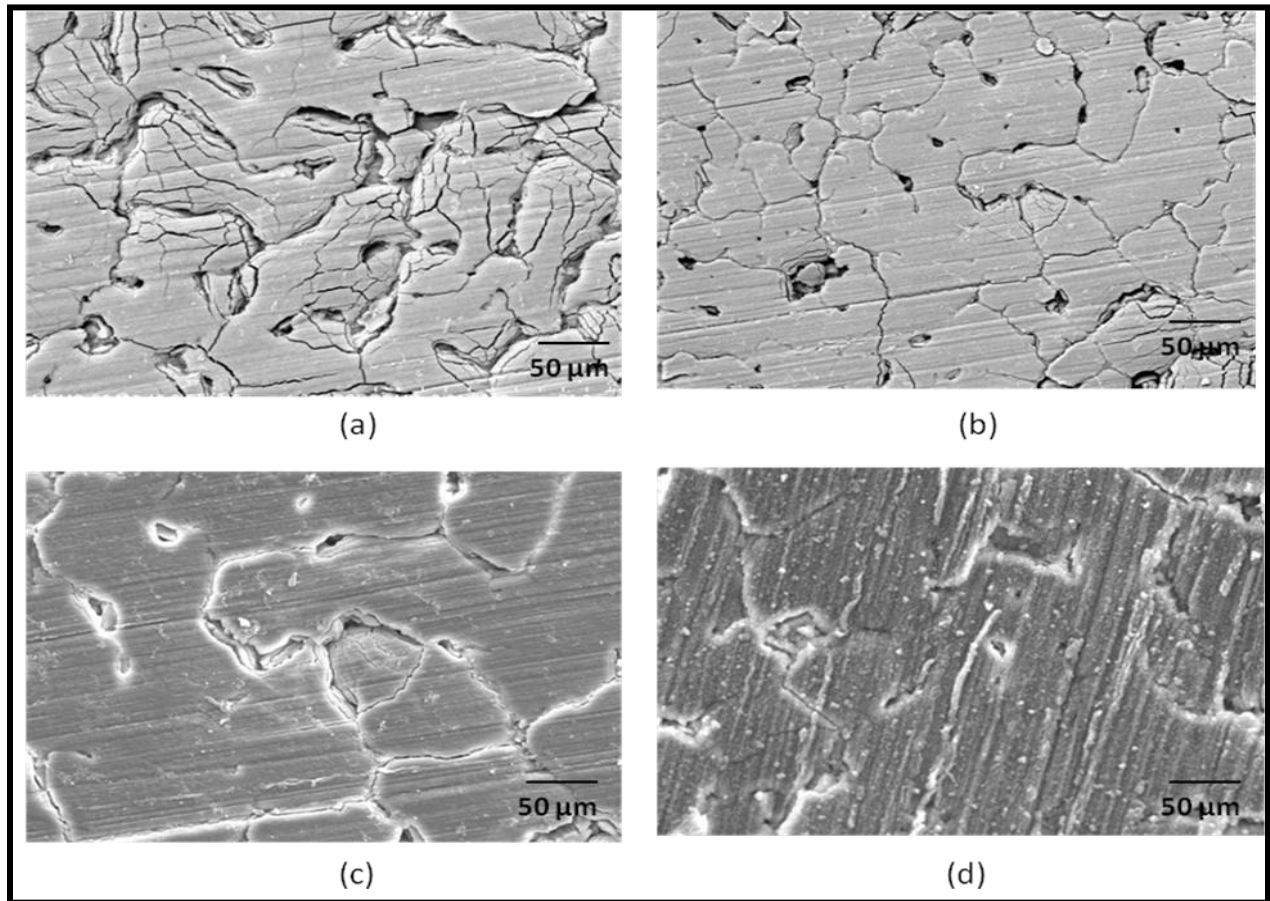


Figure 4.2: SEM micrographs of the surface morphology of the Mg-6Zn-Ca alloy with alkali pretreatment for different durations: (a) 24 h, (b) 48 h, (c) 72 h and (d) 240 h

To further strengthen the fact, that the alkaline pretreatment develops a protective hydroxide layer on the magnesium alloy surface, electrochemical test were performed. The potentiodynamic polarization plots of the alloy before and after the different pre-treatments are shown in Figure 4.4.

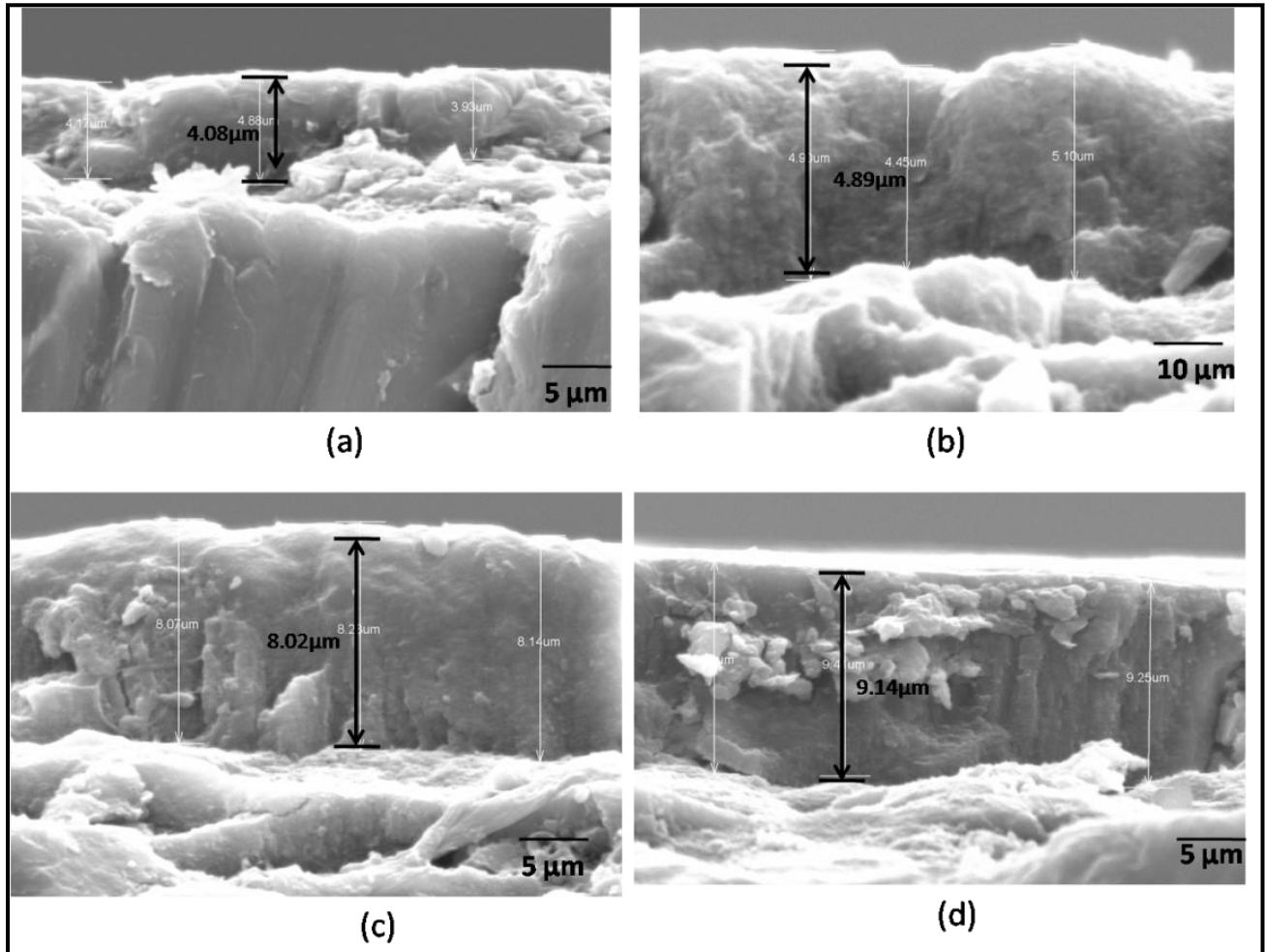


Figure 4.3: SEM micrographs of crosssections of Mg-6Zn-Ca alloy with alkali pretreatment for different durations: (a) 24 h, (b) 48 h, (c) 72 h and (d) 240 h.

The corrosion potential (E_{corr}) and the corrosion current density (i_{corr}) derived from the potentiodynamic polarization curves are presented in Table 4.2. A positive shift in E_{corr} represents a lesser susceptibility to corrosion. E_{corr} of the alloy alkali-treated for 48, 72 and 240 h

shifted towards the nobler direction by 90-100 mV, in comparison to the untreated alloy. The respective similarities in the E_{corr} and i_{corr} as well as in the shape of the anodic plots of all the pretreated and the untreated alloys suggest the dissolution mechanism to be the same [98]. However, the pretreated samples invariably showed a decrease in the current density, with the 240 h treated samples showing a decrease by an order of magnitude as compared to the untreated alloy. E_{corr} of this sample shifted to a nobler direction by about 100 mV.

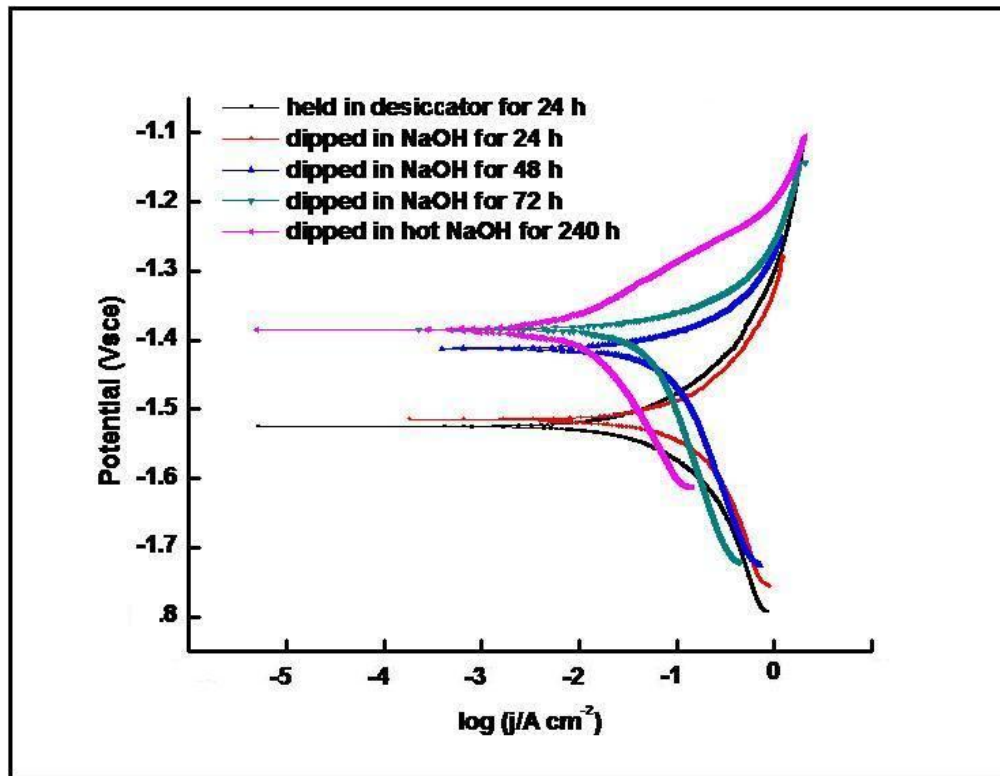


Figure 4.4: Potentiodynamic polarization of different pretreated samples as compared to bare in *m*-SBF at $(36.5 \pm 0.5) ^\circ\text{C}$

Table 4.2: Corrosion potential and corrosion current densities derived from plots in Figure 4.4

Samples	E_{corr} (V)	i_{corr} (i/A cm²)
Bare Mg-6Zn-Ca alloy held in desiccator for 24 h	-1.57	2.5 x10 ⁻²
Alloy dipped in NaOH for 24 h	-1.55	3.1 x10 ⁻²
Alloy dipped in NaOH for 48 h	-1.43	3.1 x10 ⁻²
Alloy dipped in NaOH for 72 h	-1.38	1.7 x10 ⁻²
Alloy dipped in hot NaOH for 240 h	-1.38	8.9 x10 ⁻³

4.2 Development, Characterization and Evaluation of Coating systems

The optimized alkaline pretreated specimen was further coated with three different developed coating systems. The three coating systems were developed by mixing hydrolyzed silanes in different mixing ratios and were applied by dipping for 5-10 min, dried in air for 15 minutes and finally cured for 1h at 120°C. The coatings systems developed on magnesium alloy are:

- DEPETES:MTEOS based coating system
- DEPETES:BTESPT based coating system
- GPTMS:MTEOS based coating system

4.2.1 DEPETES:MTEOS based coating system

To develop the silane coating system, it is necessary to develop understanding of hydrolysis of the silane and the curing conditions of the developed coating system. Therefore, hydrolysis conditions were established and optimized for individual silanes before mixing them in different ratios to develop the sol-gel for the coating. The coated specimens were cured at two different

temperatures to optimize the curing temperature for the coating before proceeding for further characterization and evaluation.

A. Study of hydrolysis of 2-Diethylphosphatoethyl triethoxysilane (DEPETES)

As discussed previously (section 2.5.1 and 4.1) the presence of many hydroxyl groups in the silane solution induces a good wettability on magnesium surface. Hydrolysis of 2-Diethylphosphatoethyl triethoxysilane (DEPETES) was carried out in a solution of water and ethanol. Two batches of different volume ratios of water/ethanol, 5/90/5 (batch 1) and 5/50/44 (batch 2) of silane, water and ethanol respectively, were prepared and acetic acid was used to maintain a pH 5 of the solution and was used to study hydrolysis and subsequent condensation.

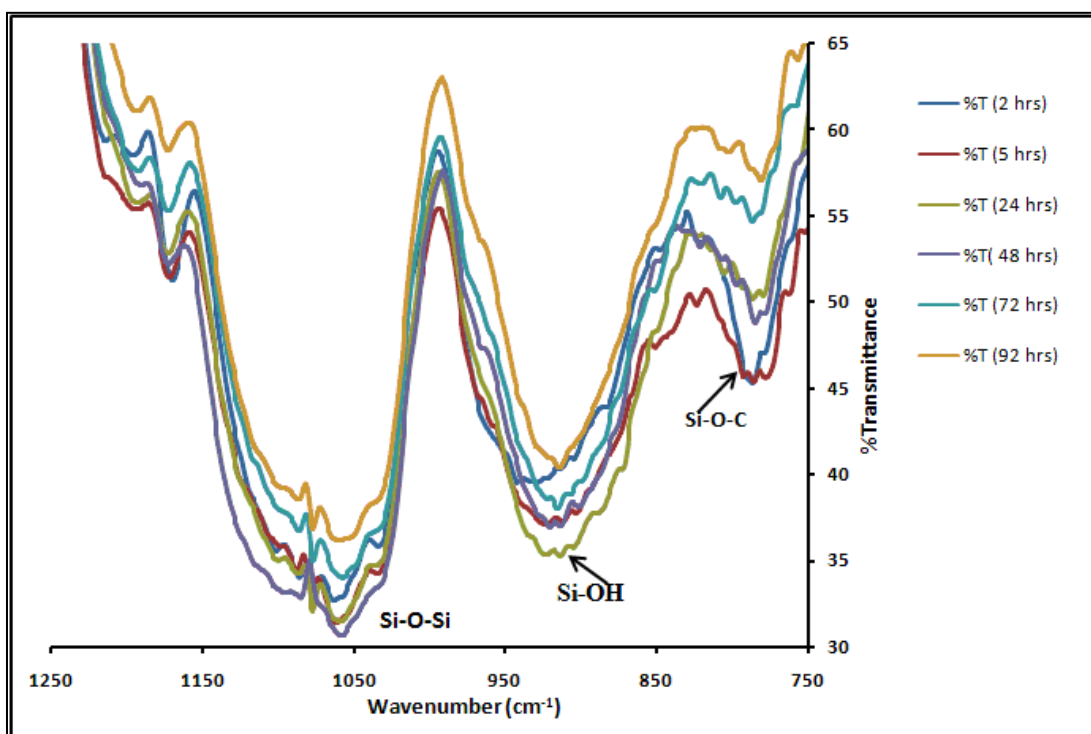


Figure 4.5: Time dependent FTIR spectra of hydrolysis and condensation of DEPETS

batch 1

In Figure 4.5 the 790 cm^{-1} and 1080 cm^{-1} peak belong to silicone (Si-O-C) vibration band that corresponds to symmetric and asymmetric stretching respectively. These bands present in precursors were involved in hydrolysis reaction during the sol-gel process. Therefore, Si-O-C peaks had a maximum intensity at 2 h and 5 h, the intensity decreased with time but even after 92 h did not completely disappear, indicating that the reaction had progressed very slowly. With time, the Si-O-C bond converts gradually into Si-OH (silanol) which was confirmed by FTIR peak observed at $880\text{-}900\text{ cm}^{-1}$. Initially, there was an increase in the silanol precursor intensity up to 24 h and then it decreased as shown in Figure 4.5. It seems that the hydrolysis reaction was predominant till 1st day of ageing then condensation reaction took over. The resulting condensation reaction produced the siloxane linkage which was revealed at peak intensity of 1050 cm^{-1} for asymmetric stretching vibration of Si-O-Si.

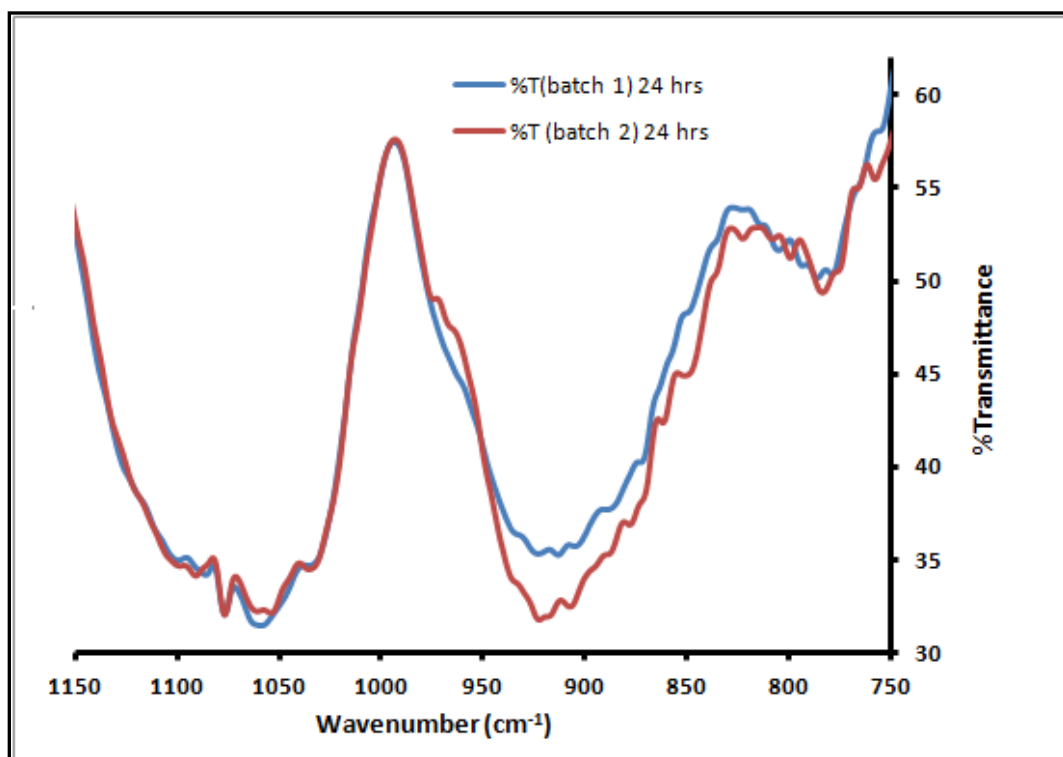


Figure 4.6: Comparative spectra of batch 1 and batch 2 DEPETES after 24 h hydrolysis

The spectra for the two batches were compared. The intensity of Si-OH is greater for batch 2 (Figure 4.6), indicating the silane/water/ethanol ratio to be optimum for this batch. This ratio was used for further studies.

The 10 days pretreated samples were immersed in the silane solution mixtures with different DEPETES:MTEOS volume ratios (1:1, 1:2, 1:3 and 1:4) for 5-7 min and drip dried in air for 15 min. Curing was carried out at 120°C for 1 h to enhance the cross linking within the silane to form a dense network within the coating which may resist the electrolyte ingress through the silane layer.

B. Methyl triethoxy silane (MTEOS) hydrolysis at two different pH

The hydrolysis of MTEOS was carried out at two different pHs (pH 5 (MT-O) and pH 4 (MT-N)) in a solution of water and ethanol (Figure 4.7). Two batches of silane/ethanol/water, 3/75/22, were prepared and pH was maintained using acetic acid. This solution mixture was stirred for 3 days to facilitate the formation of maximum hydroxyls during hydrolysis reaction.

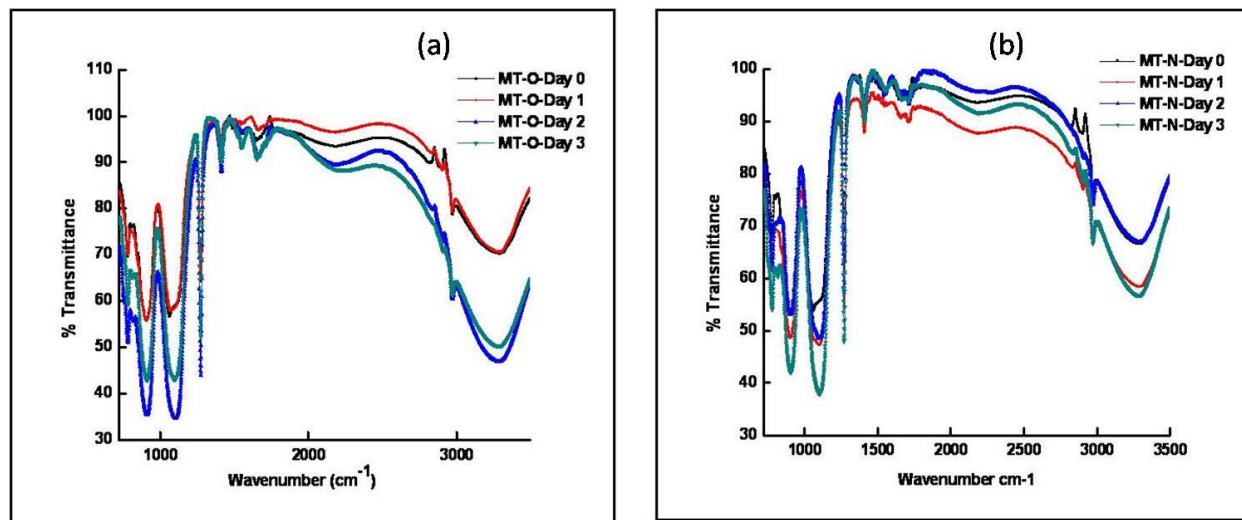


Figure 4.7: Time dependent FTIR Spectra to study hydrolysis and condensation of MTEOS at a) pH 5, b) pH 4

The Si-O-C bond (790 cm^{-1}) changes to the Si-OH (silanol) with time due to hydrolysis reaction, Maximum hydroxyls were found to be formed after 48 h of hydrolysis at pH 5. This was confirmed by a peak observed at $880\text{-}900\text{ cm}^{-1}$ as compared to peak observed after 3 days in case of solution at pH 4. The resulting condensation reaction produced the siloxane linkage which was confirmed by the intense FTIR peak at 1050 cm^{-1} that corresponds to asymmetric stretching vibration of Si-O-Si that can be seen in both the spectra. The spectra also exhibit an O-H stretching region around 3450 cm^{-1} which is represented by a broad band, where freely vibrating OH groups and hydrogen bonded OH groups are apparent. This is possibly formed in the hydrolysis reaction of the alkoxy groups of MTEOS. The peak intensity of Si-OH was found to be more intense at pH 5 as compared to pH 4, thereby confirming more number of free hydroxyl groups available for adhesion to the magnesium alloy surface at pH 5. Therefore, pH 5 was used in further studies.

C. Curing at two different temperatures

When the substrate is immersed in the silane solution during coating process, silanes adhere to the substrate through hydrogen bond with metal hydroxide/oxide present on the surface. During curing, Si-O-Si bonds increase in number, at the expense Si-OH and Si-OEt bonds.

Curing of DEPETES:MTEOS coated specimen was carried out at two different temperatures (100°C and 120°C) and the intensity of peak at 1050 cm^{-1} representing the Si-O-Si linkage was found to be greater at 120°C when compared to 100°C . Also, absence of a peak at 3400 cm^{-1} implies the loss of water content retained in the coating. Therefore, 120°C was found to be optimized curing temperature to carry out further experiments (Figure 4.8).

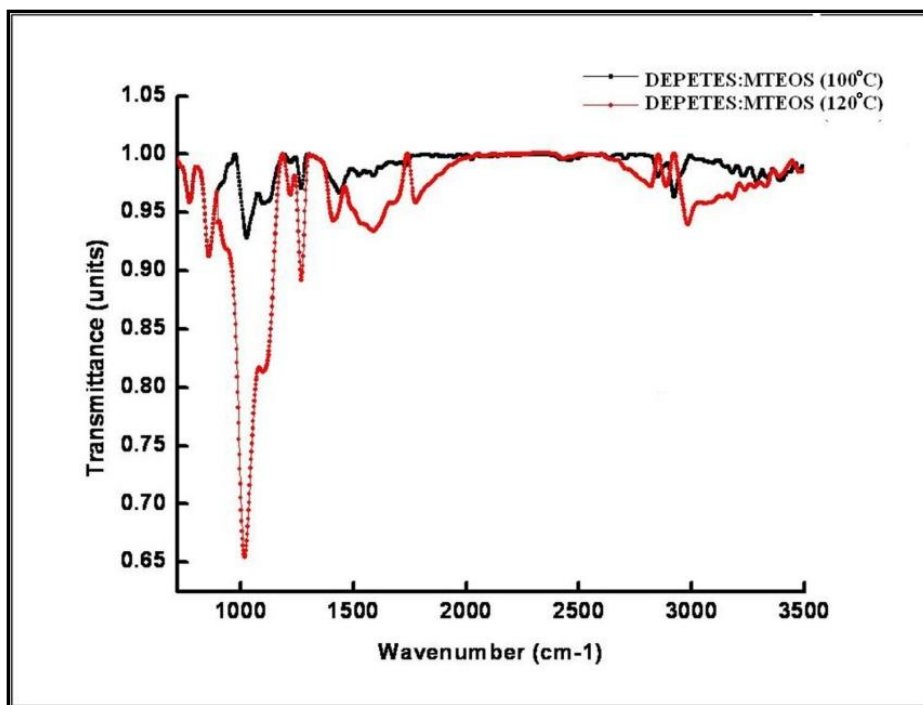


Figure 4.8: FTIR spectra of cured sample of DEPOTES:MTEOS at 100 and 120°C

4.2.1.1 Surface characterization of the silane coated alloy

The coated magnesium alloy surface was characterized using FTIR and SEM. EDAX was used for chemical analysis of the coated surface.

A) Structural Analysis - (by Fourier transform infrared spectroscopy (FTIR))

When certain metallic samples are immersed in the silane solution during the coating process, silanes bond with the sample through hydrogen bonding, with metal oxide/hydroxide present on the metallic surface. During curing, Si-O-Si bonds increase in number at the expense of the Si-OH and Si-OEt bonds. The curing of the alkali-pretreated silane-coated alloy was done at 120 °C. The extent of curing in silane coatings developed with the different DEPOTES:MTEOS volume ratios was examined by FTIR. In the case of the 1:1 coating, peaks that correspond to Si-O-C (symmetric), Si-O-Et (asymmetric) and Si-OH, were observed at 790 cm^{-1} , 1389 cm^{-1} and 880 cm^{-1} , respectively. The peak that appears at 1050 cm^{-1} (Figure 4.9)

corresponds to the asymmetric stretching of Si-O-Si linkage observed in 1:2, 1:3 and 1:4 case confirms the formation of a cross-linked siloxane network structure in the film. It is to be noted that the Si-O-Si band has lower intensity in the coating with a 1:1 DEPOTES:MTEOS ratio; this indicates lesser cross linkage as compared to the coating with the 1:4 ratio that showed the maximum intensity of Si-O-Si peak. The Si-OH and Si-O-C were absent in 1:2, 1:3 and 1:4 ratio coatings developed, indicating the consumption of all Si-OH and Si-O-C for the formation of Si-O-Si linkage in these cases. Also the peak at 1389 cm^{-1} corresponding to Si-OEt seen with maximum intensity in 1:1 has gradually decreased and observed to be absent completely in 1:4 ratio indicating the consumption of all Si-OEt to form Si-O-Si in case of 1:4 ratio.

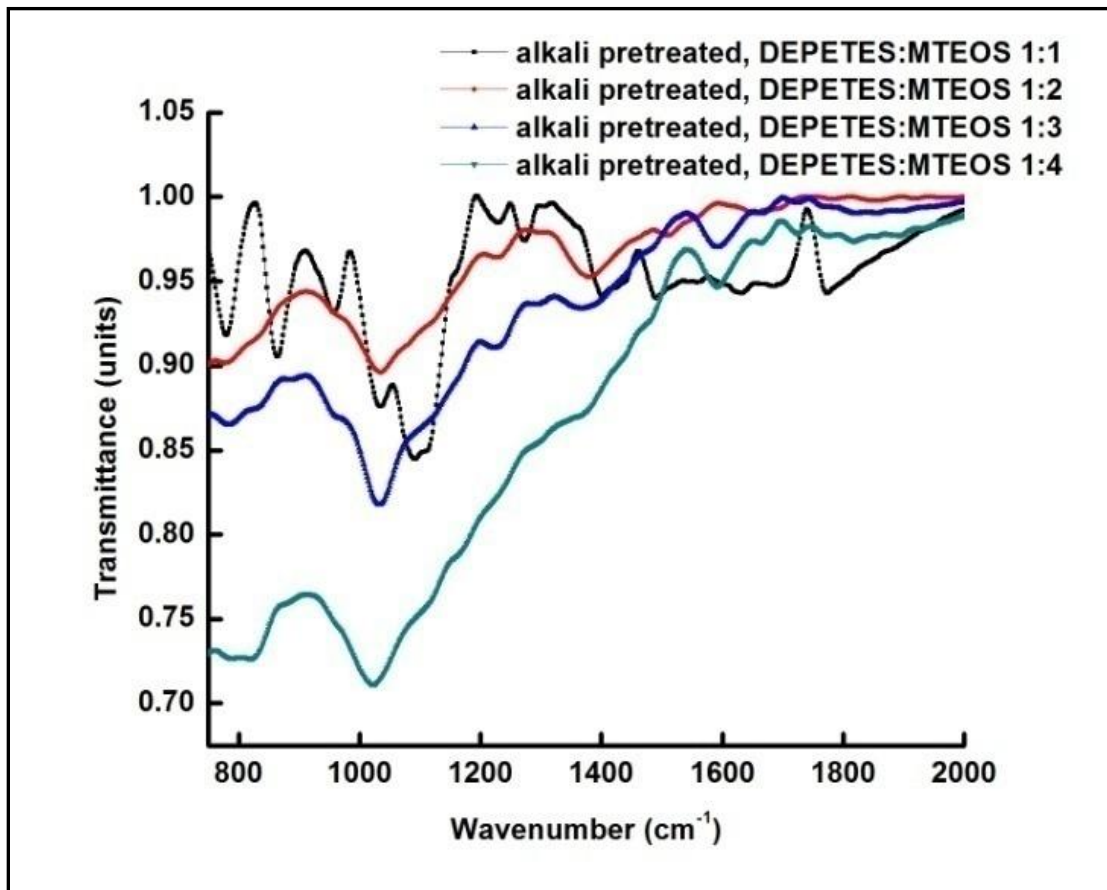


Figure 4.9: FTIR spectra of cured alkali-pretreated alloy dipped in mixtures of silanes in different DEPOTES:MTEOS volume ratios: (a) 1:1, (b) 1:2, (c) 1:3 and (d) 1:4

B) Surface morphology and chemical analysis of silane coated alloy

SEM analysis was used to observe the surface morphology and crosssectional thickness of the coating on magnesium alloy. The thickness of this coating was $\sim 16.1 \mu\text{m}$, as shown in Figure 4.10. Surface morphologies of the alloy specimens, alkali pre-treated for 240 h and then dipped in silane mixtures of different DEPETES:MTEOS volume ratios are shown in Figure 4.11. Samples coated with a DEPETES:MTEOS ratio of 1:4 was found to be the most defect-free (Figure 4.11 d). As expected, the polymeric coating primarily contained C, P, Mg and Si, as determined with the help of EDAX analysis (shown in Figure 4.12 below).

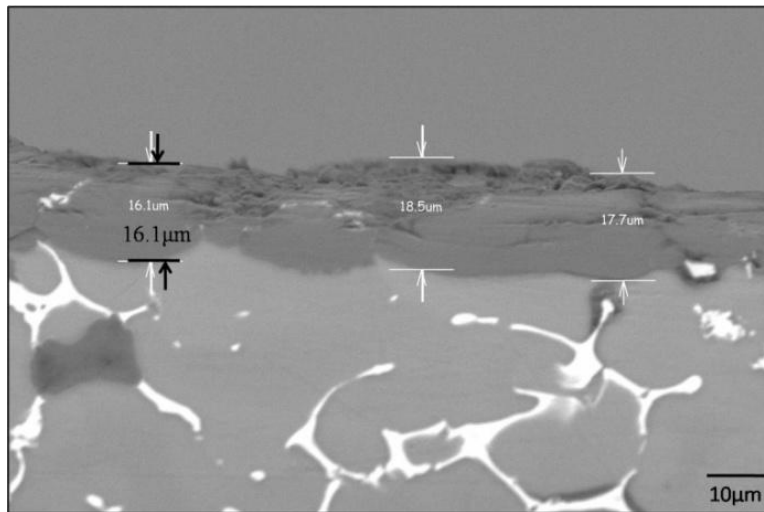


Figure 4.10: SEM micrograph of crosssectional thickness of the 1:4 DEPETES:MTEOS coated sample

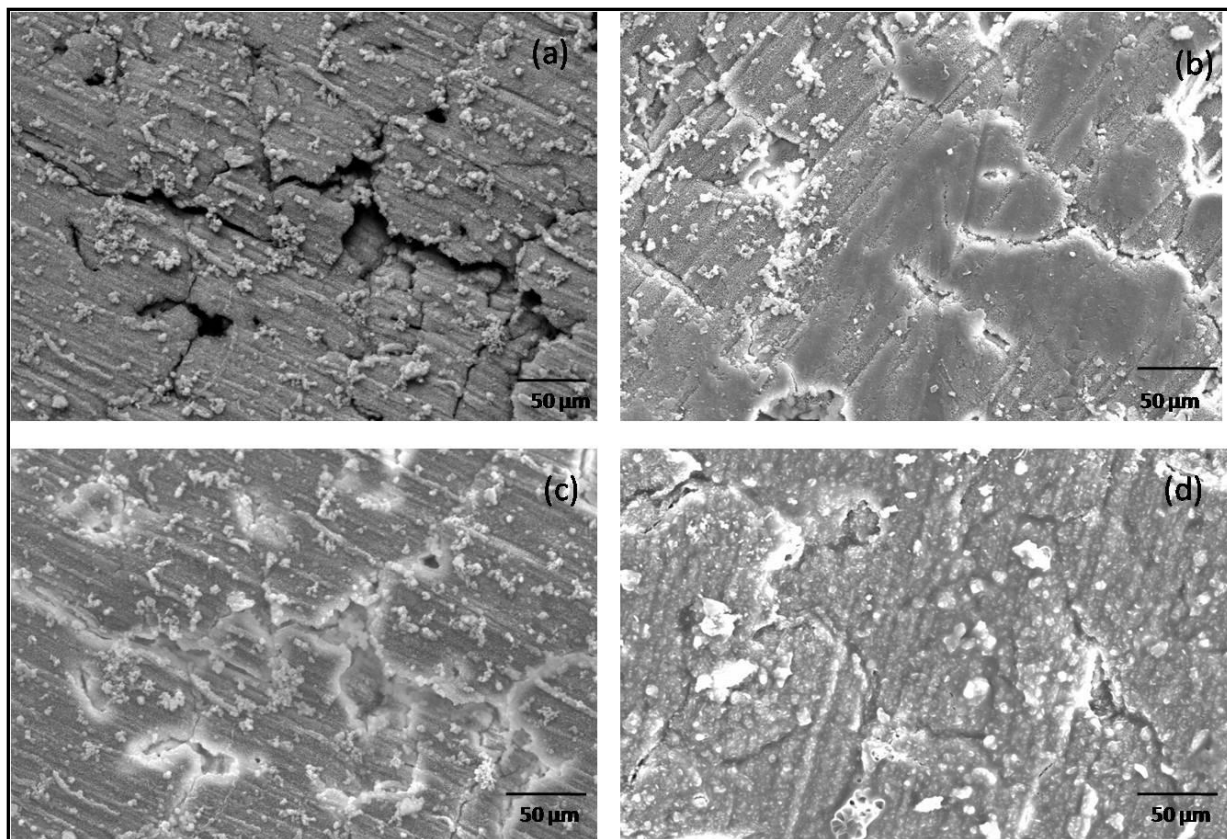


Figure 4.11: SEM micrographs of the surface morphology of alkali-pretreated alloy dipped in mixtures of silanes in different DEPOTES:MTEOS volume ratios of: (a) 1:1, (b) 1:2, (c) 1:3 and (d) 1:4.

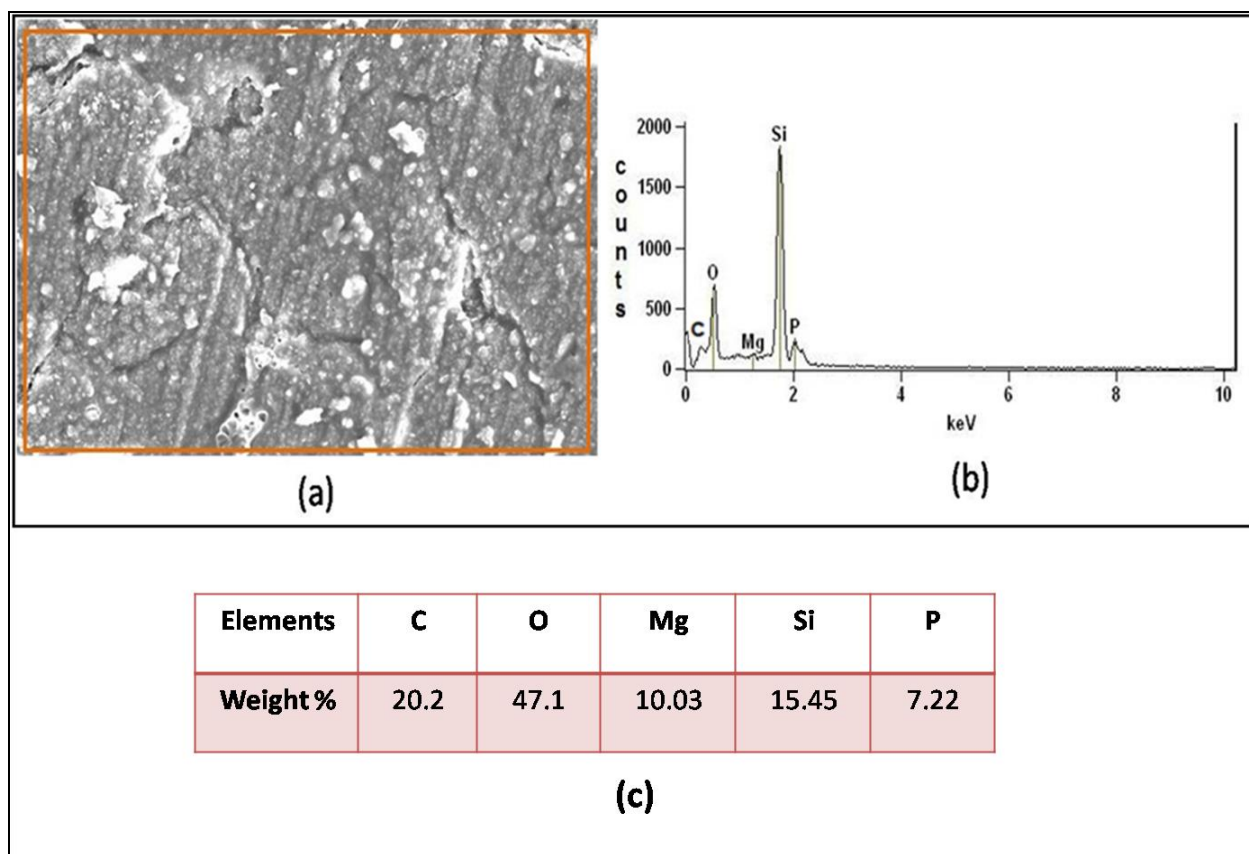


Figure 4.12: (a) SEM micrograph, (b) EDAX graph and (c) Elemental analysis of 1:4 DEPETES:MTEOS coated sample

4.2.1.2 Performance Evaluation of DEPETES:MTEOS silane coated Mg-6Zn-Ca alloy

A) Electrochemical investigation of DEPETES:MTEOS silane coated Mg 6Zn-Ca alloy

Figure 4.13 shows the potentiodynamic polarization plots for the bare and silane-coated samples in *m*-SBF at 36.5 °C. The corrosion potential (E_{corr}) and the corrosion current density (i_{corr}), derived from the potentiodynamic polarization curves are presented in Table 4.3. Current densities in the corresponding anodic and cathodic parts of the polarization scans of all the coated samples were significantly lower in comparison to the bare alloy. The maximum

improvement was seen in the coating with a DEPETES:MTEOS volume ratio of 1:4, as suggested by an order of magnitude lower current density of samples with this coating, as compared to the bare alloy. Also, the corrosion potential (E_{corr}) of the 1:4 coated alloy was ~150 mV more noble as compared to the bare alloy, implying its considerably lesser susceptibility to corrosion.

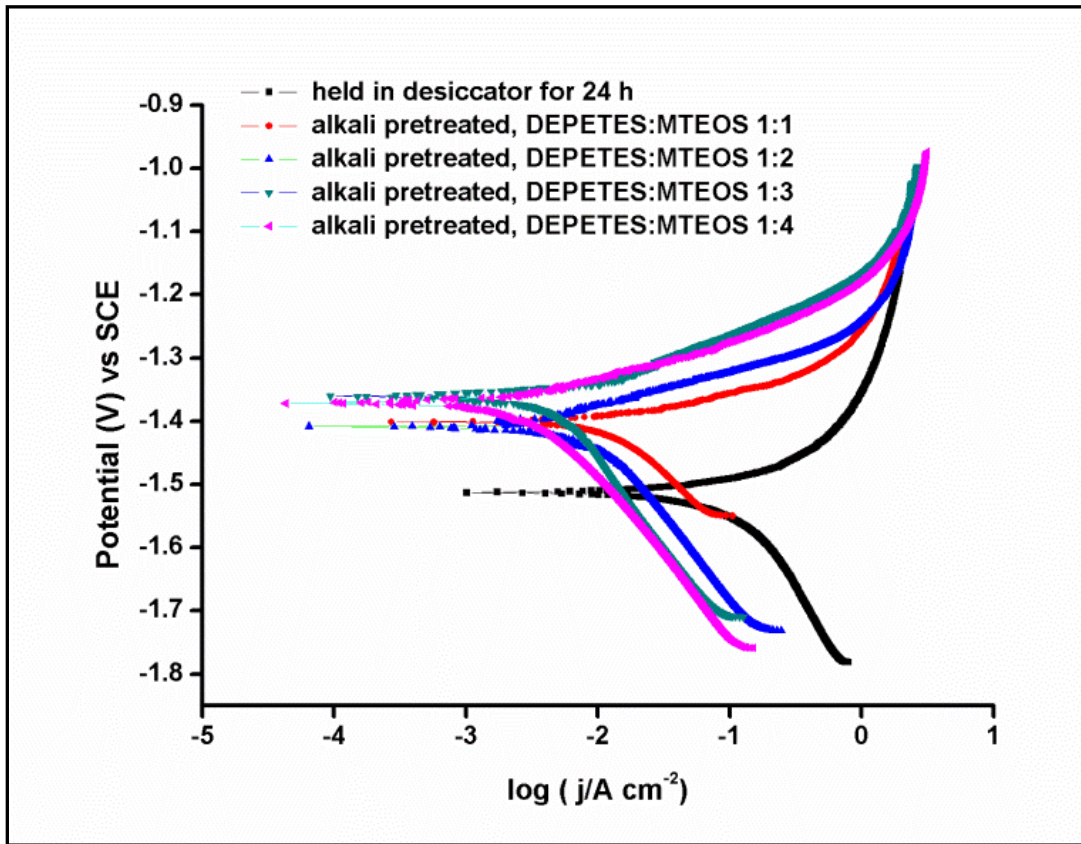


Figure 4.13: Potentiodynamic polarization in *m*-SBF at (36.5 ± 0.5) °C of the alloy coated with different DEPETES:MTEOS ratios of coating formulations

Table 4.3: Corrosion potential and corrosion current densities derived from plots in Figure 4.13

Samples	E_{corr} (V)	i_{corr} ($\mu\text{A cm}^{-2}$)
Bare Mg-6Zn-Ca alloy held in desiccator for 24 h	-1.57	6.3×10^{-2}
Alkali pretreated, DEPETES:MTEOS 1:1	-1.40	1.5×10^{-2}
Alkali pretreated, DEPETES:MTEOS 1:2	-1.40	7.9×10^{-3}
Alkali pretreated, DEPETES:MTEOS 1:3	-1.37	6.3×10^{-3}
Alkali pretreated, DEPETES:MTEOS 1:4	1.36	1.9×10^{-3}

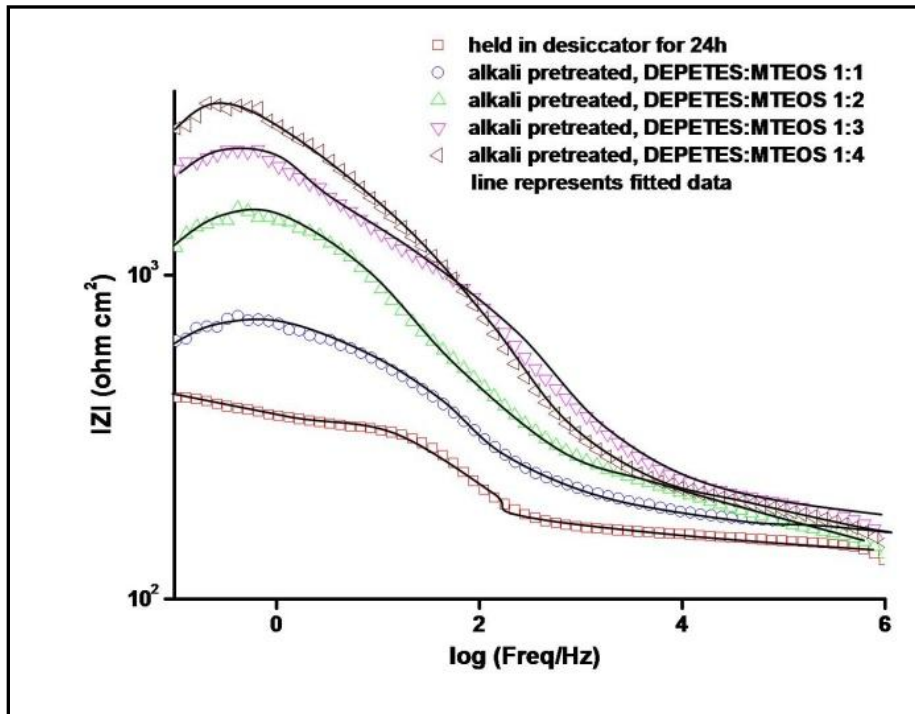


Figure 4.14: Bode plots in *m*-SBF at $(36.5 \pm 0.5)^\circ\text{C}$ of the alloy coated with different DEPETES:MTEOS ratios of coating formulations.

The EIS data for the bare and DEPETES:MTEOS coated Mg-6Zn-1Ca alloy are shown in Bode impedance plots in Figure 4.14. In a Bode impedance plot, the magnitude of impedance at the lowest frequency represents the polarization resistance. The impedance at the lowest frequency for all coated samples increases gradually with the change in the DEPETES:MTEOS ratio from 1:1 to 1:4 in the coating formulation ratio (Figure 4.14). The coating with DEPETES:MTEOS ratio of 1:4 improved the corrosion resistance of the bare alloy by an order of magnitude.

For developing mechanistic understanding, the experimental impedance data were analyzed using an appropriate electrical equivalent circuit (EEC). The EEC with two time constants, as shown in Figure 4.15 (a), was used to simulate the experimental impedance data for the bare alloy and EEC with 3 time constants was proposed for the coated alloy (Figure 4.15 (b)) considering the interfaces of sample/surface hydroxide/*m*-SBF solution and sample/ surface hydroxide/silane film/*m*-SBF solution. In corrosion processes, each of these interfaces can be represented as a parallel combination of a capacitance and a resistance. In Figure 4.15 (a) EEC, R_s is the solution resistance and the surface film is represented by a parallel combination of the constant phase element (CPE), Q_f , and the film resistance R_f formed by the hydroxide. The electrical double layer is represented by another CPE, Q_{dl} , and a charge transfer resistance R_{ct} [98] whereas in Figure 4.15 (b) EEC, the R_f and C_f represents the silane film. In the simulation of experimental data, the CPE behavior is generally attributed to the distributed surface reactivity, roughness, electrode porosity.

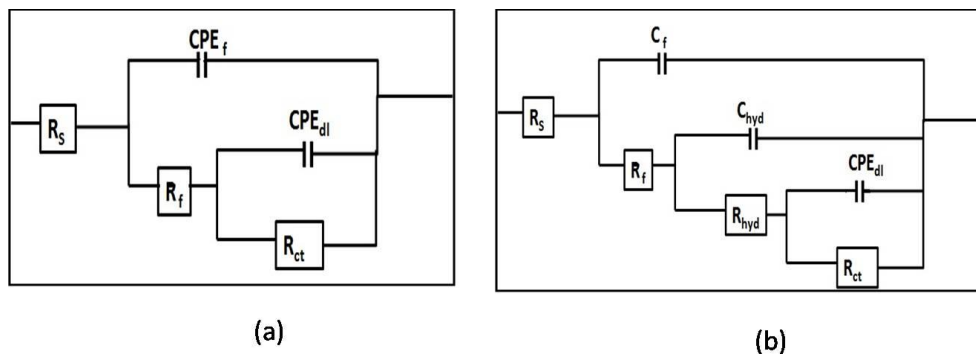


Fig 4.15: (a) The electrical equivalent circuit fitted to the experimentally obtained impedance data of the bare Mg-6Zn-Ca alloy, (b) DEPETES:MTEOS (1:4) coated sample

Simulation was conducted using EEC, $R_s(CPE_f(R_f(CPE_{dl}R_{ct})))$ and a comparison with the simulated results based upon other EECs suggested that $R_s(CPE_f(R_f(CPE_{dl}R_{ct})))$ was the closest fit to the experimental impedance data for the uncoated alloy with a relatively low chi square value (5.09×10^{-4}) as well as a low error (2.2%) in impedance measurement. The calculated parameters for the proposed EEC are shown in Table 4.4.

For the coated alloy, simulation was conducted using 3 time constant EEC, and a comparison with the simulated results based upon other EECs suggested that $R_s(C_f(R_f(C_{hyd}(R_{hyd}(CPE_{dl}R_{ct}))))$ was the closest fit to the experimental impedance data. The calculated parameters for the proposed EEC are shown in Table 4.5.

Table 4.4: Calculated parameters of the proposed EEC for the uncoated sample

Bare alloy	$CPE_f/F\text{ cm}^{-2}$	n	$R_f/\Omega\text{cm}^2$	$CPE_{dl}/F\text{ cm}^{-2}$	N	$R_{ct}/\Omega\text{cm}^2$	Chi squared value	Measured error in impedance/%	$R_p/\Omega\text{ cm}^2$
	6.3×10^{-5}	0.8	119.4	6.5×10^{-3}	0.9	36.69	5.09×10^{-4}	<2.257	156.09

Table 4.5: Calculated parameters of the proposed EEC for the DEPOTES:MTEOS coated

Samples after the simulation of experimental data

Parameters	DEPOTES:MTEOS (1:1)	DEPOTES:MTEOS (1:2)	DEPOTES:MTEOS (1:3)	DEPOTES:MTEOS (1:4)
$R_f/[\Omega\text{ cm}^2]$	35.16	51.25	103	105.1
$C_f/[F\text{ cm}^{-2}]$	4.95×10^{-6}	3.76×10^{-7}	2.95×10^{-7}	1.57×10^{-7}
$R_{hyd}/[\Omega\text{ cm}^2]$	129.4	182.6	410.01	487.8

$C_{hyd}/[F\ cm^{-2}]$	1.133×10^{-5}	4.2×10^{-6}	2.52×10^{-6}	2.442×10^{-6}
$CPE_{dl}/[F\ cm^{-2}]$	1.8×10^{-4}	7.384×10^{-5}	5.4×10^{-5}	4.37×10^{-5}
n	0.84	0.87	0.86	0.7
$R_{ct}/[\Omega\ cm^2]$	169.2	563.1	797.9	1336
$R_p/[\Omega\ cm^2]$	333	797	1311	1929
Chi squared value	4.94×10^{-3}	9.35×10^{-3}	8.05×10^{-3}	8.5×10^{-3}
Measured error in impedance/[%]	<7.02	<7.616	<8.97	<9.221

B) Time dependent degradation of 1:4 DEPETES:MTEOS coated alloy

The coating developed with 1:4 DEPETES:MTEOS ratio showed the best corrosion resistance among the coatings with the silane mixtures in different ratios and coatings of other three ratios were found to be completely degraded within few hours of immersion. This improvement is due to the reasonably intact nature of the silane coating developed with 1:4 DEPETES:MTEOS ratio. In spite of the highly environment-friendly nature of the silane coating process as well as the coatings themselves, such coatings reportedly fail to offer an adequate long-term solution for corrosion resistance and protection, as result of micropores, cracks and areas with low cross-link density. Such defects facilitate the diffusion of aggressive electrolyte to the coating/sample interface, thereby developing sites for corrosion initiation. Therefore, the alloy coated with the silane formulation that provided the maximum corrosion resistance in short-term tests (that is, DEPETES:MTEOS, 1:4) was subjected to extended immersions in *m*-SBF, and the durability of corrosion resistance due to the coating was investigated after different durations of immersion.

As shown in Figure 4.16 and Table 4.6, following 110 h of immersion, the value of $|Z|_{0.1Hz}$ for 1:4 ratio was similar to that of the initial $|Z|_{0.1Hz}$ of bare Mg-6Zn-Ca alloy. After 110 h of

constant immersion, the silane coating loses its potential to protect the sample in *m*-SBF at (36.5 ± 0.5) °C. The bode plots exhibit systematic variations resulting from the changes in coating resistance due to diffusion of chloride ions through the coating subsequently leading to corrosion of the bare Mg-6Zn-Ca. An increase in C_f and C_{hyd} is observed with increased immersion time, which is attributed to the uptake of the electrolyte into the coating. It is noted that C_f and C_{hyd} values attribute to the physical properties of the coatings themselves, which includes being thicker or physically not allowing water to diffuse as rapidly. The increase in these values with decrease in R_p value (Table 4.6) attributes to the onset or progression of corrosion processes at the surface of the metal and subsequently the detachment of the epoxy coating from the sample. The charge transfer resistance (R_{ct}) is able to yield information regarding the rate of the corrosion process occurring at the metal sample beneath the coating. A decline in the R_{ct} value of is observed following 110 h of immersion, which corresponds with the increasing extent of corrosion.

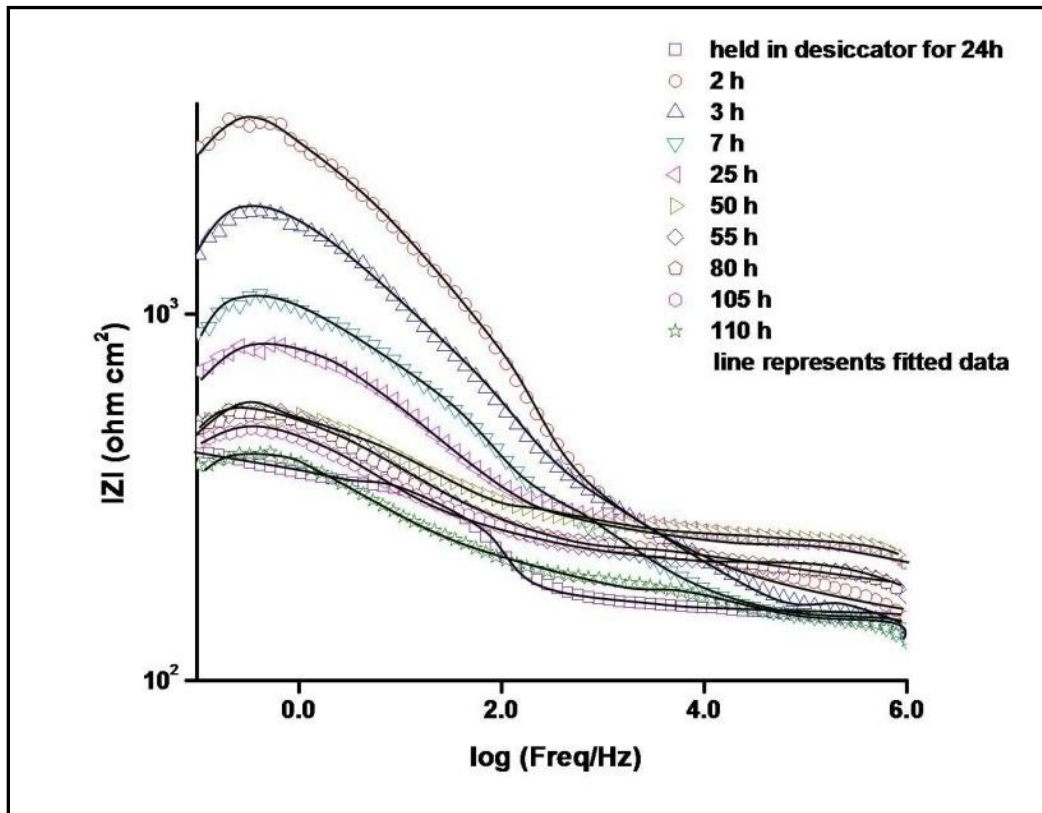


Figure 4.16: Bode plots of the alloy silane coated with DEPETES:MTEOS ratio of 1:4, after different durations of immersion in *m*-SBF at (36.5 ± 0.5) °C

Table 4.6: Values of the different components in the EEC after the simulation of experimental data for the time dependent degradation of 1:4 (DEPTES: MTEOS) coated sample

Immersion time (h)	$R_f/[\Omega \text{ cm}^2]$	$C_f/[F \text{ cm}^{-2} \times 10^{-7}]$	$R_{hyd}/[\Omega \text{ cm}^2]$	$C_{hyd}/[F \text{ cm}^{-2} \times 10^{-6}]$	$CPE/[F \text{ cm}^{-2} \times 10^{-5}]$	n	$R_{ct}/[\Omega \text{ cm}^2]$	$R_p/[\Omega \text{ cm}^2]$
2	105.1	1.57	487.8	2.44	4.37	0.7	1336	1929
5	82.33	2.5	224.4	3.43	7.0	0.78	744.2	1051
7	67.7	3.8	172.4	4.72	12.3	0.81	330.6	570
25	25.96	4.4	95.97	5.6	14.0	0.82	225.3	350
50	16.75	5.7	49.9	5.23	33.0	0.84	116.8	215
80	21.87	6.2	52.21	6.30	40.0	0.87	135.8	208
110	24.39	6.6	42.86	6.40	59.0	0.86	95	161

As established through polarization and EIS tests in *m*-SBF at $(36.5 \pm 0.5) ^\circ\text{C}$, the silane coating with a DEPTES:MTEOS ratio of 1:4 showed substantially superior corrosion resistance to all other treatments; this is attributed to the most defect-free surface developed due to the 1:4 coating (Figure 4.10). This is in agreement with the FTIR spectra and SEM micrographs, which showed the maximum intensity of crosslinking of Si-O-Si peak and a comparatively lesser defective coating in the case of the 1:4 ratio DEPTES:MTEOS coating.

C) Hydrogen evolution

One of the major drawbacks of Mg as biomaterial is the concurrent formation of H_2 gas when it corrodes in body fluid [31]. The evolved H_2 can accumulate and form gas pockets that may lead to necrosis of the neighboring tissues and delay healing. However, if H_2 is generated slowly enough, it can be transported away from the implant, and thus, can be tolerated by the body.

Thus, the study of the variation of the hydrogen evolution rate with exposure time is of great importance. The overall reaction for Mg corrosion ($\text{Mg} + 2\text{H}_2\text{O} = \text{Mg}^{2+} + 2\text{OH}^- + \text{H}_2$) consists of the anodic dissolution of magnesium and cathodic hydrogen evolution. The dissolved oxygen in the test solution is reported to make little contribution to the cathodic process [43] and so experiments were carried out without de-aeration. Dissolution of one magnesium atom generates one hydrogen gas molecule. In other words, the evolution of one mole of hydrogen gas corresponds to the dissolution of one mole of magnesium. Therefore, the estimation of the generated hydrogen also indicates the magnesium dissolution rate. Using the set-up shown in Figure 3.4, triplicate runs were carried out to examine reproducibility of the hydrogen evolution data [148].

The evolved hydrogen was collected in a measuring cylinder above the corroding samples, as shown in the Figure 3.4. Each sample, of dimensions $28 \times 22 \text{ mm}^2$ of the bare Mg-6Zn-Ca alloy and the silane-coated sample was placed at the bottom of a 1000 ml beaker in a 500 ml solution of *m*- SBF at approximately 37°C for 216 hrs. The hydrogen evolution rates were monitored as a function of immersion time.

As seen in Figure 4.17, hydrogen evolution rates were the highest for the bare alloy and the alloy with 1:1 DEPETES:MTEOS coating throughout the entire duration of immersion, whereas, the rate was lowest for the optimized 1:4 DEPETES:MTEOS-coated sample. The hydrogen evolving from the samples with a protective coating exhibited a trend similar to the pH change, that is, a much smaller amount of hydrogen was evolved from the 1:4 ratio coated sample compared to the bare Mg-6Zn-Ca alloy samples. The undulations in the corrosion rate or the hydrogen evolution rate of alloy magnesium alloys is usually attributed to the formation of the corrosion products which adhere to the corroding surface [153].

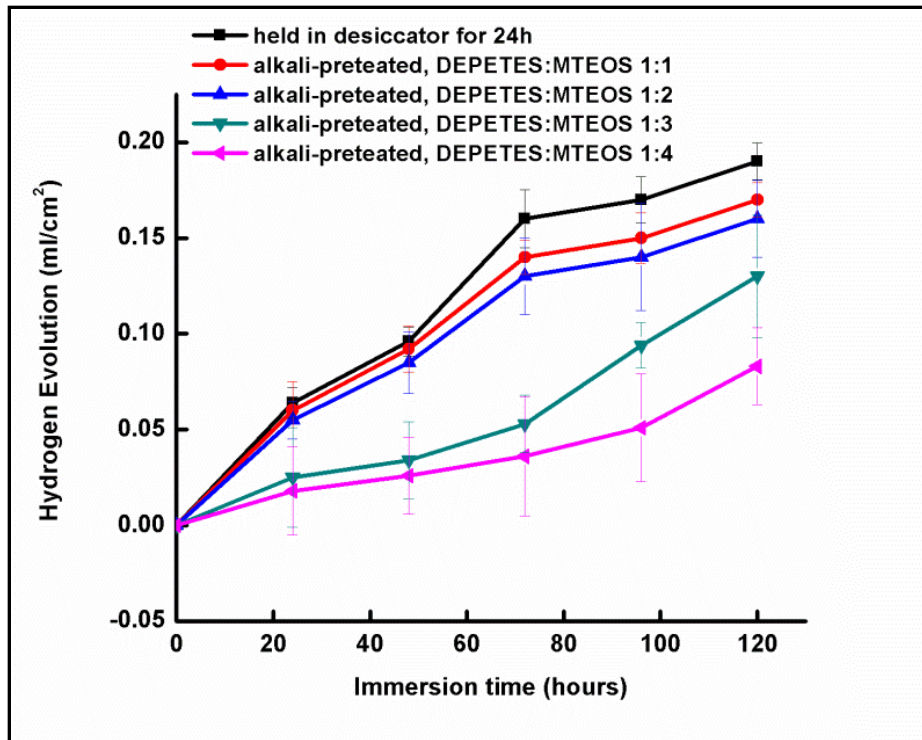


Figure 4.17: Hydrogen evolution of bare and coated alloys, as a function of immersion time *m*-SBF at $(36.5 \pm 0.5) ^\circ\text{C}$

D) pH study

Local alkalization can unfavorably affect the pH-dependent physiological reaction balances in the vicinity of the magnesium implant and may even lead to an alkaline poisoning effect if the local *in vivo* pH exceeds 7.8 [9]. Therefore, the change in pH in the bare and the coated alloys was monitored throughout all the corrosion tests. The data in Figure 4.18 suggests that the pH of the alloy coated with the 1:4 DEPETES:MTEOS silane mixture remained below 7.8, whereas, the pH became much higher for the bare alloy and the alloy coated with DEPETES:MTEOS silane mixtures of other ratios.

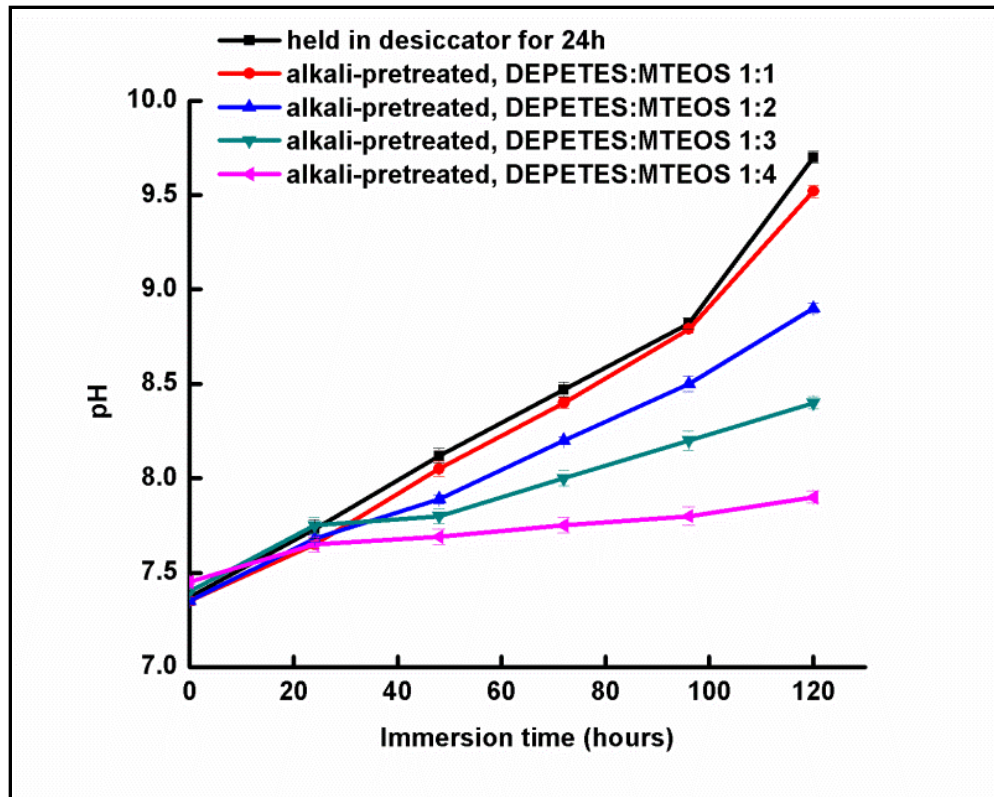


Figure 4.18: Variation of pH as a function of immersion time *m*-SBF at $(36.5 \pm 0.5) ^\circ\text{C}$.

4.2.1.3 Mechanical analysis of the silane coating on the Mg-6Zn-Ca alloy

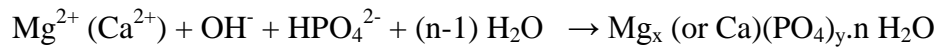
The adhesion of the coatings was determined in accordance with ASTM D3359. The coatings showed strong adhesion with a rating of 5B; this rating corresponds to the best ASTM rating. Also, pencil hardness of the coatings, as determined in accordance with ASTM D3363-92a, was found to be 4H. Probably, the cracks on the surface are not deep enough to affect the sample and coating adhesion.

4.2.1.4 Post corrosion analysis of 1:4 DEPETES:MTEOS coated alloy

Figure 4.19 shows SEM images of the uncoated and the 1:4 DEPETES:MTEOS coated alloy after immersion in *m*-SBF for 110 h. The uncoated alloy developed the usual mud-like morphology with cracks, whereas, the coated alloy had significantly lesser number of cracks,

confirming the ability of the coating to provide corrosion resistance to the alloy in *m*-SBF. EDAX of the coated samples indicated the presence of oxygen, magnesium, calcium, zinc and phosphorous on the surface of the corroded sample. The presence of oxygen and magnesium is consistent with a corrosion product of Mg (OH)₂, while the calcium and phosphorous can be associated with *m*-SBF [154].

The crystalline corrosion products shown in Figure 4.19b were characterized by XRD. The XRD spectrum in Figure 4.20 confirmed the formation of magnesium phosphates as suggested by the following equations [155] along with magnesium hydroxide and magnesium:



Each of the chemically-different hydrated forms of magnesium phosphates is known to be non-toxic and is shown to support osteoblast differentiation and function [148, 156]. The HCO₃⁻ and HPO₄²⁻ in *m*-SBF can react with the OH⁻ generated during magnesium dissolution, which induces precipitation of insoluble carbonates and phosphates in the corrosion product layer. The presence of insoluble carbonates and phosphates on the magnesium alloy immersed in *m*-SBF has been reported by many studies [148, 155, 157].

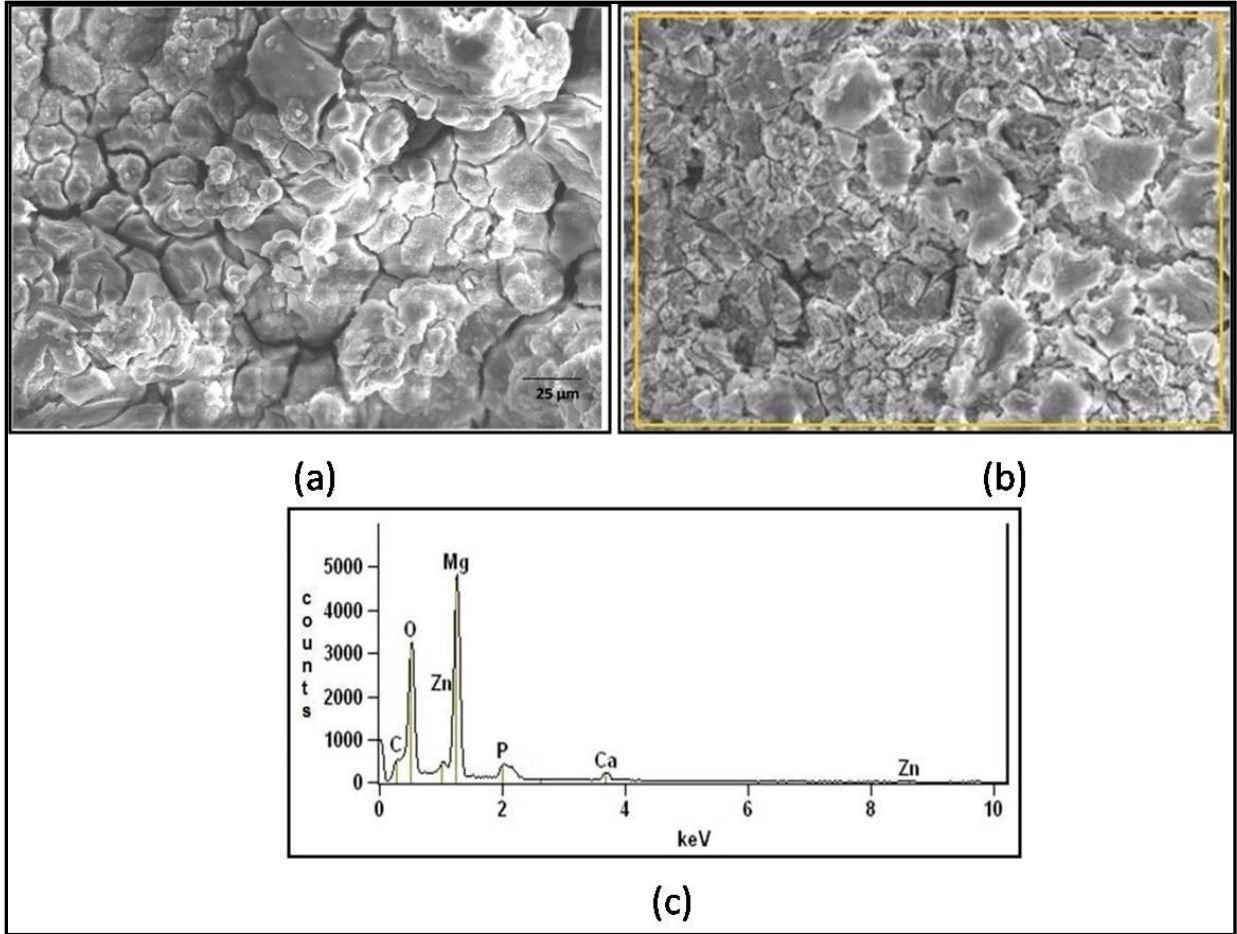


Figure 4.19: SEM micrographs of: (a) bare Mg-6Zn-Ca alloy and (b) 1:4 DEPETES:MTEOS-coated samples, (c) EDAX of 1:4 MTEOS-coated samples, after immersion for 110 hrs in *m*-SBF at (36.5 ± 0.5) °C

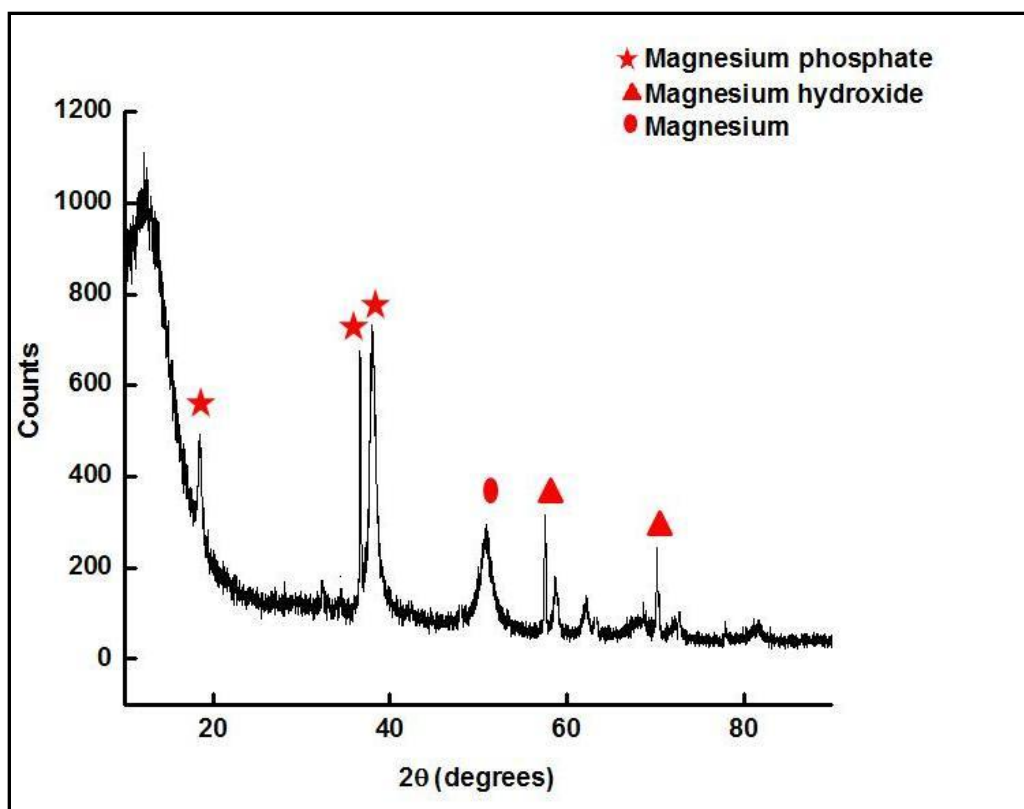


Figure 4.20: XRD spectra of the 1:4 DEPETES:MTEOS coated alloy after immersion for 110 h in *m*-SBF at $(36.5 \pm 0.5) ^\circ\text{C}$

The DEPETES:MTEOS coating system considerably delayed the degradation of Mg-6Zn-Ca alloy by 110 h, thereby reducing the surface reactivity and reducing the hydrogen evolution and pH change. But we further explored and studied another long chain precursor BTESPT in combination with DEPETES, to see its effect on further reducing the corrosion phenomenon.

4.2.2 DEPETES:BTESPT based coating system

The hydrolysis of DEPETES was studied and reported at two different pH and hydrolysis conditions were optimized respectively. The coating sol was developed by mixing the two independently hydrolyzed silanes in different ratios. The coated specimens were cured at two

different temperatures to optimize the curing temperature for the coating before proceeding for further characterization and evaluation.

A) BTESPT hydrolysis study at two different pH

In case of BTESPT, hydrolysis was done at pH 5 (TS-N-) and pH 6.5 (TS-O-) (reported [33]) with silane/ethanol/water volume ratio as 5/90/5 and pH was adjusted using acetic acid. The aging was studied for 3 days for both solutions and it was observed that at pH 6.5 the maximum silanol formation occurs after 3 days (peak at 880-900 cm^{-1}) whereas at pH 5 solution even after 3 days there is only a very weak peak of Si-OH, implying that the silanol formation had just started after 3 days when pH is 5 (Figure 4.21). Further investigations were carried out with formulation with pH 6.5.

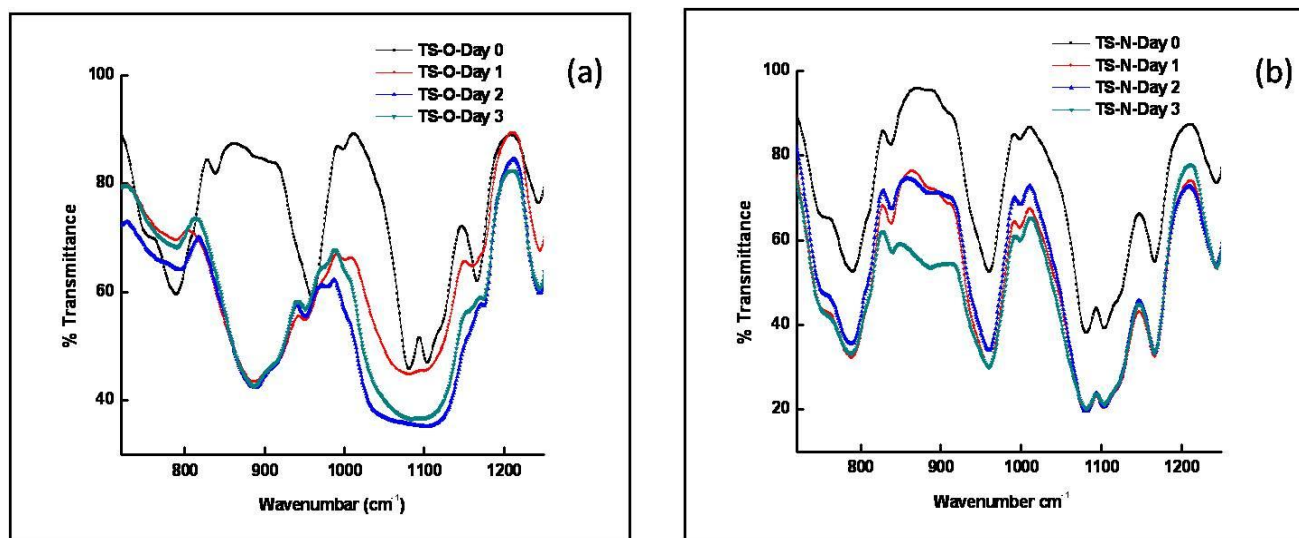


Figure 4.21: Time dependent FTIR Spectra study of hydrolysis and condensation of Tetrasulfide silane at a) pH 6.5, b) pH 5

B) Curing at two different temperatures

The Curing of DEPETES:BTESPT was studied at two different temperatures, 100°C and 120°C. Figure 4.22 shows that the intensity of peak at 1050 cm^{-1} representing the Si-O-Si linkage is more intense at 120°C and the intensity of Si-OH peak concurrently decreased. Also absence of a peak at 3400 cm^{-1} implies the loss of water content retained in the coating. Therefore, 120°C was optimized as the curing temperature.

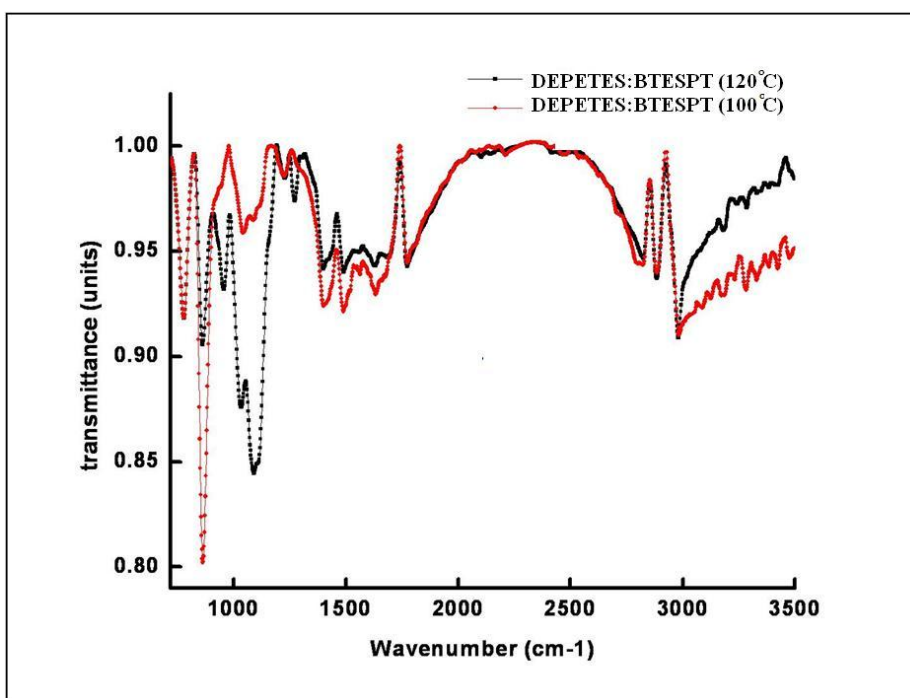


Figure 4.22: FTIR spectra of cured sample of DEPETES:BTESPT at 100°C and 120°C

4.2.2.1 Surface characterization of the silane coated alloy

The coated magnesium alloy surface was characterized using FTIR and SEM. EDAX was used for chemical analysis of the coated surface.

A) Structural Analysis – by Fourier transform infrared spectroscopy (FTIR)

The curing of the alkali-pretreated silane-coated alloy was done at 120 °C. The extent of curing in silane coatings developed with the different DEPETES:BTESPT volume ratios were examined by FTIR. The peak that appears at 1050 cm⁻¹ (Figure 4.23) corresponds to the asymmetric stretching of Si-O-Si linkage observed in each case confirms the formation of a cross-linked siloxane network structure in the film. It is to be noted that the Si-O-Si band has lower intensity in the coating with a 1:1 DEPETES:BTESPT ratio; this indicates lesser cross linkage as compared to the coating with the 1:4 ratio that showed the maximum intensity of Si-O-Si peak. In the case of the 1:1 coating, peaks that correspond to Si-O-C (symmetric), Si-O-Et (asymmetric) and Si-OH, were observed at 790 cm⁻¹, 1389 cm⁻¹ and 880 cm⁻¹, respectively. The Si-OH peak was absent in coatings developed with other silane ratios, indicating the consumption of all Si-OH for the formation of Si-O-Si linkage in these cases.

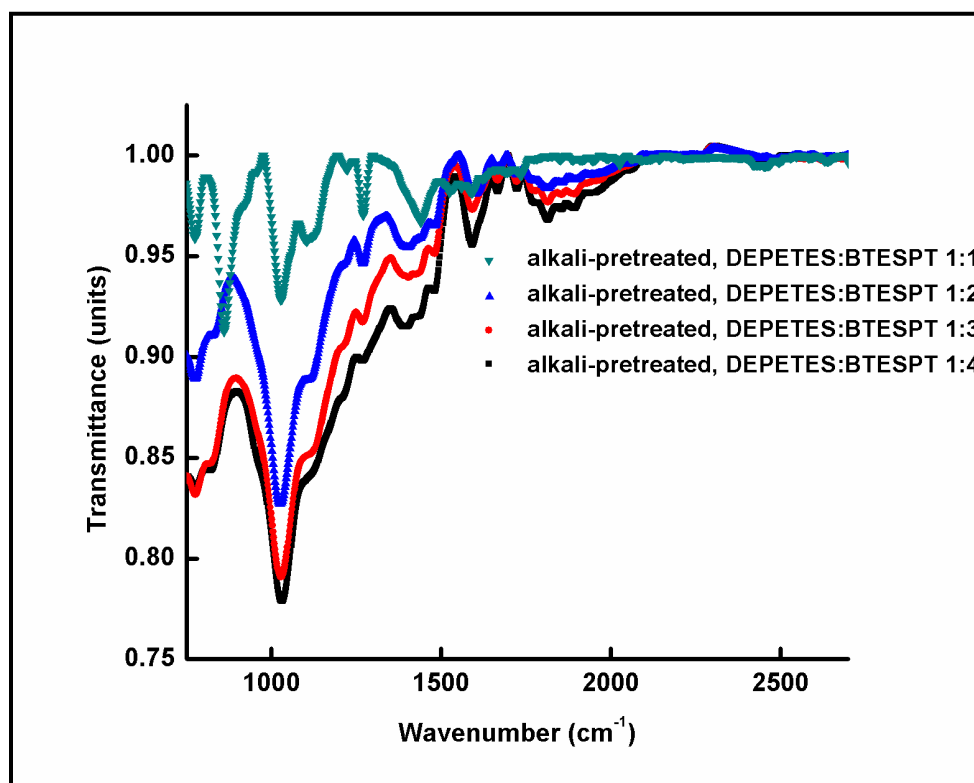


Figure 4.23: FTIR spectra of cured alkali-pretreated alloy dipped in mixtures of silanes in different DEPETES:BTESPT volume ratios: (a) 1:1, (b) 1:2, (c) 1:3 and (d) 1:4

B) Surface morphology and chemical analysis of silane coated alloy

The cross-sectional thickness of the developed coating on the alloy observed to be $\sim 16\mu\text{m}$, as shown in Figure 4.24. Surface morphologies of the alloy specimens alkali pre-treated for 240 h and then dipped in silane mixtures of different DEPETES:BTESPT volume ratios are shown in Figure 4.25. Samples coated with a DEPETES:BTESPT ratio of 1:4 was found to be the most defect-free (Figure 4.25d). The chemical analysis showed the presence of C, S, P, Si and Mg in the polymeric coating, as determined with the help of EDAX analysis (shown in Figure 4.26 below).

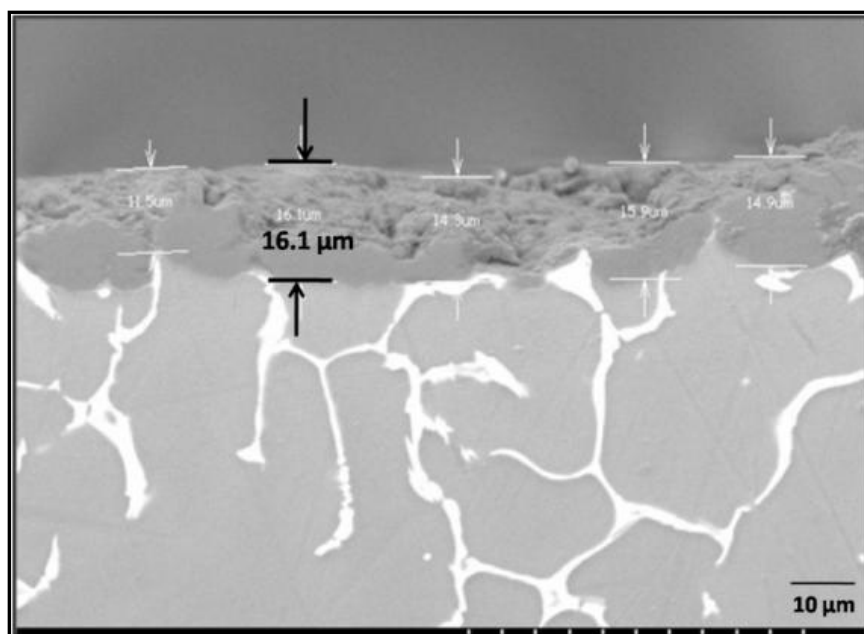


Figure 4.24: SEM micrograph of cross-sectional thickness of the 1:4 DEPETES:BTESPT coated sample

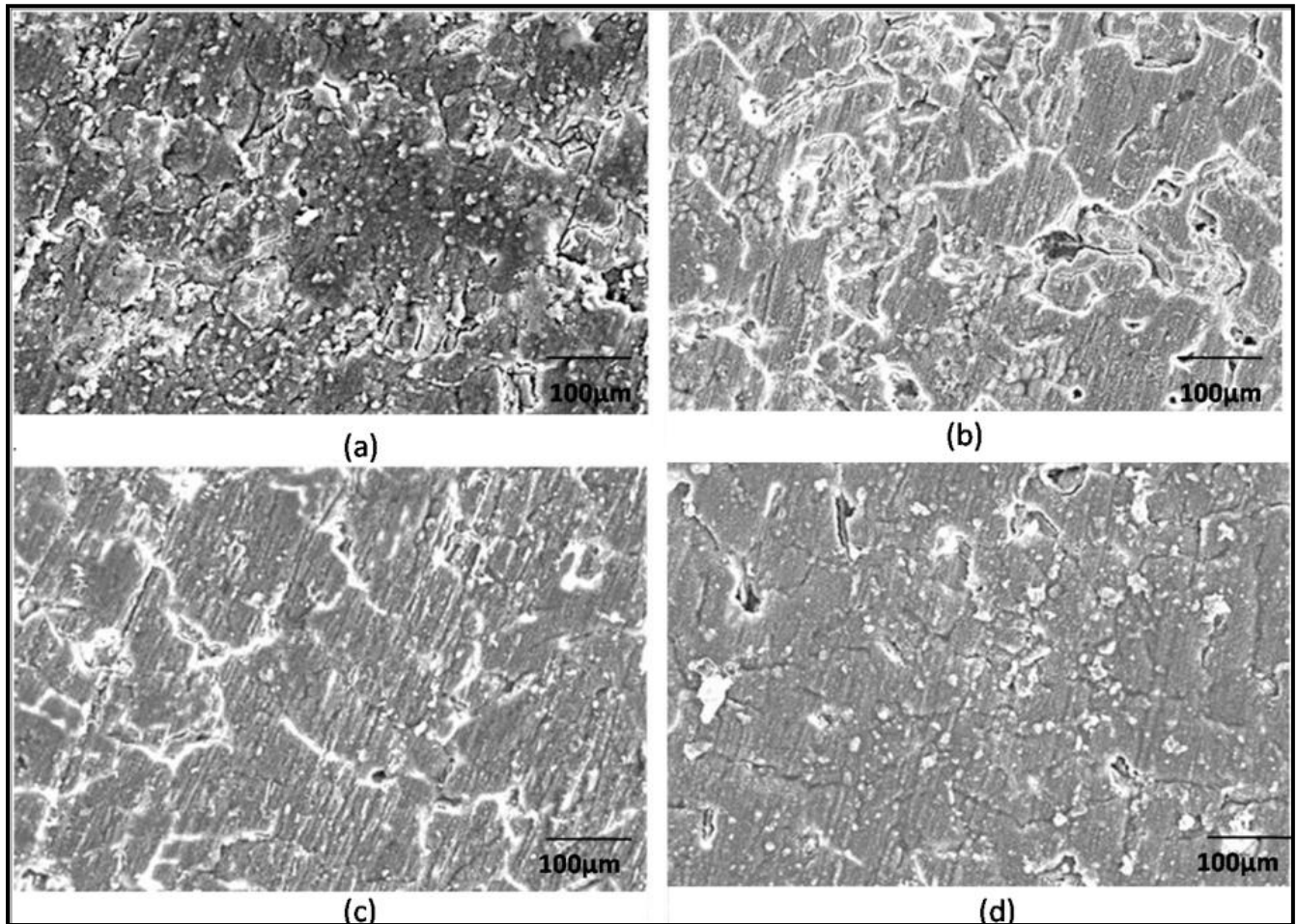


Figure 4.25: SEM micrographs of the surface morphology of alkali-pretreated alloy dipped in mixtures of silanes in different DEPETES:BTESPT volume ratios of: (a) 1:1, (b) 1:2, (c) 1:3 and (d) 1:4.

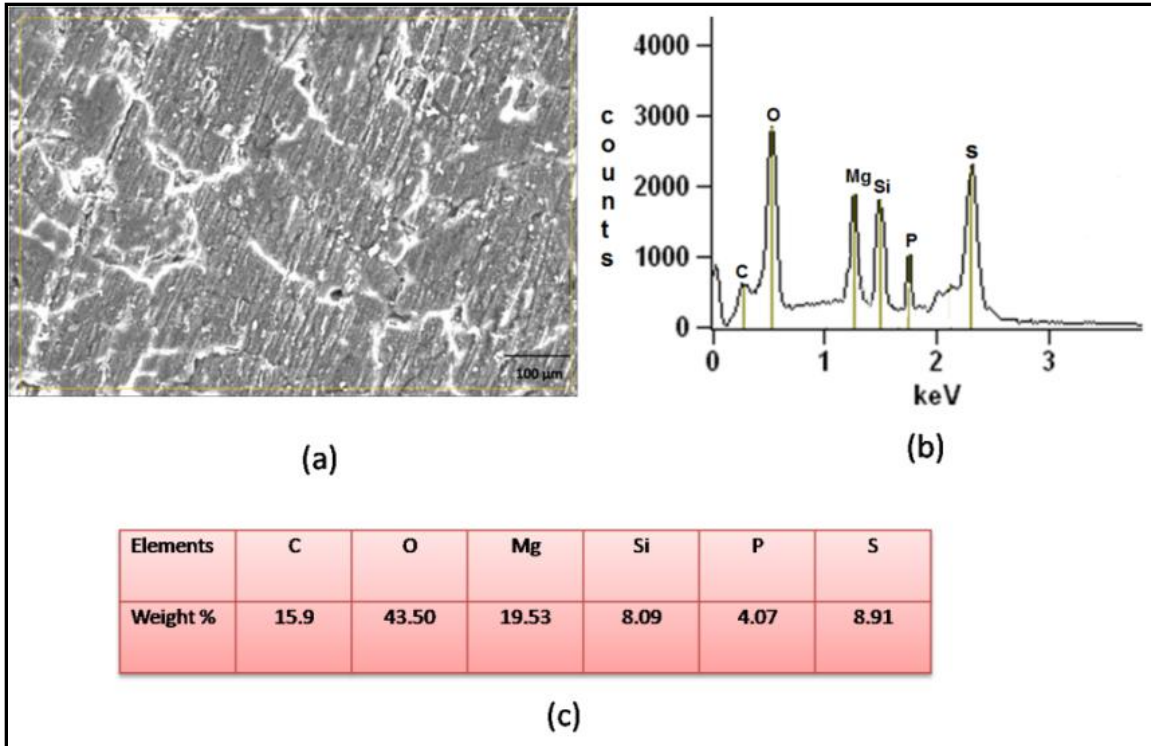


Figure 4.26: (a) SEM micrograph, (b) EDAX graph and (c) Elemental analysis of 1:4 DEPETES:BTESPT coated sample

4.2.2.2 Performance Evaluation of DEPETES:BTESPT silane coated Mg-6Zn-Ca alloy

A) Electrochemical investigation of silane coated Mg-6Zn-Ca alloy

Figure 4.27 shows the potentiodynamic polarization plots for the bare and silane-coated samples in *m*-SBF at 36.5 °C. The corrosion potential (E_{corr}) and the corrosion current density (i_{corr}) derived from the potentiodynamic polarization curves are presented in Table 4.7. Current densities in the corresponding anodic and cathodic parts of the polarization scans of all the coated samples were significantly lower in comparison to the bare alloy. The maximum improvement was seen in the coating with a DEPETES:BTESPT volume ratio of 1:4, as suggested by 2 orders of magnitude lower current density of samples with this coating, as compared to the bare alloy. Also, the corrosion potential (E_{corr}) of the 1:4 coated alloy was ~150

mV more noble as compared to the bare alloy, implying its considerably lesser susceptibility to corrosion.

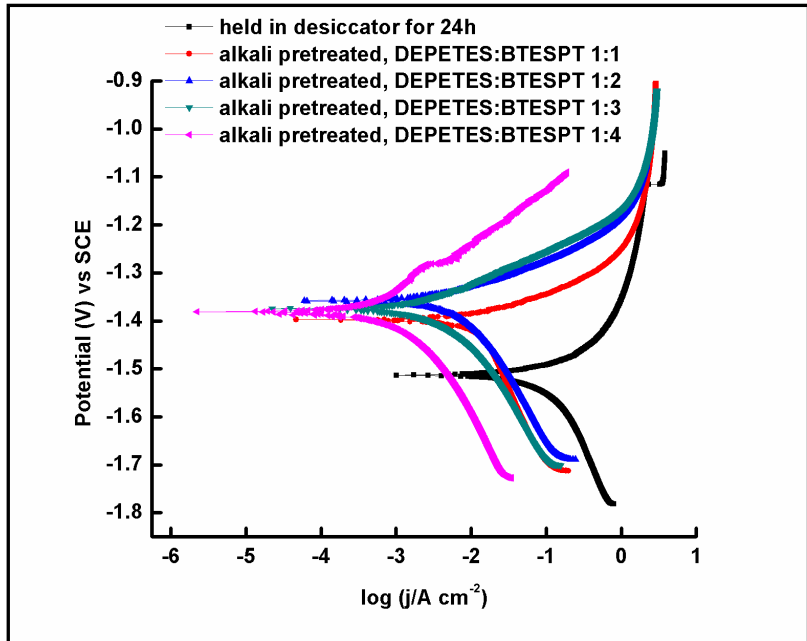


Figure 4.27: Potentiodynamic polarization in *m*-SBF at $(36.5 \pm 0.5) \text{ }^\circ\text{C}$ of the alloy coated with different DEPETES:BTESPT ratios of coating formulations

Table 4.7: Corrosion potential and corrosion current densities derived from plots in Figure 4.27.

Samples	E_{corr} (V)	i_{corr} (i/A cm^2)
Bare Mg-6Zn-Ca alloy held in dessicator for 24 h	-1.57	6.3×10^{-2}
Alkali pretreated, DEPETES:BTESPT 1:1	-1.39	1.5×10^{-2}
Alkali pretreated, DEPETES:BTESPT 1:2	-1.35	3.1×10^{-3}
Alkali pretreated, DEPETES:BTESPT 1:3	-1.37	1.5×10^{-3}
Alkali pretreated, DEPETES:BTESPT 1:4	-1.38	6.3×10^{-4}

The EIS data for the bare and coated Mg-6Zn-1Ca alloy are shown in Bode impedance plots in Figure 4.28. In a Bode impedance plot, the magnitude of impedance at the lowest frequency represents the polarization resistance. The impedance at the lowest frequency for all coated samples increases gradually with the change in the DEPETES:BTESPT ratio from 1:1 to 1:4 in the coating formulation ratio (Figure 4.28 and Table 4.8). The coating with DEPETES:BTESPT ratio of 1:4 improved the corrosion resistance of the bare alloy by 2 orders of magnitude.

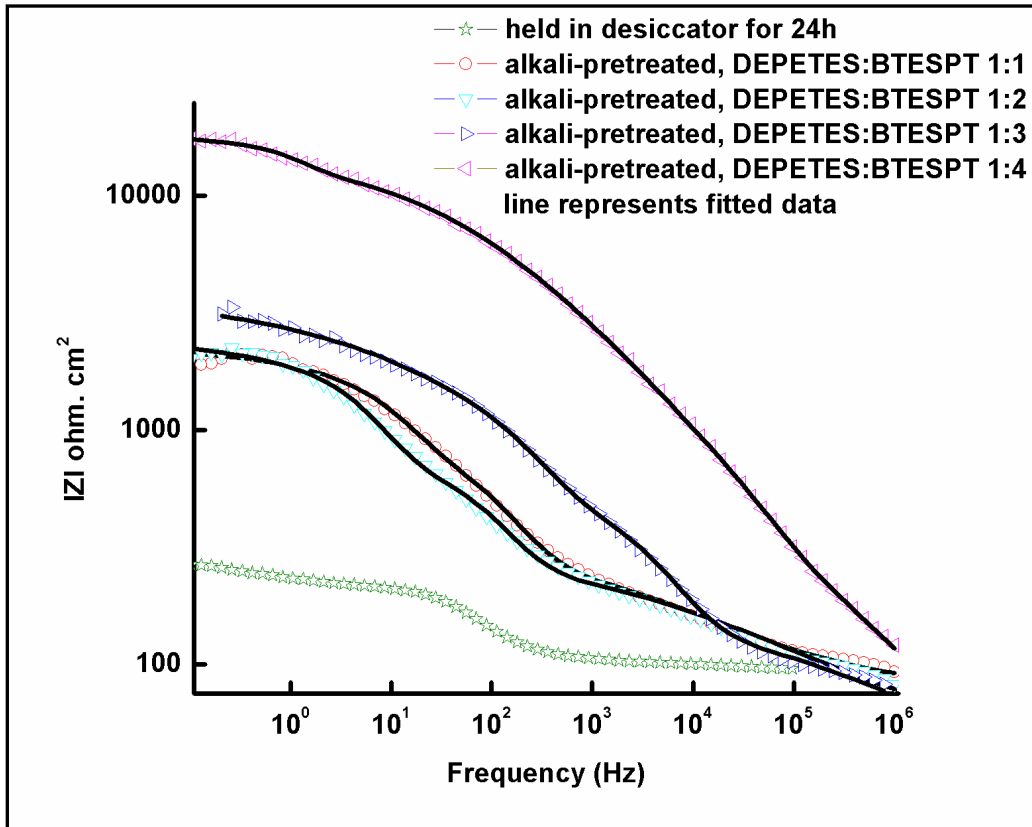


Figure 4.28: Bode plots in *m*-SBF at (36.5 ± 0.5) °C of the alloy coated with different DEPETES:BTESPT ratios of coating formulations.

Table 4.8: Impedance at the lowest frequency for the bare and coated alloys, derived from plots in Figure 4.28

Samples	Impedance $ Z (\Omega \text{ cm}^2)$
Bare Mg-6Zn-Ca alloy	$<10^2$
DEPETES:BTESPT 1:1	1.9×10^3
DEPETES:BTESPT 1:2	2.8×10^3
DEPETES:BTESPT 1:3	3.1×10^3
DEPETES:BTESPT 1:4	1.7×10^4

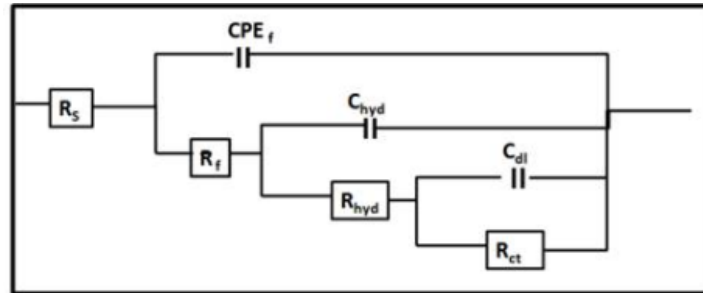


Figure 4.29: The electrical equivalent circuit that fits the experimentally-obtained impedance data of sample coated with a mixture of DEPETES and BTESPT

An EEC with three time constants was proposed for the DEPETES:BTESPT coated alloy (Figure 4.29) to represent the interfaces: a sample/surface hydroxide/*m*-SBF solution and a sample/surface hydroxide/silane film/*m*-SBF solution [12]. Again, these interfaces are

represented as a parallel combination of a capacitance and a resistance. In Figure 4.29 EEC, R_s is the solution resistance and the silane-coated surface is represented by a parallel combination of the constant phase element CPE_f and the coating film resistance R_f . The hydroxide layer is represented by C_{hyd} and hydroxide film resistance by R_{hyd} . The electrical double layer is represented as C_{dl} , and a charge transfer resistance R_{ct} .

Table 4.9: Parameters calculated using EEC in Figure 4.29 for the alloy coated with different ratios of DEPETES:BTESPT, and dipped in *m*-SBF

Parameters	DEPETES:BTESPT volume ratios			
	1:1	1:2	1:3	1:4
$R_f/[\Omega \text{ cm}^2]$	266.6	256	1107	5679
$CPE_f/[F \text{ cm}^{-2}]$	3.0×10^{-5}	4.2×10^{-5}	8.14×10^{-6}	2.5×10^{-6}
n	0.53	0.48	0.61	0.6
$R_{hyd}/[\Omega \text{ cm}^2]$	991.4	701	962.1	9178
$C_{hyd}/[F \text{ cm}^{-2}]$	2.1×10^{-6}	3.6×10^{-6}	1.21×10^{-6}	7.47×10^{-8}
$C_{dl}/[F \text{ cm}^{-2}]$	2.4×10^{-5}	2.5×10^{-5}	6.5×10^{-5}	1.5×10^{-5}
$R_{ct}/[\Omega \text{ cm}^2]$	803.2	1257	863.7	1151
Chi squared value	4.05×10^{-3}	3.35×10^{-3}	4.44×10^{-3}	6.27×10^{-4}
Measured error in impedance/[%]	<6.368	<5.784	<6.664	<2.503
$R_p/[\Omega \text{ cm}^2]$	2060	2214	2933	16008

As suggested by the data in Tables 4.9, R_f , R_{hyd} and R_{ct} for all the coated samples are higher than the R_f and R_{ct} of the untreated bare alloy. Polarization resistance (R_p), which is a measure of the corrosion resistance of the alloy sample coated with a silane volume ratio of 1:4 is considerably higher ($16008 \Omega \text{ cm}^2$) than R_p for the bare alloy ($156.09 \Omega \text{ cm}^2$), suggesting substantial corrosion resistance of the coated alloy. Since capacitance is directly proportional to the area of the capacitor, the relatively lower capacitance in the case of the 1:4 coated sample (order of $CPE_f 10^{-6} \text{ F cm}^{-2}$ and $C_{hyd} 10^{-8} \text{ F cm}^{-2}$) in comparison to the bare alloy as well as those for coatings with 1:1, 1:2, 1:3 ratios of silane mixtures implies that there is a decrease in the active area of corrosion in the case of the alloy with the 1:4 coating.

As established through polarization and EIS tests in *m*-SBF at $(36.5 \pm 0.5) ^\circ\text{C}$, the silane coating with a DEPETES:BTESPT ratio of 1:4 showed substantially superior corrosion resistance to all other treatments; this is attributed to the most defect-free surface developed due to the 1:4 coating (Figure 4.28). This is in agreement with the FTIR spectra and SEM micrographs, which showed the maximum intensity of crosslinking of Si-O-Si peak and a comparatively lesser defective coating in the case of the 1:4 ratio DEPETES:BTESPT coating. Further, SEM micrographs in which a 1:4 DEPETES:BTESPT coated sample showed a comparatively lesser defective coating.

B) Time dependent degradation of 1:4 DEPETES:BTESPT coated alloy

The coating developed with 1:4 DEPETES:BTESPT showed the best corrosion resistance among other ratios. Therefore, the alloy coated with the silane formulation that provided the maximum corrosion resistance in short-term tests (that is, DEPETES:BTESPT, 1:4) was subjected to extended immersions in *m*-SBF, and the durability of corrosion resistance due to the coating was investigated after different durations of immersion. Coatings of other three ratios were found to be completely degraded within few hours of immersion. As shown in Figure 4.30 and Table 4.10, corrosion resistance of the coated samples, as represented by their impedance at the lowest

frequency decreased gradually with increasing immersion time, and became similar to that of the bare alloy after 175 h.

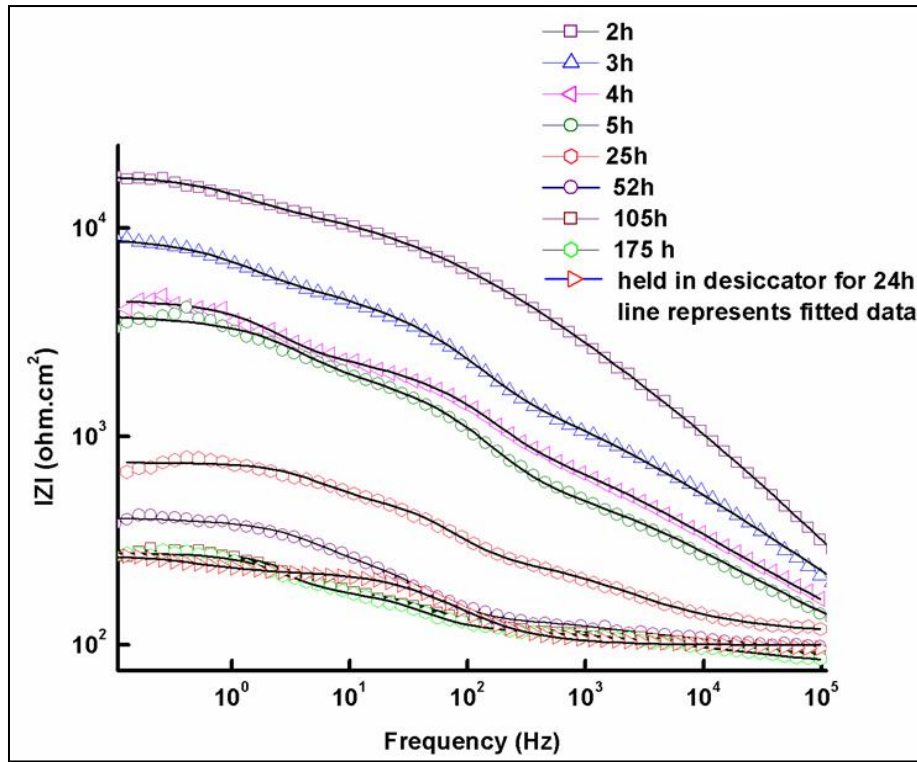


Figure 4.30: Bode plots of the alloy silane coated with DEPETES:BTESPT ratio of 1:4, after different durations of immersion in *m*-SBF at (36.5 ± 0.5) °C.

Table 4.10: Parameters calculated using EEC in Figure 4.29 for the alloy coated with the DEPETES:BTESPT volume ratio of 1:4, dipped in *m*-SBF for different durations

Immersion Time [h]	$R_f/[\Omega \text{ cm}^2]$	$CPE_f/[F \text{ cm}^{-2}]$	n	$R_{hyd}/[\Omega \text{ cm}^2]$	$C_{hyd}/[F \text{ cm}^{-2}]$	$C_{dl}/[F \text{ cm}^{-2}]$	$R_{ct}/[\Omega \text{ cm}^2]$	$R_p/[\Omega \text{ cm}^2]$
2	5679	2.5×10^{-6}	0.6	9178	7.47×10^{-8}	1.5×10^{-5}	1151	16008
3	2448	1.23×10^{-5}	0.44	3979	4.5×10^{-7}	4.1×10^{-5}	2846	9275
4	1436	2.8×10^{-5}	0.40	1887	5.01×10^{-7}	4.4×10^{-5}	1647	4970

5	808	1.7×10^{-5}	0.48	1566	1.1×10^{-6}	3.6×10^{-5}	1425	3800
25	181	1.8×10^{-5}	0.6	264	9.3×10^{-6}	1.5×10^{-4}	193	640
52	50.41	13.1×10^{-5}	0.64	168	2.6×10^{-5}	2.9×10^{-4}	95.93	315
105	47.7	8.0×10^{-5}	0.67	74.95	4.5×10^{-5}	5.6×10^{-4}	89.96	212
175	45.87	10.2×10^{-5}	0.54	69.78	6.2×10^{-5}	7.2×10^{-4}	84.96	198

Table 4.10 suggests that R_f , R_{hyd} and R_{ct} decreased with time; this attributes the degradation of corrosion resistance to the combined degradation of the coating and the hydroxide layer.

C) Hydrogen evolution

As seen in Figure 4.31, hydrogen evolution rates were the highest for the bare alloy and the alloy with 1:1 DEPETES:BTESPT coating throughout the entire duration of immersion of 216 h, whereas, the hydrogen evolution rate has decreased with increase in ratio from 1:1-1:4. It was found to be lowest for the optimized 1:4 DEPETES:BTESPT-coated sample. The hydrogen evolving from the samples with a protective coating exhibited a trend similar to the pH change, that is, a much smaller amount of hydrogen was evolved from the 1:4 ratio coated sample compared to the bare Mg-6Zn-Ca alloy samples.

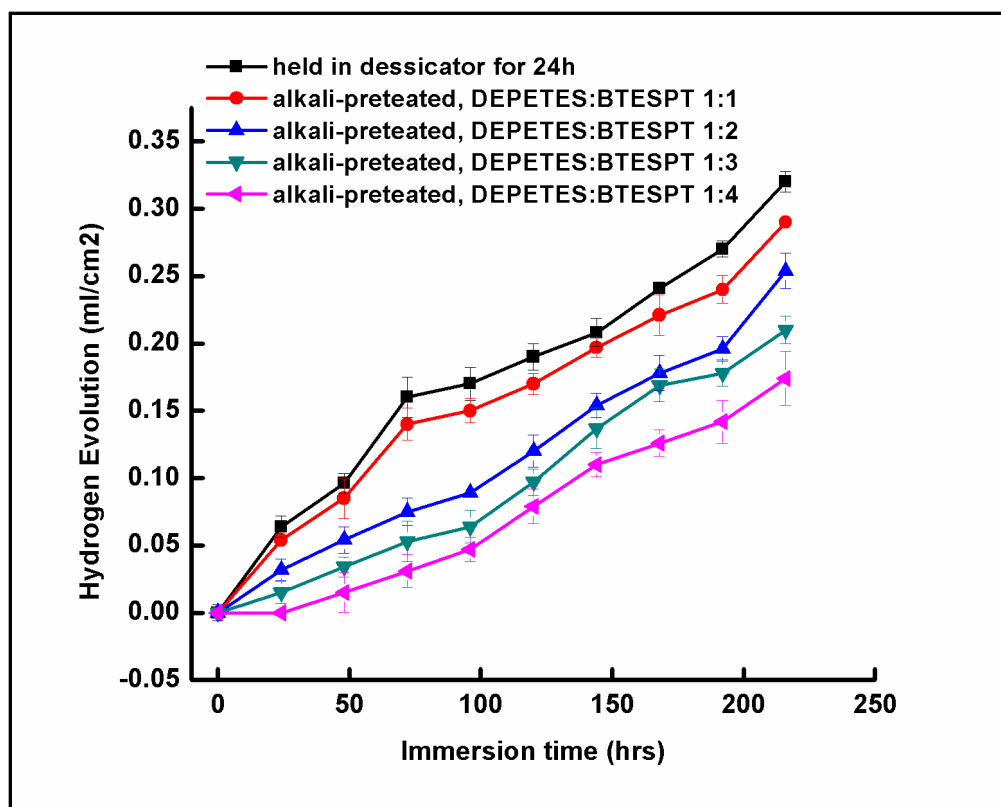


Figure 4.31: Hydrogen evolution of bare and coated alloys, as a function of immersion time *m*-SBF at $(36.5 \pm 0.5) ^\circ\text{C}$.

D) pH study

The change in pH in the bare and the coated alloys was monitored throughout all the corrosion tests. The data in Figure 4.32 suggests that the pH of the alloy coated with the 1:4 DEPETES:BTESPT silane mixture remained below 7.8, whereas, the pH became much higher for the bare alloy and the alloy coated with DEPETES:BTESPT silane mixtures of other ratios.

4.2.2.3 Mechanical analysis of the DEPETES:BTESPT silane coating on the Mg-6Zn-Ca alloy

The coatings showed strong adhesion with a rating of 5B in accordance with ASTM D3359; this rating corresponds to the best ASTM rating. Also, pencil hardness of the coatings, as determined in accordance with ASTM D3363-92a, was found to be 4H.

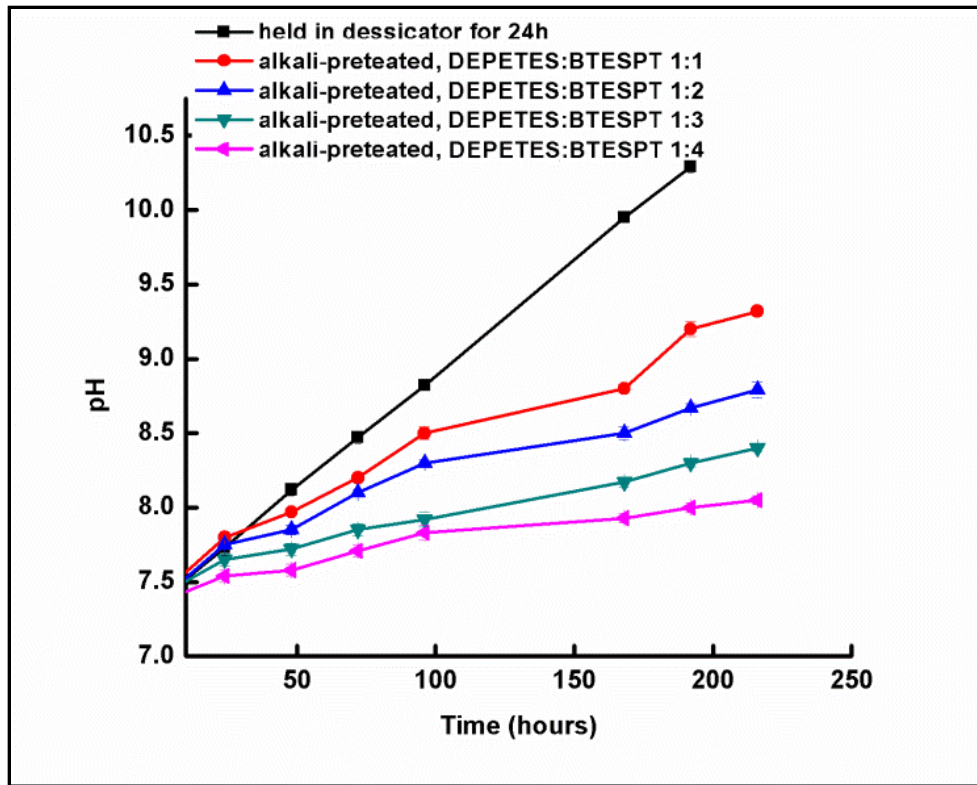


Figure 4.32: Variation of pH as a function of immersion time *m*-SBF at (36.5 ± 0.5) °C.

4.2.2.4 Post Corrosion Analysis of 1:4 DEPETES:BTESPT coated alloy

Figure 4.33 shows SEM images of 1:4 DEPETES:BTESPT coated alloy after immersion in *m*-SBF for 216 h. EDAX of the coated samples indicated the presence of Si, S, oxygen, magnesium, calcium and phosphorous on the surface of the corroded sample. The presence of oxygen and magnesium is consistent with a corrosion product of $Mg(OH)_2$, while the calcium and phosphorous can be associated with *m*-SBF [154].

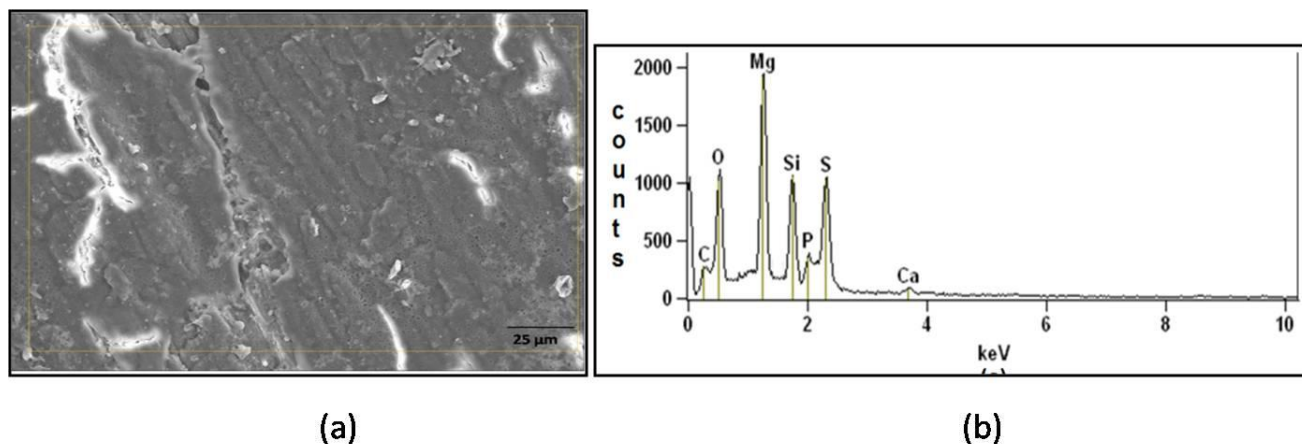
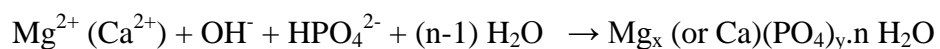


Figure 4.33 a) SEM micrograph, b) EDAX of 1:4 DEPETES:BTESPT-coated samples, after immersion for 216 hrs in *m*-SBF at $(36.5 \pm 0.5) ^\circ\text{C}$

The crystalline corrosion products shown in Figure 4.33(a) were characterized by XRD. The XRD spectrum in Figure 4.34 confirmed the formation of salts of magnesium phosphate, as suggested by the following equation [155] along with magnesium hydroxide and magnesium.



Till now, through both the coating systems, we were able to achieve a significant delay in corrosion and thereby reducing the surface reactivity of the magnesium alloy. Further we explored new coating system based on GPTMS and MTEOS, to see its effect on the corrosion performance of the alloy.

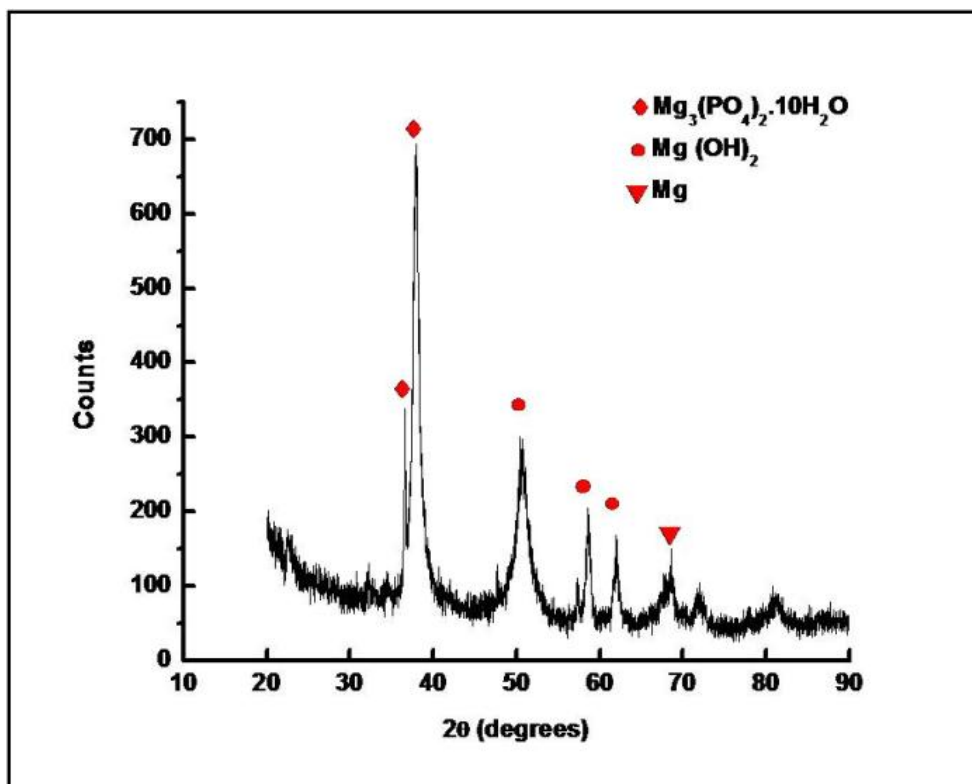


Figure 4.34: XRD spectra of the 1:4 DEPETES:BTESPT coated alloy after immersion for 216 hrs in *m*-SBF at $(36.5 \pm 0.5) ^\circ C$

4.2.3 GPTMS:MTEOS based coating system

The sol gel coating was developed by mixing the two silanes in different molar ratios and hydrolyzing for definite period of time. The coated sample were cured at $120^\circ C$ and were characterized and evaluated.

4.2.3.1 Surface characterization of silane coated alloy

The coated magnesium alloy surface was characterized using FTIR and SEM. EDAX was used for chemical analysis of the coated surface.

A) Structural Analysis –by Fourier transform infrared spectroscopy (FTIR)

Curing of alkali-pretreated silane coated alloy was done at 120 °C, and the extent of curing in silane coatings developed with the different GPTMS:MTEOS volume ratios were examined by FTIR. For the coating, 790 cm^{-1} and 880 cm^{-1} peak respectively correspond to Si-O-C (symmetric) and Si-OH. The Si-OH peak intensity was maximum for coating with 1:1 ratio, that decreased considerably for 2:1 and was, in fact, absent for the coating with 3:1 ratio, indicating consumption of all Si-OH for the formation of Si-O-Si linkage in this case. The 790 cm^{-1} peak was found to be absent in the cases of coatings with 2:1 and 3:1 ratios, suggesting the conversion of Si-OEt to Si-OH and further Si-O-Si bond due to crosslinking. The peak appearing at 1050 cm^{-1} in Figure 4.35 that corresponds to the asymmetric stretching of Si-O-Si linkage, was observed in each case, and confirms the formation of a cross-linked siloxane network structure in the film. It is noted that the Si-O-Si band has a significantly lower intensity in the case of the coating with a 1:1 GPTMS:MTEOS, indicating a lesser extent of cross linking as compared to the coating with the 3:1 ratio that showed maximum intensity for the Si-O-Si peak.

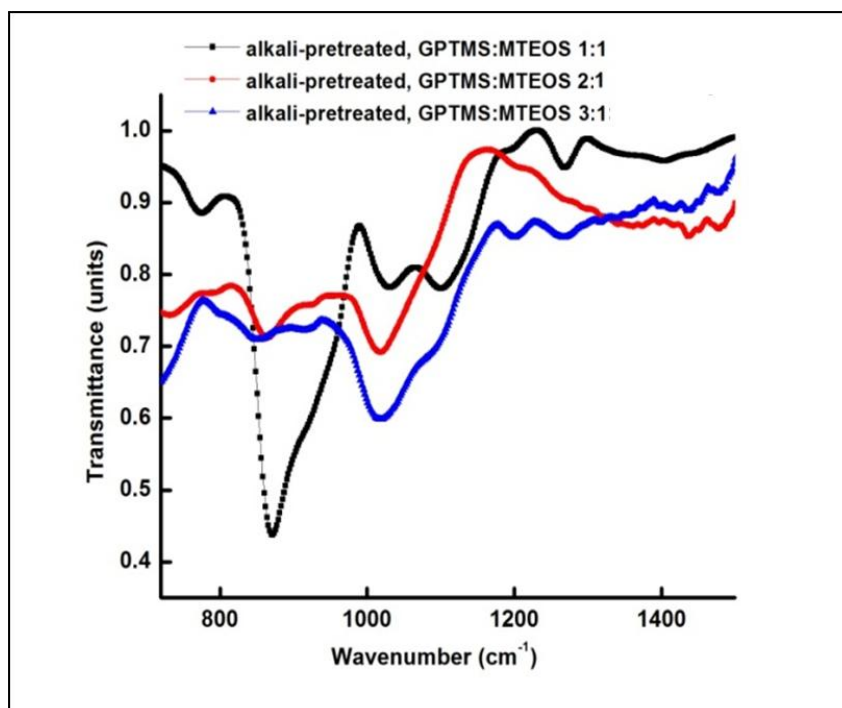


Figure 4.35: FTIR spectra of cured alkali-pretreated alloy dipped in mixtures of silanes in different GPTMS:MTEOS volume ratios: (a) 1:1, (b) 2:1 and (c) 3:1

B) Morphology, chemical and mechanical properties of silane coated alloy

The thickness of developed coating was observed to be $21\mu\text{m}$, as shown in Figure 4.36. Surface morphologies of the alloy coated with different mixtures of GPTMS:MTEOS molar ratios are shown in Figure 4.37. Specimens coated with a GPTMS:MTEOS ratio of 3:1 was found to be the most defect-free (Figure 4.37 c). EDAX analysis of the coated alloy showed the presence of Si, Mg, Ca O and carbon (Figure 4.37 d). Pencil hardness of the coatings, as determined in accordance with ASTM D3363-92a, was found to be 4H and also adhesion of the coatings (determined in accordance with ASTM D3359) showed a strong adhesion (rating 5B that corresponds the best ASTM rating).

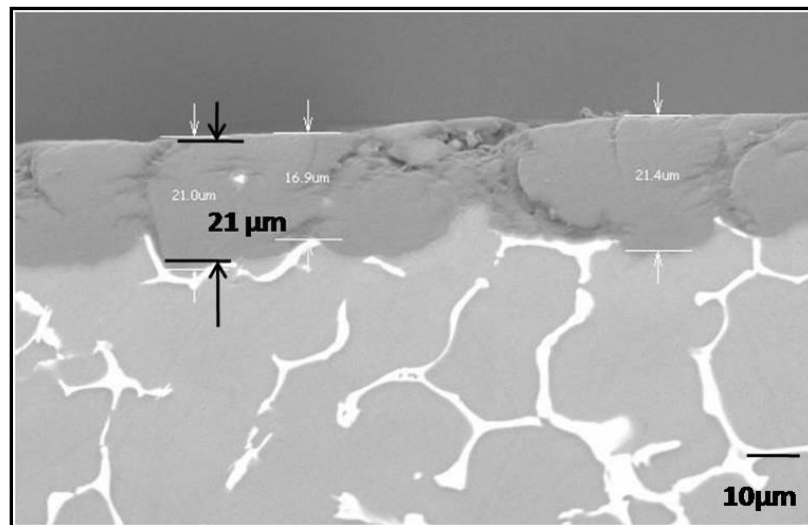


Figure 4.36: SEM micrograph of crosssectional thickness of the 3:1 GPTMS:MTEOS coated sample

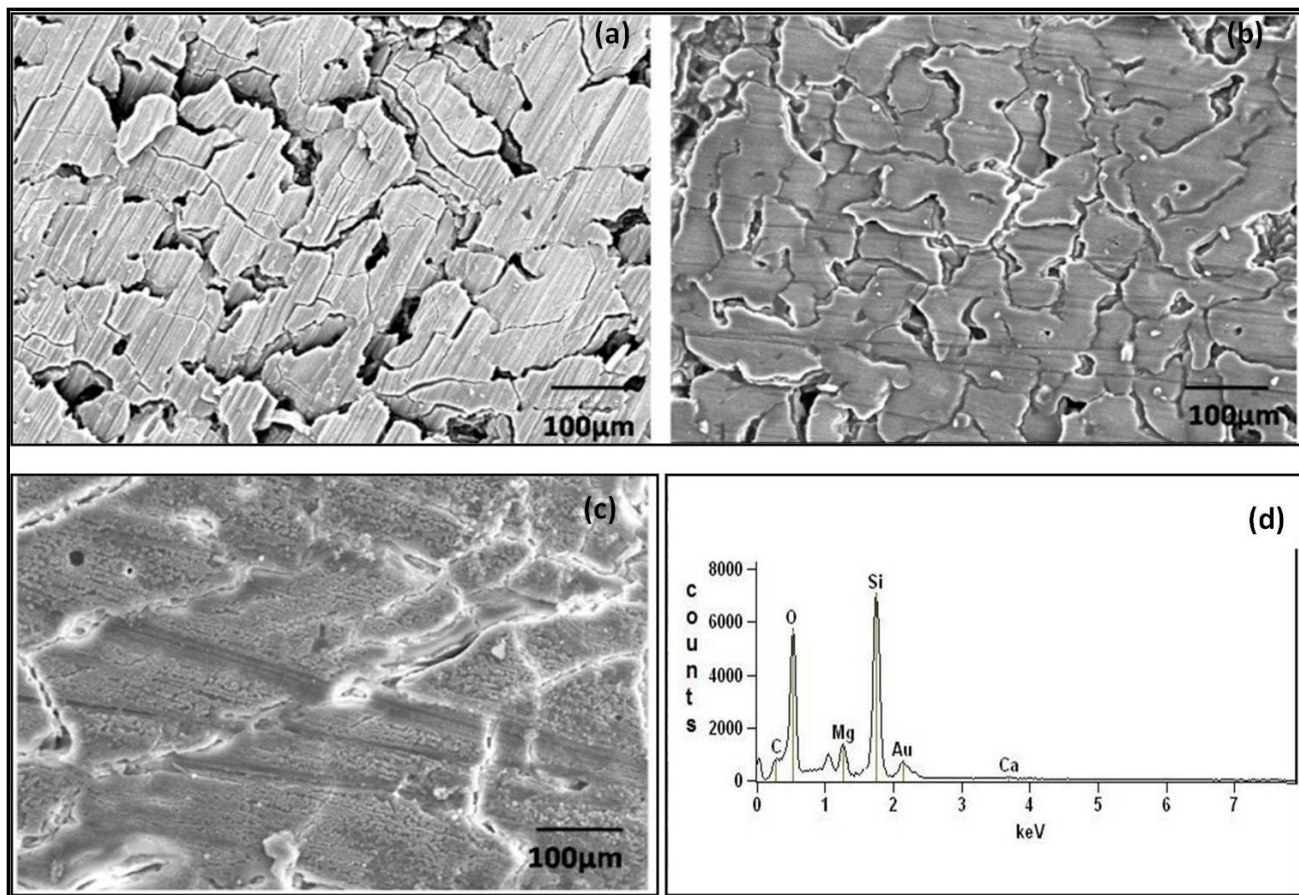


Figure 4.37: SEM micrographs of the surface morphology of alkali-pretreated alloy dipped in mixtures of silanes in different GPTMS:MTEOS volume ratios of: (a) 1:1, (b) 2:1, (c) 3:1 and (d) EDAX elemental analysis of 3:1 GPTMS:MTEOS coated specimen

4.2.3.2 Performance Evaluation of GPTMS:MTEOS silane coated Mg-6Zn-Ca alloy

A) Electrochemical investigation of GPTMS:MTEOS silane coated alloy

Figure 4.38 shows the potentiodynamic polarization plots for the bare and GPTMS:MTEOS silane-coated specimens in *m*-SBF at 36.5 °C. The corrosion potential (E_{corr}) and the corrosion current density (i_{corr}) derived from these plots are presented in Table 4.11. The corrosion potential (E_{corr}) of the alloy coated with the 3:1 ratio was ~340 mV more noble as compared to the bare alloy. Also, the current densities in the anodic and cathodic parts of the polarization

scans of the alloy with the 3:1 coating were two orders of magnitude lower, as compared to the bare alloy (Table 4.11). As evident from Figure 4.36 and Table 4.11, the coatings with the GPTMS:MTEOS ratios of 2:1 and 1:1 resulted in considerably less noble shifts in E_{corr} as well as the decrease in current densities.

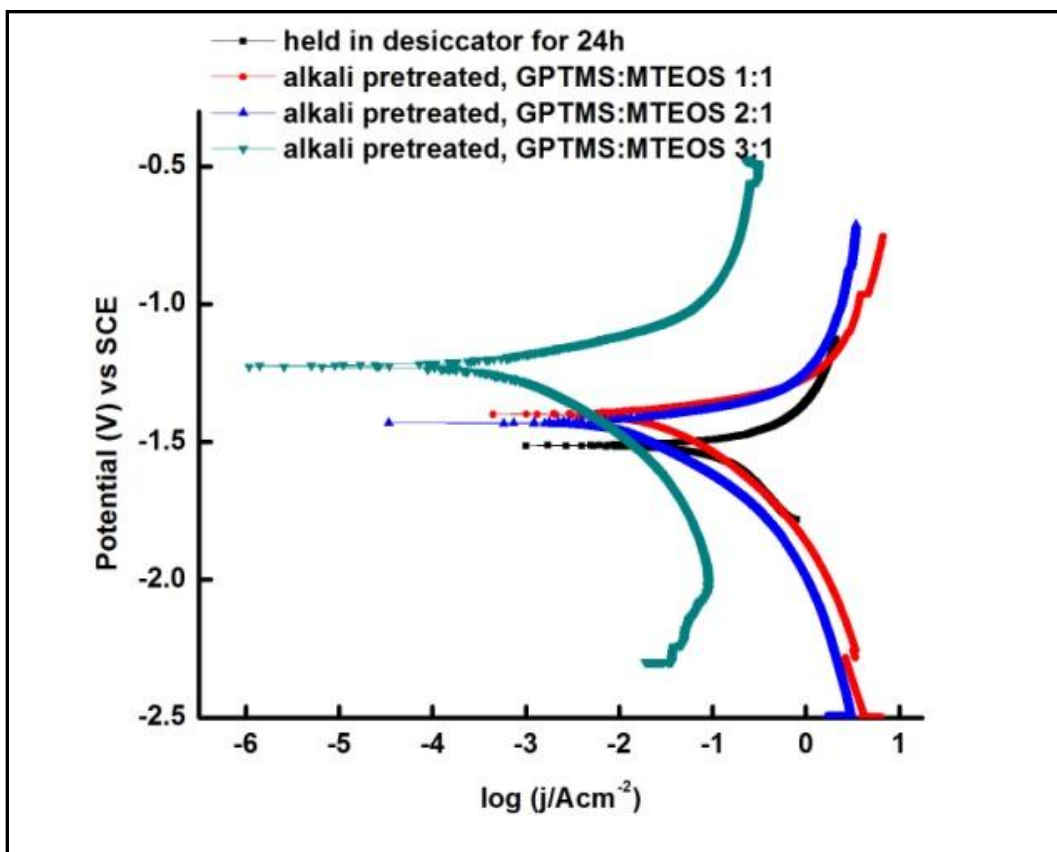


Figure 4.38: Potentiodynamic polarization in *m*-SBF at (36.5 ± 0.5) °C of the alloy coated with different GPTMS:MTEOS ratios of coating formulations

Table 4.11: Corrosion potential and corrosion current densities derived from plots in Figure 4.38

Samples	E_{corr} (V)	i_{corr} (i/A cm²)
Bare Mg-6Zn-Ca alloy held in dessicator for 24 h	-1.57	6.3 x10 ⁻²
Alkali pretreated, GPTMS:MTEOS 1:1	-1.40	3.1 x10 ⁻²
Alkali pretreated, GPTMS:MTEOS 2:1	-1.43	1.2 x10 ⁻²
Alkali pretreated, GPTMS:MTEOS 3:1	-1.23	8.9 x10 ⁻⁴

The EIS data for the bare and GPTMS:MTEOS coated Mg-6Zn-1Ca alloy are shown in the form of Bode impedance plots in Figure 4.39. In Bode impedance plot, the magnitude of impedance at the lowest frequency represents the polarization resistance. The impedance at the lowest frequency for all coated specimens increased systematically with the change in the GPTMS:MTEOS ratio from 1:1 to 3:1 in the coating formulation (Figure 4.39 and Table 4.12). The coating with GPTMS:MTEOS, 3:1 ratio provided improvement in corrosion resistance of bare Mg-6Zn-Ca alloy by 5 orders of magnitude.

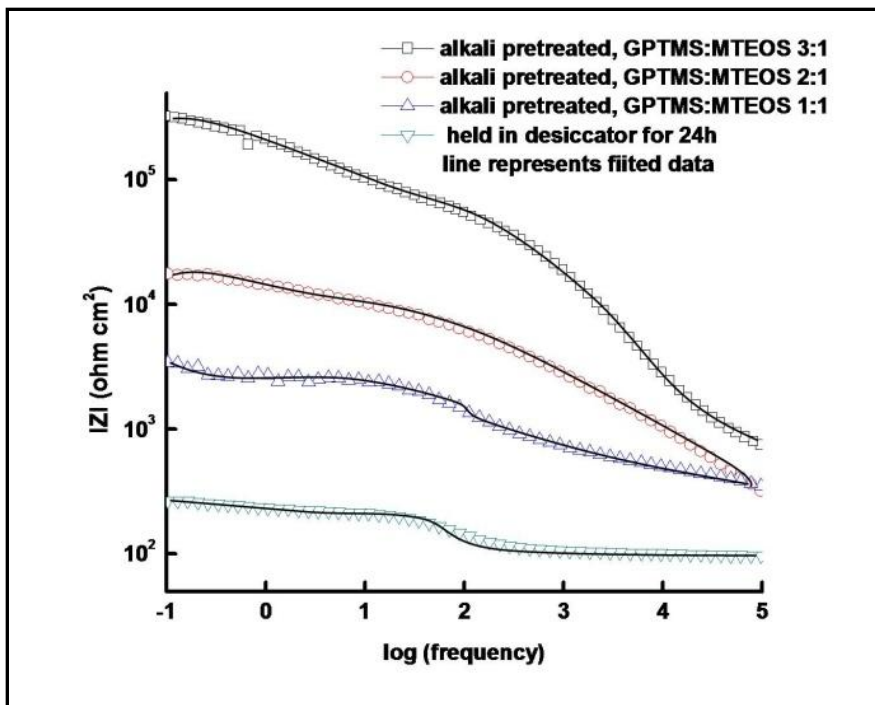


Figure 4.39: Bode plots in *m*-SBF at $(36.5 \pm 0.5)^\circ\text{C}$ of the alloy coated with different GPTMS:MTEOS ratios of coating formulations.

Table 4.12: Impedance at the lowest frequency for the bare and coated alloys, derived from plots in Figure 4.39

Samples	Impedance $ Z (\Omega \text{ cm}^2)$
Bare Mg-6Zn-Ca alloy	$<10^2$
GPTMS:MTEOS 1:1	5×10^3
GPTMS:MTEOS 2:1	2×10^4
GPTMS:MTEOS 3:1	4×10^5

B) Time dependent degradation of GPTMS:MTEOS coated alloys

Coatings with each of the three GPTMS:MTEOS ratios provided significant improvement in the corrosion resistance (impedance) of the alloy. Alloys with the three coatings were subjected to extended immersions in *m*-SBF, and the durability of corrosion resistance due to the coating was investigated after different durations of immersion.

An EEC with three time constants, as shown in Figure 4.40 was proposed for the GPTMS:MTEOS coated alloy to represent the interfaces: a substrate/surface hydroxide/*m*-SBF solution and a substrate/surface hydroxide/silane film/*m*-SBF solution. These interfaces are represented as a parallel combination of a capacitance and a resistance. In this EEC, R_s is the solution resistance and the silane-coated surface is represented by a parallel combination of the constant phase element CPE_f and the coating film resistance R_f . The hydroxide layer is represented by C_{hyd} and hydroxide film resistance by R_{hyd} . The electrical double layer is represented as C_{dl} , and a charge transfer resistance R_{ct} .

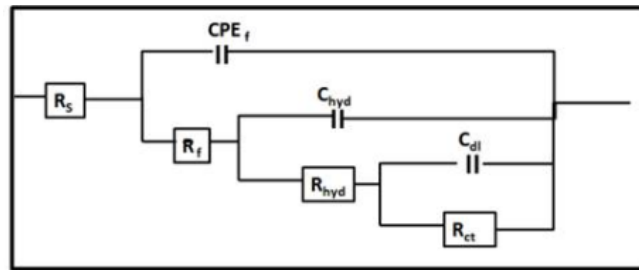


Figure 4.40: The electrical equivalent circuit that fits the experimentally-obtained impedance data of sample coated with a mixture of GPTMS:MTEOS

As shown in Figure 4.41, the time dependent immersion showed the durability of 1:1 GPTMS:MTEOS ratio for 24 h (Figure 4.41 a), 2:1 GPTMS:MTEOS for 100 h (Figure 4.41 b) and 3:1 GPTMS:MTEOS for 280h (Figure 4.41 c). After 24 h of constant immersion, the 1:1 GPTMS:MTEOS silane coating loses its potential to protect the sample in *m*-SBF at (36.5 ± 0.5)

°C similarly 2:1 GPTMS:MTEOS loses its protective property in 100 h and 3:1 GPTMS:MTEOS survives for 280 h.

The R_f value is a measure of the resistance through the pores of the coatings and is inversely proportional to the extent and number of defects in the coating. The evolution of R_f with the exposure time in the electrolyte gives information about the coating capacity to avoid the formation of pores across the film due to its degradation. High R_f values are attributed to the protective property of coatings during electrolyte exposure. As evident from Figure 4.41 and Table 4.13 GPTMS:MTEOS, 3:1 showed a significantly high R_f , proving to be highly crosslinked and protective coating.

An increase in C_f and C_{hyd} is observed with increased immersion time, which is attributed to the uptake of the electrolyte into the coating. It is noted that C_f and C_{hyd} values attribute to the physical properties of the coatings themselves, which includes being thicker or physically not allowing water to diffuse as rapidly.

The increase in these values with decrease in R_p value (Table 4.13 - 4.15) attributes to the onset or progression of corrosion processes at the surface of the metal and subsequently the detachment of the epoxy coating from the sample.

The charge transfer resistance (R_{ct}) is able to yield information regarding the rate of the corrosion process occurring at the metal sample beneath the coating. A decline in the R_{ct} value is observed following different time of immersion for all the 3 ratios of immersion, which corresponds with the increasing extent of corrosion.

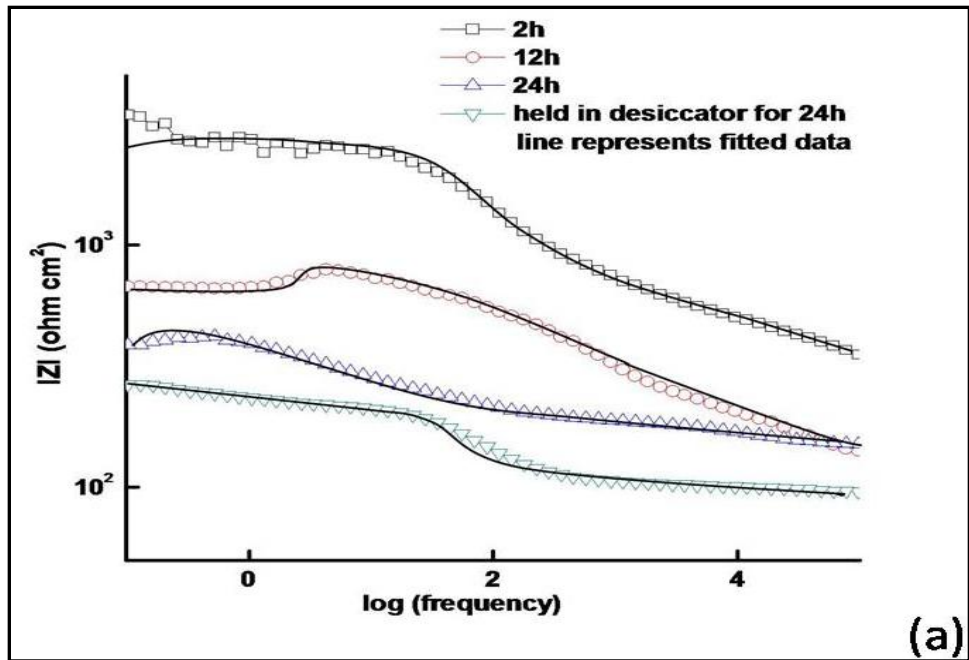


Figure 4.41 (a) : Bode plots of the alloy silane coated with 1:1 GPTMS:MTEOS, after different durations of immersion in *m*-SBF at $(36.5 \pm 0.5)^\circ\text{C}$

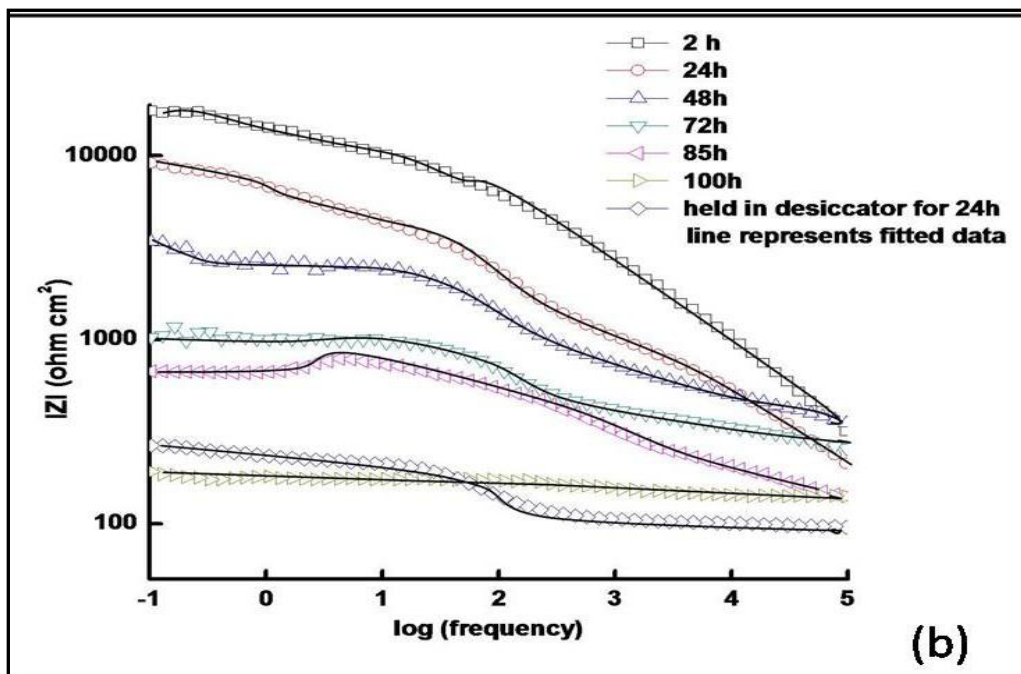


Figure 4.41 (b): Bode plots of the alloy silane coated with 2:1, GPTMS:MTEOS after different durations of immersion in *m*-SBF at $(36.5 \pm 0.5)^\circ\text{C}$

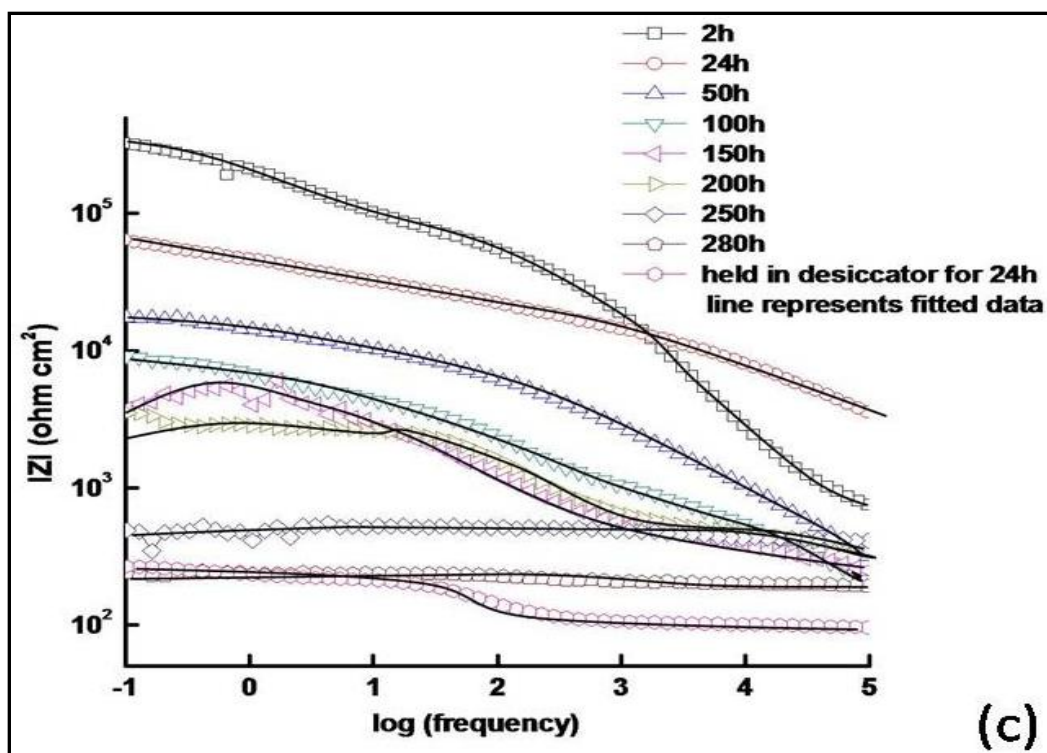


Figure 4.41 (c): Bode plots of the alloy silane coated with 3:1 GPTMS:MTEOS, after different durations of immersion in *m*-SBF at $(36.5 \pm 0.5) ^\circ\text{C}$

Table 4.13: Parameters calculated using EEC in Figure 4.40 for the alloy coated with the 1:1 GPTMS:MTEOS, dipped in *m*-SBF at $(36.5 \pm 0.5) ^\circ\text{C}$ for different durations

Immersion Time [h]	$R_f/[\Omega \text{ cm}^2]$	$CPE_f/[F \text{ cm}^{-2}]$	n	$R_{hyd}/[\Omega \text{ cm}^2]$	$C_{hyd}/[F \text{ cm}^{-2}]$	$C_{dl}/[F \text{ cm}^{-2}]$	$R_{ct}/[\Omega \text{ cm}^2]$	$R_p/[\Omega \text{ cm}^2]$
2	1765	1.7×10^{-5}	0.48	1535	1.3×10^{-6}	3.6×10^{-5}	1400	4700
12	283	5.4×10^{-5}	0.6	274	2.5×10^{-5}	1.8×10^{-4}	193	750
24	50.41	14.1×10^{-5}	0.63	168	9.2×10^{-5}	2.7×10^{-4}	102	320.41

Table 4.14: Parameters calculated using EEC in Figure 4.40 for the alloy coated with the 2:1 GPTMS:MTEOS, dipped in *m*-SBF for different durations

Immersion Time [h]	$R_f/[\Omega \text{ cm}^2]$	$CPE_f/[F \text{ cm}^{-2}]$	n	$R_{hyd}/[\Omega \text{ cm}^2]$	$C_{hyd}/[F \text{ cm}^{-2}]$	$C_{dl}/[F \text{ cm}^{-2}]$	$R_{ct}/[\Omega \text{ cm}^2]$	$R_p/[\Omega \text{ cm}^2]$
2	16079	2.7×10^{-6}	0.63	9178	7.47×10^{-7}	1.7×10^{-5}	7261	32458
24	4448	1.2×10^{-5}	0.42	2551	4.5×10^{-6}	4.2×10^{-5}	2776	9775
48	2436	2.3×10^{-5}	0.40	1987	5.01×10^{-6}	4.8×10^{-5}	1947	6370
72	408	2.7×10^{-5}	0.45	466	2.1×10^{-5}	5.2×10^{-5}	226	1100
85	351	2.8×10^{-5}	0.61	334	7.3×10^{-5}	1.6×10^{-4}	145	830
100	85	10.1×10^{-5}	0.63	156	8.0×10^{-5}	2.8×10^{-4}	99	340

Table 4.15: Parameters calculated using EEC in Figure 4.40 for the alloy coated with the 3:1 GPTMS:MTEOS, dipped in *m*-SBF for different durations

Immersion Time [h]	$R_f/[\Omega \text{ cm}^2]$	$CPE_f/[F \text{ cm}^{-2}]$	n	$R_{hyd}/[\Omega \text{ cm}^2]$	$C_{hyd}/[F \text{ cm}^{-2}]$	$C_{dl}/[F \text{ cm}^{-2}]$	$R_{ct}/[\Omega \text{ cm}^2]$	$R_p/[\Omega \text{ cm}^2]$
2	184679	6.5×10^{-6}	0.59	122256	9.1×10^{-8}	8.5×10^{-6}	78073	385008
24	36050	1.2×10^{-5}	0.44	22979	4.5×10^{-7}	4.1×10^{-5}	13246	72275
50	8636	1.8×10^{-5}	0.40	6787	5.1×10^{-7}	4.9×10^{-5}	4147	19570
100	3235	2.7×10^{-5}	0.48	2766	2.1×10^{-6}	5.3×10^{-5}	2599	8600
150	2181	4.8×10^{-5}	0.6	1464	6.3×10^{-6}	6.3×10^{-5}	1595	5240
200	850	8.1×10^{-5}	0.64	1268	7.6×10^{-6}	7.2×10^{-5}	997	3115
250	245	9.1×10^{-5}	0.67	200	4.4×10^{-5}	8.3×10^{-4}	267	712
280	85	11.2×10^{-5}	0.54	97	6.5×10^{-5}	8.5×10^{-4}	93	285

The coating developed with 3:1 GPTMS:MTEOS ratio showed the best corrosion resistance among the coatings with the other silane mixtures in different ratios. All the ratios were subjected to extended immersions in *m*-SBF, and the durability of corrosion resistance due to the coating was investigated after different durations of immersion.

C) Hydrogen Evolution

As seen in Figure 4.42, hydrogen evolution rates were the highest for the bare alloy and the alloy with 1:1 GPTMS:MTEOS coating throughout the entire duration of immersion of 360h, whereas, the rate was lowest for the optimized 3:1 GPTMS:MTEOS coated sample. Consistent with the polarization and EIS data (Figure 4.38, 4.39 and 4.41), among the three coatings, the hydrogen evolution rate was the highest for the coating with 1:1 ratio of GPTMS:MTEOS, and it was the lowest for coating with the ratio of 3:1.

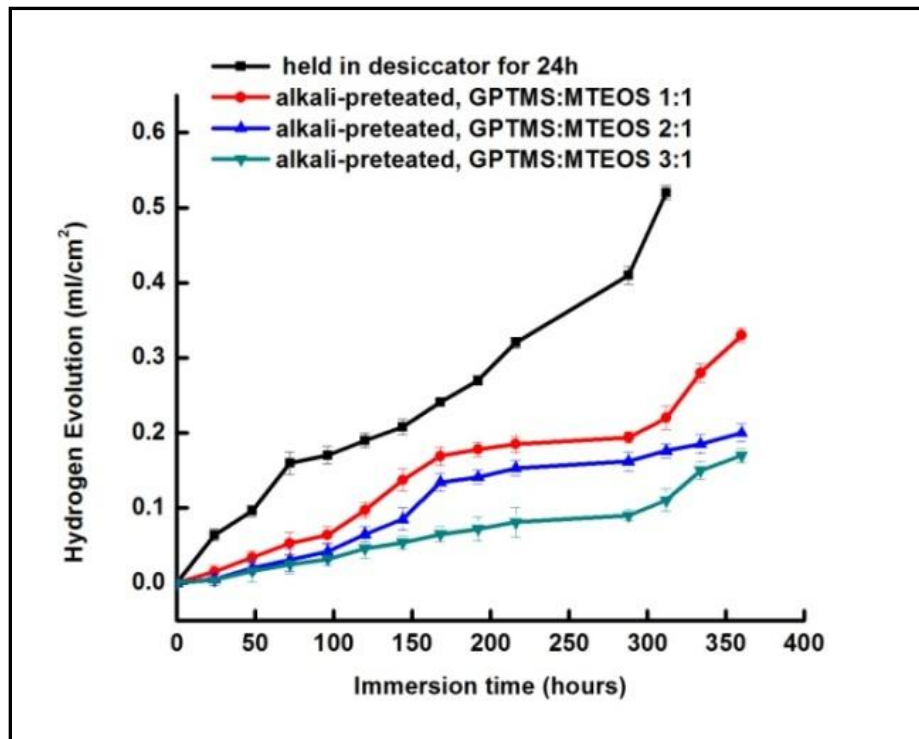


Figure 4.42: Hydrogen evolution of bare and coated alloys, as a function of immersion time *m*-SBF at $(36.5 \pm 0.5) ^\circ\text{C}$

D) pH study

The change in pH in the bare and the coated alloys was monitored throughout all the corrosion tests. The data in Figure 4.43 suggests that the pH of all the GPTMS:MTEOS coated alloy remained below 7.8. The change increase in pH is drastically low in all the ratios as compared to bare alloy. The specimens exhibited similar trend of pH change and hydrogen evolution from the samples with a protective coating, that is, a much smaller amount of hydrogen was evolved and minimum increase in pH was observed from the 3:1 ratio coated sample compared to the bare Mg-6Zn-Ca alloy samples.

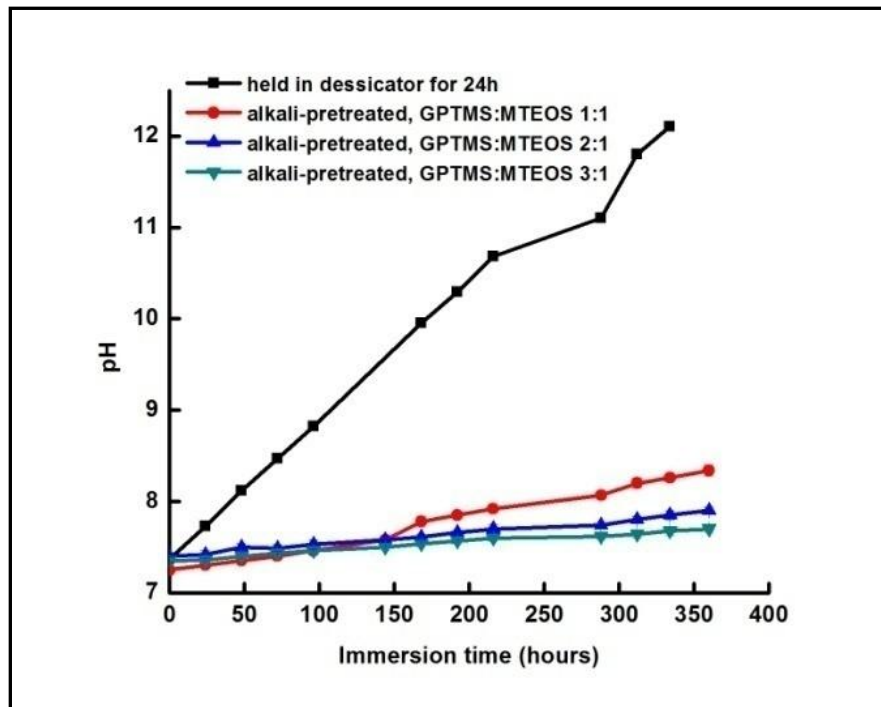


Figure 4.43: Variation of pH as a function of immersion time *m*-SBF at $(36.5 \pm 0.5) ^\circ\text{C}$.

4.2.3.3 Post corrosion analysis

SEM image in Figure 4.44 a shows morphology of the alloy coated with the 3:1 ratio of GPTMS:MTEOS, after immersion in *m*-SBF for 280 h. The micrograph show a rough surface

layer formed on the specimen with precipitates formed due to corrosion of the specimen in the *m*-SBF. EDAX spectrum of this surface indicated the presence of Si, oxygen, magnesium, calcium and zinc on the surface of the corroded specimen.

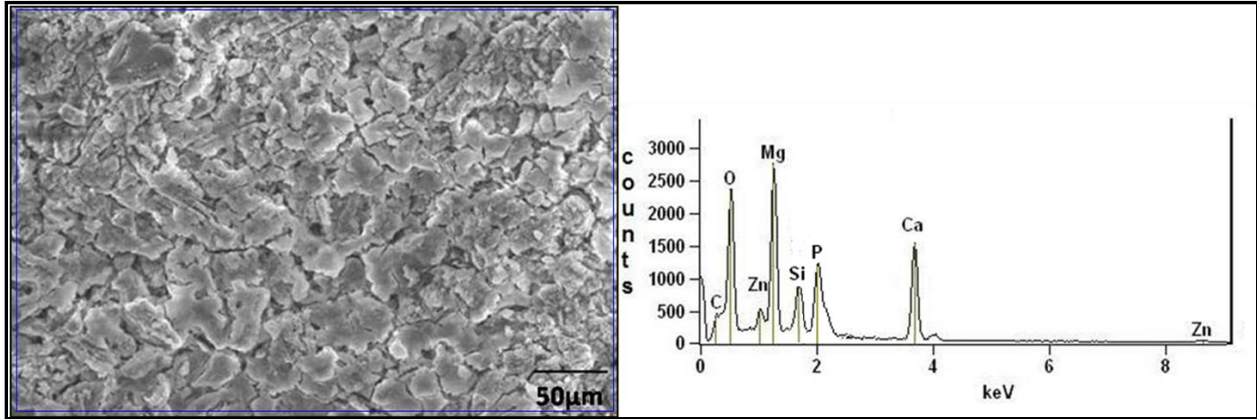


Figure 4.44: a) SEM micrographs, (b) EDAX of 3:1 GPTMS:MTEOS-coated samples, after immersion for 280 h in *m*-SBF at $(36.5 \pm 0.5)^\circ\text{C}$

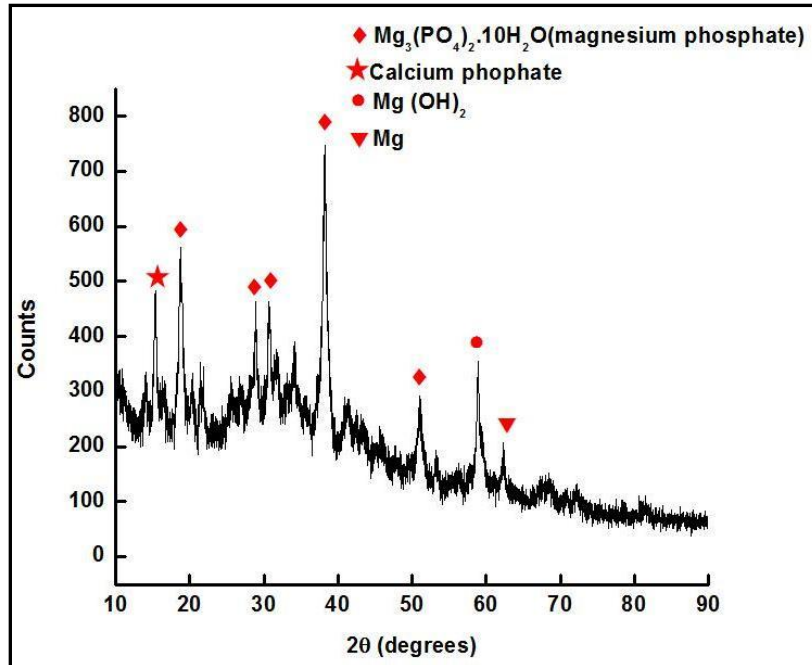
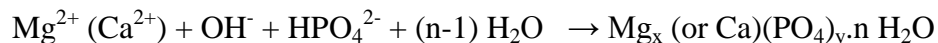


Figure 4.45: XRD spectra of the 3:1 GPTMS:MTEOS coated alloy after immersion for 280 h in *m*-SBF at $(36.5 \pm 0.5)^\circ\text{C}$

The crystalline corrosion products shown in Figure 4.44 were characterized by XRD. The XRD spectrum in Figure 4.45 confirmed the formation of salts of magnesium and calcium phosphate, as suggested by the following equation [155] along with magnesium hydroxide and magnesium:



4.3 In vitro biocompatibility tests

4.3.1 Biocompatibility investigation of GPTMS:MTEOS coating system

4.3.1.1 Cell morphology and attachment observations

The successful attachment of cells onto the surface of alloy specimen is a major characteristic in determining a favourable biological response towards the alloy implants. Figure 4.46 shows the electron micrographs depicting successful attachment and cell morphology of the MG-63 osteosarcoma cells on the surface of bare Mg-6Zn-Ca and 3:1 GPTMS:MTEOS silane coated Mg-6Zn-Ca after 1, 3, 7 and 14 days. The positive control cells show normal morphology and steady crowding of cells is observed over the experimental time period. The cell attachment on the surface of bare Mg-6Zn-Ca specimen show strong differences even from the first day of study. It showed no or a very low number of cells attached on the surface which further decreased over the fortnight due to the specimen undergoing corrosion and thereby evolving hydrogen on the surface. The micrographs on day 3 and 7 show rounded up and fewer numbers of cells with the specimen primarily covered by the corrosion products. In contrast, the coated specimen shows initiation of attachment of cells on day 1 with spherical cellular morphology. By the end of day 3, these cells are seen to properly attach to the surface and the cytoplasm of these cells is seen to be successfully spread, forming filopodia, to achieve normal cellular morphology (can be seen clearly at higher magnification (Figure 4.47)). By day 7, it was observed that the cells were successfully dividing as an increase in the number of viable cells could be seen. Also, initiation of corrosion of the specimen could also be observed. Micrograph captured on day 14 of the study showed the formation of thin cellular layer covering the specimen along with the corrosion products accumulating in the region. The cells can be seen flattened and attach tightly on coated surfaces with their filopodium. These results indicate the facilitation of the cell

attachment by the coating on to the specimen which delays the corrosion of the alloy and help in improvement of the biological response towards the intended implant specimen.

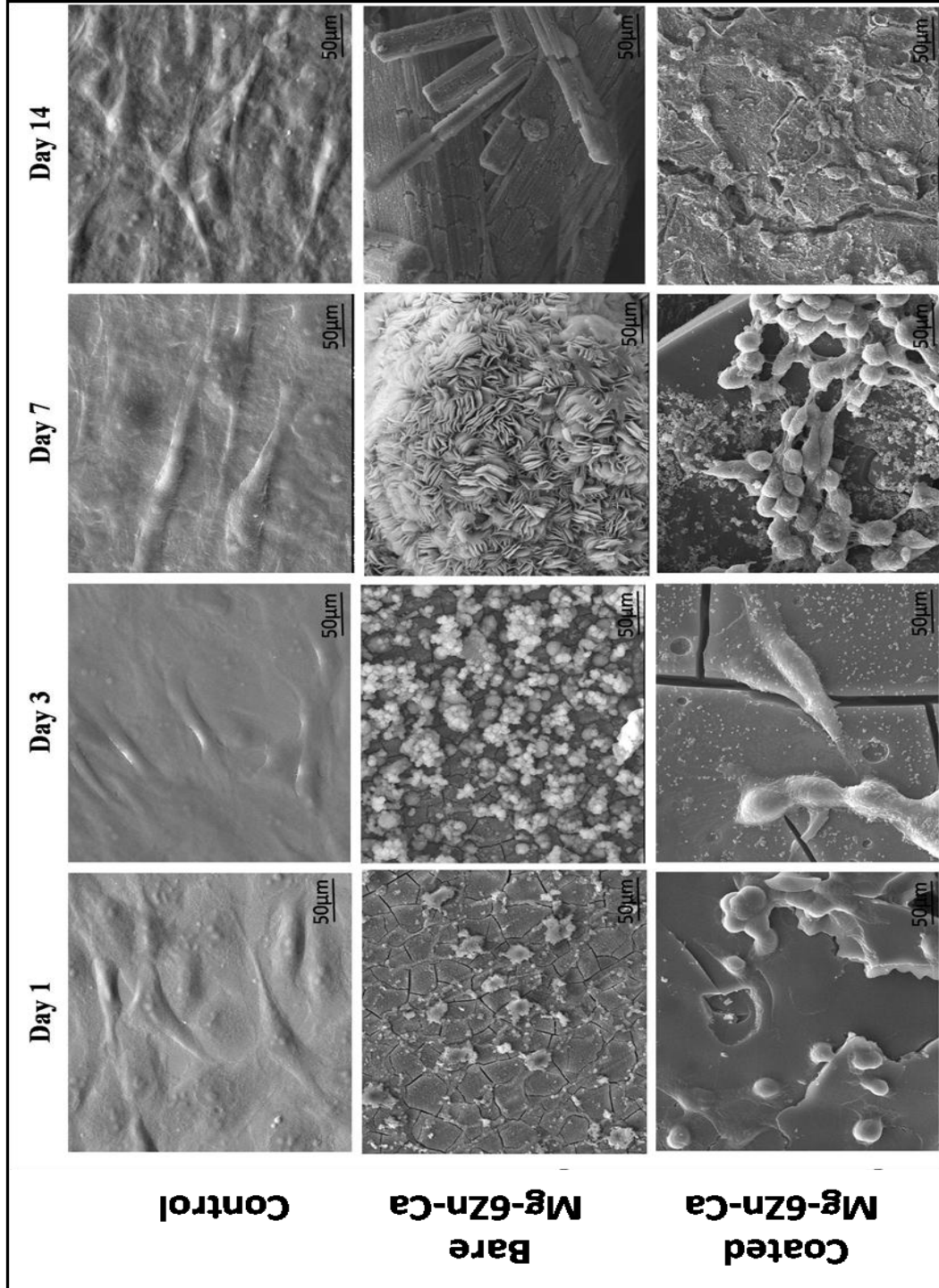


Figure 4.46: Electron micrographs depicting attachment of the MG-63 cells after culturing for 1, 3, 7 and 14 day on bare Mg-6Zn-Ca and 3:1 GPTMS:MTEOS silane coated Mg-6Zn-Ca

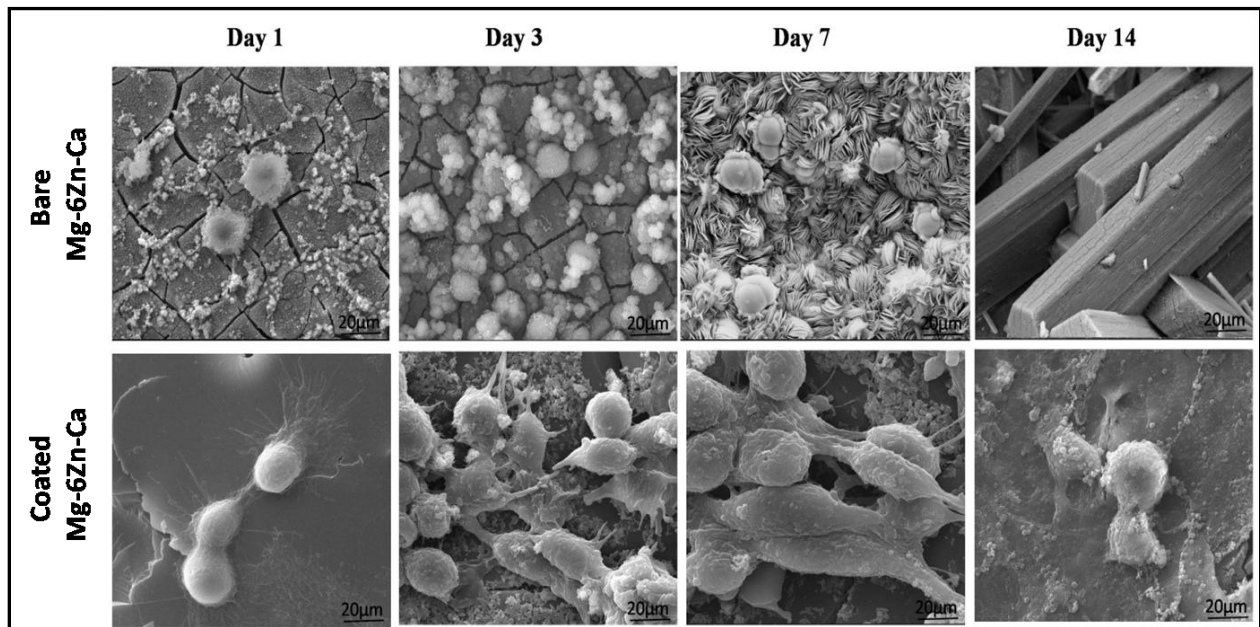


Figure 4.47: Electron micrographs depicting attachment of the MG-63 cells after culturing for 1, 3, 7 and 14 day on bare Mg-6Zn-Ca and 3:1 GPTMS:MTEOS silane coated Mg-6Zn-Ca.

4.3.1.2 Cell viability and proliferation

Figure 4.48 (a) shows the percentage cell proliferation represented against the proliferation of the positive control. It was observed that the cells proliferated better on the 3:1 GPTMS:MTEOS coated Mg-6Zn-Ca specimen as against the bare Mg-6Zn-Ca sample ($p < 0.05$). The bare Mg-6Zn-Ca specimen show a significant reduction in cell proliferation activity of the MG-63 cells on and after 3 days of culturing. This reduction could largely be attributed to the sample undergoing corrosion and evolving hydrogen in the environment of tissue culture medium causing a severe increase in the pH of the culture medium. This increased alkalinity of the growth medium makes the environment unfavorable for cell growth and division and is largely responsible for the cell deaths which were present on 1st day of the study. In contrast to the bare specimen, the coated alloy specimen was seen to support the cell proliferation over longer time durations and to an appreciable cell number density. The sol – gel based silane coatings hide the corrosive surface of the alloy and delay the specimen corrosion to considerable time duration. The water-based tissue

culture medium is seen to initiate the degradation of this coating not before the 7 day of the experiment. The reduction in cell population seen on day 7 and day 14 as compared to day 3 is not much which is in agreement with the information obtained from the electron micrographs.

The quantification of DNA ($\mu\text{g}/\text{cell}$) was evaluated after 1, 3, 7 and 14th day of culturing over the alloy specimens (Figure 4.48 b) using the cell number density on the surfaces of specimens. The DNA content of MG-63 cells over the bare and silane coated specimen was found to be in accordance to the cell proliferation activity. The viable cells present on the surface of these specimens are seen to be at their highest on the 1st day, decreasing significantly on the bare specimen. While a gradual reduction of cell number was observed for the silane coated specimen. The two sample *t* test analysis of the difference of the population means were found to be significantly different at $p < 0.01$ while no significant difference was found at $p < 0.001$. Also, at $p < 0.01$ the population variances were not significantly different.

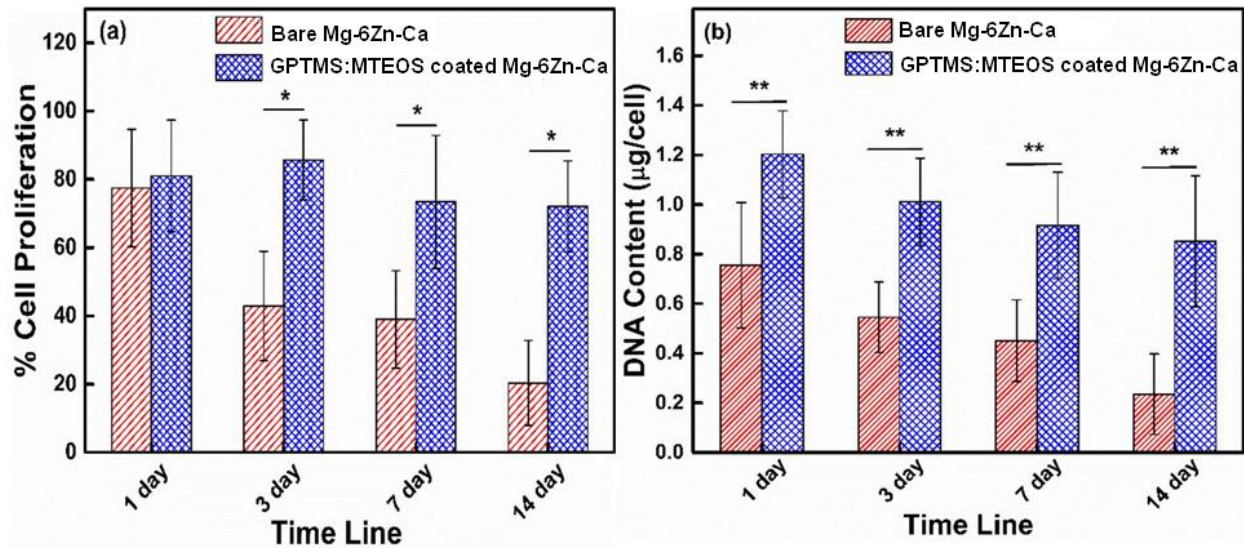


Figure 4.48 (a) Percentage cell proliferation observed on bare Mg-6Zn-Ca and 3:1 GPTMS:MTEOS coated Mg-6Zn-Ca calculated against positive control; at $p < 0.05$ level the difference of means were found to be significantly different (b) DNA content of MG-63 cells on the bare Mg-6Zn-Ca and GPTMS:MTEOS coated Mg-6Zn-Ca

4.3.1.3 Alkaline phosphatase activity (ALP) assay

Figure 4.49 shows the behavior of ALP activity of MG-63 cells cultured over a period of 14 days. Similar tendencies to the cell proliferation behavior were also observed for the ALP activity, a marker of the cell differentiation behavior. For cells cultured over bare Mg-6Zn-Ca specimen, moderate ALP activity was observed till day 3 which showed only a slight increase on day 7 while negligible change was observed on day 14. In contrast, the cells cultured over the 3:1 GPTMS:MTEOS coated Mg-6Zn-Ca specimen showed moderate increase in ALP activity till 3rd day of study and substantially shot up on day 7 to further reduce on the 14th day of the study. The alkaline phosphatase (ALP) activity of the cells on coated samples showed higher expression levels compared to bare Mg-6Zn-Ca alloy. This higher ALP expression observed in the silane coating system confirms the enhancement of cell function and activity at least at an early stage of differentiation [158].

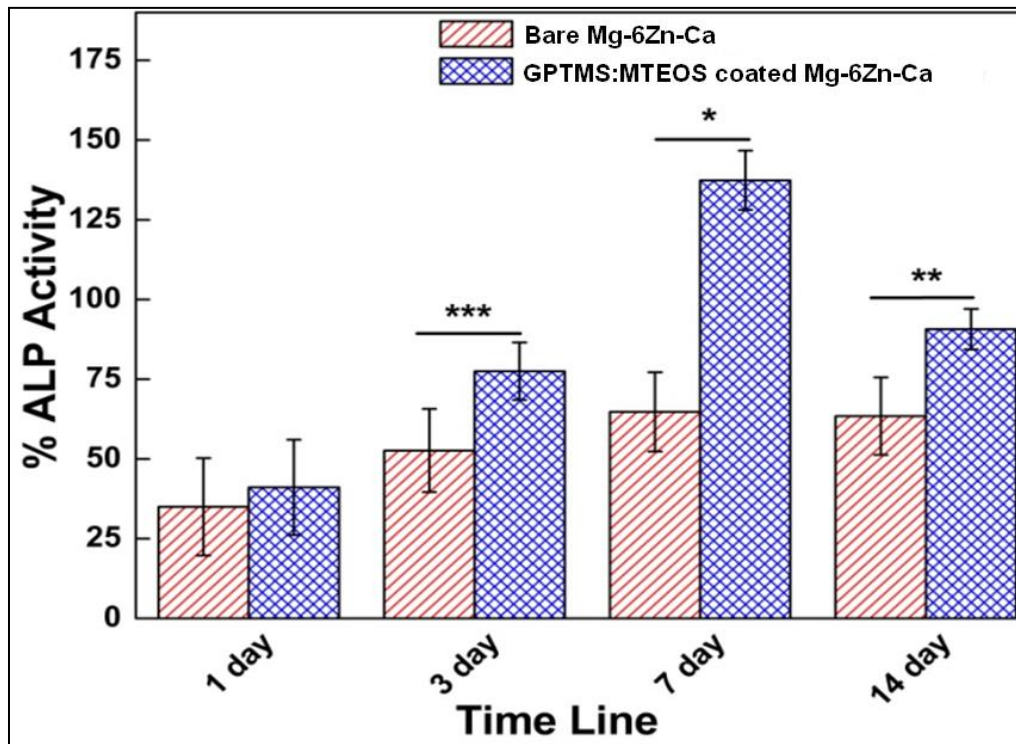


Figure 4.49: Percentage ALP activity of MG-63 cells cultured on bare Mg-6Zn-Ca and GPTMS:MTEOS coated Mg-6Zn-Ca calculated against ALP activity observed in positive control MG-63 cells; at $p < 0.05$, 0.01 and 0.001 level the difference of means were found to be significantly different between bare Mg-6Zn-Ca and GPTMS:MTEOS coated Mg-6Zn-Ca

4.3.2 Biocompatibility investigation of 1:4 DEPETES:BTESPT coating system

4.3.2.1 Cell morphology and attachment observations

Figure 4.50 shows the electron micrographs depicting successful attachment and cell morphology of the MG-63 osteosarcoma cells on the surface of bare Mg-6Zn-Ca and 1:4 DEPETES:BTESPT silane coated Mg-6Zn-Ca after 1, 3, 7 and 14 days. After 1 day incubation, on the bare Mg-6Zn-Ca only single isolated cells were observed and cell spreading was poor. In contrast 1:4 DEPETES:BTESPT coated specimen, strong formation of the actin cytoskeleton can be observed, and the cells are well spread, covering most of the surface (Figure 4.50). Some cells were also found to be connected with each other. After 3 and 5 days culture, the cells were found to be very well connected together and after 14 days culture the cells can be seen flattened and attach tightly on coated surfaces with their extended filopodium. These results indicate the improved biocompatibility of the coated surface due to increased corrosion resistance of the coated surface as compared to bare magnesium alloy.

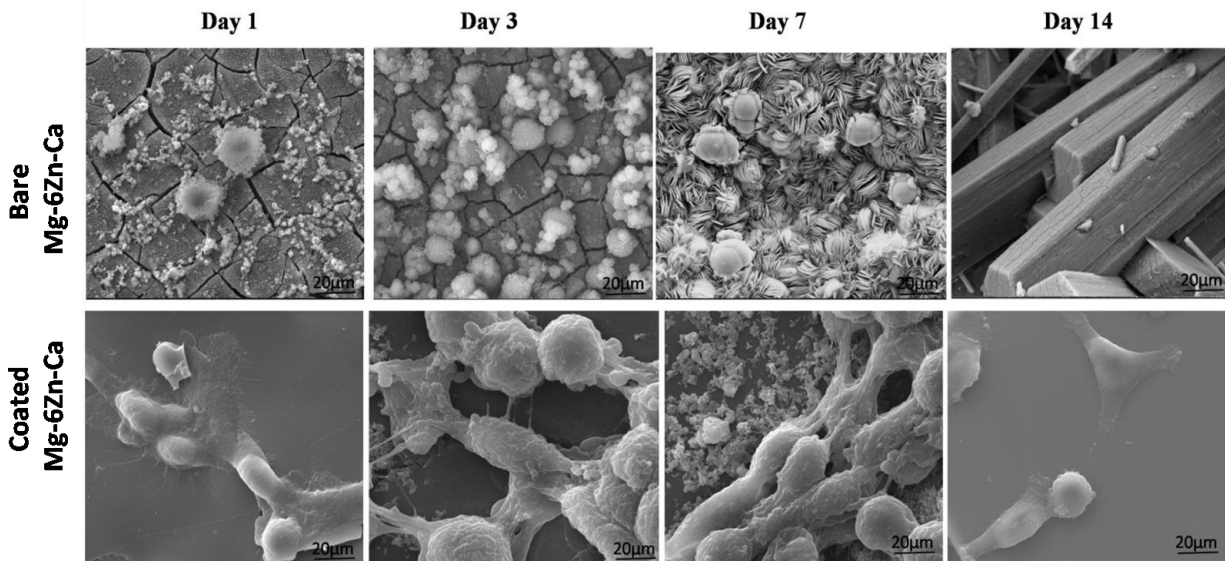


Figure 4.50: Electron micrographs depicting attachment of the MG-63 cells after culturing for 1, 3, 7 and 14 day on bare Mg-6Zn-Ca and 1:4 DEPETES:BTESPT silane coated Mg-6Zn-Ca.

4.3.2.2 Cell viability and proliferation

Figure 4.51 (a) shows the percentage cell proliferation represented against the proliferation of the positive control. It was observed that the cells proliferated better on the 1:4 DEPETES:BTESPT coated Mg-6Zn-Ca specimen as against the bare Mg-6Zn-Ca sample. The bare Mg-6Zn-Ca specimen show a significant reduction in cell proliferation activity of the MG-63 cells on and after 3 days of culturing because of its high reactivity in the media. This increased alkalinity of the growth medium makes the environment unfavorable for cell growth and division. In contrast to the bare specimen, the coated alloy specimen was seen to support the cell proliferation over longer time durations and to an appreciable cell number density. The sol – gel based silane coatings hide the corrosive surface of the alloy and delay the specimen corrosion to considerable time duration. This result is similar to the result obtained in 3:1 GPTMS:MTEOS based coating system.

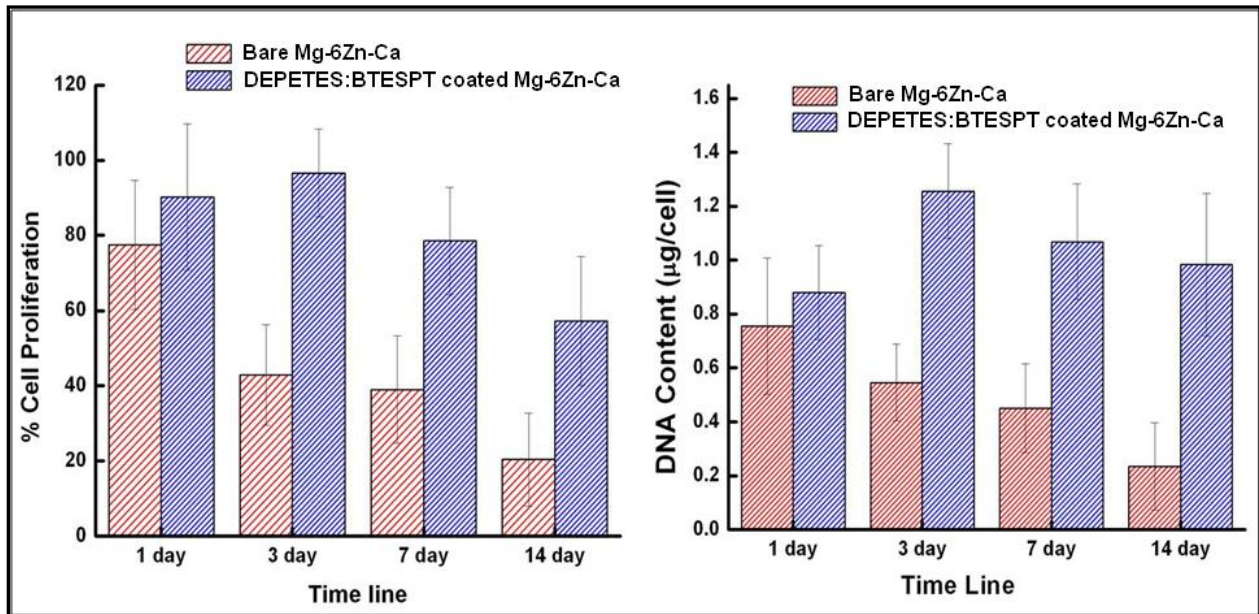


Figure 4.51: (a) Percentage cell proliferation observed on bare Mg-6Zn-Ca and 1:4 DEPETES:BTESPT coated Mg-6Zn-Ca calculated against positive control and (b) DNA content of MG-63 cells on the bare Mg-6Zn-Ca and 1:4 DEPETES:BTESPT coated Mg-6Zn-Ca

4.3.2.3 Alkaline phosphatase activity (ALP) assay

Figure 4.52 shows the behavior of ALP activity of MG-63 cells cultured over a period of 14 days on bare magnesium and 1:4 DEPETES:BTESPT coated specimen. For cells cultured over bare Mg-6Zn-Ca specimen, moderate ALP activity was observed till day 3 which showed only a slight increase on day 7 while negligible change was observed on day 14. In contrast, the cells cultured over the 1:4 DEPETES:BTESPT coated Mg-6Zn-Ca specimen showed moderate increase in ALP activity till 3rd day of study and substantially shot up on day 7 to further reduce on the 14th day of the study. The alkaline phosphatase (ALP) activity of the cells on coated samples showed higher expression levels compared to bare Mg-6Zn-Ca alloy. This result is similar to the result obtained in 3:1 GPTMS:MTEOS based coating system.

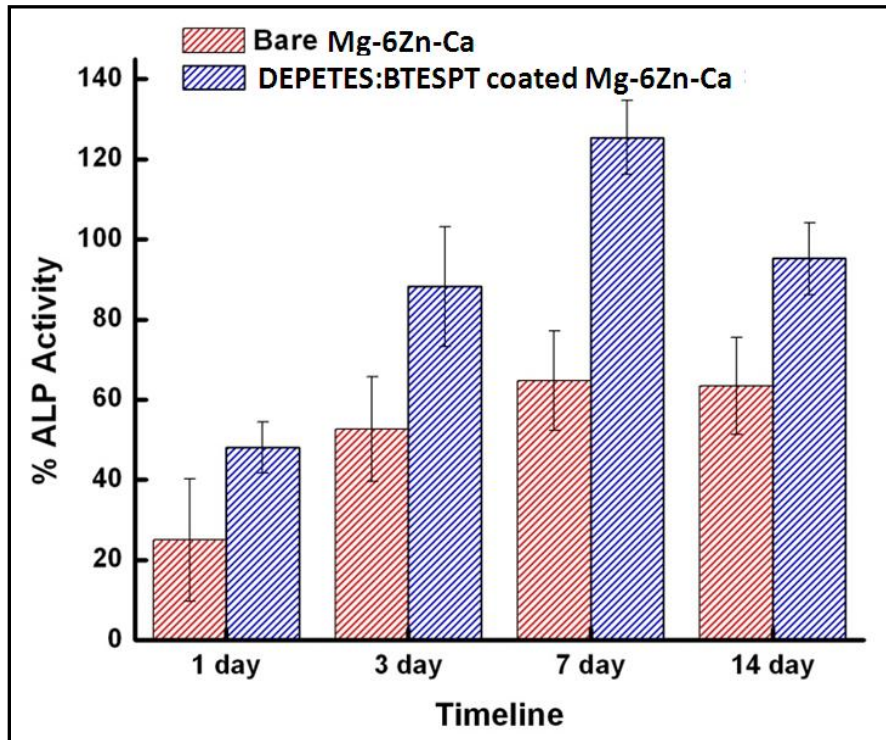


Figure 4.52: Percentage ALP activity of MG-63 cells cultured on bare Mg-6Zn-Ca and 1:4 DEPETES:BTESPT coated Mg-6Zn-Ca calculated against ALP activity observed in positive control MG-63 cells

4.3.2.4 XRD Analysis of formed corrosion products on the coated surface in DMEM

The corrosion products formed on the surface of the bare and coated Mg-6Zn-Ca alloy after immersion in the DMEM media at $(36.5 \pm 0.5) ^\circ\text{C}$ were also analyzed by XRD. The XRD spectrum in Figure 4.53 confirmed the formation of salts of magnesium and calcium phosphates and carbonates, as suggested by the following equation [155] along with magnesium hydroxide:

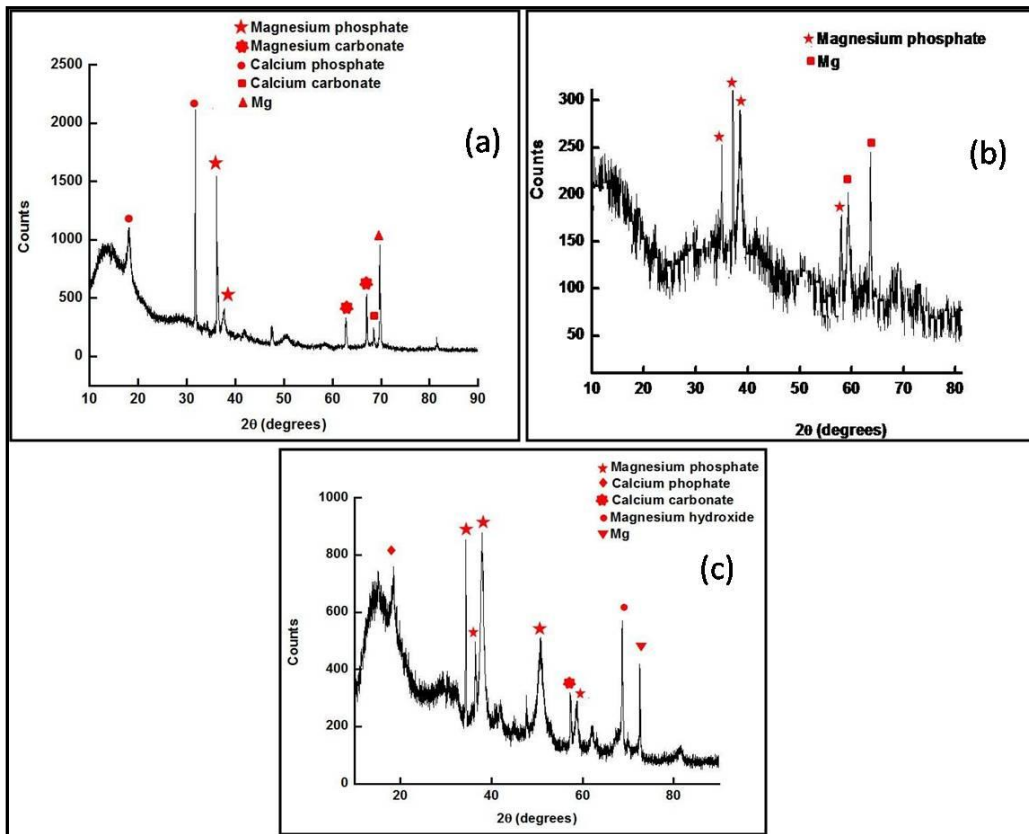
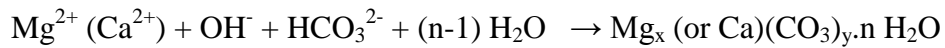
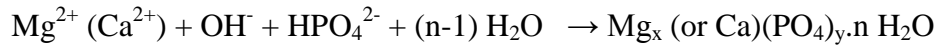


Figure 4.53: XRD images of the MG-63 cells on (a) bare Mg-6Zn-Ca alloy, (b) 1:4 DEPETES:BTESPT coated Mg-6Zn-Ca alloy and (d) 3:1 GPTMS:MTEOS coated Mg-6Zn-Ca samples after culturing in DMEM

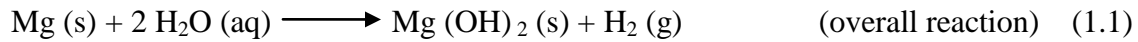
These different hydrated forms of magnesium phosphates are known to be non toxic supports osteoblast differentiation and function [148, 156]. The HCO_3^- and HPO_4^{2-} in *m*-SBF and DMEM can react with the OH^- generated during magnesium dissolution, which induces precipitation of insoluble carbonates and phosphates in the corrosion product layer. The presence of insoluble carbonates and phosphates on the magnesium alloy immersed in *m*-SBF has been reported by many studies [148, 155, 157, 159]. Calcium phosphate coated implants has been known to enhance bone bonding with the implant surfaces, in addition to accelerating bone growth.

Chapter 5

General Discussion

Corrosion of Magnesium alloy

Magnesium dissolution in aqueous environments generally proceeds by electrochemical reaction with water to produce magnesium hydroxide and hydrogen gas as shown in the equations below. These equations also suggest that this mechanism is insensitive to the oxygen concentration [21, 34].



However, the presence of several anions such as, chloride, sulphate and nitrate in the aqueous solution hinder the formation of the surface film and/or disrupts the existing film, resulting in accelerated corrosion [21, 34]. Sensitivity to impurities and inability to develop robust passive film below pH 11 accounts for different types of magnesium corrosion problems, such as general, galvanic corrosion, pitting corrosion and stress corrosion cracking [21].

The evolution of hydrogen and the associated pH changes are not desirable in *in-vivo* biological situations. These can cause a delay in the growth of tissues. Corrosion resistance during initial stages is necessary to allow implants to maintain their mechanical integrity in bone healing phase. Therefore, a coating is required to enable biodegradation at a desired rate by offering limited barrier function.

Choice of Mg-6Zn-Ca alloy was based primarily on bio-compatibility of the alloying elements (Zn and Ca). Therefore, to exploit the biocompatibility properties of magnesium alloy, we need to control the degradation of the alloy by developing some surface coating.

Surface modification through silane based Coating

Silanes have been widely used as coupling agents in clinical applications for more than 50 years, particularly in dentistry as adhesion promoters and their use has been proved to be safe. However, the frequent use has been limited due to bond degradation associated with the hydrolytic cleaving of the siloxane bonds and degradation is expected when water penetrates into coating/alloy interface resulting in detachment of the silane coating. Since the purpose of silane coating on biodegradable implant material is to control the degradation for a limited period (and not a long lasting protection), it has potential to serve as a coating system with desired properties.

It has been reported earlier that strongly negative surfaces (such as PO_4H_2 , COOH and OH -terminated surfaces), possess greater induction capability for the heterogeneous nucleation and growth of calcium/magnesium phosphates and carbonates [125] (Figure 5.1).

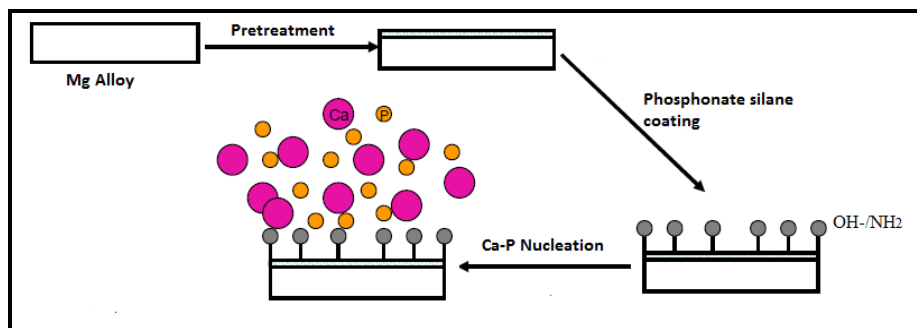


Figure 5.1: Proposed biological response of phosphonate silane based coating system

Effect of surface Pre-treatment

Prior to application of sol-gel based silane coating on the alloy, the magnesium surface should possess a uniform and adherent hydroxide layer to provide enough OH^- groups for silane to bind with the alloy surface. Therefore, optimized surface pre-treatment for the alloy was established in alkaline solution. The magnesium alloy has to be pretreated at pH 12, in hot NaOH for 240 h before application of silane to develop an adherent and uniform hydroxide on the surface. To establish this pretreatment, the alloy was pretreated for various time intervals to produce the suitable hydroxide. Also its protective nature was confirmed using electrochemical techniques. A positive shift in E_{corr} represents a lesser susceptibility to corrosion. E_{corr} of the alloy alkali-treated for 48, 72 and 240 h shifted towards the nobler direction by 90-100 mV, in comparison to the untreated alloy. However, the pretreated samples invariably showed a decrease in the current density, with the 240 h treated samples showing a decrease by an order of magnitude as compared to the untreated alloy. The sol-gel based silane coating was applied on the alloy with the aim of delaying the fast corrosion of the alloy in the simulated physiological environment. Fig 5.2 shows the probable reaction mechanism of the as-developed coatings.

Modification using DEPETES:MTEOS coating system

With the background described above, in the first approach of development of phosphonate silane based coating system, a composite coating system of phosphonate silane (DEPETES) with MTEOS as a precursor was developed by mixing the two in different volume ratios to study the

effect of different ratios on corrosion resistance and biocompatibility. The thickness of this coating was found to be ~ 16.1 μm . Electrochemical investigation revealed that the corrosion current densities in the corresponding anodic and cathodic parts of the polarization scans of all the coated specimens were significantly lower in comparison to the bare alloy. The corrosion potential (E_{corr}) of the 1:4 coated alloy was ~ 150 mV more noble as compared to the bare alloy, implying its considerably lesser susceptibility to corrosion. The EIS data showed an improvement of 1 order of magnitude of impedance in case of 1:4 coated as compared to bare Mg alloy. The time dependent electrochemical investigation showed that the coating with the optimized ratio (1:4 DEPETES:MTEOS) helped in controlling the corrosion of the bare magnesium sample upto 110 h in *m*-SBF at (36.5 ± 0.5) $^{\circ}\text{C}$ thereby retarding the concurrent hydrogen evolution and suppressing the abrupt increase in pH.

Modification using DEPETES:BTESPT based coating system

Since an observed delay of 110 h was not enough for magnesium alloy to be used as body implant, therefore, further DEPETES was crosslinked with BTESPT, a long chain silane precursor with S-S hydrophobic linkage in different volume ratios with an assumption of increasing the hydrophobicity of the crosslinked film and further delaying the degradation of the alloy. The thickness of this coating was found to be ~ 16 μm . Electrochemical investigation revealed that the current densities in the corresponding anodic and cathodic parts of the polarization scans of all the coated specimens were significantly lower in comparison to the bare alloy. The improvement was maximum for the coating with DEPETES:BTESPT volume ratio of 1:4, as suggested by 2 orders of magnitude lower current density of this sample as compared to the bare alloy. Also, the corrosion potential (E_{corr}) of the 1:4 coated alloy was ~ 150 mV more noble as compared to the bare alloy implying its considerably less susceptibility to corrode. The coating with DEPETES:BTESPT ratio of 1:4 improved the impedance of the bare alloy by 2 orders of magnitude and also decreased the current density by 2 orders of magnitude. This system further retarded the dissolution for upto 175 h in *m*-SBF at (36.5 ± 0.5) $^{\circ}\text{C}$ and also retarded the hydrogen evolution and abrupt increase in pH.

The improvement through phosphonate silane, DEPETES achieved in the above two coatings is quite comparable to the improvement Khramov et al [129] reported on AZ31 alloy with DEPETES:MTEOS based coating system in dilute Harrison's solution. Although a significant shift in E_{corr} towards the noble position had been achieved in the developed system DEPETES:MTEOS and DEPETES:BTESPT as compared to the one reported earlier.

Modification using GPTMS:MTEOS based coating system

In the third, non-phosphonate silane based coating system approach, a sol-gel based crosslinked coating of GPTMS and MTEOS was developed (Figure 5.3). GPTMS and MTEOS were used in different molar ratios to optimized coating chemistry. The thickness of developed coating was observed to be 21 μm . Electrochemical investigation revealed that the corrosion potential (E_{corr}) of the alloy coated with the 3:1 ratio was ~340 mV more noble as compared to the bare alloy. Also, the current densities in the anodic and cathodic parts of the polarization scan of the alloy with the 3:1 coating were two orders of magnitude lower, as compared to the bare alloy. This GPTMS:MTEOS coating system when mixed in the optimized ratio delayed the corrosion of provided coatings significantly delaying the corrosion of bare Mg-6Zn-Ca alloy for upto 280 h (Figure 3) in *m*-SBF at $(36.5 \pm 0.5) ^\circ\text{C}$ and also retarded hydrogen evolution and suppressed increase in pH. Therefore, maximum delay in rapid corrosion has been achieved with GPTMS:MTEOS, 3:1 coating system.

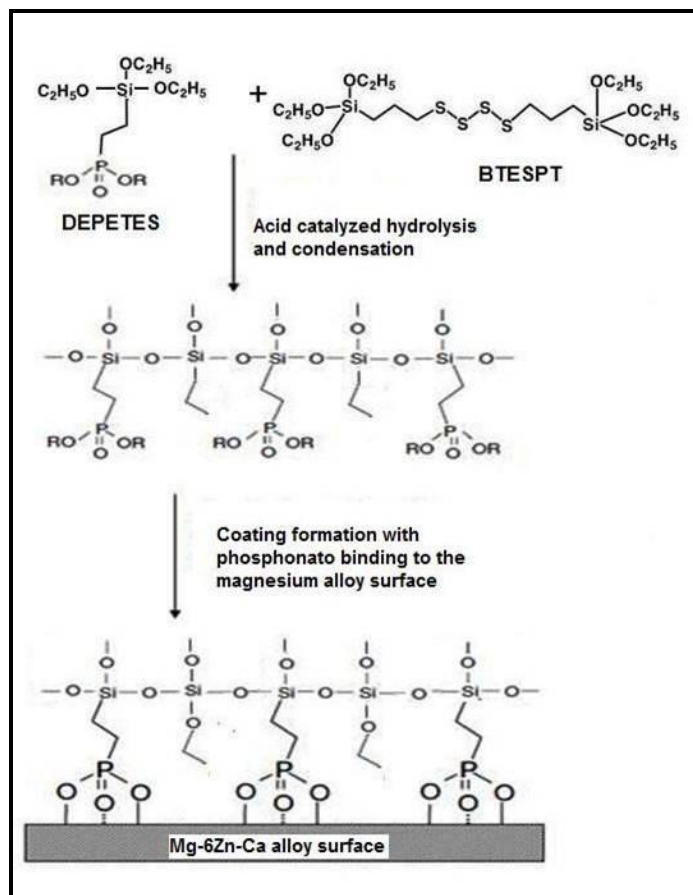


Figure 5.2: Proposed reaction mechanism for the developed Phosphonate silane based sol-gel coating

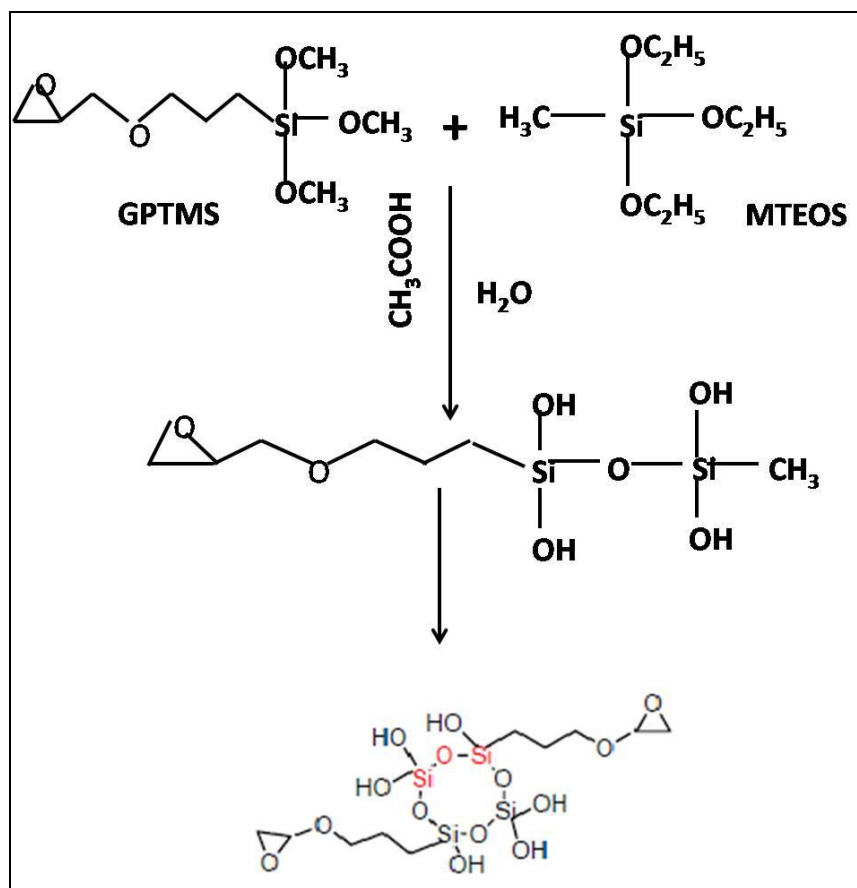


Figure 5.3: Schematic representation of hydrolysis and condensation of GPTMS and MTEOS

Degradation Mechanism of silane coated alloy

Therefore, maximum delay in rapid corrosion has been achieved with GPTMS:MTEOS, 3:1 coating system. In all the coated samples the anodic dissolution reactions rates were also slowed as the silane coating blocks mass transport of Mg^{2+} . At the same time, the formation of Si-O-Mg bonds at the interface also blocks some anodic reactions and reduces the corrosion current. The shift of corrosion potential towards the cathodic direction also indicates that the hydrophobic silane film acts as a physical barrier to retard the electrolyte penetration as observed from potentiodynamic polarization study.

Therefore, sol-gel based silane coating systems that were applied on the alloy with the aim of delaying its fast corrosion in the simulated physiological environment showed considerable improvement in corrosion resistance since they provided a protective barrier between the sample and the corrosive medium to inhibit the corrosion of the Mg-6Zn-Ca alloy. Therefore, the undesirable excessive rate of formation of by-products of Mg alloy corrosion (e.g., hydrogen gas or hydroxide ions) in the *m*-SBF solution was mitigated.

Since silane based coatings are water based coatings that provide temporary barrier, when immersed continuously, the silane coatings hydrolyze and water eventually penetrates and reach the coating/alloy interface (Figure 5.4). Also, since the siloxane hydrolysis is a reversible process, the Si-O-Si bonds convert back to Si-OH bonds. Initially, a very low degradation rate is observed due to the protective nature of silane coating on the alloy surface of the samples (Figure 5.4b). The polarization and EIS study indicate the formation of protective films at the early stage for all the developed silane coating systems, R_f , R_{hyd} and R_{ct} were found to be decrease with time. This behavior suggests the degradation of the coating and the hydroxide layer simultaneously, thereby decreasing the overall impedance of the coating system.

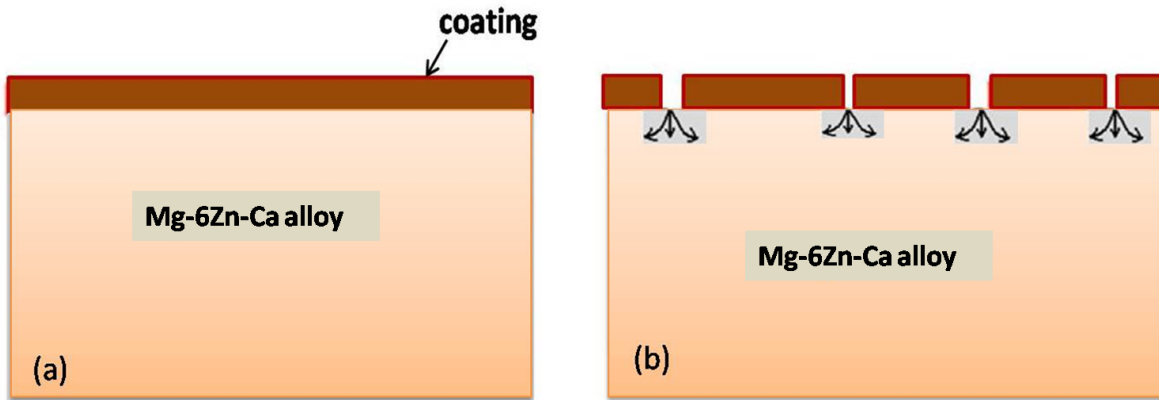


Figure 5.4: Schematic degradation diagram, (a) initial surface condition of the coated magnesium alloy and (b) degraded polymeric coating upon degradation [86]

With the progress of the degradation process, the protective layer starts to break down and reactive surface gets exposed to the corrosion medium decreases the impedance of the coating system (Figure 4.16, 4.29 and 4.39). This inadequacy of coating systems can be attributed to the presence of inherent intermetallics on the magnesium alloy surface which can interfere with the development of robust hydroxide surface (section 4.1). The resulting micropores, surface defects/ discontinuities and areas with low cross-link density may all have damaging influence. These areas facilitate the diffusion of aggressive electrolytes to the coating/sample interface and provide preferential sites for corrosion initiation. Therefore, the improved achieved in this study may be sufficient for implants required for short term applications; but it may be inadequate for longer service life.

Corrosion of the coated sample in the immersion state in *m*-SBF induces precipitation of some insoluble carbonates and phosphates in the corrosion product layer that has been known to support osteoblast formation, and hence, the silane coating can be considered biologically active (Figure 5.5).

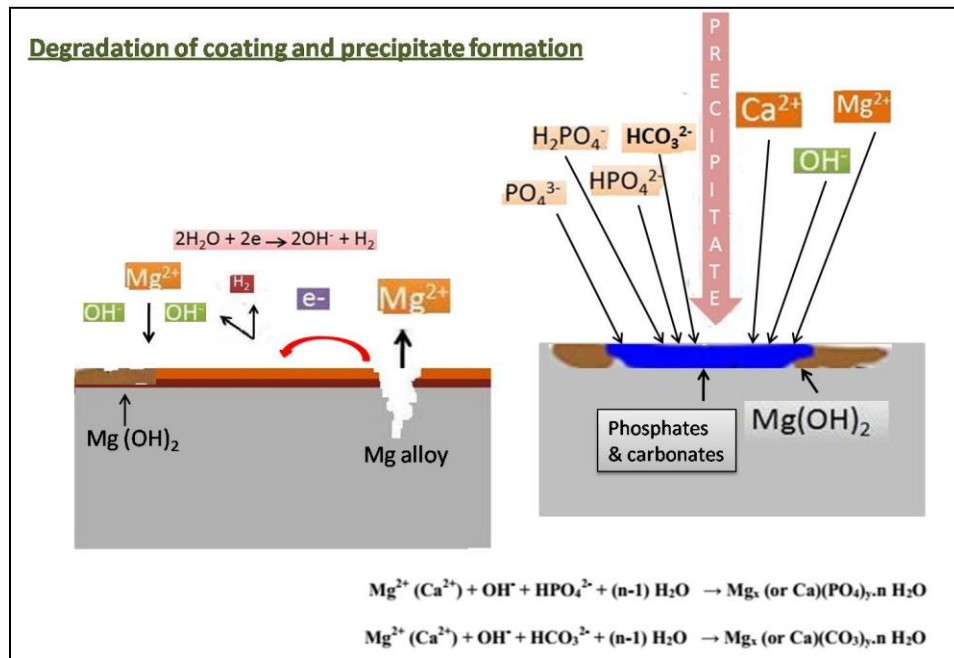


Figure 5.5: Mechanism for formation of Ca/Mg phosphates and carbonates

Cytotoxicity behavior of silane coated alloy

Cell behavior and response to biomaterials is an important factor for evaluation of the material's biocompatibility. The in-vitro biocompatibility study carried out using human osteoblast cells (MG-63) showed that Mg sample reacted vigorously with the culture medium DMEM, producing hydroxide ions and hydrogen gas. Local alkalization and hydrogen bubbles produced an unfavorable environment for the cells to attach. Therefore, only few cells were detected on the bare Mg-6Zn-Ca alloy samples. By contrast, numerous cells were found to be attached well to the surfaces of DEPOTES:BTESPT and GPTMS:MTEOS coated Mg-6Zn-Ca alloy, having a relatively flattened and stretched shape, as shown in Figure 4.46, 4.47 and 4.50. Therefore, good biocompatibility and favorable morphology of the DEPOTES:BTESPT and GPTMS:MTEOS coated Mg-6Zn-Ca alloy provided a suitable interaction environment, simultaneously enlarging the bioactive surface area as compared to bare alloy. The bioactive silane coated surface has also supported the improved proliferation of cells and their further differentiation on the coated surface as compared to bare Mg-6Zn-Ca alloy.

Therefore, the results observed in this research study clearly demonstrate that the silane based coatings have the ability of improving the cell survival rate, cell adhesion and further improving the subsequent cellular reactions like differentiation. The XRD analysis of the corrosion products formed on the surface of the silane coated alloys confirms the presence of calcium carbonates, calcium phosphates, magnesium carbonates and magnesium phosphates that have been reported to enhance osteoblast activity and thereby accelerate bone growth.

Therefore, the developed coating systems on the Mg-6Zn-Ca alloy can find their use as bioabsorbable microclip, being used in endoscopic surgeries and wound closures where the existing devices resorb within 2 weeks. They can also be used as bioabsorbable surgical skin staples which are usually removed after 10-12 days of post surgery. These coated magnesium alloy can also be used to replace Kirchner wires (K-wires) which are temporarily and frequently used for the stabilization of small fragments where healing is predictably quick. K-wires are used for temporary fixation during some operations and are usually removed 2-3 weeks post operation.

Chapter 6

Conclusions

Three different approaches of silane coatings, viz., phosphonato silane approach (DEPETES with MTEOS and BTESPT as precursor) and non-phosphonato silanes approach (GPTMS with MTEOS) were investigated to create bio-compatible coatings on Mg-6Zn-Ca (wt%) alloy.

- 1) The first approach, DEPOTES:MTEOS resulted in a coating which controls the dissolution of Mg-6Zn-Ca alloy up to 110 h. Silane coatings of other three ratios were found to be completely degraded within few hours of immersion. Hence, the time dependent data is not included in the present discussion
- 2) In the second approach, DEPOTES:BTESPT based coating system provides the corrosion resistance to the alloy up to 175 h, respectively. Silane coatings of other three ratios were found to be completely degraded within few hours of immersion. Hence, the time dependent data is not included in the present discussion.
- 3) The third approach, 3:1 GPTMS:MTEOS based coating system, delayed the degradation of the alloy up to 280 h, respectively.
- 4) Pre-treatment is one of the important factors in creating a perfect coating. The best pre-treatment was found to be pre-treatment with the hot NaOH for 240 h to provide a reasonably defect-free surface morphology for the silane adhesion.
- 5) The Comparative corrosion behavior of the three coatings confirmed that superiority of GPTMS:MTEOS coating system in comparison to other two coating systems. GPTMS:MTEOS coating system also showed a significant decrease in hydrogen evolution and lesser increase in pH, which are both desirable for the use of magnesium alloys as implants.

- 6) In-vitro cell culture studies carried out on two coating systems viz., DEPETES:BTESPT and GPTMS:MTEOS as compared to uncoated system confirm that the both the coated systems were superior to bare Mg-6Zn-Ca alloy in terms of cell attachment, proliferation and differentiation capability on the coated surface.
- 7) Both the coated systems when immersed in *m*-SBF and DMEM led to the formation of a rough, C and P-containing surface layer, which initially enhance the cell adhesion on the surface, making the surface biocompatible for cells.
- 8) The main outcome of this work is that this study can be now implemented to use Mg-6Zn-Ca alloy as an implant with a coating which can heal a damaged body part up to a time period upto 280 h. These coated magnesium alloy can be used as bioabsorbable surgical skin staples (needs to be removed after 10-12 days of post surgery), micro-clips(needs to degrade within 2 weeks) and pins used in fingers dislocation or fracture which are predicted to heal quickly.

Future Scope

- 1) Work can be done further to reduce corrosion resistance by using new silane combinations to improve the dissolution rate of magnesium alloy and increase the life of coating.
- 2) To study the mechanical properties of coated alloy in stress condition
- 3) To study the formability of the coated Mg-6Zn-Ca alloy.

List of publications

From thesis

- 1) Swati Gaur, A.S. Khanna, R.K. Singh Raman, "Silane-coated magnesium implants with improved in vitro corrosion resistance and biocompatibility", (Under review), Journal of Biomedical Materials Research A
- 2) Swati Gaur, R.K. Singh Raman, A.S. Khanna, "In vitro investigation of biodegradable polymeric coating for corrosion resistance of Mg-6Zn-Ca alloy in simulated body fluid", Materials Science & Engineering c , vol. 42 (2014), 91-101
- 3) Swati Gaur, A.S. Khanna, R.K. Singh Raman, "In vitro evaluation of degradation of biodegradable silane based coating on Mg-Zn-Ca alloy in physiological Environment", Materials Science forum Vol 765 (2013) pp 803-807
- 4) Swati Gaur, A.S. Khanna, R.K. Singh Raman, "Development of biodegradable coating for controlled dissolution of a magnesium alloy as an implant" Materials Science forum Vol 828-829 (2015) pp 321-326

Other Publications

- 5) Swati, Ruchi Grover Wankhede and Anand Khanna, Indian Patent , " A fast – cure underwater epoxy coating composition", Patent no. 266579
- 6) Anand Khanna and Swati Gaur, "GREEN COATINGS: A new wave in corrosion Prevention", Chemical World, March (2010)
- 7) Swati Gaur and Anand Khanna "Coatings on Stainless steels", SSPC news bulletin, vol 7, issue no. 3, Dec, 2013

References

- [1] Mitsuo N. Recent research and development in titanium alloys for biomedical applications and healthcare goods. *Science and Technology of Advanced Materials* 2003;4:445.
- [2] Hubbell JA. Biomaterials in Tissue Engineering. *Nat Biotech* 1995;13:565-76.
- [3] Manivasagam G, Dhinasekaran D, Rajamanickam A. Biomedical implants: Corrosion and its prevention-a review. *Recent Patents on Corrosion Science* 2010;2:40-54.
- [4] Hendra Hermawan DRaJRPD. *Metals for Biomedical Applications: InTech*; 2011
- [5] Shaw BA, Sikora E, Virtanen S. Fix, heal, and disappear: A new approach to using metals in the human body. *The Electrochemical Society Interface* 2008;17:45.
- [6] Staiger MP, Pietak AM, Huadmai J, Dias G. Magnesium and its alloys as orthopedic biomaterials: A review. *Biomaterials* 2006;27:1728-34.
- [7] !!! INVALID CITATION !!!
- [8] Shaw BA, Sikora E, Virtanen S. Fix, heal, and disappear: A new approach to using metals in the human body. *Electrochemical Society Interface* 2008;17:45-9.
- [9] Song G. Control of biodegradation of biocompatible magnesium alloys. *Corrosion Science* 2007;49:1696-701.
- [10] Song G, Song S. A Possible Biodegradable Magnesium Implant Material. *Advanced Engineering Materials* 2007;9:298-302.
- [11] Witte F. The history of biodegradable magnesium implants: A review. *Acta Biomaterialia* 2010;6:1680-92.
- [12] Witte F, Hort N, Vogt C, Cohen S, Kainer KU, Willumeit R, et al. Degradable biomaterials based on magnesium corrosion. *Current Opinion in Solid State and Materials Science* 2008;12:63-72.
- [13] Brar HS, Platt MO, Sarntinoranont M, Martin PI, Manuel MV. Magnesium as a biodegradable and bioabsorbable material for medical implants. *JOM* 2009;61:31-4.
- [14] Chen Y, Xu Z, Smith C, Sankar J. Recent advances on the development of magnesium alloys for biodegradable implants. *Acta biomaterialia* 2014;10:4561-73.
- [15] Avedesian MM, H. Baker and A.S.M.I.H Committee. *Magnesium and Magnesium alloys. Materials park, OH:: ASM International*; 1999.
- [16] Choudhary L, Singh Raman RK. Magnesium alloys as body implants: Fracture mechanism under dynamic and static loadings in a physiological environment. *Acta biomaterialia* 2012;8:916-23.
- [17] Kannan MB, Raman RKS. In vitro degradation and mechanical integrity of calcium-containing magnesium alloys in modified-simulated body fluid. *Biomaterials* 2008;29:2306-14.
- [18] Seal CK, Vince K, Hodgson MA. Biodegradable surgical implants based on magnesium alloys – A review of current research. *IOP Conference Series: Materials Science and Engineering* 2009;4:012011.
- [19] Witte F. The history of biodegradable magnesium implants: A review. *Acta biomaterialia* 2010;6:1680-92.
- [20] Wolf FI, Cittadini A. Chemistry and biochemistry of magnesium. *Molecular Aspects of Medicine* 2003;24:3-9.
- [21] Makar GL, Kruger J. Corrosion of magnesium. *International Materials Reviews* 1993;38:138-53.

- [22] Quach N-C, Uggowitzer PJ, Schmutz P. Corrosion behaviour of an Mg-Y-RE alloy used in biomedical applications studied by electrochemical techniques. *Comptes Rendus Chimie* 2008;11:1043-54.
- [23] Xu L, Pan F, Yu G, Yang L, Zhang E, Yang K. In vitro and in vivo evaluation of the surface bioactivity of a calcium phosphate coated magnesium alloy. *Biomaterials* 2009;30:1512-23.
- [24] Al-Abdullat Y, Tsutsumi S, Nakajima N, Ohta M, Kuwahara H, Ikeuchi K. Surface modification of magnesium by NaHCO₃ and corrosion behavior in Hank's solution for new biomaterial applications. *Materials Transactions* 2001;42:1777-80.
- [25] Chiu KY, Wong MH, Cheng FT, Man HC. Characterization and corrosion studies of fluoride conversion coating on degradable Mg implants. *Surface and Coatings Technology* 2007;202:590-8.
- [26] Xu L, Zhang E, Yang K. Phosphating treatment and corrosion properties of Mg-Mn-Zn alloy for biomedical application. *Journal of Materials Science: Materials in Medicine* 2009;20:859-67.
- [27] Yang J, Cui F, Lee IS. Surface modifications of magnesium alloys for biomedical applications. *Annals of Biomedical Engineering* 2011;39:1857-71.
- [28] Gray JE, Luan B. Protective coatings on magnesium and its alloys — a critical review. *Journal of Alloys and Compounds* 2002;336:88-113.
- [29] Kulekci M. Magnesium and its alloys applications in automotive industry. *Int J Adv Manuf Technol* 2008;39:851-65.
- [30] Song G. Recent Progress in Corrosion and Protection of Magnesium Alloys. *Advanced Engineering Materials* 2005;7:563-86.
- [31] Song G, Atrens A. Understanding Magnesium Corrosion—A Framework for Improved Alloy Performance. *Advanced Engineering Materials* 2003;5:837-58.
- [32] Avedesian MM, Baker H, Committee ASMIIH. Magnesium and magnesium alloys. Materials Park, OH: ASM International; 1999.
- [33] Montemor MF, Ferreira MGS. Electrochemical study of modified bis-[triethoxysilylpropyl] tetrasulfide silane films applied on the AZ31 Mg alloy. *Electrochimica Acta* 2007;52:7486-95.
- [34] Song GL, Atrens A. Corrosion Mechanisms of Magnesium Alloys. *Advanced Engineering Materials* 1999;1:11-33.
- [35] Pourbaix M. Atlas of electrochemical equilibria in aqueous solutions. Oxford; New York: Pergamon Press; 1966.
- [36] G errard Eddy Jai Poinern SB, Derek Fawcett. Biomedical Magnesium Alloys: A Review of Material Properties, Surface Modifications and Potential as a Biodegradable Orthopaedic Implant. *American Journal of Biomedical Engineering* 2012;Vol. 2 pp. 218-40.
- [37] Song G, Atrens A. Understanding magnesium corrosion. A framework for improved alloy performance. *Advanced Engineering Materials* 2003;5:837-58.
- [38] Choudhary L, Singh Raman RK, Hofstetter J, Uggowitzer PJ. In-vitro characterization of stress corrosion cracking of aluminium-free magnesium alloys for temporary bio-implant applications. *Materials Science and Engineering: C* 2014;42:629-36.
- [39] MedMarket Diligence, Report #M625, .
- [40] Xin Y, Hu T, Chu PK. In vitro studies of biomedical magnesium alloys in a simulated physiological environment: A review. *Acta Biomaterialia* 2011;7:1452-9.
- [41] Pişkin E. Biodegradable polymeric matrices for bioartificial implants. *The International journal of artificial organs* 2002;25:434-40.

- [42] Poinern GEJ, Brundavanam S, Fawcett D. Biomedical Magnesium Alloys: A Review of Material Properties, Surface Modifications and Potential as a Biodegradable Orthopaedic Implant. *American Journal of Biomedical Engineering* 2012;2:218-40.
- [43] Andreiotelli M, Wenz HJ, Kohal R-J. Are ceramic implants a viable alternative to titanium implants? A systematic literature review. *Clinical Oral Implants Research* 2009;20:32-47.
- [44] Webster TJ, Ergun C, Doremus RH, Siegel RW, Bizios R. Enhanced functions of osteoblasts on nanophase ceramics. *Biomaterials* 2000;21:1803-10.
- [45] Chew K, Zein, S. and Ahmad, A. The corrosion scenario in human body: Stainless steel 316L orthopaedic implants. *Natural Science* 2012;4:184-8.
- [46] Rack HJ, Qazi JI. Titanium alloys for biomedical applications. *Materials Science and Engineering: C* 2006;26:1269-77.
- [47] Niinomi M. Mechanical properties of biomedical titanium alloys. *Materials Science and Engineering: A* 1998;243:231-6.
- [48] Castleman LS, Motzkin SM, Alicandri FP, Bonawit VL, Johnson AA. Biocompatibility of nitinol alloy as an implant material. *Journal of biomedical materials research* 1976;10:695-731.
- [49] Seal CK, et al. Biodegradable surgical implants based on magnesium alloys – A review of current research. *IOP Conference Series: Materials Science and Engineering* 2009;4:012011.
- [50] Gu XN, Zheng YF. A review on magnesium alloys as biodegradable materials. *Frontiers of Materials Science in China* 2010;4:111-5.
- [51] Ma E, Xu J. Biodegradable Alloys: The glass window of opportunities. *Nature Materials* 2009;8:855-7.
- [52] Zberg B, Uggowitzer PJ, Löffler JF. MgZnCa glasses without clinically observable hydrogen evolution for biodegradable implants. *Nature Materials* 2009;8:887-91.
- [53] Bobby Kannan M, Singh Raman RK. A mechanistic study of in vitro degradation of magnesium alloy using electrochemical techniques. *Journal of Biomedical Materials Research - Part A* 2010;93:1050-5.
- [54] Kannan MB, Raman RKS. Magnesium alloys as biodegradable implants. *Gold Coast, QLD2009*. p. 83-6.
- [55] Oyane A, Kim HM, Furuya T, Kokubo T, Miyazaki T, Nakamura T. Preparation and assessment of revised simulated body fluids. *Journal of Biomedical Materials Research - Part A* 2003;65:188-95.
- [56] Zainal Abidin NI, Martin D, Atrens A. Corrosion of high purity Mg, AZ91, ZE41 and Mg₂Zn_{0.2}Mn in Hank's solution at room temperature. *Corrosion Science* 2011;53:862-72.
- [57] Kirkland NT, Lespagnol J, Birbilis N, Staiger MP. A survey of bio-corrosion rates of magnesium alloys. *Corrosion Science* 2010;52:287-91.
- [58] Xin Y, Huo K, Tao H, Tang G, Chu PK. Influence of aggressive ions on the degradation behavior of biomedical magnesium alloy in physiological environment. *Acta Biomaterialia* 2008;4:2008-15.
- [59] Hornberger H, Virtanen S, Boccaccini AR. Biomedical coatings on magnesium alloys – A review. *Acta biomaterialia* 2012;8:2442-55.
- [60] Li Z, Gu X, Lou S, Zheng Y. The development of binary Mg–Ca alloys for use as biodegradable materials within bone. *Biomaterials* 2008;29:1329-44.
- [61] Witte F, Fischer J, Nellesen J, Crostack H-A, Kaese V, Pisch A, et al. In vitro and in vivo corrosion measurements of magnesium alloys. *Biomaterials* 2006;27:1013-8.

- [62] Rosalbino F, De Negri S, Saccone A, Angelini E, Delfino S. Bio-corrosion characterization of Mg-Zn-X (X = Ca, Mn, Si) alloys for biomedical applications. *Journal of Materials Science: Materials in Medicine* 2010;21:1091-8.
- [63] Witte F, Kaese V, Haferkamp H, Switzer E, Meyer-Lindenberg A, Wirth CJ, et al. In vivo corrosion of four magnesium alloys and the associated bone response. *Biomaterials* 2005;26:3557-63.
- [64] Xu L, Yu G, Zhang E, Pan F, Yang K. In vivo corrosion behavior of Mg-Mn-Zn alloy for bone implant application. *Journal of Biomedical Materials Research - Part A* 2007;83:703-11.
- [65] Zhang E, Yin D, Xu L, Yang L, Yang K. Microstructure, mechanical and corrosion properties and biocompatibility of Mg-Zn-Mn alloys for biomedical application. *Materials Science and Engineering C* 2009;29:987-93.
- [66] Li Z, Gu X, Lou S, Zheng Y. The development of binary Mg-Ca alloys for use as biodegradable materials within bone. *Biomaterials* 2008;29:1329-44.
- [67] Zhang S, Li J, Song Y, Xie C, He Y, Jiang Y. In vitro degradation, hemolysis and MC3T3-E1 cell adhesion of biodegradable Mg-Zn alloy. *Materials Science and Engineering: C* 2009;29:1907-12.
- [68] Gu X, Zheng Y, Zhong S, Xi T, Wang J, Wang W. Corrosion of, and cellular responses to Mg-Zn-Ca bulk metallic glasses. *Biomaterials* 2010;31:1093-103.
- [69] Zberg B, Uggowitzer PJ, Löffler JF. MgZnCa glasses without clinically observable hydrogen evolution for biodegradable implants. *Nat Mater* 2009;8:887-91.
- [70] Zhang E, Yin D, Xu L, Yang L, Yang K. Microstructure, mechanical and corrosion properties and biocompatibility of Mg-Zn-Mn alloys for biomedical application. *Materials Science and Engineering: C* 2009;29:987-93.
- [71] Zhang S, Zhang X, Song Y, Zhang Y, Jiang Y, Bian Y. Research on an Mg-Zn alloy as a degradable biomaterial. *Acta biomaterialia* 2010;6:626-40.
- [72] Feyerabend F, Fischer J, Holtz J, Witte F, Willumeit R, Hort N. Evaluation of short-term effects of rare earth and other elements used in magnesium alloys on primary cells and cell lines. *Acta biomaterialia* 2010;6:1834-42.
- [73] Witte F, Hort N, Kainer KU, Willumeit R. Degradable biomaterials based on magnesium corrosion. *Current Opinion in Solid State and Materials Science* 2008;12:63-72.
- [74] Drynda A, Deinet N, Braun N, Peuster M. Rare earth metals used in biodegradable magnesium-based stents do not interfere with proliferation of smooth muscle cells but do induce the upregulation of inflammatory genes. *Journal of Biomedical Materials Research Part A* 2009;91A:360-9.
- [75] Hort N, Huang Y, Fechner D, Witte F, Kainer KU, Feyerabend F. Magnesium alloys as implant materials – Principles of property design for Mg-RE alloys. *Acta biomaterialia* 2010;6:1714-25.
- [76] Xu L, Yu G, Zhang E, Pan F, Yang K. In vivo corrosion behavior of Mg-Mn-Zn alloy for bone implant application. *Journal of Biomedical Materials Research Part A* 2007;83A:703-11.
- [77] Chashschin VP, Artunina GP, Norseth T. Congenital defects, abortion and other health effects in nickel refinery workers. *Science of The Total Environment* 1994;148:287-91.
- [78] Drynda A, Deinet N, Braun N, Peuster M. Rare earth metals used in biodegradable magnesium-based stents do not interfere with proliferation of smooth muscle cells but do induce the upregulation of inflammatory genes. *Journal of Biomedical Materials Research - Part A* 2009;91:360-9.

- [79] Gunde P, Hänzi AC, Sologubenko AS, Uggowitzer PJ. High-strength magnesium alloys for degradable implant applications. *Materials Science and Engineering A* 2011;528:1047-54.
- [80] Gray JE, Luan B. Protective coatings on magnesium and its alloys - A critical review. *Journal of Alloys and Compounds* 2002;336:88-113.
- [81] Lorenz C, Brunner JG, Kollmannsberger P, Jaafar L, Fabry B, Virtanen S. Effect of surface pre-treatments on biocompatibility of magnesium. *Acta biomaterialia* 2009;5:2783-9.
- [82] Jo J-H, Kang B-G, Shin K-S, Park D-S, Koh Y-H. Hydroxyapatite coating on magnesium with MgF₂ interlayer for enhanced corrosion resistance and biocompatibility. *Journal of Materials Science: Materials in Medicine* 2011;22:2437-47.
- [83] Kim S-M, Jo J-H, Lee S-M, Estrin Y, Lee J-W, Koh Y-H. Hydroxyapatite-coated magnesium implants with improved in vitro and in vivo biocorrosion, biocompatibility, and bone response. *Journal of Biomedical Materials Research Part A* 2014;102:429-41.
- [84] Li N, Li YD, Wang YB, Li M, Zheng YF. Corrosion resistance and cytotoxicity of a MgF₂ coating on biomedical Mg–1Ca alloy via vacuum evaporation deposition method. *Surface and Interface Analysis* 2013;45:1217-22.
- [85] Zhang XP, Zhao ZP, Wu FM, Wang YL, Wu J. Corrosion and wear resistance of AZ91D magnesium alloy with and without microarc oxidation coating in Hank's solution. *J Mater Sci* 2007;42:8523-8.
- [86] Li JN, Cao P, Zhang XN, Zhang SX, He YH. In vitro degradation and cell attachment of a PLGA coated biodegradable Mg–6Zn based alloy. *J Mater Sci* 2010;45:6038-45.
- [87] Gao JH, Shi XY, Yang B, Guan FX, Guan SK. Fabrication and characterization of bioactive composite coatings on Mg–Zn–Ca alloy by MAO/sol–gel. *Journal of Materials Science: Materials in Medicine* 2011;22:1681-7.
- [88] Huang J-j, Ren Y-b, Zhang B-c, Yang K. Preparation and property of coating on degradable Mg implant. *Chinese Journal of Nonferrous Metals* 2007;17:1465.
- [89] Yang J, Cui F, Lee IS. Surface modifications of magnesium alloys for biomedical applications. *Annals of biomedical engineering* 2011;39:1857-71.
- [90] Liu X, Yue Z, Romeo T, Weber J, Scheuermann T. Biofunctionalized anti-corrosive silane coatings for magnesium alloys. *Acta biomaterialia* 2013;9:8671-7.
- [91] van Ooij WJ, Zhu D, Stacy M, Seth A, Mugada T, Gandhi J, et al. Corrosion protection properties of organofunctional silanes - An overview. *Tsinghua Science and Technology* 2005;10:639-64.
- [92] Wang D, Bierwagen GP. Sol-gel coatings on metals for corrosion protection. *Progress in Organic Coatings* 2009;64:327-38.
- [93] Subramanian V, Van Ooij WJ. Effect of the Amine Functional Group on Corrosion Rate of Iron Coated with Films of Organofunctional Silanes. *Corrosion* 1998;54:204-15.
- [94] Palomino LM, Suegama PH, Aoki IV, Montemor MF, De Melo HG. Electrochemical study of modified cerium-silane bi-layer on Al alloy 2024-T3. *Corrosion Science* 2009;51:1238-50.
- [95] van Ooij WJ, Zhu D, Stacy M, Seth A, Mugada T. Corrosion Protection Properties of Organofunctional Silanes—An Overview. *Tsinghua Science & Technology* 2005;10:639-64.
- [96] Zucchi F, Grassi V, Frignani A, Trabanelli G. Inhibition of copper corrosion by silane coatings. *Corrosion Science* 2004;46:2853-65.
- [97] Tesoro G. Silane coupling agents, Edwin P. Plueddemann, Plenum, New York, 1982, 235 pp. Price: \$37.50. *Journal of Polymer Science: Polymer Letters Edition* 1983;21:503-.

- [98] Chakraborty Banerjee P, Singh Raman RK. Electrochemical impedance spectroscopic investigation of the role of alkaline pre-treatment in corrosion resistance of a silane coating on magnesium alloy, ZE41. *Electrochimica Acta* 2011;56:3790-8.
- [99] Pagliaro M, Royal Society of C. Silica-based materials for advanced chemical applications. Cambridge: RSC Pub.; 2009.
- [100] Jenney CR, DeFife KM, Colton E, Anderson JM. Human monocyte/macrophage adhesion, macrophage motility, and IL-4- induced foreign body giant cell formation on silane-modified surfaces in vitro. *Journal of Biomedical Materials Research* 1998;41:171-84.
- [101] Kirchner C, Liedl T, Kudera S, Stölzle S, Fertig N, Parak WJ. Cytotoxicity of Colloidal CdSe and CdSe/ZnS Nanoparticles. *Nano Letters* 2004;5:331-8.
- [102] Kotov NA, Winter JO, Clements IP, Kam NWS, Patolsky F, Ballerini L. Nanomaterials for Neural Interfaces. *Advanced Materials* 2009;21:3970-4004.
- [103] Ballarre J, Manjubala I, Schreiner WH, Orellano JC, Fratzl P, Cere S. Improving the osteointegration and bone-implant interface by incorporation of bioactive particles in sol-gel coatings of stainless steel implants. *Acta biomaterialia* 2010;6:1601-9.
- [104] Ehlert N, Badar M, Christel A, Lohmeier SJ, Mueller PP, Behrens P. Mesoporous silica coatings for controlled release of the antibiotic ciprofloxacin from implants. *Journal of Materials Chemistry* 2011;21:752-60.
- [105] Ahmed A, Bonner C, Desai TA. Bioadhesive microdevices with multiple reservoirs: A new platform for oral drug delivery. *Journal of Controlled Release* 2002;81:291-306.
- [106] Borck A, Rzany A, Wittchow E. IMPLANT MADE OF A BIOCORRODIBLE METALLIC MATERIAL HAVING A COATING MADE OF AN ORGANOSILICON COMPOUND 2008.
- [107] Osaka T, Matsunaga T, Nakanishi T, Arakaki A, Niwa D, Iida H. Synthesis of magnetic nanoparticles and their application to bioassays. *Analytical and Bioanalytical Chemistry* 2006;384:593-600.
- [108] Killian MS, Wagener V, Schmuki P, Virtanen S. Functionalization of metallic magnesium with protein layers via linker molecules. *Langmuir* 2010;26:12044-8.
- [109] Nanci A, Wuest JD, Peru L, Brunet P, Sharma V, Zalzal S, et al. Chemical modification of titanium surfaces for covalent attachment of biological molecules. *Journal of Biomedical Materials Research* 1998;40:324-35.
- [110] Nanci A, Wuest JD, Peru L, Zalzal S, McKee MD. Chemical modification of titanium surfaces for covalent attachment of biological molecules. *Journal of biomedical materials research* 1998;40:324-35.
- [111] Lévesque SG, Shoichet MS. Synthesis of cell-adhesive dextran hydrogels and macroporous scaffolds. *Biomaterials* 2006;27:5277-85.
- [112] Suppakarn N, Sanmaung S, Ruksakulpiwa Y, Sutapun W. Effect of surface modification on properties of natural hydroxyapatite/polypropylene composites. 2008. p. 511-4.
- [113] Huang LY, Yang MC. Hemocompatibility of layer-by-layer hyaluronic acid/heparin nanostructure coating on stainless steel for cardiovascular stents and its use for drug delivery. *Journal of Nanoscience and Nanotechnology* 2006;6:3163-70.
- [114] Wu Z, Jiang Y, Kim T, Lee K. Effects of surface coating on the controlled release of vitamin B1 from mesoporous silica tablets. *Journal of Controlled Release* 2007;119:215-21.
- [115] Maver U, Godec A, Bele M, Srčić S, Jamnik J. Novel hybrid silica xerogels for stabilization and controlled release of drug. *International Journal of Pharmaceutics* 2007;330:164-74.

- [116] Quintanar-Guerrero D, Ganem-Quintanar A, Nava-Arzaluz MG, Pinon-Segundo E. Silica xerogels as pharmaceutical drug carriers. *Expert opinion on drug delivery* 2009;6:485-98.
- [117] Ballarre J, Manjubala I, Schreiner WH, Orellano JC, Fratzl P, Ceré S. Improving the osteointegration and bone-implant interface by incorporation of bioactive particles in sol-gel coatings of stainless steel implants. *Acta Biomaterialia* 2010;6:1601-9.
- [118] Carlyle W, Tedeschi E. ENDOVASCULAR STENT WITH PRESERVATIVE COATING. 2003.
- [119] Ehlert N, Badar M, Christel A, Lohmeier SJ, Luessenhop T, Stieve M, et al. Mesoporous silica coatings for controlled release of the antibiotic ciprofloxacin from implants. *Journal of Materials Chemistry* 2011;21:752-60.
- [120] Wang Y, Wang P, Kohls D, Hamilton WA, Schaefer DW. Water absorption and transport in bis-silane films. *Physical Chemistry Chemical Physics* 2009;11:161-6.
- [121] Ying J, Jana N, Zheng Y. Water-Soluble, surface-functionalized nanoparticle for bioconjugation via universal silane coupling. WO Patent 2,006,080,895; 2006.
- [122] Bariana M, Aw MS, Kurkuri M, Losic D. Tuning drug loading and release properties of diatom silica microparticles by surface modifications. *International Journal of Pharmaceutics* 2013;443:230-41.
- [123] Guo R, Du X, Zhang R, Deng L, Dong A, Zhang J. Bioadhesive film formed from a novel organic-inorganic hybrid gel for transdermal drug delivery system. *European Journal of Pharmaceutics and Biopharmaceutics* 2011;79:574-83.
- [124] Petersen S, Kaule S, Teske M, Minrath I, Schmitz K-P, Sternberg K. Development and In Vitro Characterization of Hyaluronic Acid-Based Coatings for Implant-Associated Local Drug Delivery Systems. *Journal of Chemistry* 2013;2013:11.
- [125] Toworfe GK, Composto RJ, Shapiro IM, Ducheyne P. Nucleation and growth of calcium phosphate on amine-, carboxyl- and hydroxyl-silane self-assembled monolayers. *Biomaterials* 2006;27:631-42.
- [126] Thevenot P, Hu W, Tang L. Surface chemistry influences implant biocompatibility. *Current Topics in Medicinal Chemistry* 2008;8:270-80.
- [127] Kim J, Wong KC, Wong PC, Kulinich SA, Metson JB, Mitchell KAR. Characterization of AZ91 magnesium alloy and organosilane adsorption on its surface. *Applied Surface Science* 2007;253:4197-207.
- [128] Khramov AN, Balbyshev VN, Kasten LS, Mantz RA. Sol-gel coatings with phosphonate functionalities for surface modification of magnesium alloys. *Thin Solid Films* 2006;514:174-81.
- [129] Khramov AN, Johnson JA. Phosphonate-functionalized ORMOSIL coatings for magnesium alloys. *Progress in Organic Coatings* 2009;65:381-5.
- [130] Pathak SS, Khanna AS. Synthesis and performance evaluation of environmentally compliant epoxysilane coatings for aluminum alloy. *Progress in Organic Coatings* 2008;62:409-16.
- [131] Pathak SS, Khanna AS, Sinha TJM. HMMM cured corrosion resistance waterborne ormosil coating for aluminum alloy. *Progress in Organic Coatings* 2007;60:211-8.
- [132] Davis SR, Brough AR, Atkinson A. Formation of silica/epoxy hybrid network polymers. *Journal of Non-Crystalline Solids* 2003;315:197-205.
- [133] Zandi-zand R, Ershad-langroudi A, Rahimi A. Silica based organic-inorganic hybrid nanocomposite coatings for corrosion protection. *Progress in Organic Coatings* 2005;53:286-91.

- [134] Khramov AN, Balbyshev VN, Voevodin NN, Donley MS. Nanostructured sol–gel derived conversion coatings based on epoxy- and amino-silanes. *Progress in Organic Coatings* 2003;47:207-13.
- [135] Zhu D, van Ooij WJ. Corrosion protection of AA 2024-T3 by bis-[3-(triethoxysilyl)propyl]tetrasulfide in sodium chloride solution.: Part 2: mechanism for corrosion protection. *Corrosion Science* 2003;45:2177-97.
- [136] Cabral AM, Duarte RG, Montemor MF, Ferreira MGS. A comparative study on the corrosion resistance of AA2024-T3 substrates pre-treated with different silane solutions: Composition of the films formed. *Progress in Organic Coatings* 2005;54:322-31.
- [137] Zhu D, Ooij WJv. Enhanced corrosion resistance of AA 2024-T3 and hot-dip galvanized steel using a mixture of bis-[triethoxysilylpropyl]tetrasulfide and bis-[trimethoxysilylpropyl]amine. *Electrochimica Acta* 2004;49:1113-25.
- [138] Buzzi S, Jin K, Uggowitzer PJ, Tosatti S, Gerber I, Löffler JF. Cytotoxicity of Zr-based bulk metallic glasses. *Intermetallics* 2006;14:729-34.
- [139] Hänzi AC, Gerber I, Schinhammer M, Löffler JF, Uggowitzer PJ. On the in vitro and in vivo degradation performance and biological response of new biodegradable Mg–Y–Zn alloys. *Acta biomaterialia* 2010;6:1824-33.
- [140] Fischer J, Prosenc MH, Wolff M, Hort N, Willumeit R, Feyerabend F. Interference of magnesium corrosion with tetrazolium-based cytotoxicity assays. *Acta biomaterialia* 2010;6:1813-23.
- [141] Fischer J, Prosenc MH, Wolff M, Hort N, Willumeit R, Feyerabend F. Interference of magnesium corrosion with tetrazolium-based cytotoxicity assays. *Acta Biomaterialia*;6:1813-23.
- [142] ISO. 10993-5:2009. Biological evaluation of medical devices - Part 5: Tests for in vitro cytotoxicity 1999.
- [143] Oyane A, Kim HM, Furuya T, Kokubo T, Miyazaki T, Nakamura T. Preparation and assessment of revised simulated body fluids. *Journal of biomedical materials research Part A* 2003;65:188-95.
- [144] Kang Y, Xu X, Yin G, Chen A, Liao L, Yao Y, et al. A comparative study of the in vitro degradation of poly(l-lactic acid)/ β -tricalcium phosphate scaffold in static and dynamic simulated body fluid. *European Polymer Journal* 2007;43:1768-78.
- [145] Duan Y, Liu K, Chen J, Zhang X. [Effects of simulated body fluid flowing rate on bone-like apatite formation on porous calcium phosphate ceramics]. *Hang tian yi xue yu yi xue gong cheng= Space medicine & medical engineering* 2002;15:203-7.
- [146] Duan Y, Zhang Z, Wang C, Chen J, Zhang X. Dynamic study of calcium phosphate formation on porous HA/TCP ceramics. *Journal of Materials Science: Materials in Medicine* 2005;16:795-801.
- [147] Bobby Kannan M, Singh RK. A mechanistic study of in vitro degradation of magnesium alloy using electrochemical techniques. *Journal of biomedical materials research Part A* 2010;93:1050-5.
- [148] Xin Y, Hu T, Chu PK. Degradation behaviour of pure magnesium in simulated body fluids with different concentrations of. *Corrosion Science* 2011;53:1522-8.
- [149] Zhao S-f, Jiang Q-h, Peel S, Wang X-x, He F-m. Effects of magnesium-substituted nanohydroxyapatite coating on implant osseointegration. *Clinical Oral Implants Research* 2013;24:34-41.

- [150] Zhang B, Hou Y, Wang X, Wang Y, Geng L. Mechanical properties, degradation performance and cytotoxicity of Mg–Zn–Ca biomedical alloys with different compositions. *Materials Science and Engineering: C* 2011;31:1667-73.
- [151] Singh Raman RK. The role of microstructure in localized corrosion of magnesium alloys. *Metall and Mat Trans A* 2004;35:2525-31.
- [152] Banerjee PC, Raman RKS, Durandet Y, McAdam G. Electrochemical investigation of the influence of laser surface melting on the microstructure and corrosion behaviour of ZE41 magnesium alloy – An EIS based study. *Corrosion Science* 2011;53:1505-14.
- [153] Tang H, Xin T, Wang F. Calcium Phosphate/Titania Sol-Gel Coatings on AZ31 Magnesium Alloy for Biomedical Applications. *Int J Electrochem Sci* 2013;8:8115-25.
- [154] Zhang Y, Forsyth M, Hinton B, Wallace GG. Control of biodegradation of a Mg alloy in simulated body fluid. 2011.
- [155] Lorenz C, Brunner JG, Kollmannsberger P, Jaafar L, Fabry B, Virtanen S. Effect of surface pre-treatments on biocompatibility of magnesium. *Acta biomaterialia* 2009;5:2783-9.
- [156] Tamimi F, Nihouannen DL, Bassett DC, Ibasco S, Gbureck U. Biocompatibility of magnesium phosphate minerals and their stability under physiological conditions. *Acta biomaterialia* 2011;7:2678-85.
- [157] Xin Y, Liu C, Zhang X, Tang G, Tian X, Chu PK. Corrosion behavior of biomedical AZ91 magnesium alloy in simulated body fluids. *Journal of materials research* 2007;22:2004-11.
- [158] Ali NN, Rowe J, Teich NM. Constitutive expression of non-bone/liver/kidney alkaline phosphatase in human osteosarcoma cell lines. *Journal of Bone and Mineral Research* 1996;11:512-20.
- [159] Willumeit R, Fischer J, Feyerabend F, Hort N, Bismayer U, Heidrich S. Chemical surface alteration of biodegradable magnesium exposed to corrosion media. *Acta biomaterialia* 2011;7:2704-15.